UNIVERSITY OF CAPE TOWN
IYUNIVESITHI YASEKAPA • UNIVERSITEIT VAN KAAPSTAD

Parametric study of stiffened steel containment shell structures

Rugare B. Masendeke

Supervisor: Professor A. Zingoni

'This thesis is presented in partial fulfilment for the degree of Masters of Science in Structural engineering in the Department of Civil engineering at the University of Cape Town'

05 November 2008

Declaration

I hereby declare that this thesis is my own unaided work, both in conception and execution, and that apart from the normal guidance of my supervisor.

Name: Rugare B. Masendeke

Signature: Signed by candidate

Date: 31 March 2008

Acknowledgements

Firstly, I give all the glory to the Lord for His strength, knowledge and wisdom which made me pull through this thesis. His grace is unspeakable.

I also want to extent my heartfelt thanks my supervisor Prof. A. Zingoni for granting me this opportunity to further my studies by pursuing a Masters degree. I greatly appreciate your guidance and mentoring as I make my first steps into the academic and research field.

I wish to thank my mother and my family for their powerful prayers and encouragement during the period of my study. I thank the Lord for my close friends and brothers, Tongai, Tipeyi, Jameson and Regis for your moral support.

To everyone who was praying for me, God bless you abundantly.

Abstract

A FEM-based parametric study is undertaken to investigate the buckling behavior of meridionally and circumferentially stiffened steel cylindrical and conical shell frustum subjected to different load cases. This situation arises in different steel shell applications such as storage vessels (liquid, solid and gas) and in certain configurations of industrial process facilities. The stiffeners are flat strips of rectangular section welded on to the outer surface of the shell, either over the whole length of the shell meridian or around the circumference of the shell. It is required to establish how the elastic buckling load and mode shapes vary with respect to certain key parameters of the problem. The parameters of interest in the study include the number of stiffeners around the shell circumference and along the meridian, the stiffener-depth to shell-thickness ratio, and the stiffener depth-to-width ratio. This thesis reports the findings of the parametric study and also presents some results of experimental tests on laboratory small-scale models of stiffened cylindrical and conical frusta.

List of symbols

The following symbols are used in this thesis:

Nomenclature

A cross sectional area of shell;

A_r area of cross section of ring stiffener;

A_s stringer cross-sectional area;

b stringer thickness;

C_s buckling stress coefficient for cylinders under shear load;

D shell bending rigidity;

d stringer depth;

E Young's modulus;

e_s stringer eccentricity;

f_y yield stress;

G shear modulus;

I_s stringer centroidal moment of inertia about axis parallel to the cone wall;

K shell extensional rigidity;

K_c buckling stress coefficient for moderately long cylinders under axial compression;

K_p buckling stress coefficient for cylinders under uniform external pressure;

K_s buckling stress coefficient for cylindrical panels under axial compression;

K_b buckling stress coefficient for cylinders under bending;

K_{ST} stringer buckling coefficient;

L vertical length of shell;

L_e slant length of cone;

m number of meridional half waves;

N number of stringers;

n number of circumferential full waves;

P squash load;

P_{cr} elastic critical buckling load;

P_{cyl} classical buckling load of un-stiffened cylinders;

P_{con} classical buckling load of un-stiffened conical frustum;

P_x, P_y in-plane direct stress resultants

p_o applied uniform external pressure;

p_{cr} critical uniform external pressure;

R radius of cylinder;

$R(x)$ radius of cone at any point;

R_1 small radius of conical frustum;

R_2 large radius of conical frustum;

R_e equivalent radius of conical frustum;

R_f radius to the outer flange of stiffener;

R_r radius from centre of cylinder to centroid of stiffener;

$r_2(x)$ principal radius of curvature;

S_{xy} in-plane shear stress resultant

s width of cylindrical panel or equivalent conical panel;

T applied torque;

t shell thickness;

t_s smeared shell thickness of shell;

u, v, w axial, circumferential, and radial displacements ;

V applied shear force;

x meridional coordinate measured from small end ;

y circumferential cylindrical co-ordinate;

w lateral displacement;

Greek symbols

α cone tapering angle

σ_x Axial membrane stress;

σ_θ hoop membrane stress;

σ_{cr} critical elastic buckling stress;

σ_y yeild stress;

τ shear membrane stresses;

τ_{cr} critical shear membrane stresses;

λ eigenvalue;

$\zeta(x)$ stiffening ratio of cone = $A_s/(st)$;

η total curvature parameter of panel

η_p plasticity correction factor;

ξ curvature parameter;

μ Poisson's ratio = 0.3;

φ angular distance between stiffeners;

γ factor to account for the difference between theoretical and experimental results

λ_{cr} linear meridional bending half wavelength of a buckle;

Δ end shortening;

Subscripts

1 small-radius end;

2 large-radius end;

cr critical

x meridionally; and

θ circumferentially.

Abbreviations

EC3 Eurocode 3

FE Finite element

FEM Finite element model

ECCS European Convention for Construction steelwork

LBA Linear buckling analysis

List of tables

Chapter 4

Table 4.1 Overview of finite element models....46

Chapter 5

Table 5.1 Stiffened cylindrical shell models dimensions (L=300mm)....53
Table 5.2 Stiffened conical shell models dimensions (L=300mm, β=20°)....54

Chapter 6

Table 6.1 Mesh convergence study....58

Chapter 7

Table 7.1 Convergence study for single panel model....102
Table 7. 2 Failure mechanisms of cylindrical shells....103
Table 7. 3 Failure mechanisms of conical frustum shells....104
Table 7. 4 Results of experimental tests on stiffened cylindrical and conical shells....105
Table 7. 5 Results of experimental tests conducted at University College, London....106
Table 7. 6 Optimum stringer slenderness ratio for cylindrical and conical frustum (N=16)....109
Table 7. 7 Optimum d/t ratio for stiffened cylindrical and conical frustum (N=16)..111
Table 7. 8 Optimum ring stiffener slenderness ratio for circumferentially stiffened cylinders....113
Table 7. 9 Change over between panel buckling, local shell and stringer modes for different load cases.. 116
Table 7. 10 Change over between local shell, panel buckling and global modes for different load cases.. 118

Table 7. 11 Change over between stiffener and local shell modes for different load cases.....120

Table 7. 12 Change over between local shell and global modes for different load cases.....121

Table of Contents

Declaration.....i

Acknowledgements.....ii

Abstract.....iii

List of tables.....iv

List of symbols.....vi

Chapter 1 Introduction

1.1 Applications of steel shell structures.....1

1.2 Buckling problem in thin walled steel shell structures.....2

1.3 On the option of stiffening steel shell structures to enhance buckling capacity.....2

1.4 Towards the understanding of elastic buckling behaviour of stiffened shells.....3

Chapter 2 Literature Review

2.1 Introduction.....5

2.2 Definition of a shell and stress systems in shells.....5

2.3 Theory of Shell stability

2.3.1 Introduction.....5

2.3.2 Standard methods of Theory of Shell stability.....6

2.3.3 Differential equations of buckling of shells.....6

2.4 Elastic stability of un-stiffened cylindrical shells.....9

2.5 Elastic stability of un-stiffened conical shells.....13

2.6 Elastic stability of un-stiffened cylindrical panels.....17

2.7 Theory of stiffened shell stability.....18

2.8 Elastic stability of stiffened cylindrical shells.....21

2.9 Stiffened Conical shells.....26

2.10 Stress distribution on Stiffened Shells.....27

2.11 Effects of Parametric variation on stiffened shells.....30

2.12 Post buckling behaviour of stiffened and un-stiffened shells.....35

Chapter 3 Statement of Research and Methodology

3.1 Introduction....39
3.2 Statement and scope of research....39
3.3 Research objectives....40
3.4 Methodology
3.4.1 Introduction....40
3.4.2 Finite element modelling....40
3.4.3 Experimental work....42
3.4.4 Analytical solutions....42

Chapter 4 Finite element modelling
4.1 Introduction....43
4.2 Fundamentals of finite element analysis of shell structures....43
4.2.1 Eigenvalue buckling prediction....43
4.3 Geometry and materials....44
4.4 Models description....45
4.5 Boundary conditions and Loading....47
4.6 Mesh and elements
4.6.1 Elements type....48
4.6.2 Choosing the appropriate element for an analysis type....49
4.6.3 Mesh convergence study....50
4.7 Solution procedure....50

Chapter 5 Experimental testing

5.1 Introduction....52
5.2 Geometry and materials of specimen....52
5.3 Test rig and measurement system....55
5.4 Overview of test results....56
5.4.1 Results for material tensile strength....56
5.4.1 Results for axial compression....57

Chapter 6 Finite element results

6.1 Introduction....58
6.2 Mesh convergence study....58

6.3 Finite element model validation.....59
6.4 Effect of varying key parameters of stiffened shells on Elastic buckling load
6.4.1 Introduction.....59
6.4.2 Meridionally stiffened cylinders.....60
6.4.3 Circumferentially stiffened cylinders.....65
6.4.4 Meridionally stiffened conical frustum.....69
6.4.5 Circumferentially stiffened conical frustum.....74
6.5 Effect of varying key parameters of stiffened cylindrical shells on buckling modes.....80
6.5.1 Introduction.....80
6.5.2 Stringer stiffened cylindrical shells under axial Compression.....80
6.5.3 Stringer stiffened cylindrical shells under uniform external pressure.....83
6.5.4 Stringer stiffened cylindrical shells under shell edge shear load.....85
6.5.5 Ring stiffened cylindrical shells under axial Compression.....87
6.5.6 Ring stiffened cylindrical shells under uniform external pressure.....89
6.5.7 Ring stiffened cylindrical shells under shell edge shear load.....91

6.6 Effect of varying key parameters of stiffened conical shell frustum on buckling modes.....93
6.6.1 Introduction.....93
6.6.2 Stringer stiffened conical shell frustum under axial compression.....93
6.6.3 Stringer stiffened conical shell frustum under external pressure.....95
6.6.4 Stringer stiffened conical shell frustum under shell edge shear.....97
6.6.5 Ring stiffened conical shell frustum under

axial compression....99
6.6.6 Ring stiffened conical shell frustum under external pressure....101
6.6.7 Ring stiffened conical shell frustum under shell edge shear....103

Chapter 7 Discussion of results

7.1 Introduction....105
7.2 Mesh convergence study....105
7.3 Finite element model validation with analytical results and previous researchers' results....106
7.4 Discussion of experimental results....107
7.4.1 Description of failure mechanisms....107
7.4.2 Finite element model validation with experimental results....108
7.5 Load carrying capacity....110
7.5.1 Introduction....110
7.5.2 Meridionally stiffened cylindrical and conical frustum shells....110
7.5.3 Circumferentially stiffened cylindrical and conical frustum shells....115
7.6 Effect of varying key parameters of stiffened cylindrical and conical frustum shells on Buckling modes....118
7.6.1 Introduction....118
7.6.2 Meridionally stiffened shell....118
7.6.3 Circumferentially stiffened....123

Chapter 8 Conclusions and recommendations

8.1 Introduction....127
8.2 Validity of FEM to mode elastic buckling of stiffened shells....127
8.3 Load carrying capacity....127
8.4 Failure mode shapes....128

8.5 Recommendations.....129

References.....130

Appendix A -Finite element results

Appendix B -Experimental results

Appendix C -Buckling coefficient graphs

Chapter 1

Introduction

1.1 Applications of steel shell structures

Thin walled steel shells find their vast application as containment structures in civil and mechanical engineering industry. Zingoni (1997) attributes the popularity and basis of shell form applications in industry to their generally high strength-to-weight ratio and inherent stiffness. Shell structures offer the most efficient usage of structural material and if construction constraints are overcome they provide a natural choice for many applications due to their structural efficiency (Rotter, 1998).

Fig. 1.1 Different applications of steel containment shell structures (source Google pictures)

Steel shell structures are widely used as storage vessels for gaseous, liquid and granular materials such as water, oil, coal and industrial chemicals. Storage bins are an important link in the chain of materials handling for a large number of industries. In many cases, the ability of storage facilities to provide a reliable flow of bulk material determines the success of a plant (Pircher and Bridge, 2001).

Apart from storage, they also find diverse application in industrial process facilities with conveyance pipes, chimneys and towers, boilers and pressure vessels as examples. Further applications include marine off-shore platforms and bodies of transportation structures.

1.2 Buckling problem in thin walled steel shell structures

Steel containment structures are usually constructed as thin shells of revolution. These shells of revolution, in conical or cylindrical form, are often subjected to fundamental loading conditions which are axial or eccentric compression, bending, torsion, and internal or external pressure. Moreover, real loading conditions often result in a combination of these fundamental load cases. These fundamental load cases and combinations induce membrane compressive and/or shear stress on shells which endanger their local structural stability. As steel shells are normally quite thin, the shell instability may govern their design.

1.3 On the option of stiffening steel shell structures to enhance buckling capacity

In view of the above remarks, a structural designer is often faced with the need to enhance buckling capacity of steel shells. Amongst the options available include:

- ☐ increasing the thickness of the shell and also
- ☐ attaching stiffeners on the shell skin.

Although the former seems to be the natural and convenient option, it results in heavy and uneconomical structures. In order to obtain lighter structure, the material in the cross section can be arranged to make the cross section most resistant to the stresses that are predominant. Such a configuration is achieved by the latter option of attaching stiffeners to the shell skin. Research has revealed beyond reasonable doubt that the latter option seems to be an economic configuration as it result in increased rigidity of the shell structure and consequently, less material being used. Stiffening elements not only increase buckling resistance but also reduce imperfection sensitivity of the shells (Sridharan and Zeggane, 2001).

1.4 Towards the understanding of elastic buckling behaviour of stiffened shells

Whereas the case of unstiffened shells has been extensively studied, fewer investigations are devoted to the case of stiffened shells. As a result, the buckling behaviour of un-stiffened shells is generally well understood and simple design procedures have been developed. The ECCS, which is one of few standing design guide lines for buckling of shells even acknowledge the inadequacy to device rules which take into account all aspects of loading in a satisfactory manner (ECCS, 1988). Also, the Det norske Veritas design rules which are based on experimental data of aerospace structures are unreliably extrapolated to offshore and terrestrial structures (Green and Nelson, 1981). Owing to this, there exists a need for a comprehensive experimental and numerical investigation of stiffened shells under different load configurations. This research is devoted to yielding a deeper insight into the buckling behaviour of stiffened shells as certain design parameters of the shell and its stiffeners vary. Such a study is of considerable significance in the context of optimal design of stiffened shells. In this study parameters such as stiffener slenderness, spacing, and pattern of stiffeners on cylindrical and conical steel containment structures will be investigated extensively.

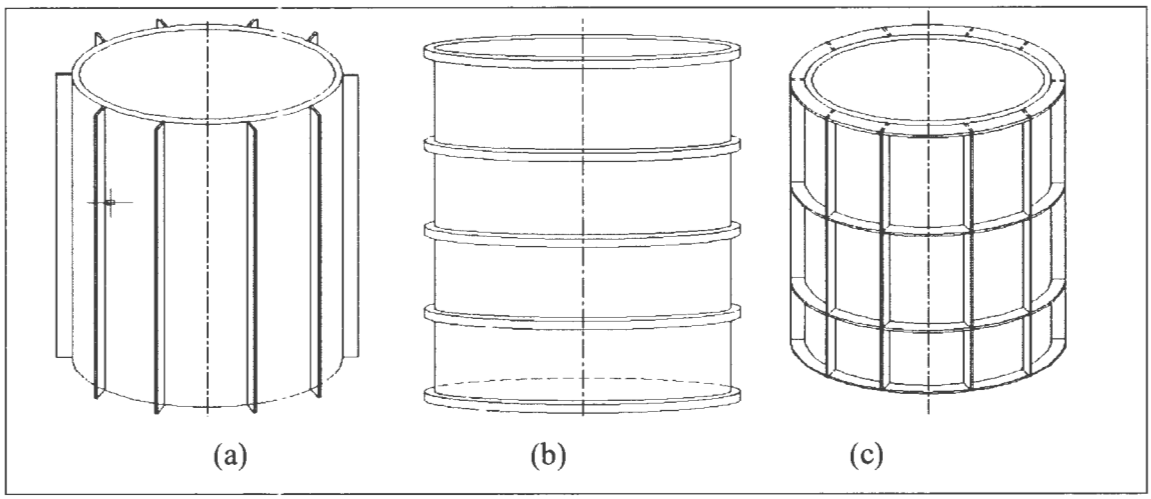

Fig. 1.2 Cylindrical shells stiffened: (a) longitudinally (b) circumferentially (c) in both directions

This current research starts by describing buckling theory of both stiffened and un-stiffened shells. Also a vivid description of different buckling modes that can be encountered in stiffened cylindrical and conical shells is given. This is followed by a

thorough review of parametric studies on stiffened shells which were previously done. A brief description of the post-buckling theory is then presented. Afterwards, a finite element based parametric study on stiffened cylindrical and conical shells is conducted and the results are verified by experimental tests on laboratory small scale models. Finally, parametric charts will be drawn from the results, which will be used to develop simple design procedures. Meanwhile, a comparison of results obtained in this current investigation with the available design guidelines will be carried out and also adequacy of safety provisions for design of stiffened shells by current design guidelines will be evaluated. Eventually, a rational approach to the design of stiffened shells will be achieved and recommendations to optimise structural design of stiffened steel containment shells will be given.

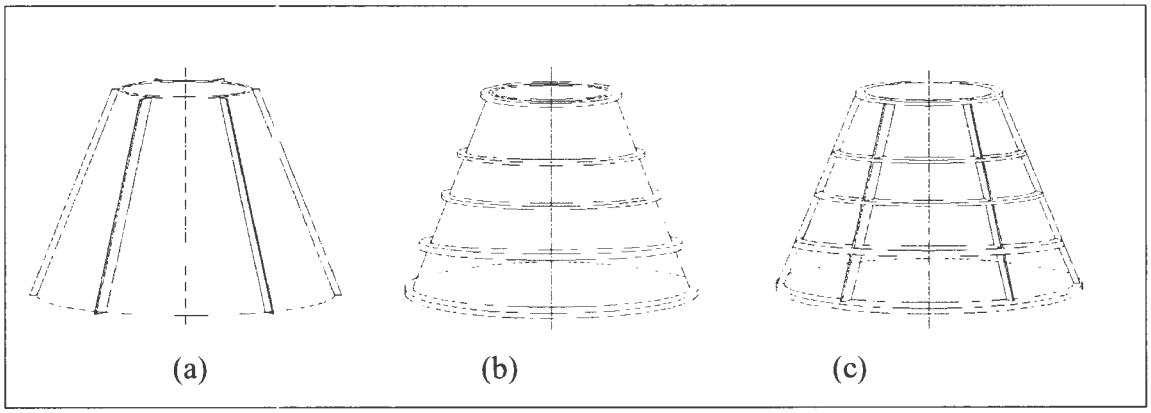

Fig. 1.3 Conical shells stiffened: (a) longitudinally (b) circumferentially (c) in both directions

Chapter 2

Literature review

2.1 Introduction

This chapter outlines the elastic buckling theory of both un-stiffened and stiffened shells. It describes the treatment of shells under different load configurations with respect to buckling. Because rigorous solutions of differential equations for real shells are seldom possible, simple approximate method which is classical equations will be presented. A comprehensive review of research done on buckling behaviour of both cylindrical and conical shells is then presented. In the review, buckling modes are also categorised. Also, different buckling modes are also reviewed. In addition to outlining the buckling theory, post-buckling behaviour of shells is also presented.

2.2 Definition of a shell and stress systems in shells

A shell is a relatively thin structure, in which material of element is bound between two curved surfaces a relatively small distance apart (Zingoni, 1997). A shell resist applied load by developing in plane forces. Shell structures offer the most efficient usage of structural material in any applications (Rotter, 1998). For the purpose of stress analysis, a shell is modelled on the basis of its middle surface (membrane surface).

2.3 Theory of Shell stability

2.3.1 Introduction

Buckling is the ultimate limit state when all or part of the structure suddenly loses its stability under the membrane compression and/or shear stresses in the shell wall. It either leads to large displacements normal to the shell surface or the structure being unable to sustain any increase in the stress resultant and great possibility of causing a catastrophic failure (EC3, 2004). The three relevant buckling membrane forces in thin walled shells are axial compression, circumferential compression and shear. These buckling membrane forces result from different load configurations. A design engineer must also consider interactive buckling (Winterstetter and Schmidt, 2002). Buckling under the former three fundamental loads is well researched and understood.

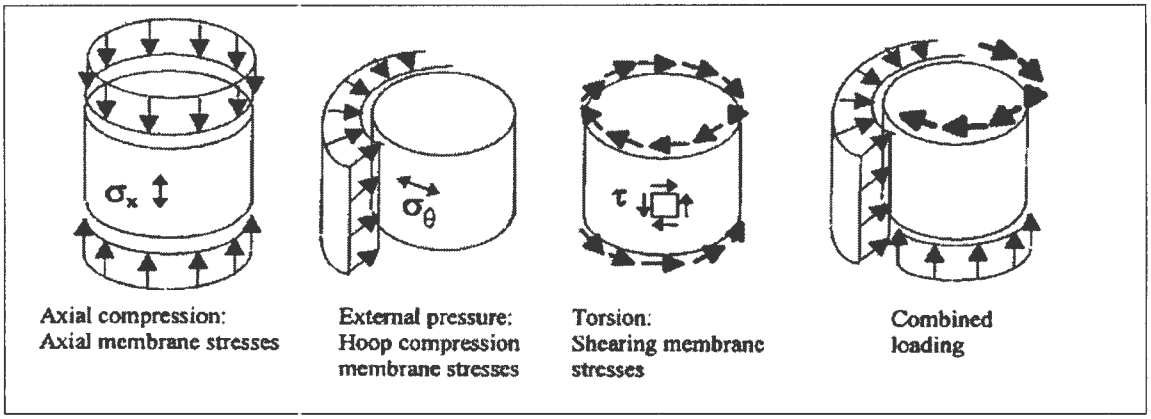

Fig. 2. 1 Fundamental load cases and combined loading (Winterstetter and Schmidt, 2002)

A shell experiences unstable equilibrium if subjected to a given compression load such that any incidental disturbance causes the shell to leave entirely its initial position of equilibrium. The change in equilibrium configuration is usually a large increase in the deflections of the shell, which may or may not be accompanied by a change in basic shape of the shell from the pre-buckled shape.

2.3.2 Standard methods of Theory of Shell stability

The stability of elastic equilibrium of compressed shells can be assessed by one of the following methods of the theory of elastic stability, which are the method of adjacent equilibrium and the energy method (Flugge, 1973). Method of adjacent equilibrium involves using the equilibrium equations, stress-strain relations and the strain-displacement equations to formulate governing differential equations for elastic bodies such as shells. The alternative, energy method, uses the principle that in a conservative system, equilibrium exists if the strain energy stored is equal to the work performed by the external loads (Chajes, 1974). When compression load exceeds critical load, the system is unstable as work done by compression load is greater than the increase in strain energy (Ugural, 1981).

2.3.3 Differential equations of buckling of shells

Using the one of the principles discussed above, different researchers developed the linear small-deflection governing equations for buckling of un-stiffened cylindrical

shells. Due to the well known difficulties of solving linear differential equations, the energy method is generally preferred to the equilibrium one.

The first classical solution was obtained by Lorenz in 1908 which was later arrived at independently by Timoshenko, Southwell, Flugge and Donnell (Chajes, 1974). Solutions for buckling under uniform lateral pressure were given by Southwell and later by von Mises. Results for cylinders subjected to torsional loading were first given by Schwerin followed by Donnell (Brush and Almroth, 1975).

Terms of relatively small magnitude surface in the process of deriving shell equations. Retaining all these terms makes the solution unachievable and equations become of little practical importance. Consequently, researchers have decided to omit some of these terms and lack of firm agreement as to which terms one should neglect has resulted in development of various shell equations, each one based on a different set of simplifications (Chajes, 1974).

Flugge derived governing deferential equations which describe comprehensively, the elastic buckling of a cylindrical shell under the most general homogeneous membrane stress action. For the same problem Timoshenko also formulated governing differential equations which are almost similar to the ones developed by Flugge. Xiang et al. examined the buckling solutions for the Timoshenko thin shell theories against the Flugge thin shell theory and they argued that Timoshenko equations are less complicated than the Flugge equations. However, Donnell achieved even much simpler and relatively uncomplicated equations which have been shown to give satisfactory results when used to deal with buckling problems. The following set of three equations with three unknowns that can be used to obtain the critical load of a cylindrical shell (Chajes, 1974).

$$\frac{\partial^2 u}{\partial x^2}+\frac{(1-\mu)}{2}\frac{\partial^2 u}{\partial y^2}+\frac{(1+\mu)}{2}\frac{\partial^2 v}{\partial x \partial y}-\frac{\mu}{R}\frac{\partial w}{\partial x}=0 \qquad (2.1)$$

$$\frac{\partial^2 v}{\partial y^2}+\frac{(1-\mu)}{2}\frac{\partial^2 v}{\partial x^2}+\frac{(1+\mu)}{2}\frac{\partial^2 u}{\partial x \partial y}-\frac{1}{R}\frac{\partial w}{\partial y}=0 \qquad (2.2)$$

$$P_x\frac{\partial^2 w}{\partial x^2}+P_y\frac{\partial^2 w}{\partial y^2}+\frac{P_y}{R}-D\left(\frac{\partial^4 w}{\partial x^4}+2\frac{\partial^4 w}{\partial x^2\partial y^2}+\frac{\partial^4 w}{\partial y^4}\right)$$
$$+\frac{1}{R}\frac{Et}{1-\mu^2}\left(\frac{\partial v}{\partial y}-\frac{w}{R}+\mu\frac{\partial u}{\partial x}\right)+2S_{xy}\frac{\partial^2 w}{\partial x\partial y}=0 \qquad (2.3)$$

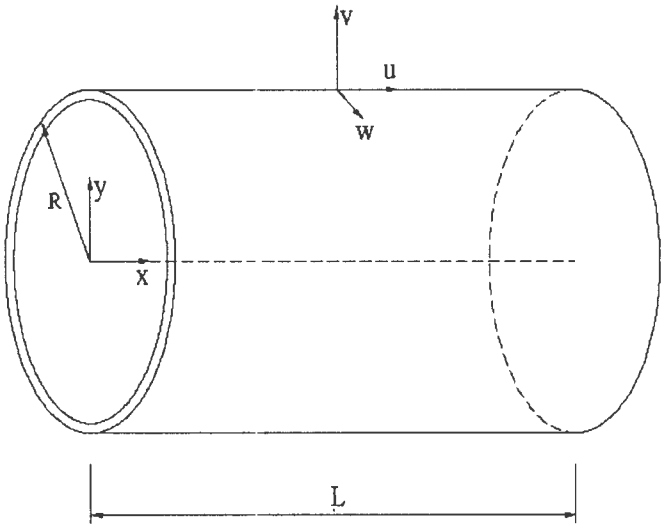

Fig. 2. 2 Notation for the differential equations

, where the symbols are defined as follows:

P_x, P_y	in-plane direct stress resultants
S_{xy}	in-plane shear stress resultant
u, *v*, *w*	axial, circumferential, and radial displace
x	axial cylindrical co-ordinate
y	circumferential cylindrical co-ordinate

In certain types of solutions it is more convenient to deal with one of the three equations. Accordingly, Donnell has reduced the three equations into a simpler and single linear eight order equation in w known as the Donnell equation (Chajes, 1974).

$$D\nabla^8 w-\nabla^4\left(P_x\frac{\partial^2 w}{\partial x^2}+P_y\frac{\partial^2 w}{\partial y^2}+2S_{xy}\frac{\partial^2 w}{\partial x\partial y}\right)+\frac{Et}{R^2}\frac{\partial^4 w}{\partial x^4}=0 \qquad (2.4)$$

Although the simplifications imposed by Donnell somewhat limit the range of applicability, the Donnell equation form the basis for more stability analyses and serve as an introduction to the more complex shell configurations (Brush and Almroth, 1975).

2.4 Elastic stability of un-stiffened cylindrical shells

2.4.1 Introduction

By imposing adequate boundary conditions into the Donnell equation, classical solutions can be obtained for cylindrical shells subjected to axial compression, external pressure, torsion and combined loading. Geometry and notation used is shown in Fig. 2.2 below.

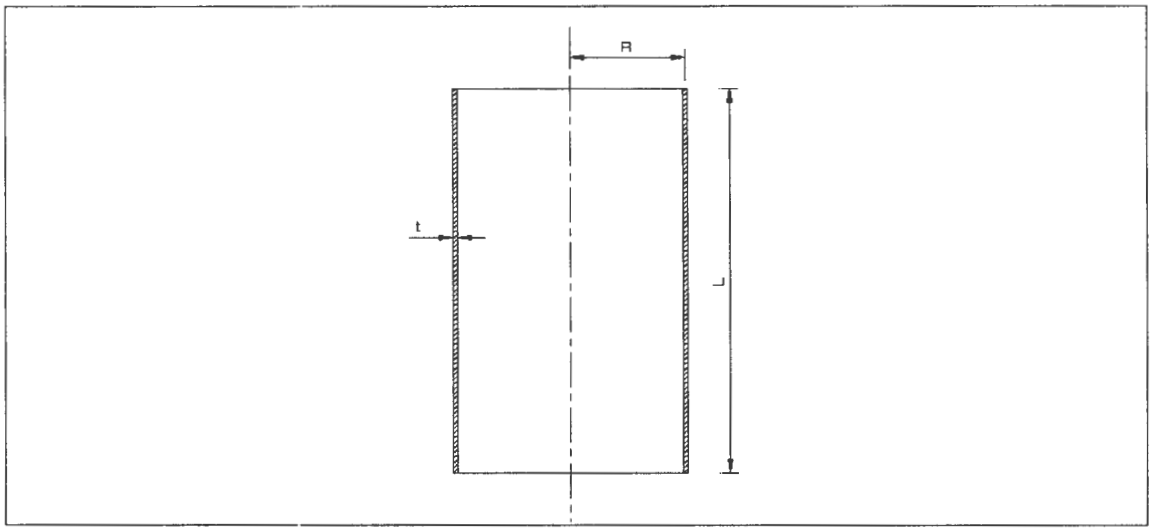

Fig. 2. 3 Un-stiffened cylindrical shell vertical section showing geometry and notation.

The following symbols will be used in the following discussion:

η_p –plasticity correction factor

μ - Poisson's ratio of the material

t – thickness of shell

L- length of cylinder

R- radius of cylinder

2.4.2 Un-stiffened Cylindrical shells under axial compression

Symmetrical buckling occurs at a particular value of compressive load if a cylindrical shell is uniformly compressed in the axial direction. The critical value of compressive load can be obtained by solving the Donnell equation described before.

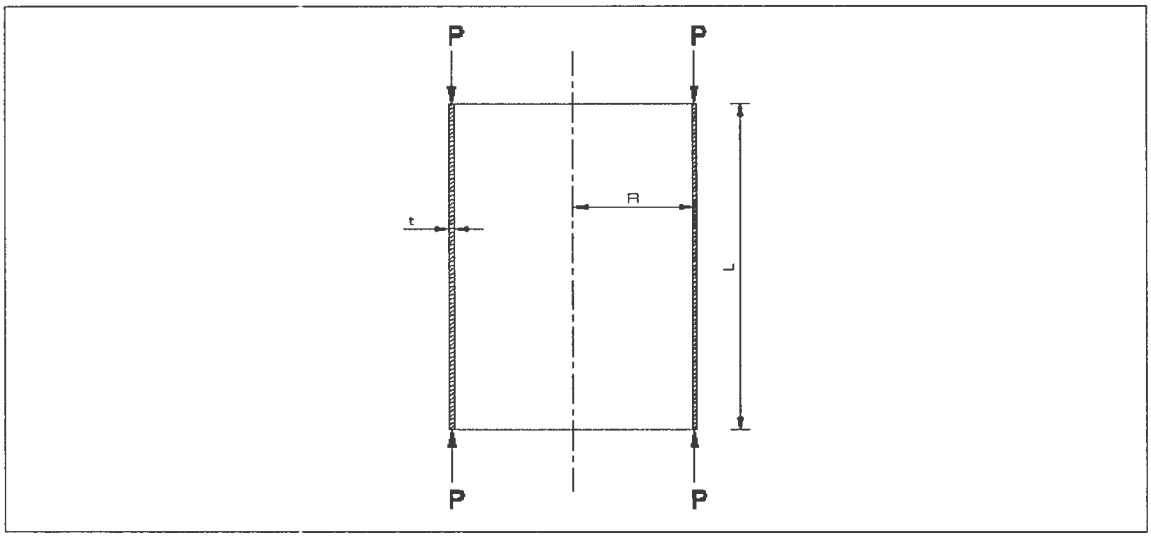

Fig. 2. 4 Un-stiffened cylindrical shell under axial compression.

The design allowable buckling stress for an unpressurised thin walled circular cylinder subjected to axial compression is given by (Baker et al.,1972) :

$$\frac{\sigma_{cr}}{\eta_p} = K_c \frac{\pi^2 E^2}{12(1-\mu^2)}\left(\frac{t}{L}\right)^2 \tag{2.5}$$

, where K_c is buckling stress coefficient and for moderately long cylinders and is given by:

$$K_c = \frac{4\sqrt{3}}{\pi^2}\gamma Z \tag{2.6}$$

where,

$$Z = \frac{L^2}{Rt}\sqrt{1-\mu^2} \tag{2.7}$$

,where γ is a factor to account for the difference between theoretical and experimental results. The classical theoretical value for γ =1 therefore,

$$K_c = \frac{4\sqrt{3}}{\pi^2} Z \tag{2.8}$$

Substituting back into equation (2.5) and putting η_p=1 for elastic buckling, an expression for classical elastic buckling is obtained (Baker et al.,1972):

$$\sigma_{cr} = \frac{E}{\sqrt{3\left(1-\mu^2\right)}}\left(\frac{t}{R}\right) \tag{2.9}$$

This formula coincides with one for non-symmetric buckling which occurs due to initial imperfections that is unintentional deviation from the assumed initial state of the structure. σ_{cr} is independent of cylindrical length. Real imperfect axially compressed shells buckle at a stress significantly below that given by the linear theory. Classical solutions show the linear meridional bending half wavelength of a buckle as (Timoshenko, 1936):

$$\lambda_{cr} = \frac{\pi\sqrt{\frac{R}{t}}}{\sqrt[4]{3(1-\mu^2)}} \tag{2.10}$$

2.4.3 Un-stiffened Cylindrical shells under shear or torsion

A torque (T) is assumed to produce a uniform shear stress around the circumference, while a shear force (V) is assumed to produce a shear stress distribution which varies harmonically (ECCS, 1988).

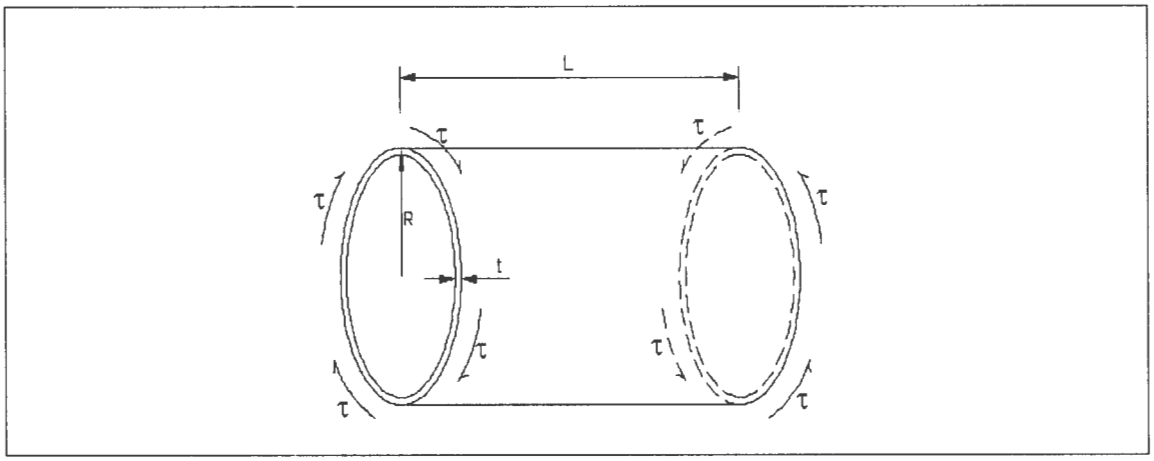

Fig. 2. 5 Un-stiffened cylindrical shell under torsion.

Baker suggests that for a circular cylinder of moderate length, the buckling stress is given by (ECCS, 1988):

$$\frac{\tau_{cr}}{\eta_p} = C_s \frac{E}{Z^{\frac{1}{4}}}\left(\frac{t}{R}\right) \tag{2.11}$$

,where C_s is a buckling stress coefficient obtained in Appendix C. The classical theoretical value for C_s=1 and for elastic buckling, the plasticity correction term η_p=1. Therefore an expression for classical elastic buckling is given by:

$$\tau_{cr} = 0.735 \frac{E}{Z^{\frac{1}{4}}} \left(\frac{t}{R} \right) \tag{2.12}$$

2.4.4 Un-stiffened Cylindrical shells under external pressure

For a simply supported cylindrical shell subjected to a uniform external pressure of p_o, the buckling stress in the circumferential direction is given by (Baker et al.,1972):

$$\frac{\sigma_{cr}}{\eta_p} = K_p \frac{\pi^2 E}{12\left(1-\mu^2\right)} \left(\frac{t}{L} \right)^2 \tag{2.13}$$

,where K_p is the buckling coefficient obtained from graphs in Appendix C. The theoretical coefficient for lateral and axial pressure is given by :

$$K_p = 1.04\sqrt{Z} \tag{2.14}$$

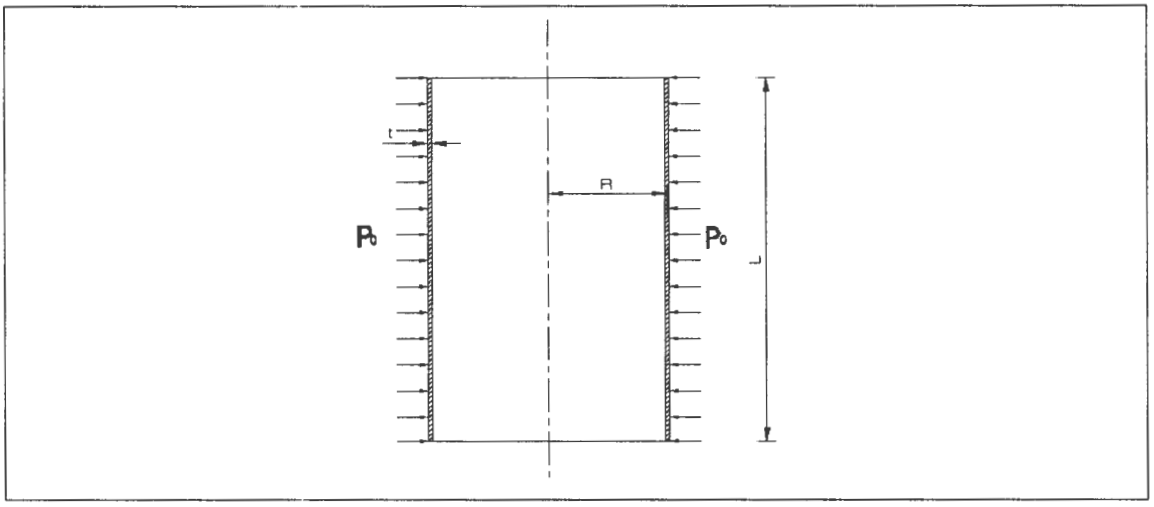

Fig. 2. 6 Un-stiffened cylindrical shell under external pressure.

The critical pressure in turn is given by (Baker et al.,1972):

$$p_{cr} = \frac{\sigma_{cr} t}{R} \tag{2.15}$$

2.5 Elastic stability of un-stiffened conical shells

2.5.1 Introduction

The equivalent cylinder approach is used to determine the buckling stress for a right circular cone subjected to axial compression, shear or torsion and lateral and axial external pressure.

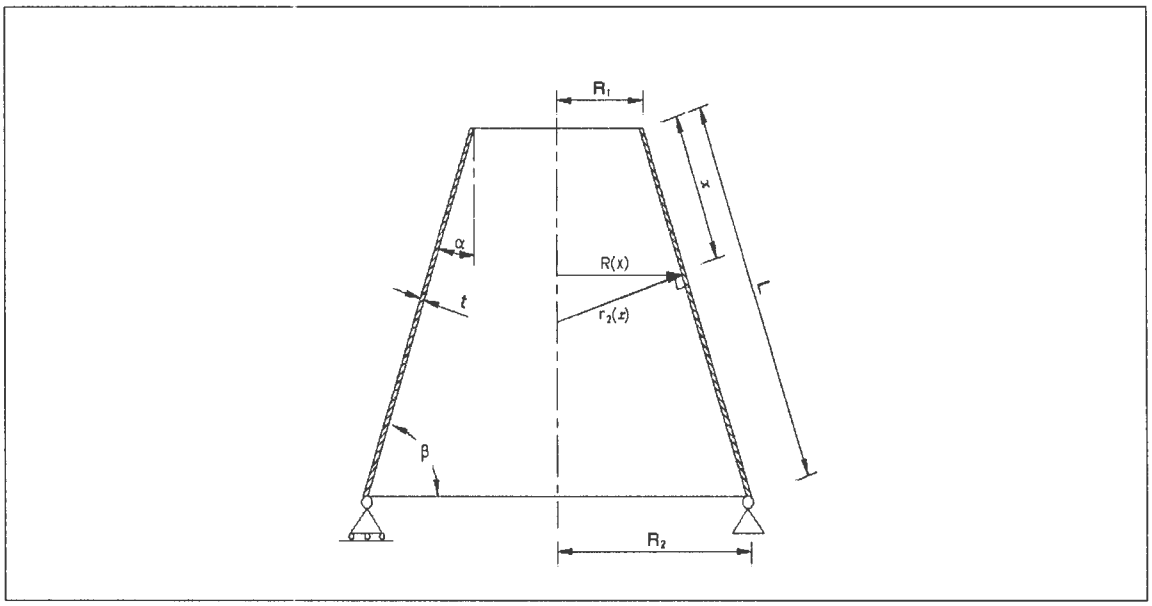

Fig. 2. 7 Un-stiffened conical shell geometry and notation.

By reference to Fig. 2.7, the equivalent radius R_e (local principal radius of curvature) for meridional compression is given by (ECCS,1988):

$$R_e = \frac{R(x)}{\cos\alpha} \tag{2.16}$$

, where x is adopted as a distance coordinate along the straight meridian, R (x) is radius of cone at any point and α is angle between axis of rotation of shell and its meridian.

R_e for circumferential compression is given by (Baker et al.,1972):

$$R_e = \frac{R_1 + R_2}{2\cos\alpha} \tag{2.17a}$$

The radius for calculating elastic critical shear stress is given by (ECCS, 1988):

$$R_e = \left(1 + \sqrt{\frac{R_1 + R_2}{2R_1}} - \sqrt{\frac{2R_1}{R_1 + R_2}}\right) R_1 \cos\alpha \tag{2.17b}$$

2.5.2 Un-stiffened conical shell under axial compression

The buckling stress of circular cone subjected to axial compression may be obtained from the formula (Baker et al.,1972):

$$\frac{\sigma_{cr}(x)}{\eta_p} = \gamma \frac{E}{\sqrt{3\left(1-\mu^2\right)}}\left(\frac{t}{R(x)}\right)\cos\alpha \tag{2.18}$$

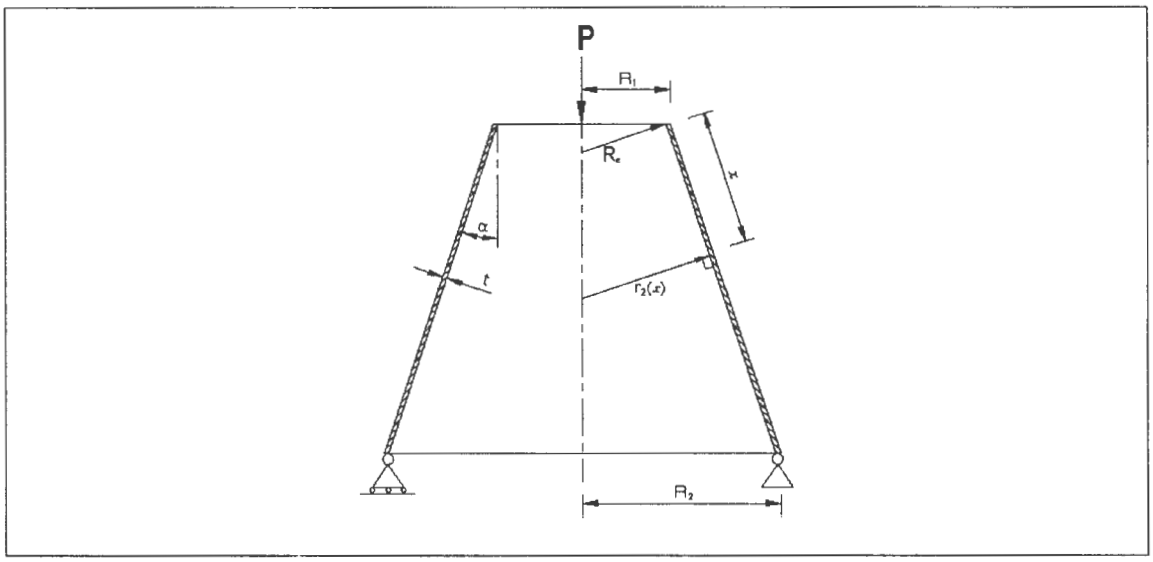

Fig. 2. 8 Un-stiffened conical shell under axial compression.

Since the minimum is sought, the critical stress at the small radius end must be considered i.e $\sigma_{cr}= \sigma_{cr}(x=0)$ and $R(x)=R_1$ hence theoretical elastic buckling stress simplifies to:

$$\sigma_{cr} = \frac{E}{\sqrt{3\left(1-\mu^2\right)}}\left(\frac{t}{R_1}\right)\cos\alpha \tag{2.19}$$

, since $\gamma=1$ and $\eta_p=1$. Once the σ_{cr} is known the total compressive load (P_{cr}) can be obtained from the equation (Baker et al.,1972) :

$$P_{cr} = 2\pi R_1 \sigma_{cr} t \cos^2\alpha \tag{2.20}$$

2.5.3 Un-stiffened conical shell under shear or torsion

Buckling stress for a right circular cone subjected to torsion is obtained from equation (Baker et al.,1972):

$$\frac{\tau_{cr}}{\eta_p} = C_s \frac{E}{Z^{\frac{1}{4}}} \left(\frac{t}{R_e}\right) \left(\frac{R_e}{R_1}\right)^2 \tag{2.21}$$

,which can be simplified to:

$$\frac{\tau_{cr}}{\eta_p} = C_s \frac{E}{Z^{\frac{1}{4}}} \left(\frac{t}{R_1 \cos\alpha}\right) R_e \tag{2.22}$$

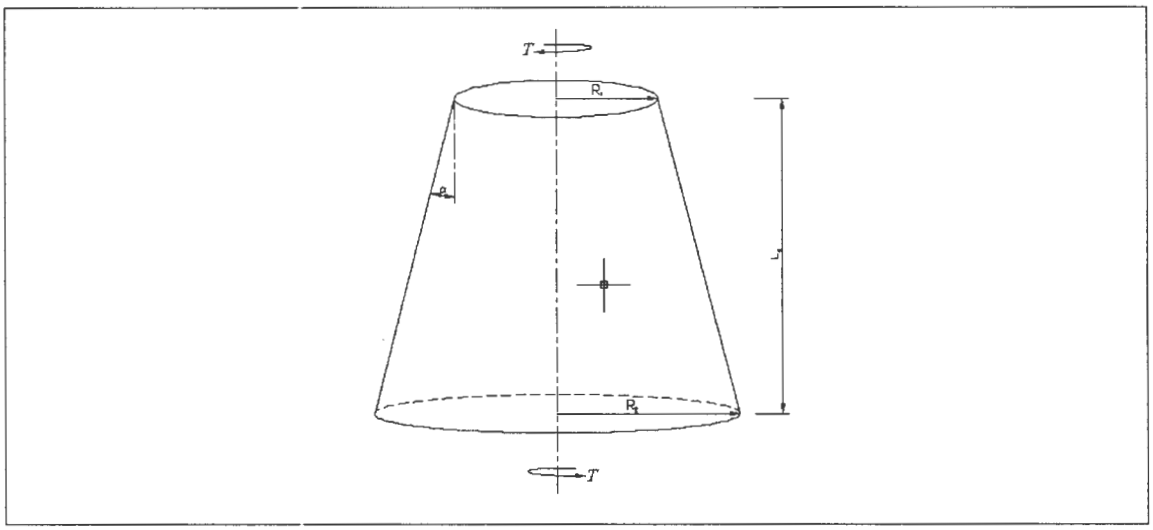

Fig. 2. 9 Un-stiffened conical shell under torsion

This equation is only valid for:

$Z > 100$ for simply supported edges and clamped edges,

$\alpha > 60^o$

, where C_s is a buckling stress coefficient obtained from graph in Appendix C. It follows that critical torque (T_{cr}) (Baker et al.,1972) :

$$T_{cr} = 2\pi R_1^2 \tau_{cr} t \tag{2.23}$$

2.5.4 Un-stiffened conical shell under lateral and external radial pressure

For a conical shell subjected to both lateral and axial uniform external radial pressure (p_o), circumferential critical buckling membrane stress (Baker et al.,1972):

$$\frac{\sigma_{cr}}{\eta_p} = K_p \frac{\pi^2 E}{12\left(1-\mu^2\right)} \left(\frac{t}{L}\right)^2 \frac{R_2}{R_e \cos\alpha} \tag{2.24}$$

K_p is a buckling-stress coefficient obtained from graphs in Appendix C where Z is given by:

$$Z = \frac{L^2}{R_e t}\sqrt{1-\mu^2} \tag{2.25}$$

R_e is given by:

$$R_e = \frac{R_1 + R_2}{2\cos\alpha} \tag{2.26}$$

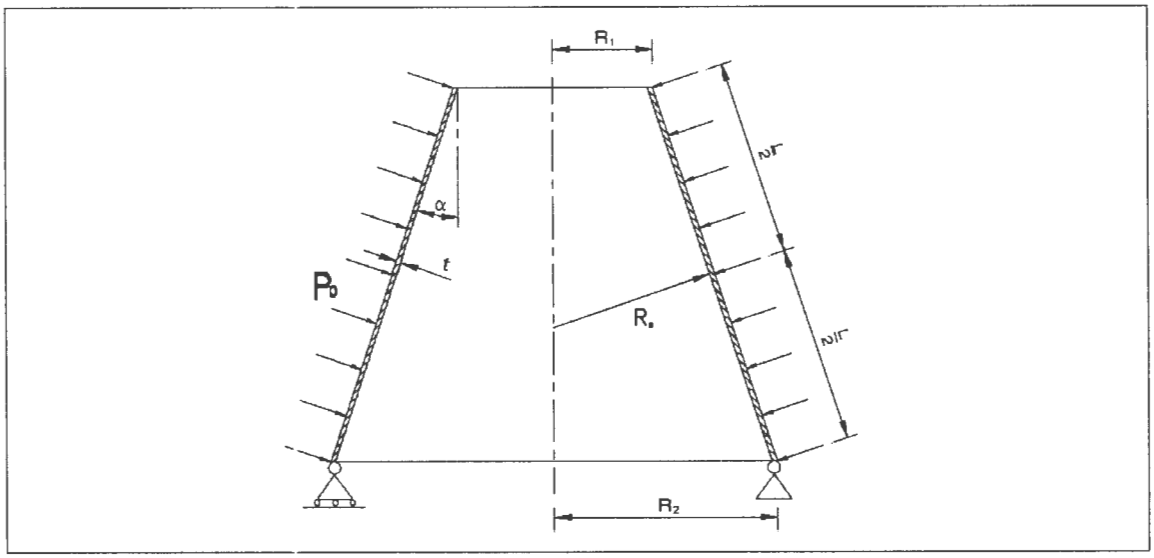

Fig. 2. 10 Un-stiffened conical shell under external pressure

The pressure (p_{cr}) for complete buckling of the shell i.e when buckles are formed right round the cone is obtained from the formula (Baker et al.,1972):

$$p_{cr} = \frac{\sigma_{cr} t}{R_2}\cos\alpha \tag{2.27}$$

2.6 Elastic stability of un-stiffened cylindrical panels

2.6.1 Introduction

Elastic buckling equations for cylindrical panels which are simple supported at the ends are given for different load cases.

2.6.2 Cylindrical panels subjected to axial compression

The buckling stress for unpressurised curved panels subject to axial compression is given by (Baker et al.,1972):

$$\frac{\sigma_{cr}}{\eta_p} = K_c \frac{\pi^2 E}{12(1-\mu^2)}\left(\frac{t}{s}\right)^2 \tag{2.28}$$

, where K_c is buckling stress coefficient given by graph in Appendix C.

2.6.3 Cylindrical panels subjected to shear

The buckling stress for unpressurised rectangular curved plates subjected to shear is given by (Baker, Kovalevsky and Rish, 1972):

$$\frac{\sigma_{cr}}{\eta_p} = K_s \frac{\pi^2 E}{12(1-\mu^2)}\left(\frac{t}{s}\right)^2 \tag{2.29}$$

, in which the buckling stress coefficient K_s is given in Appendix C. Also, Z is calculated as follows:

$$Z = \frac{L}{Rt}\sqrt{1-\mu^2} \tag{2.30}$$

2.6.4 Cylindrical panels subjected to bending

The buckling stress for curved cylindrical panel subjected to bending is given by the equation (Baker et al.,1972) :

$$\frac{\sigma_{cr}}{\eta_p} = K_b \frac{\pi^2 E}{12(1-\mu^2)}\left(\frac{t}{s}\right)^2 \tag{2.31}$$

At low values of the curvature parameter Z, the buckling coefficient for a long curved plate should approach that for a long flat plate in bending and at high values of Z it should approach that for a long cylinder in bending. These two extremes are plotted in Appendix C as the buckling coefficient to be used.

2.7 Theory of stiffened shell stability

2.7.1 Introduction

A brief discussion of failure modes is presented here.

Stiffened shells are shells that consist of a thin metal sheet stiffened by either frames (circumferential elements) or stringers (longitudinal stiffening elements) or both (Baker, Kovalevsky and Rish, 1972). Practically for steel shells, the stiffener is attached to the shell by continuous weld.

The buckling equations given in the preceding discussion are based on the assumption that the stiffeners are uniformly distributed along the circumference or meridian of a shell. Tests results have revealed that simple support edge conditions are reasonably accurate for prediction of the buckling load of a shell. Consequently, the methods of analysis given are based on the assumption of simply supported and some additional assumptions which will be specified later (ECCS, 1988). Also, loads shall be applied to the shell-stiffener structure in such a manner that its cross-sections remain plane before buckling.

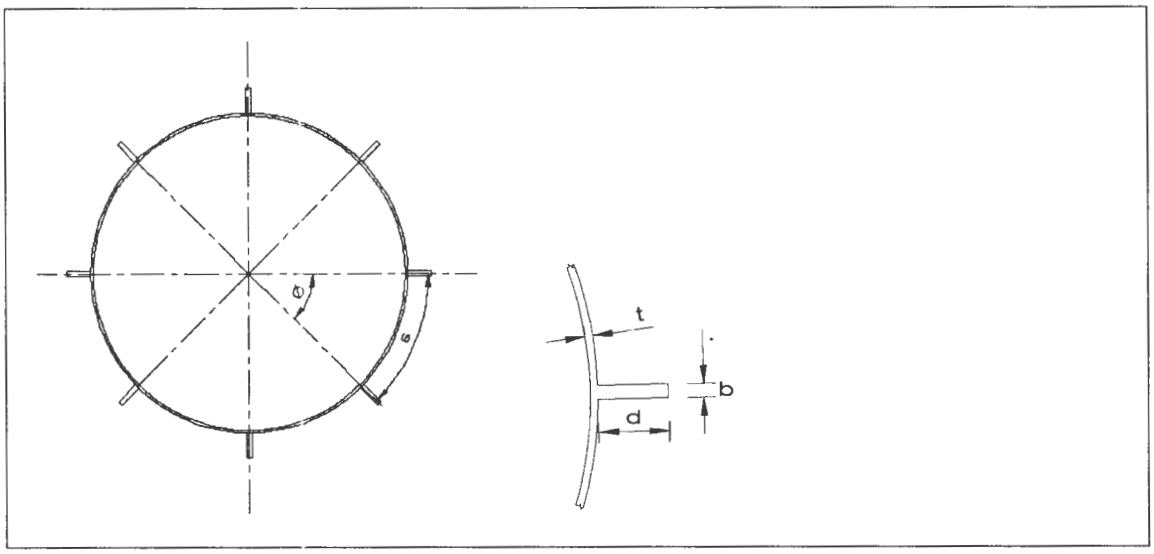

Fig. 2. 11 Stiffened cylinders and stiffener geometry

2.7.2 Types of Stiffeners

- *Stringer stiffener:* a local stiffening member that follows the meridian of the shell, representing a generator of the shell of revolution. It enhances buckling strength and assist with introduction of local loads (EC3, 2004).

- *Ring stiffeners*: a local stiffening member that passes around the circumference of the shell of revolution at a given point on the meridian. It is provided to increase the stability or to introduce axisymmetric local loads acting in the plane of the ring by a state of axisymmetric normal forces. It is assumed to have stiffening effect in the meridional plane of shell of revolution (EC3, 2004). The stiffening rings may either be external or internal and they should extend around the full circumference.

2.7.3 Buckling Modes of failures

Stringer and ring stiffened shells of revolutions are prone generally to distinct modes of instability, namely: material failure, buckling between stiffeners and general instability failure.

Stringer stiffened shells

- *Material Failure*: Material failure occurs as a result of applied stress exceeding the material allowable stress. Membrane theory can be used to obtain stresses in shells due to various loading conditions (Baker et al.,1972).

- *Local shell panel instability*: is characterised by shell panel between stiffeners buckling locally. The panel takes shape of one circumferential half wave with nodal lines along the shell stiffener junction (Spagnoli, 2001).

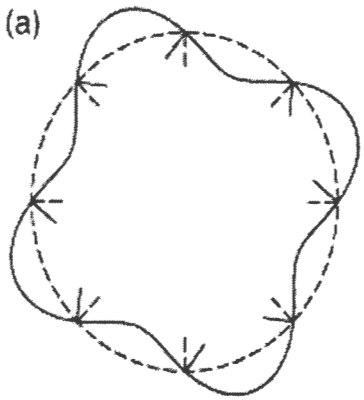

Fig. 2. 12 Circumferential profile of a shell under local shell panel buckling mode

- *Local stiffener buckling*: is characterised by flexural and torsional buckling of stiffeners (Spagnoli, 2001). Crippling of stiffener is a local instability failure of the elements of the stringers and is defined as any type of failure in which the cross sections of the stringers are distorted in their own plane but not translated or rotated (Baker, Kovalevsky and Rish, 1972). This peculiar behaviour is typical in stringers having wide, thin flanges. Crippling stress can be determined using methods of analysis of columns.

  Torsional buckling occurs when the cross section of the stringer rotates but does not distort or translate in its own plane (Baker, Kovalevsky and Rish, 1972). Figure below illustrates some typical torsional modes of instability.

- *Global stiffened panel buckling*: This mode considers overall buckling of the shell stiffener combination. Collapse takes place in a manner so as to destroy the load carrying properties of both the sheet and stringers (Baker, Kovalevsky and Rish, 1972). This failure mode is characterised by circumferential buckling wavelengths which are longer in comparison with stiffener spacing (Spagnoli, 2001).

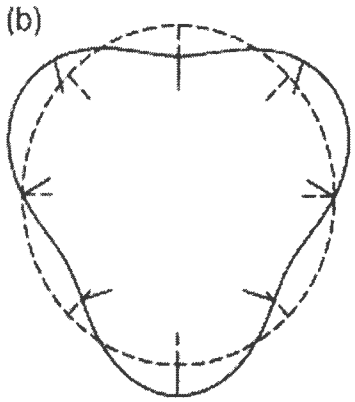

Fig. 2. 13 Circumferential profile of a shell under global stiffened panel buckling mode

Ring stiffened shells

A shell structure stiffened circumferentially and subjected to lateral and external pressure may fail in three distinct ways:

- *Material failure:* As with meridionally stiffened shells above, ring stiffened shells also exhibit this failure mode. The actual stresses in the shell must be checked against material's allowable stresses. The compressive stress in the circumferential stiffener must be compared with the local buckling of that circumferential stiffener (Baker, Kovalevsky and Rish, 1972).

- *Buckling between stiffeners:* This failure mode is typically associated with shells having relatively heavy stiffeners. The sheet buckles between the ring stiffeners while the stiffeners themselves remain undistorted in cross section. The buckling stress for this failure mode can obtained by calculating the buckling strength of unstiffened shell of length equal to the stiffener spacing.

- *General instability:* Occurs when the shell-stiffener combination buckles when a certain critical load is attained. In this buckling mode, also known as overall instability, the stiffeners lose their circularity (ECCS, 1988).

2.8 Elastic stability of stiffened cylindrical shells

2.8.1 Introduction

Baker suggested two possible approaches on the analysis of stiffened shells, these are:

- If stiffeners are widely spaced, the whole construction can be treated as a three dimensional space frame with the plate between distributing and transferring loads to the frame.
- Orthotropic shell approach where the stiffened section can be replaced with an equivalent monocoque section (Baker, Kovalevsky and Rish, 1972). However, Andrianov argued from experimental results that the later mentioned approach provides excessive values of buckling load.

2.8.2 Stringer stiffened cylindrical shells under axial compression

The region in which either shell or stringer buckling mode prevails can be evaluated by calculating the theoretical buckling stress for shell and stringer treated as isolated components (Spagnoli, 2001).

The buckling load of a stiffener can be evaluated by modelling it as a flat plate with longitudinal free side. Stringers are vulnerable to two typical failure modes which are crippling and torsional instability. Crippling is a local instability failure in which the cross sections of the stringers are distorted in their own plane but not translated or rotated (Baker, Kovalevsky and Rish, 1972). Crippling is generally associated with wide and thin stringers. Torsional instability occurs when the cross section of the stringer rotates but does not distort or translate in its own plane (Baker, Kovalevsky and Rish, 1972). The classical buckling stress for a compressed long flat plate with simply supported loaded sides is given by (Spagnoli, 2001):

$$\frac{\sigma_{cr}}{\eta_p} = K_{ST} \frac{\pi^2 E}{12(1-\mu^2)} \left(\frac{b}{d}\right)^2 \tag{2.32}$$

The stringer buckling coefficient K_{ST} is equal to 1,28 .

The local shell buckling mode stress may be calculated by idealising the shell between consecutive stringers as a cylindrical panel. For a curved cylindrical panel subjected to axial compression buckling stress is given by (Baker, Kovalevsky and Rish, 1972):

$$\frac{\sigma_{cr}}{\eta_p} = K_c \frac{\pi^2 E}{12(1-\mu^2)} \left(\frac{t}{b}\right)^2 \tag{2.33}$$

Overall buckling of shell and stiffener can be assessed on the basis of orthotropic shell theory using the following equation (Spagnoli and Chryssanthopoulos, 1999):

$$\sigma_{cr} = \frac{1}{t_{se}}\left(\frac{L}{m\pi}\right)^2\left(A_{33} + \frac{A_{12}A_{23} - A_{12}A_{22}}{A_{11}A_{22} - A_{12}^2}A_{13} + \frac{A_{12}A_{13} - A_{11}A_{23}}{A_{11}A_{22} - A_{12}^2}A_{23}\right) \tag{2.34}$$

,where the coefficients are based on the theory of smeared stringer-stiffened cylinders:

$$A_{11} = K_x\left(\frac{m\pi}{L}\right)^2 + K_{x\theta}\left(\frac{n}{r_2}\right)^2 \tag{2.35}$$

$$A_{22} = K_\theta\left(\frac{n}{r_2}\right)^2 + K_{x\theta}\left(\frac{m\pi}{L}\right)^2 \tag{2.36}$$

$$A_{33} = D_x\left(\frac{m\pi}{L}\right)^4 + \overline{D}_{x\theta}\left(\frac{n}{r_2}\right)^2\left(\frac{m\pi}{L}\right)^2 + D_\theta\left(\frac{n}{r_2}\right)^4 + \frac{K_\theta}{r_2^2} \tag{2.37}$$

$$A_{12} = \left(K_\nu + K_{x\theta}\right)\left(\frac{n}{r_2}\right)\left(\frac{m\pi}{L}\right) \tag{2.38}$$

$$A_{23} = \left(\frac{K_\theta}{r_2}\right)\left(\frac{n}{r_2}\right) \tag{2.39}$$

$$A_{13} = \frac{K_\nu}{r_2}\left(\frac{m\pi}{L}\right) + C_x\left(\frac{m\pi}{L}\right)^3 \tag{2.40}$$

and the rigidity coefficients are given by:

$$K_x = K\left(\frac{\overline{b_e}}{b_e}\right) + \frac{EA_s}{b_e} \tag{2.41}$$

$$K_\nu = \nu K \quad \text{and} \quad K_\theta = K \tag{2.42}$$

$$K_{x\theta} = \frac{Gt}{2}\left(\frac{\overline{b_e}}{b_e} + 1\right) \tag{2.43}$$

$$D_x = D\left(\frac{\overline{b_e}}{b_e}\right) + \frac{EI_s}{b_e} + \frac{EA_s e_s^2}{b_e} \tag{2.44}$$

$$D_\nu = \nu D \quad \text{and} \quad D_\theta = D \tag{2.45}$$

$$D_{x\theta} = (1-\nu)D\left(\frac{\overline{b_e}}{b_e} + 1\right) + \frac{GC_s}{2b_e} \tag{2.46}$$

$$\overline{D}_{x\theta} = 2\left(D_\nu - D_{x\theta}\right) \text{ and } C_x = \frac{EA_s e_s}{b_e} \tag{2.47}$$

$$e_s = \frac{(t+d)}{2} \; ; \; D = \frac{Et^3}{12(1-\nu^2)} ; C_s = \frac{db^3}{3} ; b_e = \frac{2\pi r_2}{N} \qquad (2.48\text{-}2.51)$$

The critical buckling stress of the shell panel between stringers can be predicted by formulation which is based on Koiter's work on buckling of cylindrical panels. Koiter and Timoshenko's theoretical critical buckling stress for cylindrical panels is calculated as a function of the total curvature parameter (η) of the panel, namely:

$$\sigma_{cr} = \frac{E\pi^2}{3(1-\nu^2)}\left(\frac{t}{s}\right)^2 (1-\eta^4) \qquad \text{valid for } \eta \leq 1 \qquad (2.52)$$

where:

$$\eta = \frac{1}{2\pi}\sqrt[4]{12(1-\nu^{2)}}\,\frac{s}{\sqrt{Rt}} \qquad (2.53)$$

While for wide panels ($\eta \rangle 1$) the buckling stress is that of an un-stiffened cylinder under axial compression and is approximated by the following formula:

$$\sigma_{cr} = 0.605\,\frac{Et}{R} \qquad \text{for } \eta \rangle 1 \qquad (2.54)$$

Koiter's curvature parameter is proportional to the one considered by the ECCS recommendations. The ECCS suggests that the local shell buckling stress depends on the curvature of the shell (ξ), the L/s ratio and the torsion stiffness of the stringers amongst other parameters. The curvature parameter is given by:

$$\xi(x) = \frac{s}{\sqrt{Rt}} \qquad (2.55)$$

In accordance to the ECCS recommendations (ECCS, 1988), the extreme conditions corresponding to a flat plate (very narrow panel) and a complete un-stiffened shell (wide panel) are considered. The elastic critical stress (σ_{cr}) for a perfect shell panel between stiffeners may be taken as equal to the higher of the elastic critical stresses for a perfect complete cylinder, which is:

$$\sigma_{cr}(x) = \frac{E}{\sqrt{3(1-\mu^2)}}\left(\frac{t}{R}\right) \qquad (2.56)$$

,for $\xi(x) \geq 2.44$ (un-stiffened shell) (ECCS, 1988) and,

$$\sigma_{cr}(x) = \frac{4\pi^2 E}{12(1-\mu^2)}\left(\frac{t}{s}\right)^2 \qquad (2.57)$$

,for $\xi(x) < 2.44$ (Flat plate) (ECCS, 1988).

However, for the behaviour between flat plate and un-stiffened shell the ECCS admits that an accurate theory yields a slightly higher buckling limit for a curved panel than the one given by the previous equations.

2.8.3 Ring stiffened cylindrical shells under external pressure

The various buckling modes which are to be considered in the design of externally pressurised stiffened cylinders are:

- Buckling between stiffeners
- Buckling between end diaphragms or heavy stiffeners (general instability)
- Tripping or local buckling of stiffeners (ECCS, 1988).

Local buckling of stiffeners

The geometric proportions of ring stiffeners must be such that local buckling of rings does not occur.

In order to ensure that the initially out of round stiffening rings have adequate strength, the maximum stress (both direct and bending) should not exceed the yield point of the stiffener material.

The circumferential direct stress in a stiffener is:

$$\sigma_{rd} = \frac{pR^2\left(1-\frac{\mu}{2}\right)}{R_f\left(t+\frac{A_r\frac{R^2}{R_r^2}}{b+2L\frac{\eta}{\delta}}\right)} \qquad (2.58)$$

Where,
p –pressure

A_r –area of cross section of ring stiffener

R_f -radius to the outer flange of stiffener

R_r –radius from centre of cylinder to centroid of stiffener

s- stiffener spacing

$$\eta = \frac{ch\ \delta - \cos\ \delta}{sh\ \delta + \sin\ \delta} \qquad (2.59)$$

$$\delta = L\left(\frac{3\left(1-\mu^2\right)}{R^2 t^2}\right)^{\frac{1}{4}} \tag{2.60}$$

Buckling between stiffeners

The elastic buckling stress of the shell is calculated from equation 2.5 with L being taken as the distance between stiffening rings i.e the unsupported length of the shell (ECCS, 1988).

Overall instability

A first approximation to the overall external buckling pressure (p_{cr}), causing perfect circular stiffeners as well as the associated perfect circular cylindrical shell to deform together into n circumferential waves is given by Brayant formula (ECCS, 1988):

$$p_{cr} = E\frac{t}{R}\psi + (n^2-1)\frac{E_r I}{R^3 s} \tag{2.61}$$

Where

$$\psi = \frac{1}{\left[n^2 - 1 + \frac{1}{2}\left(\frac{\pi R}{L}\right)^2\right]\left[\left(\frac{nL}{\pi R}\right)^2 + 1\right]^2} \tag{2.62}$$

2.9 Stiffened Conical shells

2.9.1 Introduction

Prediction of buckling strength is achieved by treating individual buckling modes separately. Prevalence of different modes can be evaluated by computation of theoretical buckling stress of shell isolated components (Spagnoli, 2001).

2.9.2 Stringer stiffened conical shells under axial compression

For shell panel instability, the critical buckling stress of the conical shell panel between stringers can be predicted by theory of cylindrical panels (Koiter 1956). The critical stress of cylindrical panel can be obtained by assuming simple support boundary conditions along shell-stringer junction provided that the stringer constrains the radial displacement along that junction. Panel curvature parameter (ξ) is used to categorise panels between the two extremes, narrow panel (flat plate) and wide panel

(unstiffened shell). Thus, the proposed critical elastic stresses for local buckling are given by:

$$\sigma_{cr}(x) = \frac{E}{\sqrt{3(1-\mu^2)}}\left(\frac{t}{r_2(x)}\right) \tag{2.63}$$

,for $\xi(x) \geq \frac{2.44}{\sqrt{\cos\beta}}$ (unstiffened shell) (Spagnoli and Chryssanthopoulos, 1999) and,

$$\sigma_{cr}(x) = \frac{4\pi^2 E}{12(1-\mu^2)}\left(\frac{t}{s(x)}\right)^2 \tag{2.64}$$

,for $\xi(x) < \frac{2.44}{\sqrt{\cos\beta}}$ (Flat plate) (Spagnoli and Chryssanthopoulos, 1999).

The critical load is estimated by multiplying the axial stress component computed above by the corresponding cross sectional area and since the minimum is sought, the critical stress at the minimum radius must be considered (Spagnoli, 2001):

$$P_{cr} = \sigma_{cr}(2\pi R_1 t + NA_s)\cos\alpha \tag{2.65}$$

Panels falling between the flat plate and unstiffened shell range exhibit higher strength than that obtained by considering unstiffened shell. However this strength increase is neglected in design codes of cylinders hence the same philosophy is adopted for conical shells (Spagnoli and Chryssanthopoulos, 1999).

For global buckling mode, critical elastic stress may be evaluated on the basis of orthotropic shell theory by smearing the stringer stiffness along the shell wall (Spagnoli and Chryssanthopoulos, 1999). The critical stress is obtained by minimizing the following expression with respect to the number of meridional (m) and circumferential waves (n):

$$\sigma_{cr} = \frac{1}{t_{se}}\left(\frac{L}{m\pi}\right)^2\left(A_{33} + \frac{A_{12}A_{23} - A_{12}A_{22}}{A_{11}A_{22} - A_{12}^2}A_{13} + \frac{A_{12}A_{13} - A_{11}A_{23}}{A_{11}A_{22} - A_{12}^2}A_{23}\right) \tag{2.66}$$

,where the coefficients are based on the theory of smeared stringer-stiffened cylinders in equation 2.35 to 2.51

2.10 Stress distribution on Stiffened Shells

2.10.1 Comparison between the behaviour of stiffened and unstiffened shells

In order to understand the difference between behaviour of unstiffened and stiffened conical shell, El Damatty et al. conducted a numerical investigation on hydrostatically loaded tanks. The study focused on three cases namely unstiffened tank, tank stiffened longitudinally with pinned boundary conditions at the bottom edge and tank stiffened longitudinally with free boundary conditions at the bottom edge. Results revealed that high stress concentrations in the form of membrane axial meridional compressive stresses and hoop tensile stresses occur at the bottom part of the cone. Distribution of the meridional displacement is presented in the Fig. 2.14 below. It is clear that larger displacement values are shown for the free stiffened case compared to the pin stiffened one. This means that the stiffeners provide less bending resistance.

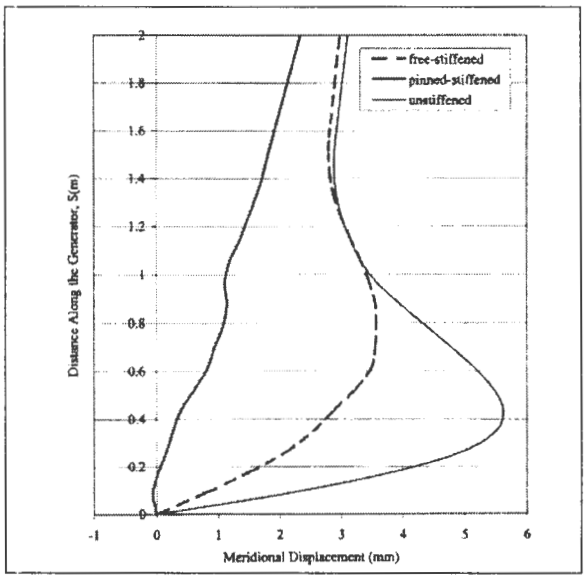

Fig. 2. 14 Meridional displacement along a generator of a stiffened and un-stiffened tank

From the same analyses, stress components are presented in Fig. 2.15 below, for both free and pinned stiffener cases with angles θ=11.25°, 33.75°,56.25° and 78.75° corresponding to stiffener locations.

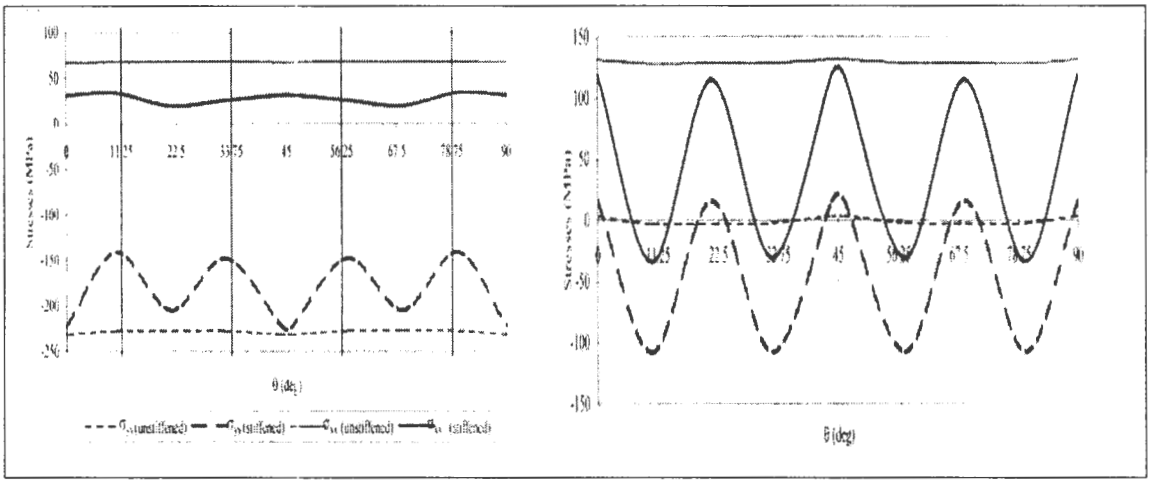

Fig. 2. 15 Stress distribution around the circumference of un-stiffened and pinned stiffened tanks (a) internal fibers (b) external fibers

It is evident from the results that by adding stiffeners, the values of axial meridional stresses in between stiffeners have decreased slightly and the same stresses at the stiffener locations have increased slightly. The total axial force for the pinned stiffened case would be less than the one associated with the unstiffened tank. The difference in axial forces is transferred to the stiffeners. It should be noticed that the maximum stress value spreads along the whole circumference for the case of the unstiffened tank, while it is localized between stiffener locations for the stiffened tanks. This explains the increase in the capacity of the tank when stiffeners are used. In general, the presence of stiffeners leads to a decrease in the mid-surface hoop stresses especially at the stiffener locations. It can also be concluded that a change of curvature occurs along the circumference of the stiffened tank leading to concave and convex circumferential bending in between and at the stiffener locations, respectively.

2.10.2 Comparison between limit load capacity of stiffened and unstiffened shells

A limit load capacity comparison was performed by El Damatty et al to examine the advantage of constructing conical tanks from stiffened panels, versus using unstiffened shells having the same volume of steel. The results clearly showed that adding stiffeners rather than increasing the shell thickness would provide major enhancement in the buckling capacity of this type of water structure. It was also noted that this increase is more pronounced if the stiffeners are anchored at their bottom edge (El Damatty et al.,2001).

Sridharan and Zeggane in another separate investigation argued that, the stiffening elements do not only enhance the buckling resistance but also reduce the imperfection-sensitivity of shells. Because of the resistance offered by the stiffeners to radial movement, local buckling modes whose nodal lines do not coincide with the location of the stiffeners are simply eliminated (Sridhran and Zeggane, 2001).

2.11 Effects of Parametric variation of stiffened shells

Shell geometric parameters strongly influence the load capacity and failure mode.

2.11.1 Load carrying capacity

Extensive studies of stiffened shells are inclined generally to the consensus that longitudinal and ring stiffeners increase the load carrying capacity of a shell structure.

Among the few investigations on the case of stringer stiffened cylinders in bending is one carried out by Chen et al using numerical method. From this study, the moment versus curvature response of the cylinders clearly shows that ultimate moment capacity of shells failing in the shell mode is less than that of shell which fails in the global buckling mode. The moment versus curvature response of cylinders with broad panels is essentially linear up to failure. However, for the case of cylinders with low s/t ratios, the moment versus curvature response departs from linearity at about one half of the ultimate moment and a significant load increase exists between the onset of buckling and the ultimate point (Chen and Elwi, 1996).

Spagnoli and Chryssanthopoulos in their study on the elastic buckling behaviour of widely stiffened conical shells under axial load came to a conclusion that critical load increases as the panel width decreases. Different panel widths were considered by varying the number of stiffeners. Furthermore, their results of the variation of critical load with respect to the tapering angle is in agreement with Seide's theoretical formula for unstiffened cones for wide panels whereas for narrow panels, the critical load decreases roughly in line with plate type response. The buckling strength start to increase after a particular value of number of stiffeners (N) is reached, which is depended on R/t ratio but independent of β. This behaviour is similar to that studied by Koiter for the case of cylindrical panels. This is illustrated in Fig. 2.16:

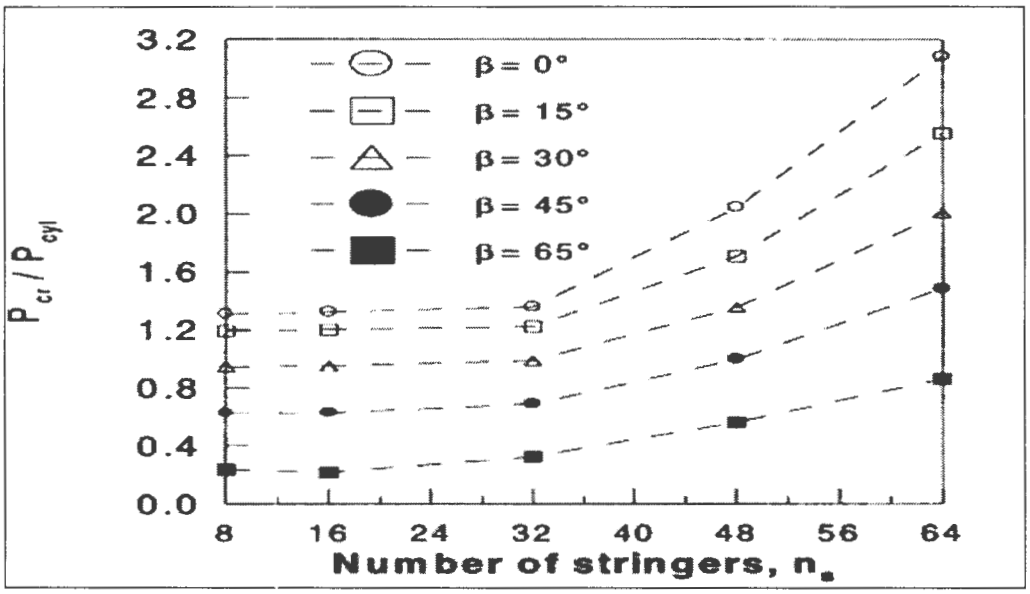

Fig. 2. 16 Variation of critical load with number of stiffeners (R_1/t=200, L/R_1=1, ζ_1=0.3)

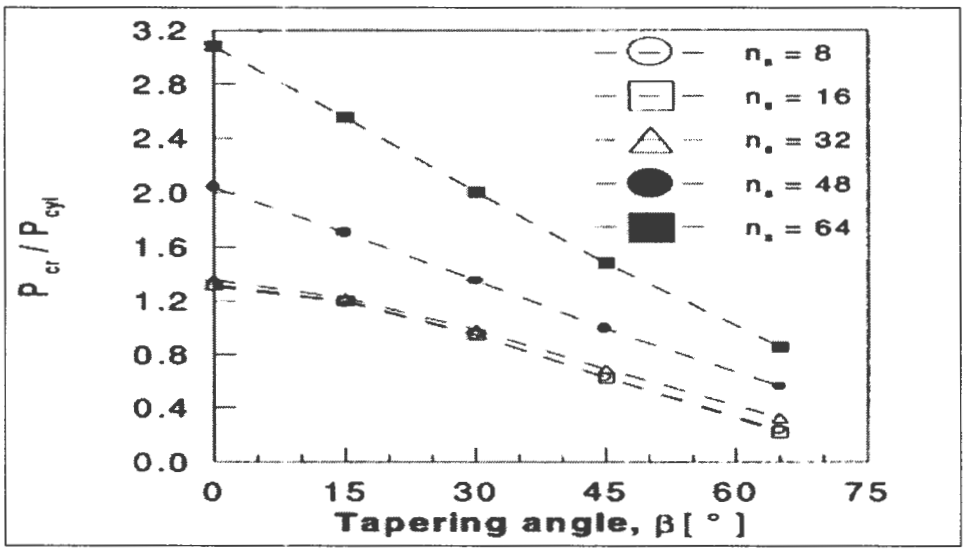

Fig. 2. 17 Variation of critical load with tapering angle (R_1/t=200, L/R_1=1, ζ_1=0.3)

Experimental investigation carried out by Krasovsky and Kostyrko on buckling of stringer cylindrical shells under axial compression, clearly revealed that the option of placing stiffeners outside is better than stiffening the inside skin of the shell (Krasovsky and Kostyrko,2007).

El Damatty et al (Damatty et al., 2001) studied the effect of varying the width of the longitudinal stiffeners on the buckling capacity of conical tanks. The results obtained clearly indicated that the larger the width of stiffener, the higher the value of critical limit load. The trend in these results can be explained by the fact that increasing the

width of the stiffener result in an increase in moment of inertia about a strong axis and consequently bending resistance of the stiffeners would increase. Maximum increase in limit loads can be achieved by choosing large values for the stiffeners' width-to-thickness aspect ratio (b_s/t_s) but should not exceed the limits for local buckling of the stiffeners.

2.11.2 Buckling modes

There have only been few investigations on the buckling behaviour of stiffened shell structures by varying geometrical parameters. Questions about buckling mode change over and prevalence of a particular mode, face a design engineer in bid to optimise a design henceforth a need arise to establish buckling mode change over limits.

A finite element based parametric study of longitudinally stiffened cylinders in bending was conducted by Chen et al. Their results distinguished general failure mode from the shell buckling mode. Results clearly shows that cylinders with broad panels that is a large stiffener spacing to shell thickness ratio or large R/t ratios are more likely to fail in shell buckling. On the other hand, nearly simultaneous failure of stiffeners and shells, which is global buckling mode, was noted for cylinders with low s/t ratios. It was also observed that deformation in the case of shell buckling is relatively smaller than that observed in the global buckling mode case. These differences show that the failure mode depends on R/t ratio reflects the shell stiffness and the s/t ratio is a parameter which reflects support provided by the stiffener (Chen and Elwi, 1996).

Experimental tests on scaled models of stringer and ring stiffened cylindrical shells of the type found in oil instillations were performed by Walker et. al. to provide reliable buckling response data for new design rules of such structures. As a first phase towards obtaining a basis for judging the accuracy of present design rules, the research concentrated on axially applied load although it was noted that the most critical combination of loading for such structures is axial compression together with external pressure. Two quite distinctly different modes of failure were exhibited by stringer stiffened shells, namely local failure and overall buckling. Generally local buckles were associated with number of stiffeners (N) =20 while overall buckling with N=40. The former was associated with appearance of local plastic buckles in the

panels, accompanied by localized rotations in the stiffeners while their common junctions remained straight. The latter was associated with deformations of the panel at stiffener junction in a single wave stretching almost the whole length of the shell. The ring stiffened cylinders of the type studied failed by local deformations close to their ends, both single and multiple bay shells. The unloading path is very steep and it may be supposed that such shells will be imperfection sensitive (Walker,Andronicou and Sridharan, 1981).

Spagnoli carried out numerical investigation on the buckling behaviour of axially compressed conical shells which are stiffened in the meridional direction. Changes of buckling modes were captured by varying stiffener slenderness, number of stiffeners and tapering angle which are the typical design parameters. In the case of sparsely stiffened cones, changeover between local and stringer modes can be obtained by varying h_w/t_w. Results shown in Fig. 2.18 depicts a mode changeover at h_w/t_w= 18 for β=15°, which is close to the change over point predicted by theory. The limit value of h_w/t_w beyond which the stringer mode is dominant, increases as the tapering angle increases. Hence, there is scope for less stringent requirements with respect to stringer buckling in highly tapered cones (Spagnoli, 2001). Also deflection graphs revealed that mode interaction between local shell and stringer modes can be expected, as is shown by the clustering of eigenvalues/eigenmodes.

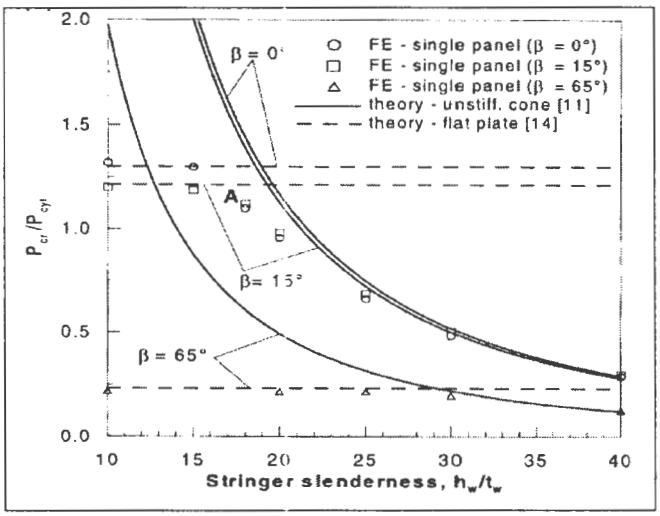

Fig. 2. 18 Local shell and stringer modes critical loads versus β variation (Spagnoli, 2001)

In the same investigation, Spagnoli proved that a changeover between local shell and global modes occurs by varying the number of stiffeners. The changeover between local and global mode at n_s=48 is depicted in Fig.2.19 (Spagnoli, 2001).

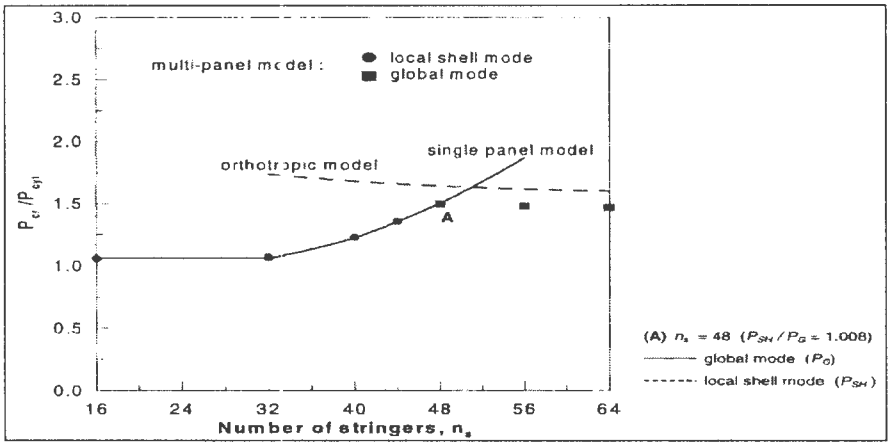

Fig. 2. 19 Local shell and global modes critical loads versus number of stringers variation (Spagnoli, 2001)

Further than that, Spagnoli also argued that a changeover between local shell and global modes can also occur in cones as a result of varying the tapering angle (Spagnoli, 2001). The influence of β on the dominant mode is illustrated in Fig. 2.20.

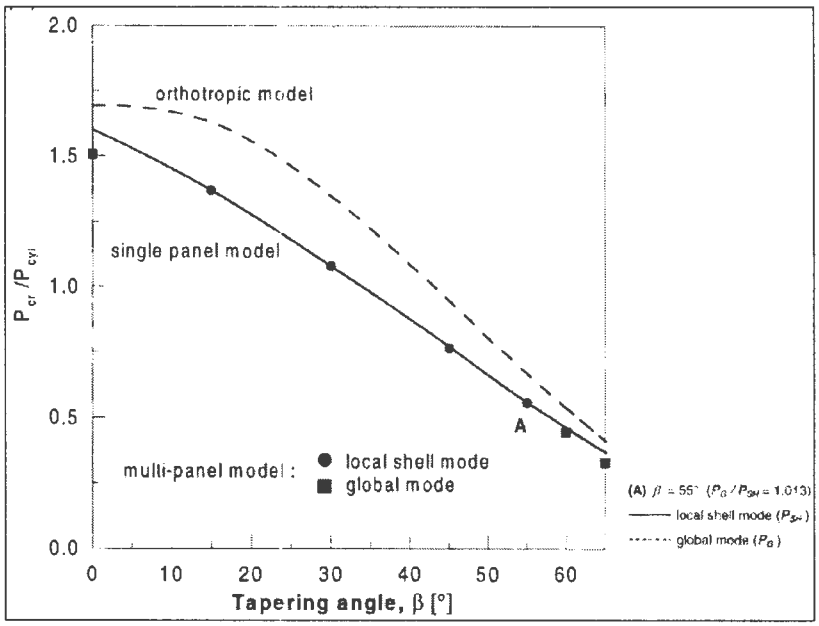

Fig. 2. 20 Local shell and global modes critical loads versus β variation (Spagnoli, 2001)

2.12 Post buckling behaviour

The buckling load is not always the maximum capacity load. There are indeed structures whose load carrying capacity is not exhausted with the appearance of visible buckles. Whether the load carried by the structure can be augmented after buckling or not depends on its post buckling behaviour (Esslinger and Geier, 1975).

The stiffening elements not only enhance the buckling resistance but also reduce the imperfection-sensitivity of the shells. Because of the resistance offered by the stiffeners to radial movement, local buckling modes whose nodal lines do not coincide with the location of the stiffeners are simply eliminated. This has the effect of minimizing the nonlinear modal interactions which are the source of imperfection-sensitivity in un-stiffened shells (Sridharan and Zeggane, 2001).

2.12.1 Post Buckling Behaviour of cylindrical shells

Due to possession of curvature unlike flat plates, cylinders develop membrane restoring forces at bifurcation point besides bending moments. At this instant of buckling, outward deflection causes tensile forces while inward deflection causes compressive forces. These membrane forces in combination with the curvature of the cylinder act in the restoring sense. The curvature of the un-deformed shell pre-dominates the buckling deformation (Esslinger and Geier, 1975).

However, in the post buckling region the radial deflections become so large that they no longer may be neglected in comparison to the curvature of the un-deformed shell. On the contrary to the effect of membrane forces at bifurcation point, the membrane compressive forces in the inward buckles push shell wall in the in ward direction. The membrane forces produced by the buckling process yield radial loads in the inward direction, over the whole circumference. The effect of these swelling radial loads is no longer restoring but on the contrary is detrimental like external pressure. For thin walled shells in the post buckling region the restoring action of the membrane forces decreases, vanishes and finally is reversed. As a result the loads, carried by the cylinder in the post buckling region, are lower that the buckling load (Esslinger and Geier, 1975).

Experimental results obtained to verify the theoretical results inevitably indicated that cylinders buckle at loads which are considerably below that given by classical theory. Experimental results varied as low as 30% of the load given by classical solution and furthermore the large degree of scatter of results was not satisfying researchers (Chajes, 1974).

A remarkable step towards understanding this problem and toward an explanation of the discrepancy between the theoretical and experimental results was achieved by Donnell in 1934 (Chajes, 1974). Donnell realised that it was not sufficient to determine the load at bifurcation but that an investigation of the post buckling behaviour was necessary. He proposed that a non linear finite deflection theory was required. To his now well known small-deflection equations, Donnell added some non linear terms similar to the ones used in formulating nonlinear plate equations and thus arrived at the von Karman-Donnell large displacement shell equations. Donnell was also aware that of the fact that the buckling pattern observed to exist during experimental tests was radically from the one assumed to exist in the classical theory. Classical theory assumed buckling pattern to consist of sinusoidal waves in both axial and circumferential directions contrary to the actual buckle pattern which consists of deep diamond shaped bulges directed primarily toward the centre of curvature (Chajes, 1974).

The first meaningful solution to the problem was obtained by von Karman and Tsien using the same large deflection equation as were used by Donnell. By approximating the lateral deflection with a function that adequately represented the actual buckle pattern of the shell, von Karman and Tsien obtained the first accurate picture of the post buckling behaviour of an axially compressed cylinder (Chajes, 1974). The results obtained are shown on Fig. 2.21.

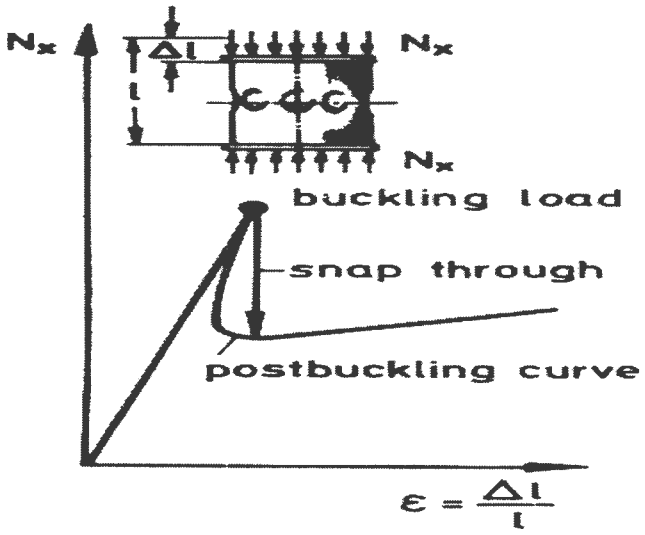

Fig. 2. 21 Buckling and post buckling behaviour of a perfect cylinder

This curve shows that the axial load required to maintain equilibrium drops sharply as critical load is reached and cylinder subsequently bends. Beyond doubt, there exist equilibrium configurations at finite deflections that can be maintained by loads considerably below the critical load. In conclusion, von Karman and Tsien suggested that there was a possibility of a cylinder jumping from the unbuckled state to the adjacent buckled configuration at a load way below the critical load. This can be triggered by even slight disturbance such as vibration of the testing machine.

Later on Donnell and Wan suggested an improvement to the analysis by introduction of initial imperfections. As a consequence of their work, initial imperfections are now generally believed to be the principal reason for the discrepancy between the classical buckling stress and the experimentally observed failure stress.

2.12.2 Post Buckling Behaviour of conical shells

Post buckling behaviour of widely stiffened conical shells under axial compression was studied by Spagnoli and Chryssanthopoulus using a numerical method based parametric study. The parameters considered are number of stiffeners and tapering angle. In general, the results show a well defined limit load followed by an unstable (unloading) initial post buckling path as shown in Fig. 2.22 :

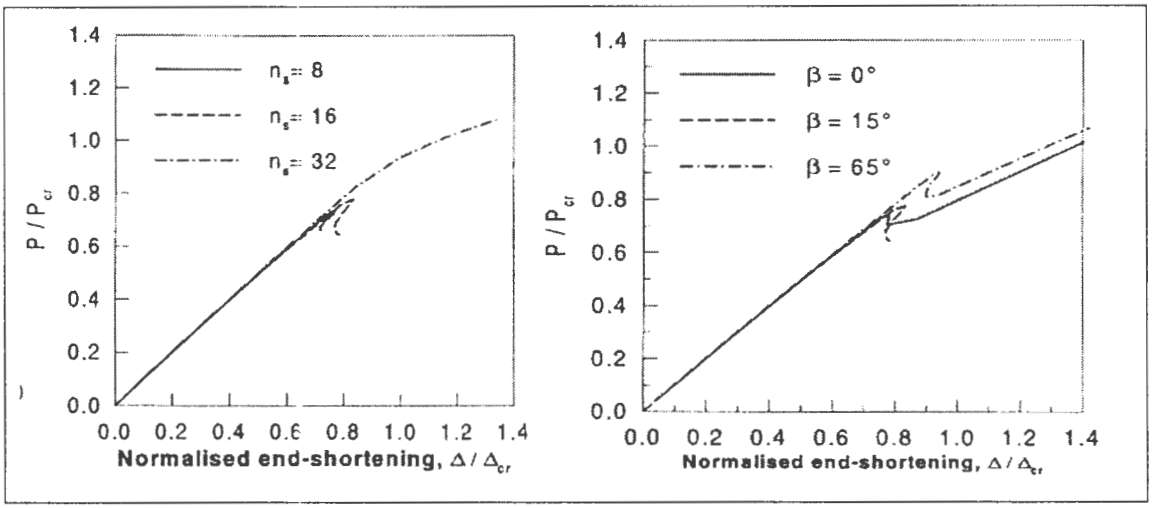

Fig.2.22 Variation of load versus end shortening (R_1/t=200, L/R_1=1, ζ_1=0.3) (a) with number of stringer stiffeners (β=15°) (b) with tapering angle (N=16)

Most importantly, the graph seems to be in strong agreement with the theory of narrow cylindrical panels for a large n_s which shows a stable post buckling path. By comparison, the change over value for the n_s is close to the one obtained by Kioter.

Chapter 3

Statement of Research and Methodology

3.1 Introduction

It is evident from the literature reviewed that there exists a need for a more comprehensive understanding of buckling behavior of stiffened steel shells.

In this chapter the statement of research is introduced with its objectives. The methodology is then discussed.

3.2 Statement and scope of research

For different load configurations, it is required to establish how the elastic buckling load and mode shapes vary on stiffened shells with respect to certain key design parameters. Only cylindrical and conical stiffened shells will be treated in this research because of their relative simplicity and also because they are the commonest shell configurations in structural applications.

In the present investigation, stiffening arrangement characterized by flat bar stiffener (rectangular cross section) welded on the outside surface of the shell is considered in all cases. Different stiffener arrangements are considered for both conical and cylindrical shells which are:

- Longitudinal(stringer) stiffening
- Circumferential(ring) stiffening

This study focuses on the following geometric parameters of stiffened shells:

- the number of stiffeners on the shell (**N**),
- the stiffener-depth to shell-thickness ratio (**d/t**),
- the stiffener depth-to-width(stiffener slenderness) ratio (**d/b**)
- the ratio of radius to shell thickness (**R/t**)

3.3 Research objectives

The main objectives of this research are as follows:

- To assess the effect of varying stiffener parameters on the elastic buckling load of stiffened cylindrical and conical frusta. Also in this research, the advantages of constructing steel containment shells using stiffened panels, versus using un-stiffened shells are verified.

- To establish how varying stiffener and shell geometric parameters influence the mode of failure of stiffened shells. The linear elastic buckling response of stiffened shells is assessed for a wide range of shell and stiffening parameters. As different parameters vary, mode interaction is expected at certain values of the parameter under study. In this case both modes interact very closely and the value of a parameter at that point is also known as the change over point. This is the case where one expects to gain a maximum increase in the critical load, while minimizing the number of stiffeners and the overall weight of the shell structure (Alinia, 2005).

3.4 Methodology

3.4.1 Introduction

The entire parametric study described in this thesis is conducted using numerical methods based on finite element modeling and these results are validated using experimental tests results and theoretical results from analytical formulas.

3.4.2 Finite element modeling

The finite element method is a technique for obtaining approximate solutions to boundary value problems. In any finite element analysis, the solution of the mathematical model of a structure is numerically approximated using finite element procedures (Chapelle and Bathe, 2003). The finite element formulation of the problem results in a system of simultaneous algebraic equations for solution, rather than requiring the solution of differential equations. These numerical methods yield approximate values of the unknowns at discrete numbers of points in the continuum. Hence this process of modeling a body by dividing it into an equivalent system of smaller bodies or

units (finite elements) interconnected at points common to two or more elements (nodal points or nodes) and/or boundary lines and/or surfaces is called discretization (Logan, 2002). Fig. 3.1 summarizes the solution process of shell analysis.

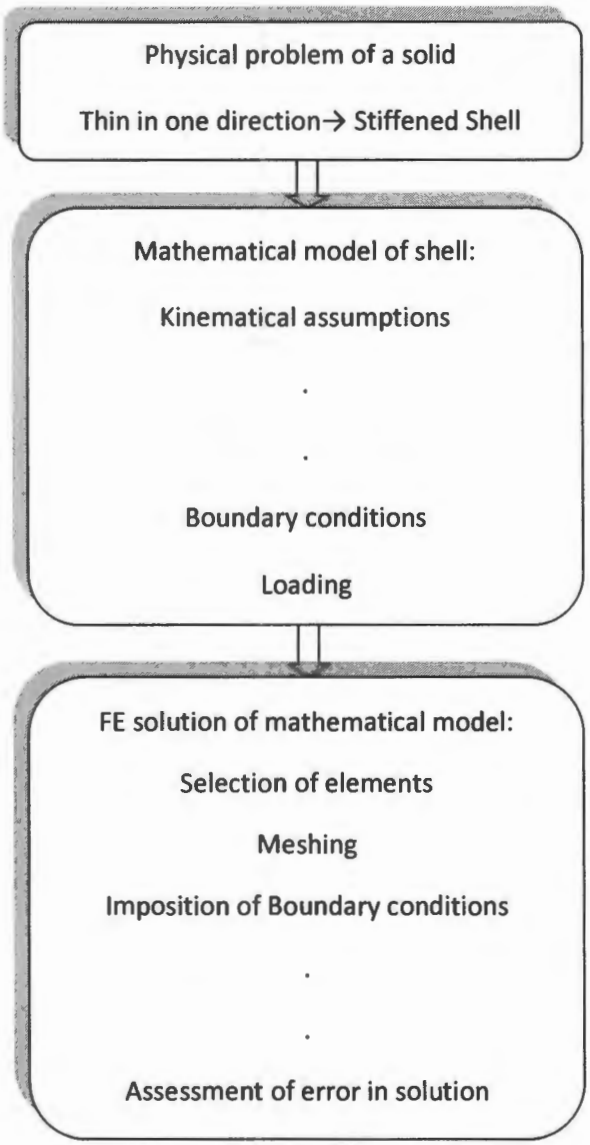

Fig. 3.1 Finite element analysis of a shell problem (Chapelle and Bathe, 2003).

In this study, the behavior of stiffened shells is investigated numerically by using ABAQUS finite element system. The theory and the solution procedure are outlined in detail in Chapter 4. One of the main advantages of this system is that it is relatively cheaper when compared with experimental testing. Finite element modeling allows simulation of complex shapes which

cannot be modeled easily theoretically or experimentally. Most importantly, numerical methods allow modeling of different load configurations which are difficult or expensive to model experimentally.

3.4.3 Experimental work

To validate the finite element results, experimental tests are conducted on laboratory small scale models of stiffened cylindrical and conical frusta.

Specimens will be fabricated from steel sheets. Only axial compression load case will be considered. A testing machine which applies axial load at a constant rate will be used. The testing machine used in these tests is called the Amsler universal testing machine.

Details of geometry and material of models and testing rig details and testing procedure are given in Chapter 5.

3.4.4 Analytical solutions

Analytical solutions of stiffened and un-stiffened cylindrical and conical shells which were presented in Chapter 2 will be used to validate elastic buckling analysis results from numerical modeling and experimental tests.

In Chapter 2, simple form classical buckling equations of un-stiffened shells were derived from Donnell governing differential equation. In finite element modeling, all results are presented as ratio of critical buckling load of stiffened shell (P_{cr}) to classical buckling load of un-stiffened shells (P_{cyl} or P_{con}). In particular, the buckling strength of stiffened shells will be presented as a normalized strength i.e P_{cr}/P_{cyl} or P_{cr}/P_{con}.

Chapter 4

Finite Element modeling

4.1 Introduction

A finite element modeling (FEM) based parametric study to investigate the buckling behavior of a meridionally and ring stiffened cylindrical and conical steel shell structures is performed using a general purposes program ABAQUS CAE 6.5. In particular, it is required to establish how elastic buckling load and modes shapes vary with respect to certain key design geometric parameters of shells subjected to different fundamental load configurations.

4.2 Fundamentals of finite element analysis of shell structures

4.2.1 Eigenvalue buckling prediction

Linear eigenvalue analysis is a linear perturbation procedure used to estimate the critical/bifurcation load of stiff structures. Stiff structures carry their design loads primarily by axial or membrane action, rather than bending action. Their response usually involves very little deformation prior to buckling hence pre-buckling is almost linear (ABAQUS, 1995).

The buckling load estimate is obtained as a multiplier of the pattern of perturbation load. For eigenvalue estimates to be reasonable, the response of perturbation loads must be elastic up to the estimated buckling load values (ABAQUS, 1995).

Shell governing equations for an arbitrarily chosen configuration during buckling can be reduced to an eigenvalue problem. Using the standard finite element approach, the governing equations for buckling then take the form of the standard eigenvalue problem (ABAQUS, 1995):

$$(K_{o}^{ij} + \lambda K_{\Delta}^{ij})\upsilon^{j} = 0 \qquad (3.10)$$

where ,

K_{o}^{ij} - stiffness matrix corresponding to the base state

K_{Δ}^{ij} - differential initial stress and load stiffness matrix

λ - eigenvalue

υ -buckling mode shapes

i and j -degrees of freedom for the whole body.

The base state stiffness is the sum of the hypo elastic tangent stiffness, initial stress stiffness and the load stiffness. The differential stiffness consists of the sum of the initial stress stiffness due to the perturbation stresses and the load stiffness due to the perturbation loads (ABAQUS, 1995).

4.3 Geometry and materials

Geometry of the stiffened conical frustum and cylindrical shells being analysed are depicted in Fig. 4.1.

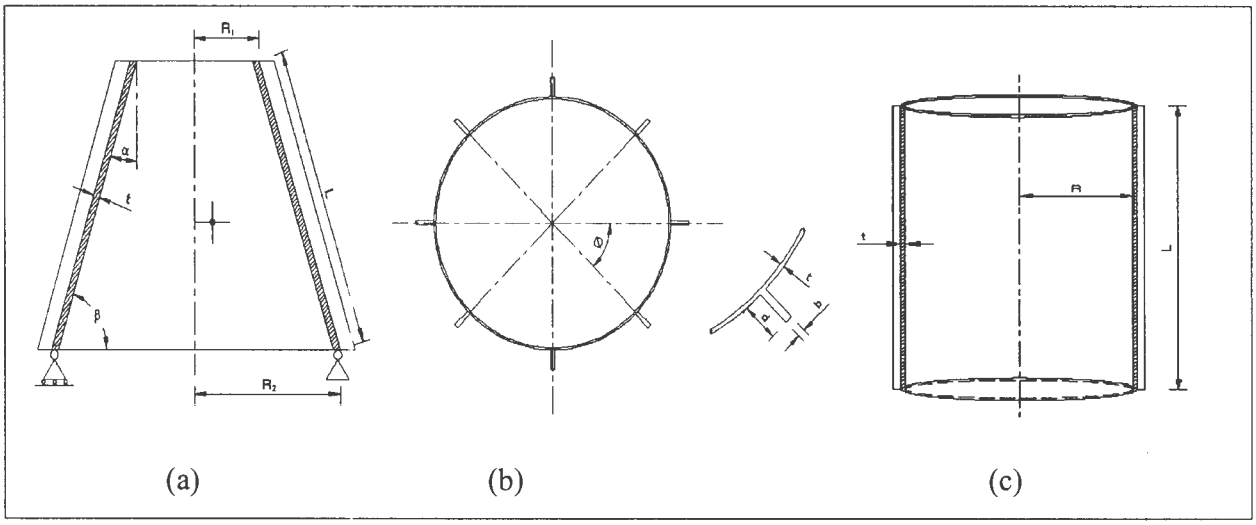

Fig. 4.1 Geometry and notation

Flat bar longitudinal (stringer) stiffening and circumferential (ring) stiffening will be considered separately for both conical and cylindrical shells. The flat bar stiffeners are placed on the outside surface of the shell as shown on in Fig. 4.1.

A broad range of these geometric parameters are investigated. The ranges of these parameters considered are the once typically encountered in civil and mechanical engineering structures:

- N from 4 to 64
- d/t from 2.5 to 12.5

- d/b from 2 to 15

Also, in all cases R/t varies from 100 to 200, which is a typical range of most industrial applications. Other geometrical parameters that are kept constant are L/R=1 and for conical frustum $\beta=30^{\circ}$ which is the most typical angle used in silos and pipe tapering practice.

The material used for both the shell and stiffeners is hot rolled structural steel, which is typically used in industrial structures. It has a Young's modulus (E) of 200 000MPa and a Poisson's ratio (μ) of 0.3.

In view of the range of R/t examined, it should be emphasized that material non-linearities will also play an important role but in this study they are assumed to have little or no effect on the results obtained. The stress versus strain relationship is assumed to be perfectly elastic. Material and geometric non linearities, with exception of pre-buckling deformations, are beyond the scope of this present study.

4.4 Models description

In this present investigation, the different modes of instability in stiffened conical and cylindrical shells under different load configurations are studied through a number of finite element models. The models are developed based on the criteria successfully verified previously by Chrystapolis. In particular, local shell and stringer buckling modes and global mode might develop in thin walled stiffened shells (Spagnoli, 2001). Buckling modes will be examined effectively in isolation, by considering the following discrete and smeared models:

- shell only model
- single panel model
- multi panel model
- orthotropic (smeared) model

The shell only model allows effective analysis of local shell buckling mode in isolation, independent of stiffener behavior. Depending on the orientation of stiffeners, this model is defined by a pair of either successive stringers or ring stiffeners.

By exploiting symmetry conditions, the single panel model is defined by a pair of either successive mid panel meridians or circumferences. This shell stringer assembly is exploited to analyze both local shell and stringer buckling modes.

The global stiffened panel mode is investigated by smearing stiffeners over the shell wall hence an orthotropic model is generated. Smeared approach is effective provided that the stiffeners are closely spaced.

Finally, a multi panel model which allows the analysis of both local shell and global modes will be considered (Spagnoli, 2001). Quarter cone and cylindrical models will be considered.

Model Reference	Model description	Model angular width	Buckling mode
Shell only	Discrete model	360°/N	Local shell
Single panel	Discrete model	360°/N	Local shell, local stringer
Multi-panel	Discrete model	90°	Local shell, local stringer, global
Orthotropic	Smeared model	90°	Global

Table 4.1 Overview of finite element models (Spagnoli and Chryssanthopoulos, 1999)

However, at least one full model will be analyzed for each parameter for the purpose of comparison with discrete models. If appropriate boundary conditions are implemented in discrete models, negligible difference from full models is expected in terms of critical loads (Spagnoli, 2001).

4.5 Boundary conditions and Loading

Boundary conditions are used to prescribe values of basic solution variables: displacements and rotations in stress/displacement analysis.

Ring circumferentially fixed rotationally free boundary conditions are applied at the top curved edges and stiffeners. This type of edge fixity is typically found in marine and aeronautical structures when the conical frustum is used as a transition element between cylinders of different diameter and is bound by heavy ring stiffeners.

The bottom edge is simply supported. Translation is restrained in all directions whilst free to rotate. The loading boundary condition is only supported in the radial and circumferential directions.

Symmetry boundary conditions are applied along the straight meridional edges of the single panel model. For shell only models u1=u2=0 boundary conditions are considered along the straight edges in order to simulate the constraints imposed by sturdy stiffeners.

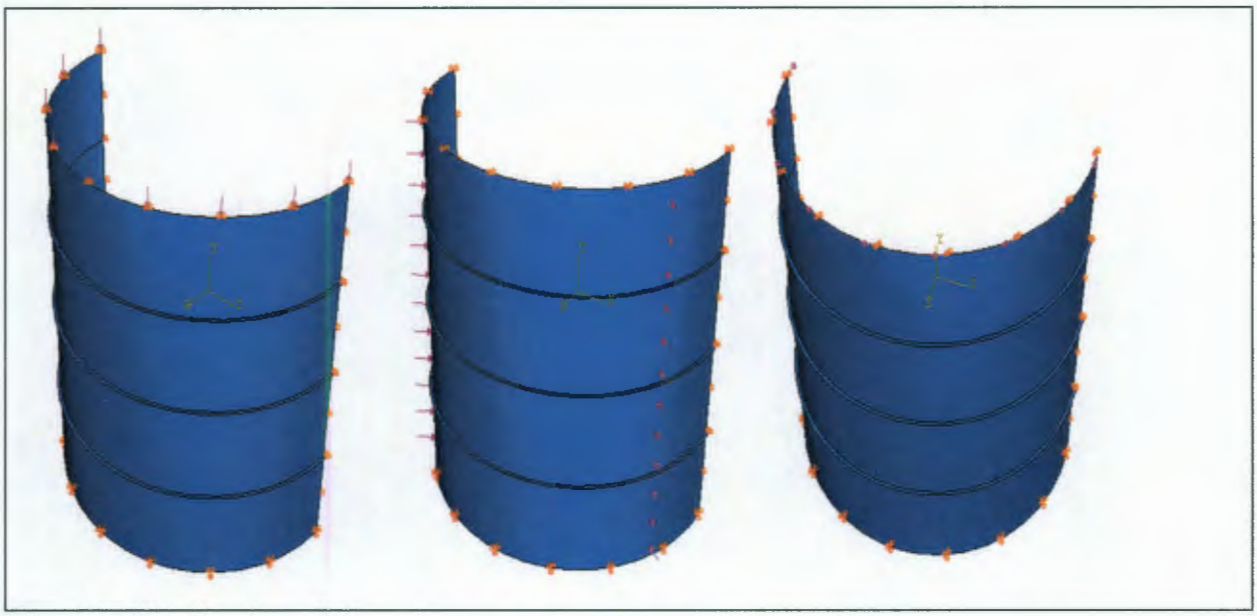

Fig. 4.2 Typical loading configuration on stiffened cylindrical shells

Different loading types are applied as shell edge load along the top edge curved edge and stiffener end. The following load cases are considered:

- compressive axial load
- uniform external pressure
- shear/torsion

4.6 Mesh and elements

4.6.1 Elements type

The ABAQUS element library provides a complete geometric modeling capability. It has an extensive element library to provide a powerful set of tools for solving many different problems. These elements are characterized by the following aspects (ABAQUS, 1995):

- family
- degrees of freedom
- number of nodes
- formulation
- integration

The unique element names identify each of the five aspects of an element. The element families which are commonly used in a stress analysis are (ABAQUS, 1995):

- continuum (solid) elements
- shell elements
- beam elements
- rigid elements
- membrane elements e.t.c

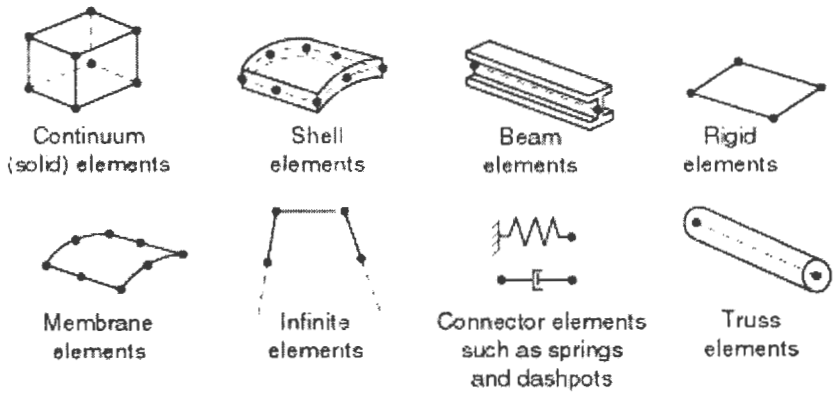

Fig. 4.3 Commonly used element families (ABAQUS, 1995)

The degrees of freedom are the fundamental variables calculated during the analysis. For a stress/displacement simulation the degrees of freedom are the translations and for shell and beam elements, the rotations at each node.

At any point in the element which is not nodes, the displacements are obtained by interpolating from the nodal displacements. The order of interpolation is determined by the number of nodes used in the element. The order of interpolation is s follows:

- linear elements
- quadratic elements
- tetrahedral elements

Element formulation refers to the mathematical theory used to define the element's behavior. All of the stress/displacement elements in ABAQUS are based on the Lagrangian or material description of behavior (element deforms with the material). Alternatively the Eulerian, or spatial formulation where description elements are fixed in space as the material flows through them (ABAQUS, 1995).

4.6.2 Choosing the appropriate element for an analysis type

Conventional shell elements are used to model structures in which one dimension, the thickness, is significantly smaller than the other dimensions. This condition is used to discretize a body by defining the geometry at a reference surface and the thickness will be defined through section

property definition. In contrast, continuum shell elements descritize an entire three dimension. Shell elements have displacement and rotational degrees of freedom while continuum shell elements have only displacement degrees of freedom.

Shell elements are to be used to model both the shell and the stiffeners walls. Four node Langrangian doubly curved shell elements, in accordance with the Mindlin-Reissner kinematic assumptions, are to be employed. The element, designated as S4R in ABAQUS, uses a selective integration rule, reduced 2 x 2 Gauss integration, which prevents mesh locking and hour-glass modes. The element has three degrees of freedom per node. The element formulation is based on large displacement and small strain analysis.

4.6.3 Mesh convergence study

A fine mesh based on the mesh convergence study, is used to ensure that the mesh adopted produces accurate buckling strength results. The relative change of eigenvalues with mesh refinement is used for convergence analysis.

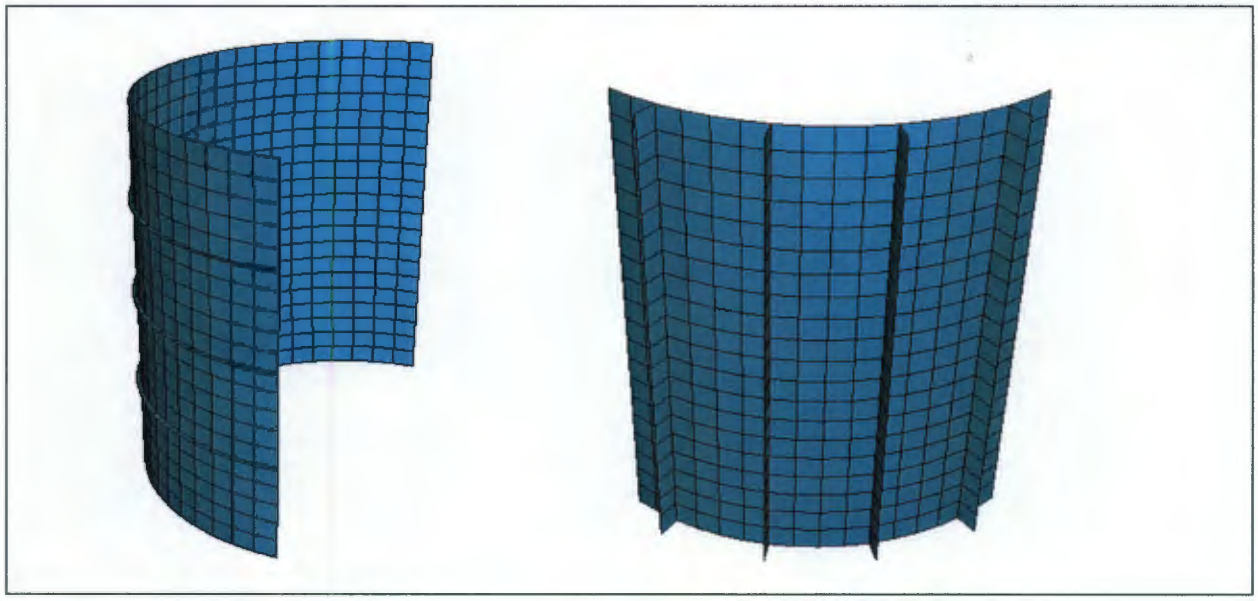

Fig. 4.4 Meshed multi panel model

4.7 Solution procedure

Membrane stresses, in most practical situations are accompanied by bending stresses which results in the shell structure behaving nonlinearly. Nonlinear equations which arise can be

linearised to yield an algebraic eigenvalue problem which can be solved to obtain a buckling load (Bagchi and Paramasivam, 1996). The basis for modeling shall be in accordance with Eurocode 3 (2004) which allows the option of performing a Linear buckling analysis (LBA). In LBA, the linearity of the theory results from the assumptions of a linear elastic material law and the small deflection theory. This LBA obtains the lowest eigenvalue at which the shell may buckle into a different deformation mode, assuming no change of geometry, no change in the direction of action of loads and no material degradation. Imperfections of all kinds are ignored (EC3, 2004). This analysis provides the basis of the critical buckling resistance evaluation. Linear buckling analysis (LBA) gives a good prediction of buckling load if the pre-buckling rotations are negligible. In practice pre-buckling rotations exist hence linear buckling analysis yield overestimated buckling loads which are un-conservative. However, for the purpose of studying the buckling behavior of a shell, the LBA is quiet satisfactory.

The elastic critical buckling load, P_{cr}, is determined from an eigenvalue analysis for different models.

CHAPTER 5

Experimental Modeling

5.1 Introduction

Verification of results from finite element analysis and theoretical studies is performed by experimental tests on laboratory small scale models of stiffened cylindrical and conical frusta shell subjected to axial compressive load.

Satisfactory description of buckling behaviour of stiffened shells can be achieved using the linear theory of orthotropic shells .However, correlation of numerical and theoretical results, with experimental results obtained within a broad range of parametric changes is found to be unsatisfactory if stiffener spacing exceeds certain limit i.e relatively too broad (Krasovsky and Kostyrko, 2007). Moreover, experimental results obtained by different researchers to verify the theoretical results inevitably indicated that shells buckle at loads which are considerably below that given by classical theory. Specifically, experimental results varied as low as 30% of the load given by classical solution and furthermore the large degree of scatter of results seems not to satisfy researchers [18]. Consequently, authenticity of using parametric results from numerical and theoretical analysis in the development of stiffened shell design equations has been questioned.

In view of the above remarks, this work presents experimental investigation carried out with the aim to study systematically the influence of the following structural factors on the mechanism of the stiffened shells carrying capacity exhaustion when subjected to an axial compressive load:

- Number of stiffeners
- Stiffeners slenderness

5.2 Geometry and materials of specimen

The geometrical characteristics of specimens are given in Fig. 5.1. All shells models are stiffened on the outside with rectangular cross section bars. The length L and L_e for both cylinders and conical frustum respectively remain constant for all test models.

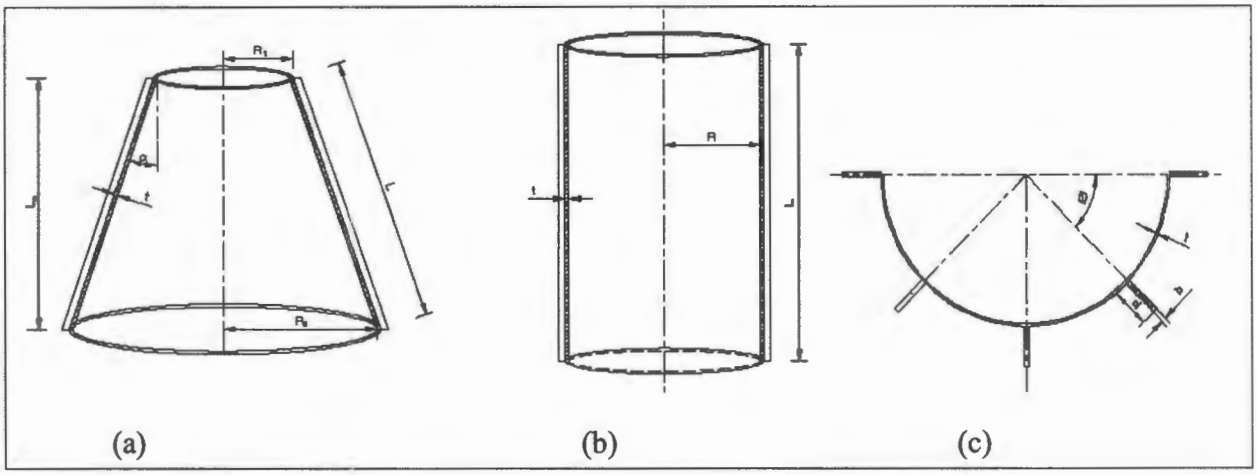

Fig 5. 1 Geometry and notation

Table 5.1 and 5.2 shows average measured dimensions of the stiffened cylinders and conical frustum shell models. Fabrications drawing with dimension details are attached in Appendix B.

Model reference	Shell dimensions		Stiffener dimensions		Number of stiffeners (N)
	R (mm)	*t (mm)*	*b (mm)*	*d (mm)*	
CYL01	100	-	-	-	No stiffeners
CYLO3	100	1.6	1.6	10	8
CYL05	100	1.6	1.6	10	20
CYL07	100	1.6	1.6	10	8
CYL09	100	1.6	1.6	10	20

Table 5.1 Stiffened cylindrical shell models dimensions (L=300mm)

Model reference	Shell dimensions			Stiffener dimensions		Number of stiffeners (N)
	R_1 (mm)	*R_2 (mm)*	*t (mm)*	*b (mm)*	*d (mm)*	
CON01	100	180	1.6	-	-	No stiffeners
CON03	100	180	1.6	1.6	10	8

CON05	**100**	**180**	**1.6**	**1.6**	**10**	**20**
CON07	**100**	**180**	**1.6**	**1.6**	**10**	**8**
CON09	**100**	**180**	**1.6**	**1.6**	**10**	**20**

Table 5.2 Stiffened conical shell models dimensions (L=300mm, β=20°)

Specimens are fabricated from steel sheets which are developed and seam welded along a single longitudinal axis. The stiffeners are made of the same material as the shell and are spot welded abreast to the shell's outer surface.

To identify the material properties, normalized tensile tests were performed on pieces of steel from the same sheet that was used to manufacture the shell and stiffener models.

E= 200 000MPa

v= 0.3

f_y= 300N/mm^2

Fig 5. 2 Typical stiffened cylindrical shell specimens

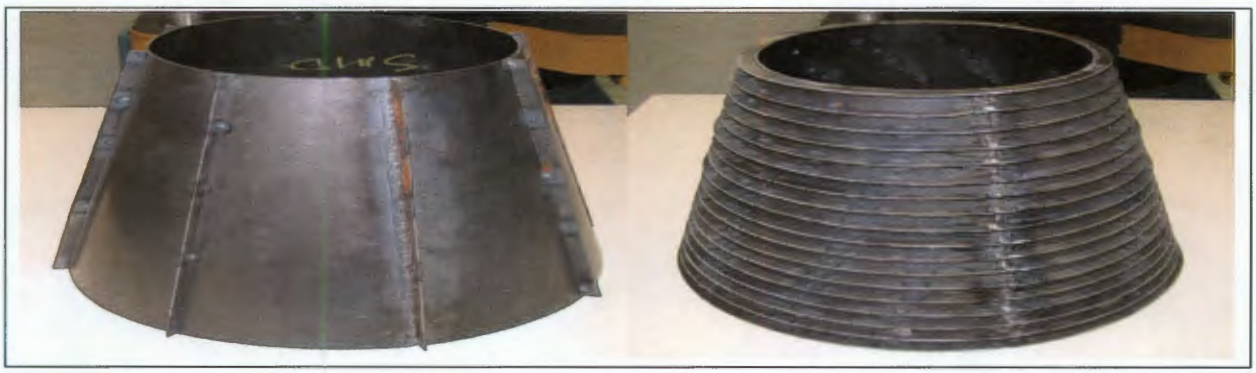

Fig 5. 3 Typical stiffened conical shell specimens

5.3 Test rig and measurement system

The models were tested in a rig shown in Fig.5.4 below. Axial compression was developed by the Amsler universal mechanical testing machine. The testing machine is driven by a variable electric motor through a low ratio gearbox, thus enabling slow kinematical loading rate of 0.05mm/min to be achieved. The force created by the jack was transmitted to the model as a uniform axial displacement through rigid circular plates sitting on ball bearings.

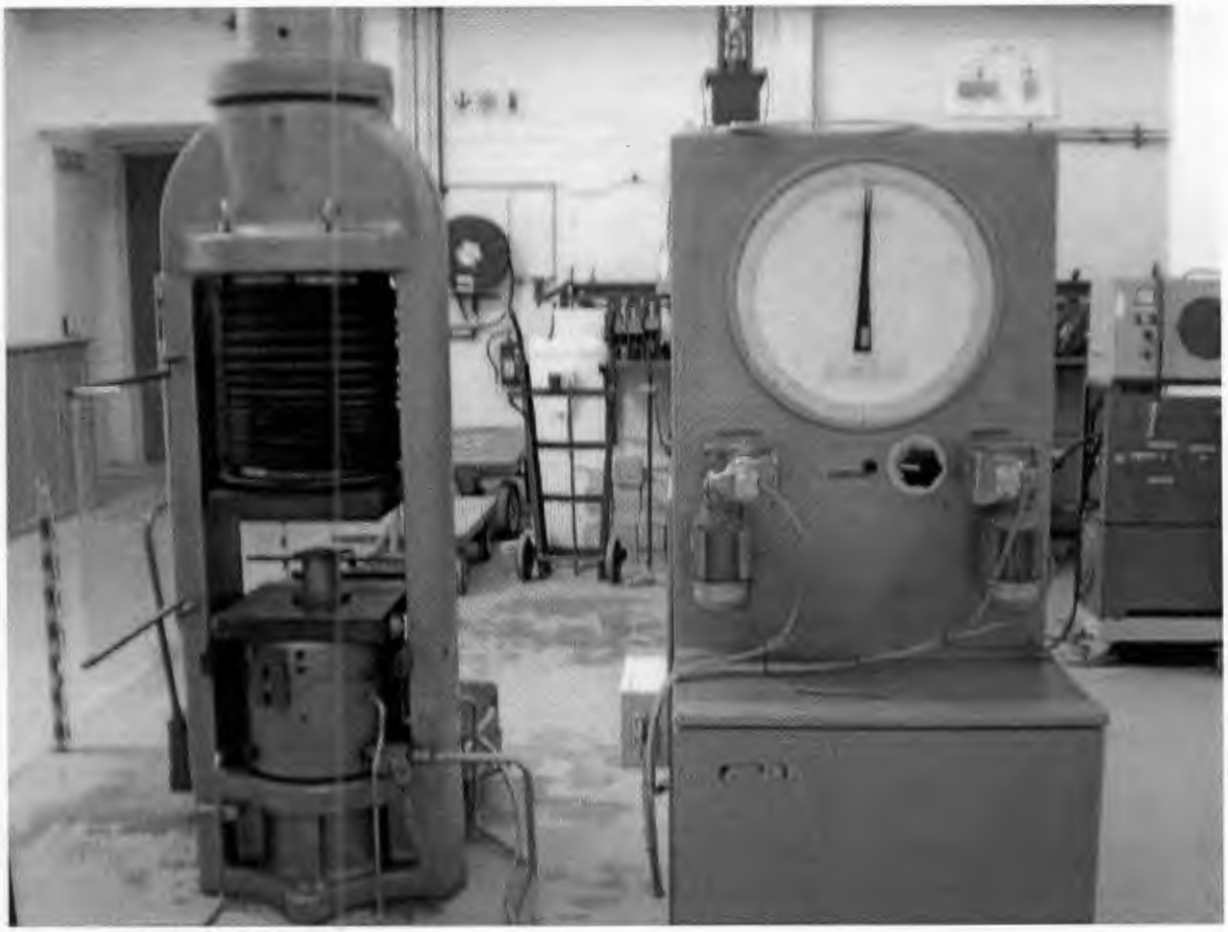

Fig 5. 4 Amsler universal mechanical testing machine

Dial gauges were fitted around the shell model and along the shell sides to measure displacement. The number of axial readings was decided based on theoretical elastic buckling modes axial half-waves for un-stiffened conical and cylindrical shells, whereas the circumferential spacing was determined in order to maintain approximately a square mesh.

5.4 Overview of test results

5.4.1 Results for material tensile strength

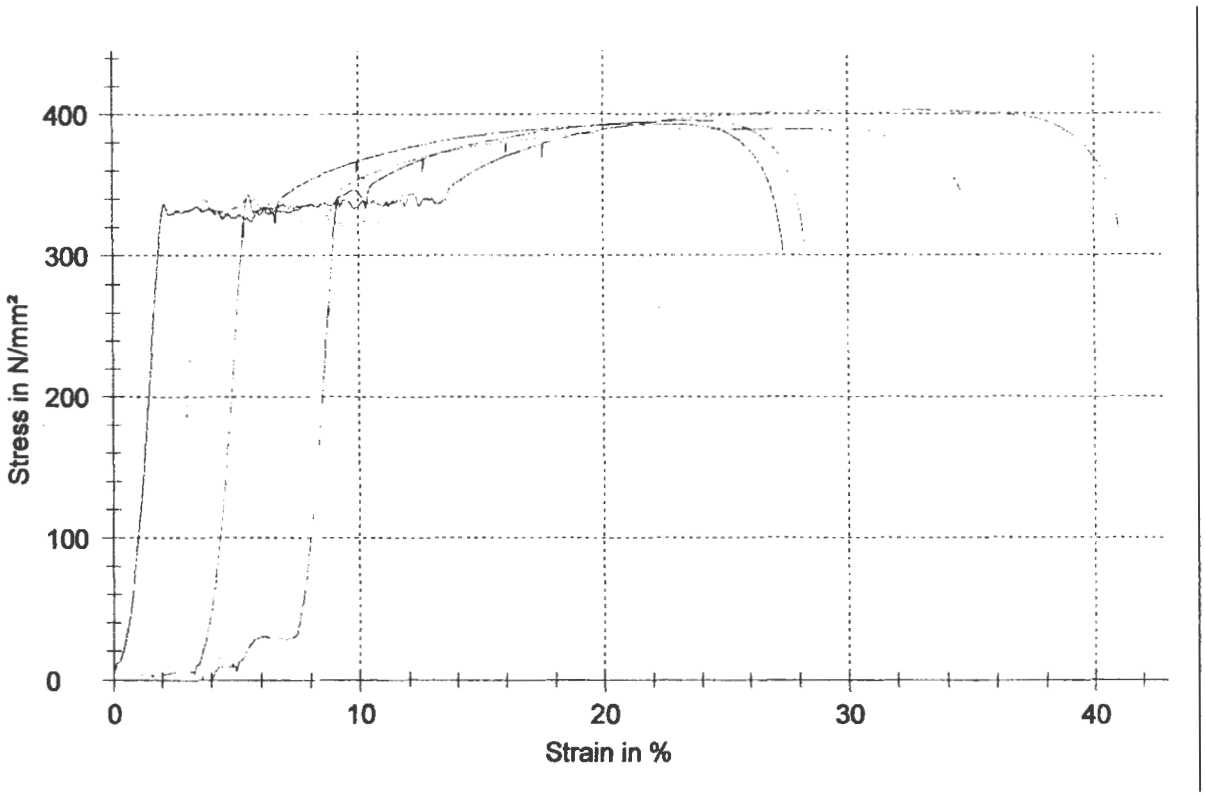

Fig 5. 5 Stress-strain graph for material used for fabrication on the specimens

5.4.1 Results for axial compression

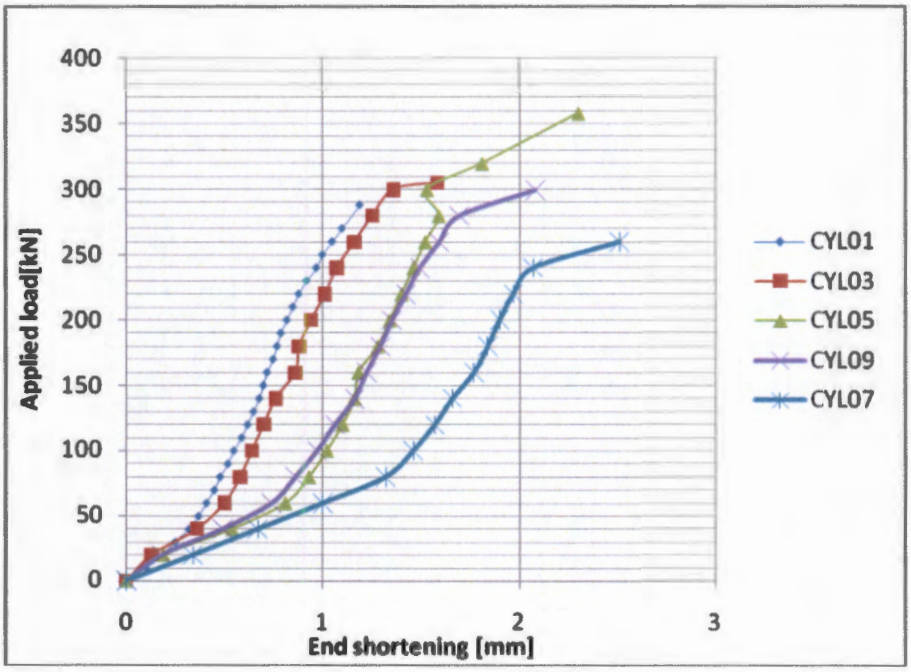

Fig 5. 6 Experimental buckling pressure for stiffened cylinders

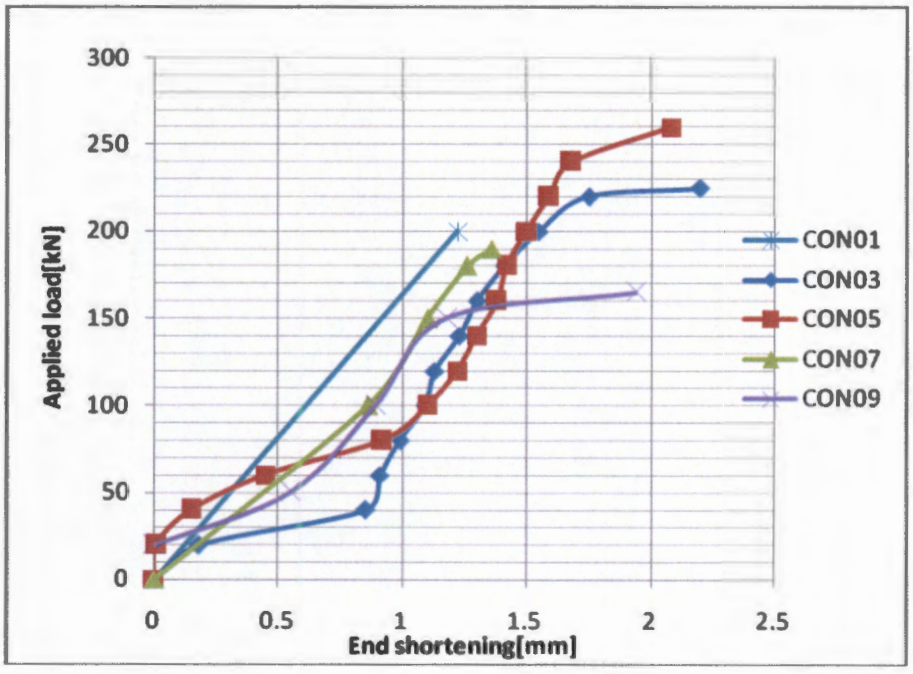

Fig 5. 7 Experimental buckling pressure for stiffened conical frusta

CHAPTER 6

Results of Finite Element studies

6.1 Introduction

Results of finite element parametric studies are presented in this chapter. ABAQUS linear buckling analysis results on how the elastic buckling load and mode shapes vary with respect to certain key parameters are presented. A discussion of the results then follows in chapter 7.

Results of various buckling modes are investigated via different finite element models. It is important to verify that these finite element models accurately predict the critical elastic buckling load of the shells. Eigenvalue analyses, is performed firstly to validate the finite element models.

Presentation then follows of the load carrying capacity and buckling modes results for a wide range of parameters defined in the earlier chapter. Only critical eigenmodes and eigenvalues are reported.

6.2 Mesh convergence study

Results of a mesh convergence study are presented for multi-panel model.

N	Axial	Circum	λ	Pcr[kN]	Model
	14	8	12783	85431	Multi panel
	14	16			
	28	**32**	**12158**	81254	Multi panel
	14	32			
8	14	32	12326	82377	Multi panel
	14	**16**			
	14	16	12771	85351	Full Model
16	**14**	**8**	**14764**	98671	Multi panel
	14	8	13919	93023	Full Model
32	14	4	5716	38201	Multi panel
	10	2	19644	131284	Full Model

Table 6.1 Mesh convergence study

6.3 Finite element model validation

A comparative study of theory with finite element results obtained from different models was performed. Due to limitation of analytical studies on the buckling strength of conical panels, only cylindrical shell models will be validated. Validity of results on cylindrical panel models will be assumed to follow for conical shells. The results are presented by plotting normalized buckling strength against total curvature in the Fig. 6.1.

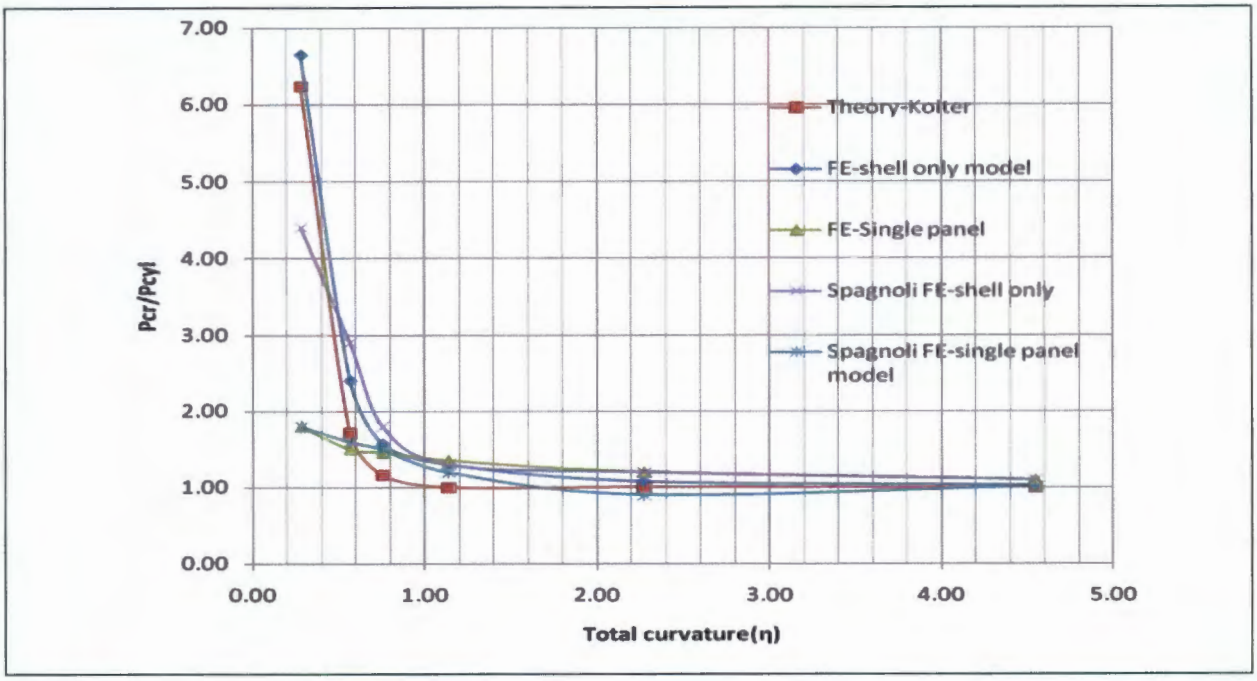

Fig. 6. 1 Comparison of FE and theoretical resultsfor cylindrical panels (R/t=100, L/R=2, ζ_1=0.3).

6.4 Effect of varying key parameters of stiffened shells on Elastic buckling load

6.4.1 Introduction

The purpose of this part of the study is to examine the advantage of stiffening cylindrical and conical over their un-stiffened counterparts that have the same volume of steel (iso-weight). Furthermore, a comparison between the option of stiffening in the meridional direction and stiffening in the circumferential direction will be conducted. Finally, the stiffener slenderness will be varied to reveal the optimum stiffener size for different shell geometry and load cases.

6.4.2 Meridionally stiffened cylinders

6.4.2.1 Deformed shapes of elastic buckled cylinders subjected to various load cases

Typical buckling shapes for stringer stiffened shells subjected to various load cases, are shown in Fig. 6.2(a-c).

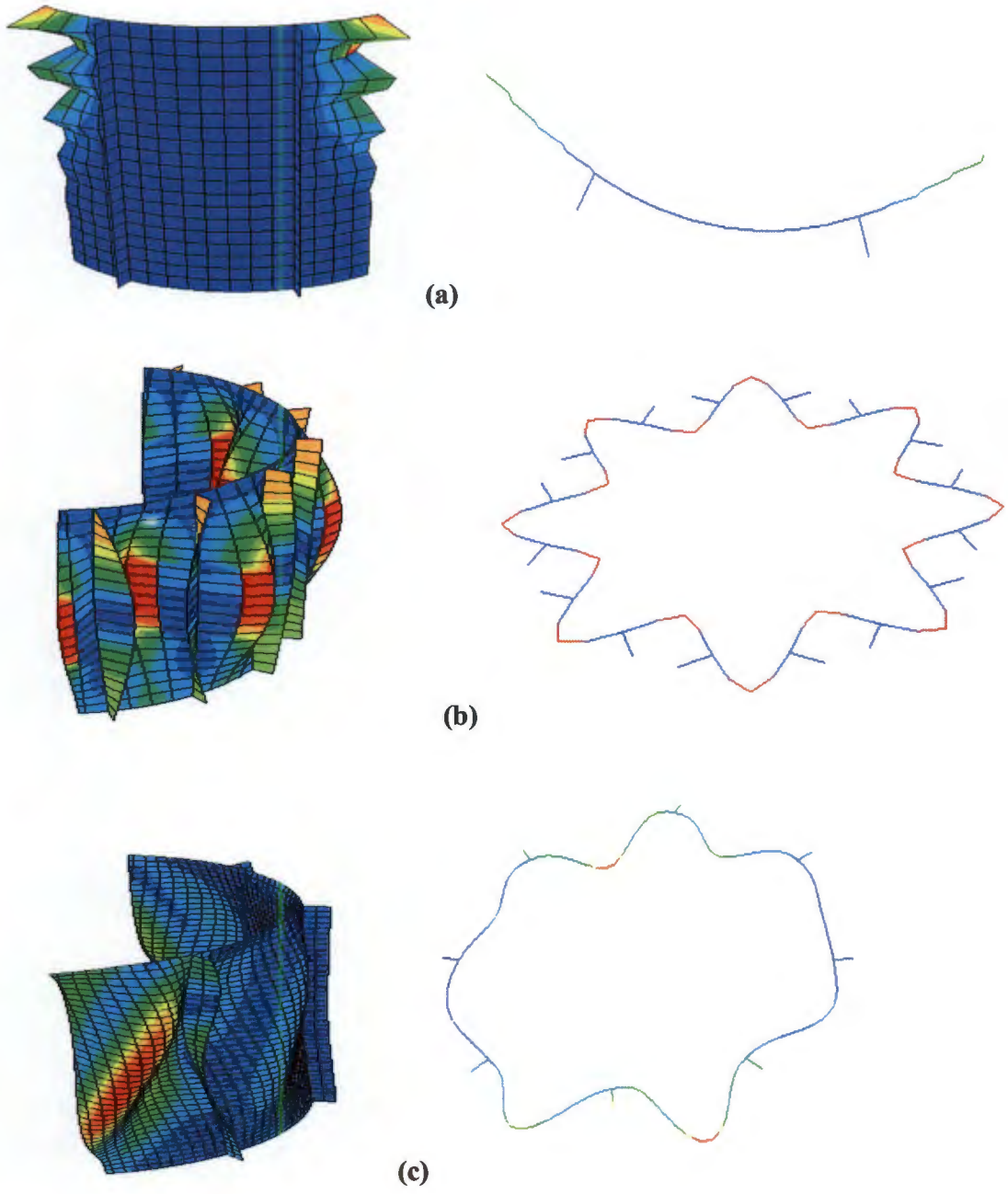

Fig. 6. 2 Deformed shapes of cylinders subjected to (a) axial compression (b) external pressure (c) shear load

6.4.2.2 Variation of elastic buckling load for cylinders of varying R/t and number of stringers (N)

The first set of results are presented for cylinders with a fixed stiffener dimensions d/b=5. By varying the R/t ratio of cylinders for different load configurations, curves in Fig. 6.3 to 6.4 are obtained.

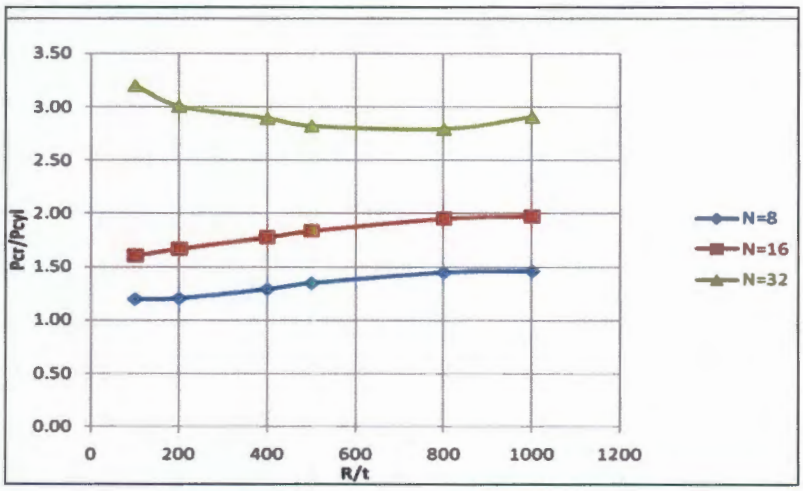

Fig. 6. 3 Axial compression: Normalised Buckling load vs R/t

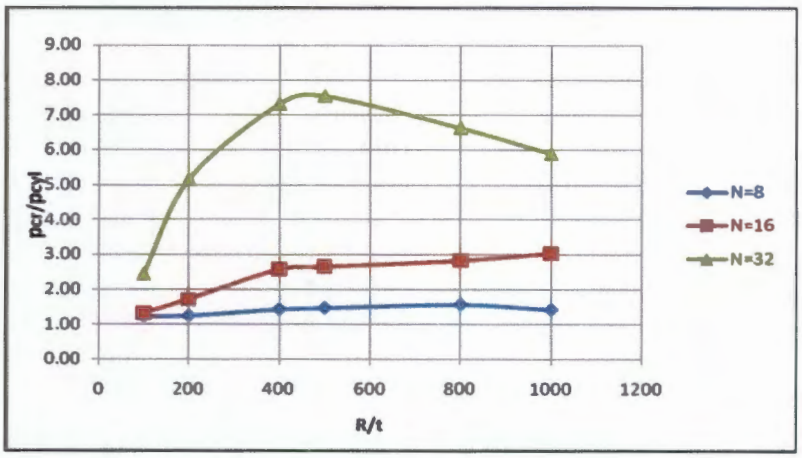

Fig. 6. 4 Uniform external pressure: Normalised Buckling load vs R/t

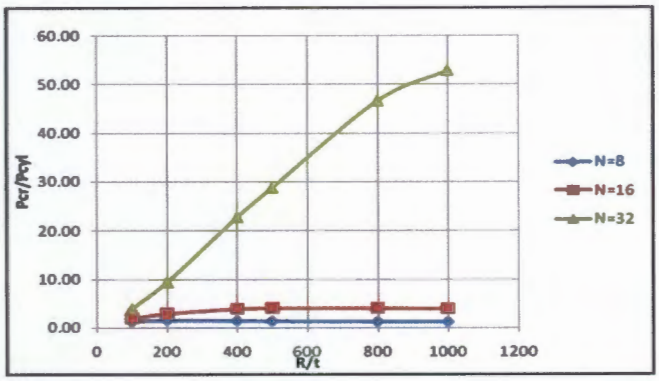

Fig. 6. 5 Shell edge shear: Normalised Buckling load vs R/t

6.4.2.3 Effect of varying number of stringers (N) on elastic buckling loads for iso-weight cylinders

The effect of varying total curvature (η) by varying number of stringers (N) for iso-weight cylinders is presented in Fig. 6.6. Cases of N between the extreme cases of wide panels (N=8) and narrow panels (N=64) are considered.

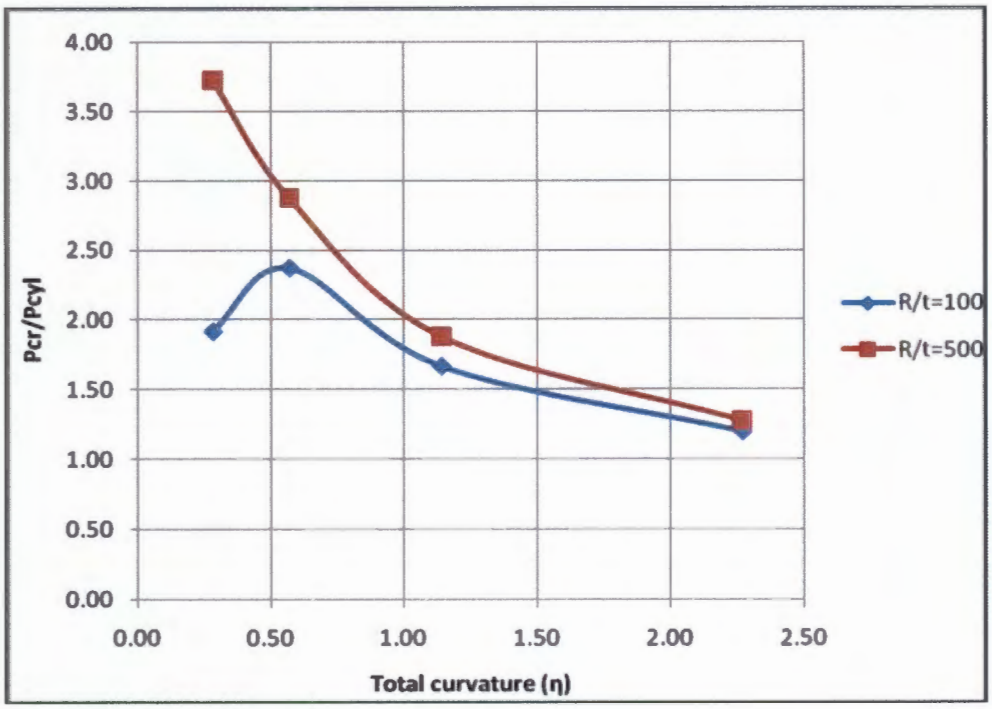

Fig. 6. 6 Axial compression: Normalised Buckling load vs total curvature (η) for iso-weight cylinders

6.4.2.4 Effect of varying stringers slenderness (d/b) on elastic buckling loads on cylinders of varying R/t

Influence of d/b is illustrated in Fig. 6.7 to 6.9, where results of a 16 stringer model under different load cases are presented.

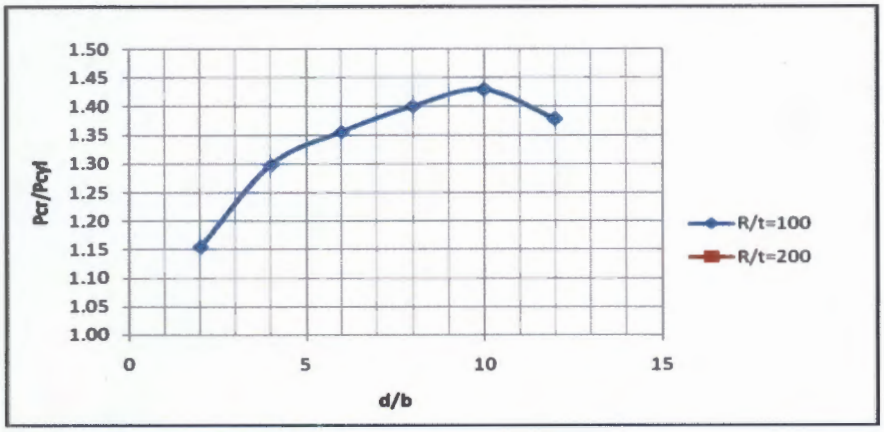

Fig. 6. 7 Axial compression: Normalised Buckling load vs d/b

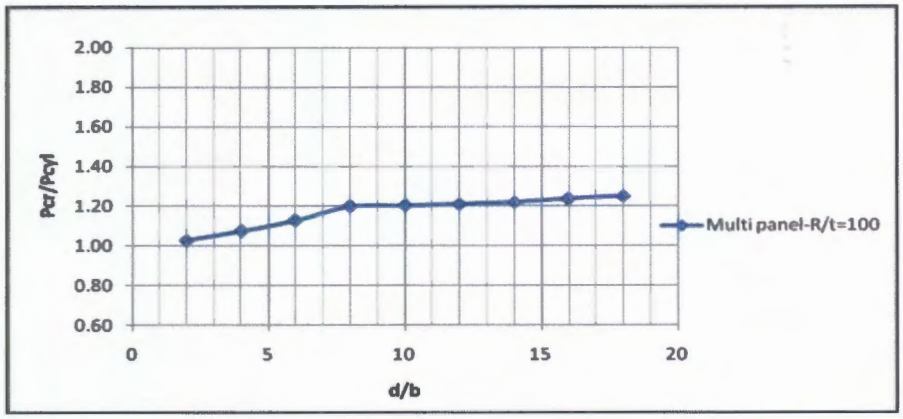

Fig. 6. 8 Uniform external pressure: Normalised Buckling load vs d/b

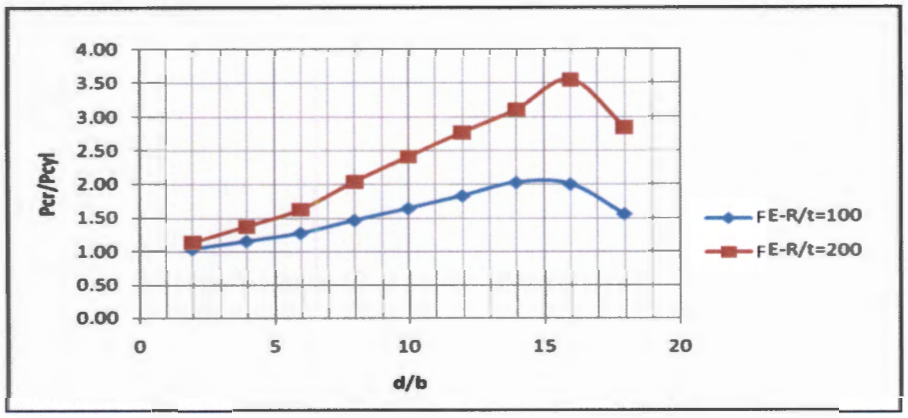

Fig. 6. 9 Shell edge shear: Normalised Buckling load vs d/b

6.4.2.5 Effect of varying stringers slenderness (d/t) on elastic buckling loads on cylinders of various d/b ratios

Effect of varying stringer slenderness on elastic buckling, was assessed using cylindrical model with fixed number of stiffeners (N=16). The results are presented in Fig. 6.10 to 6.12.

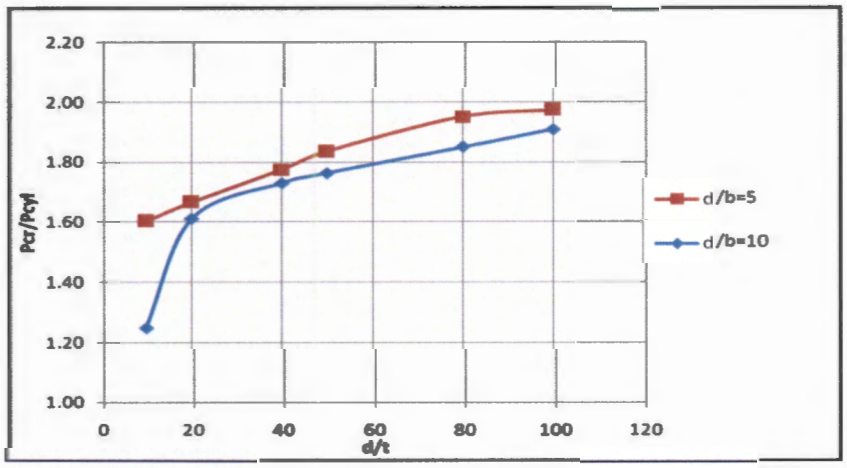

Fig. 6. 10 Axial compression: Normalised Buckling load vs d/t

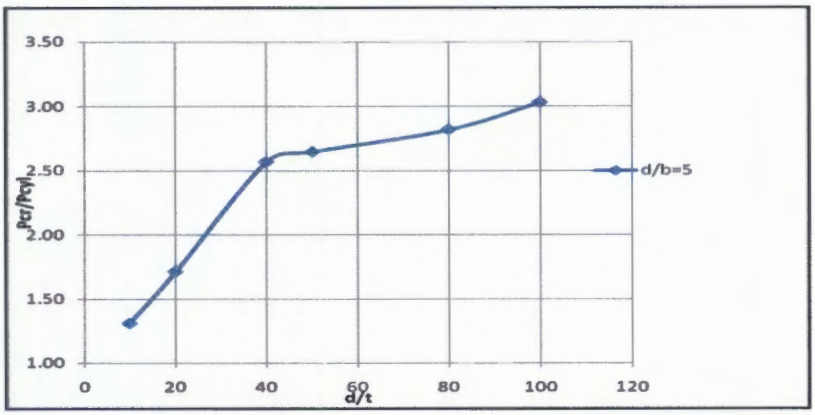

Fig. 6. 11 Uniform external pressure: Normalised Buckling load vs d/t

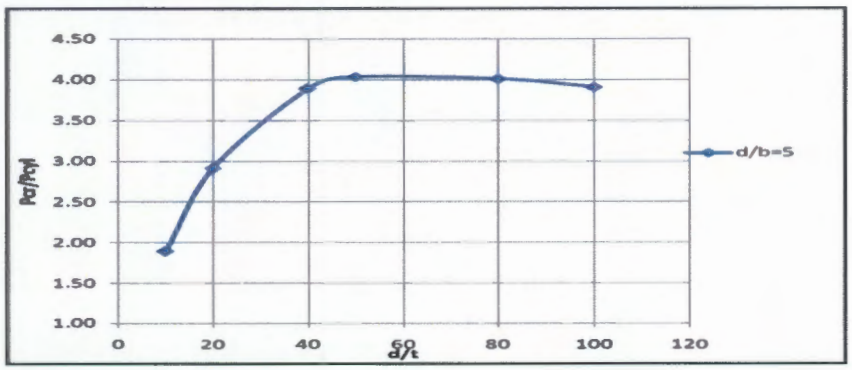

Fig. 6. 12 Shell edge shear: Normalised Buckling load vs d/t

6.4.3 Circumferentially stiffened cylinders

6.4.3.1 Deformed shapes of elastic buckled cylinders subjected to various load cases

Typical collapse modes of ring stiffened cylindrical shells are shown in Fig. 6.13(a-c) for different load cases.

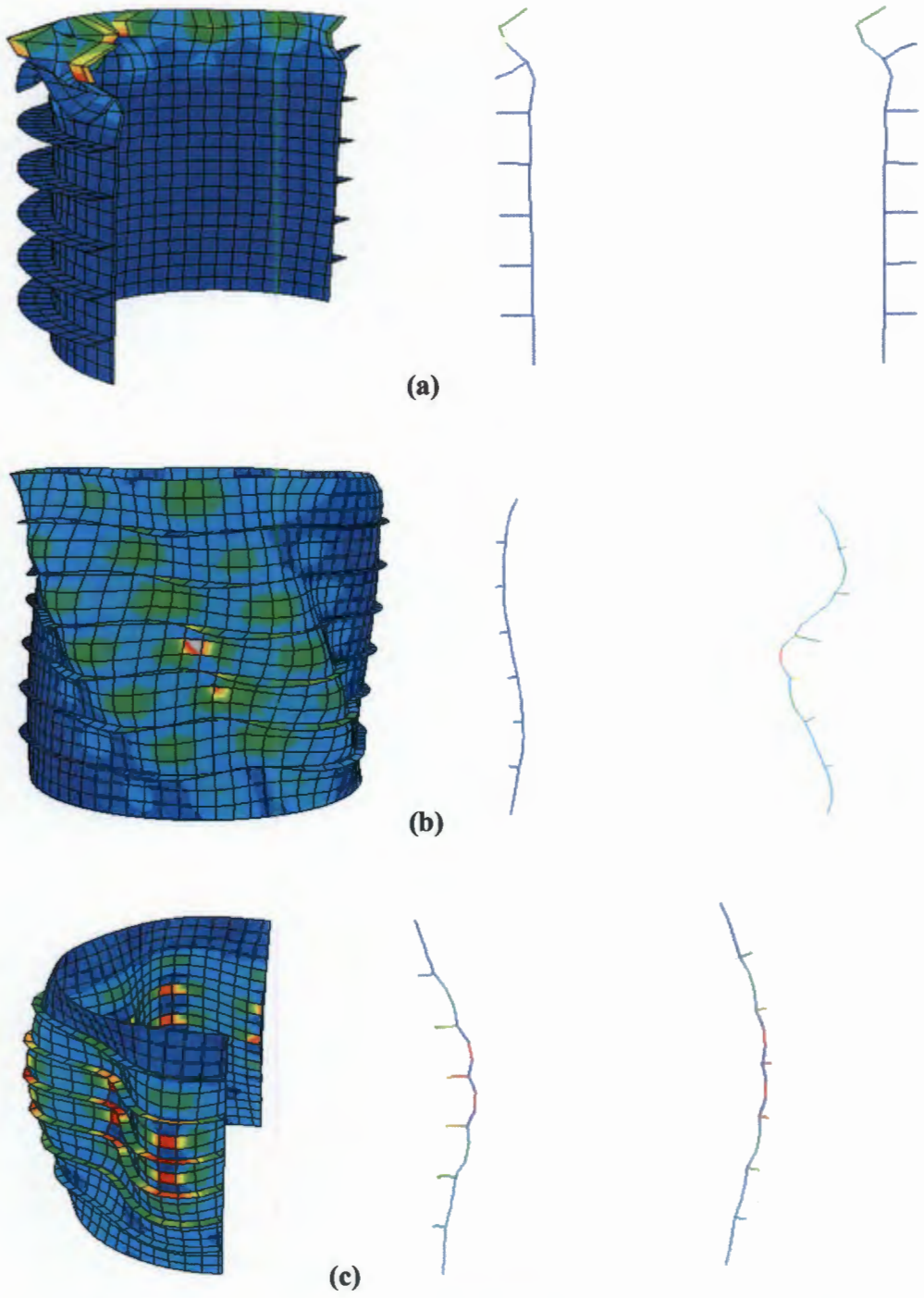

Fig. 6. 13 Deformed shapes of elastic buckled cylinders subjected to (a) axial compression (b) external pressure (c) shear load

6.4.3.2 Variation of elastic buckling load for cylinders of varying R/t and number of ring stiffeners (N)

By varying the number of ring stiffeners of d/b=1, different panel widths are considered for cylinders of various R/t ratio. The results are summarized in Fig. 6.14 up to Fig. 6.16.

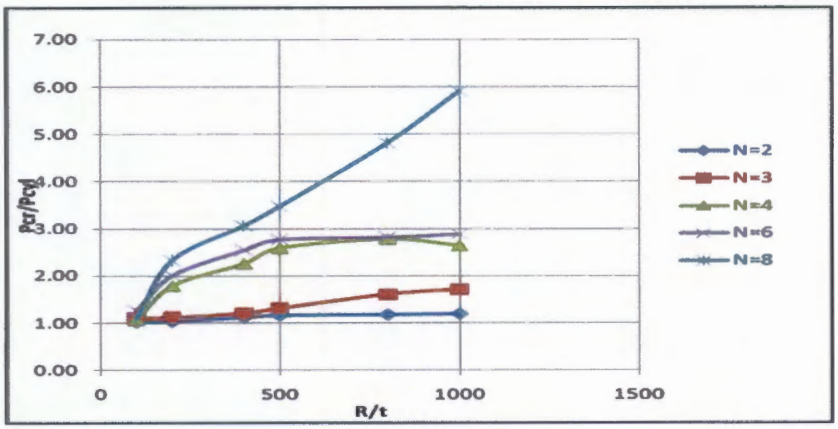

Fig. 6. 14 Axial compression: Normalised Buckling load vs R/t

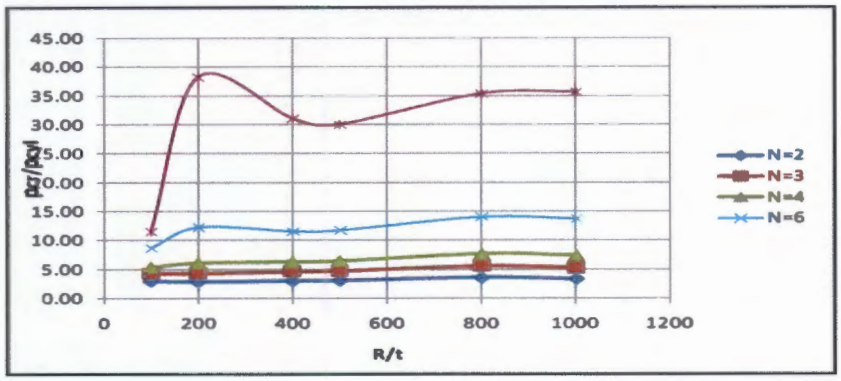

Fig. 6. 15 Uniform external pressure: Normalised Buckling load vs R/t

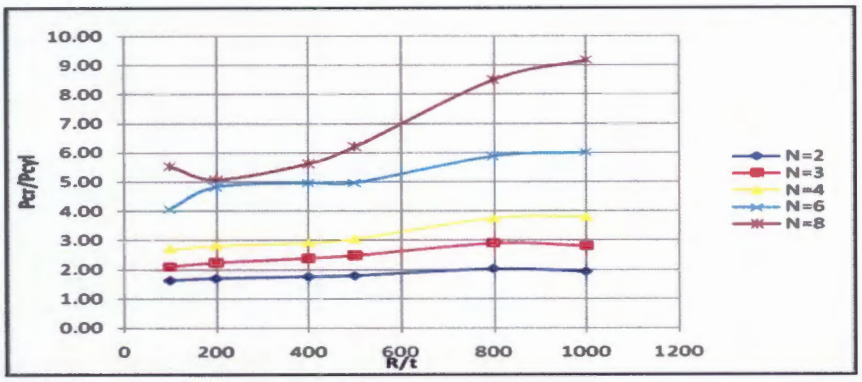

Fig. 6. 16 Shell edge shear: Normalised Buckling load vs R/t

6.4.3.3 Effect of varying ring stiffeners' slenderness (d/b) on elastic buckling loads on cylinders of varying R/t

Results of the investigation of variation of buckling load with ring stiffener slenderness for cylinders with fixed panel length (N=6) are presented in Fig. 6.17 up to 6.19.

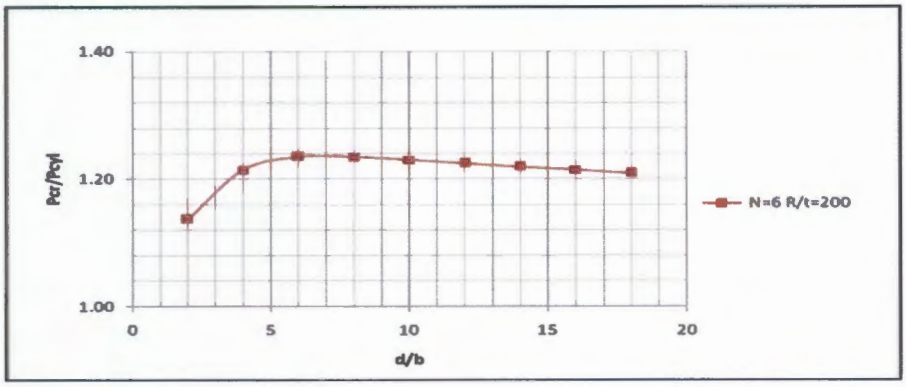

Fig. 6. 17 Axial compression: normalized elastic buckling strength vs stringer slenderness (d/b)

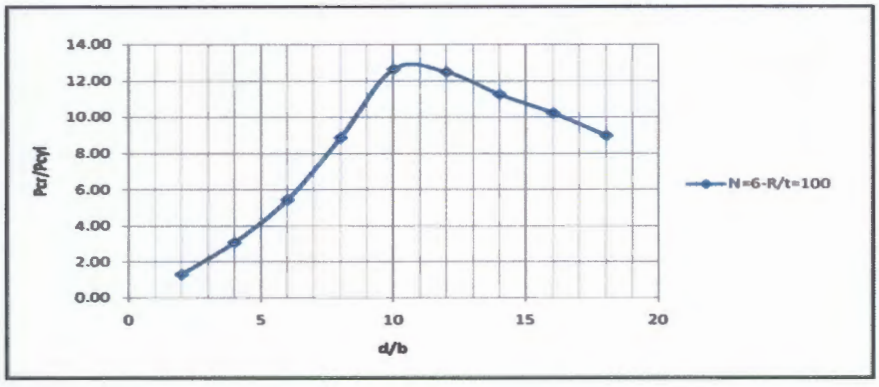

Fig. 6. 18 External pressure: normalized elastic buckling strength vs stringer slenderness (d/b)

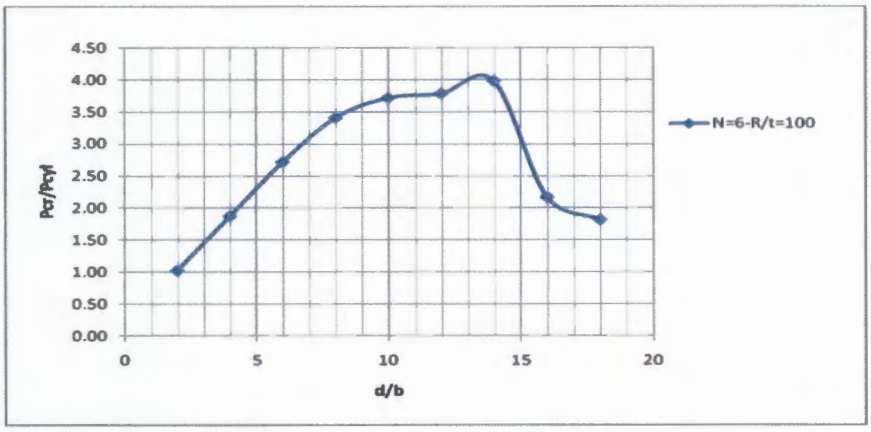

Fig. 6. 19 Shear: normalized elastic buckling strength vs stringer slenderness (d/b)

6.4.4 Meridionally stiffened conical shell frustum

6.4.4.1 Deformed shapes of elastic buckled conical shell frustum subjected to various load cases

Different deformed shapes of elastic buckled conical frustum under different load configurations are shown in Fig. 6.20(a-c).

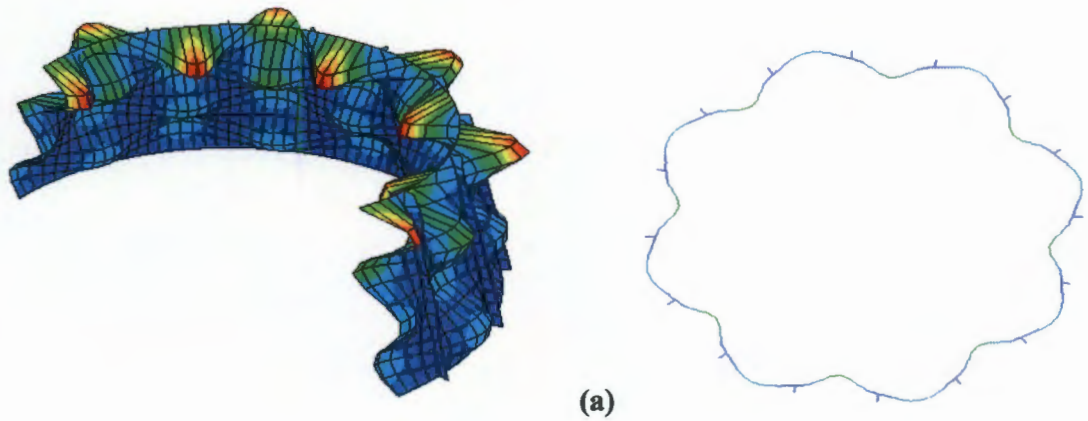

(a)

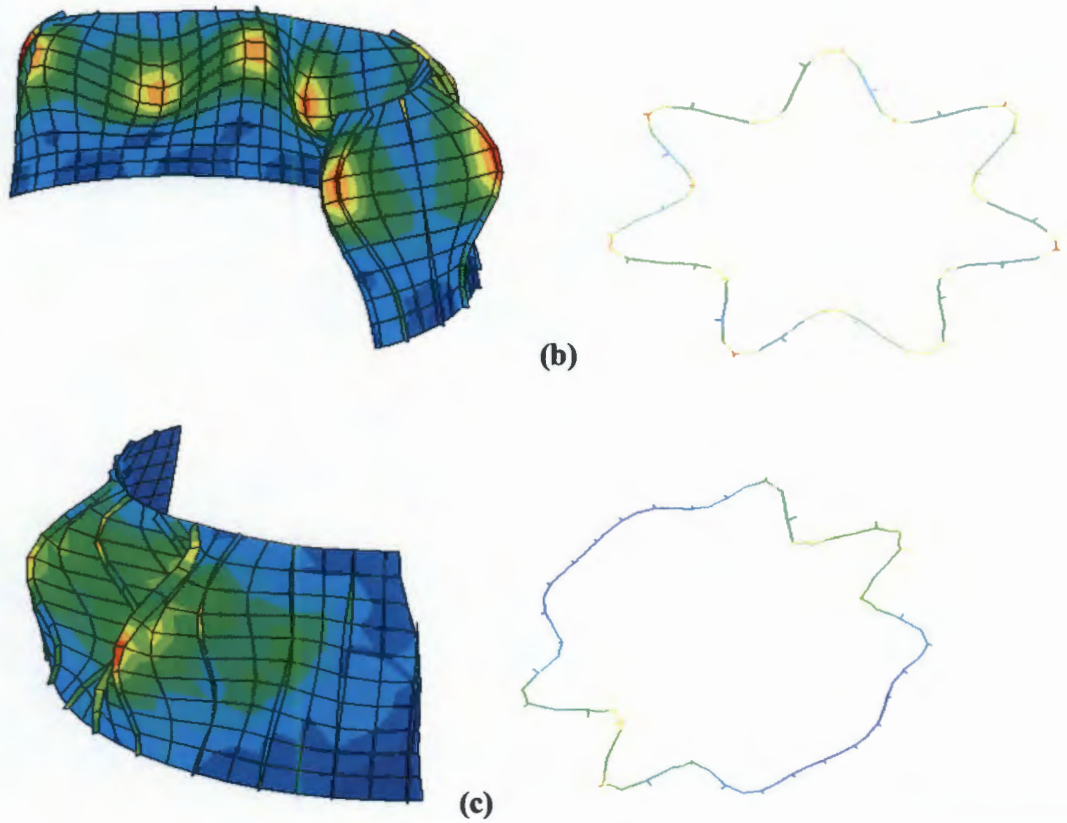

Fig. 6. 20 Deformed shapes of elastic buckled conical frustum subjected to (a) axial compression (b) external pressure (c) shear load

6.4.4.2 Variation of elastic buckling load for conical frustum of varying R/t and number of stiffeners (N).

Both the R/t ratio and panel width are varied while the slenderness ratio of the stiffeners is kept constant (d/b=5), to investigate the variation of elastic buckling load on conical frusta. The results obtained for different load configurations are presented in Fig. 6.21 to 6.23.

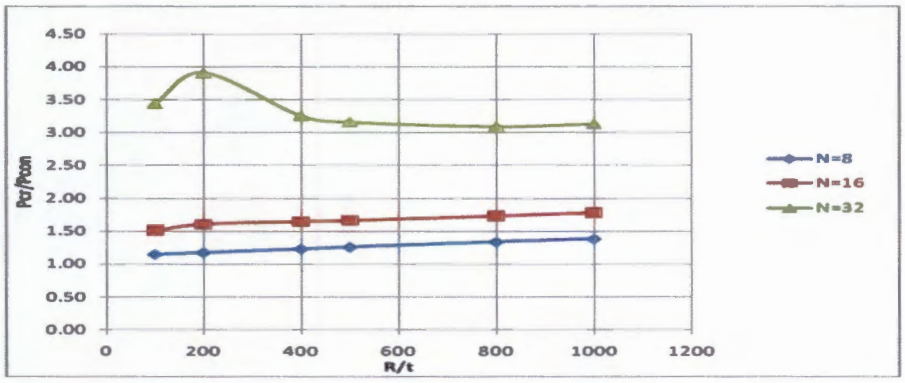

Fig. 6. 21 Axial compression: normalized elastic buckling strength vs R/t

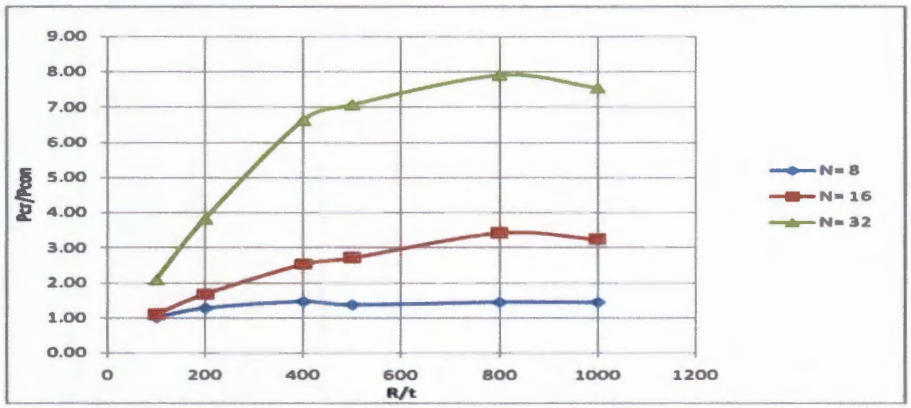

Fig. 6. 22 External pressure: normalized elastic buckling strength vs R/t

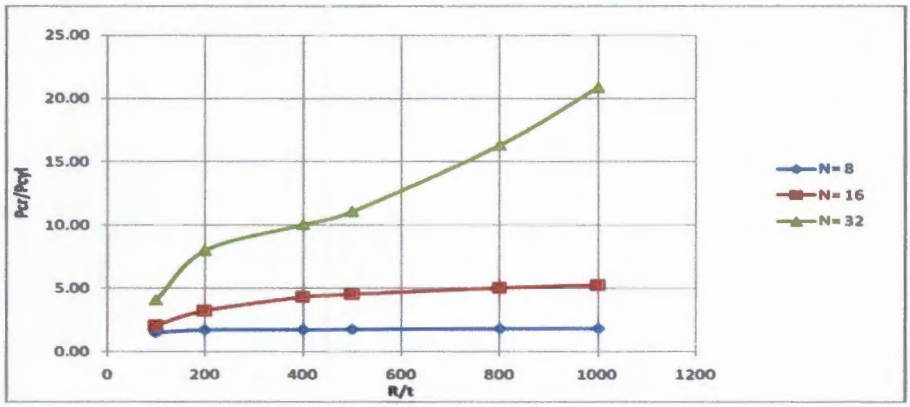

Fig. 6. 23 Shear: normalized elastic buckling strength vs R/t

6.4.4.3 Effect of varying stringer slenderness (d/b) on elastic buckling loads on conical frustum of varying R/t.

Effect of varying stiffener slenderness on elastic buckling load of stiffened conical shells with fixed number of stiffeners (N=16) was assessed. For different load cases, results are presented in Fig. 6.24 to 6.26.

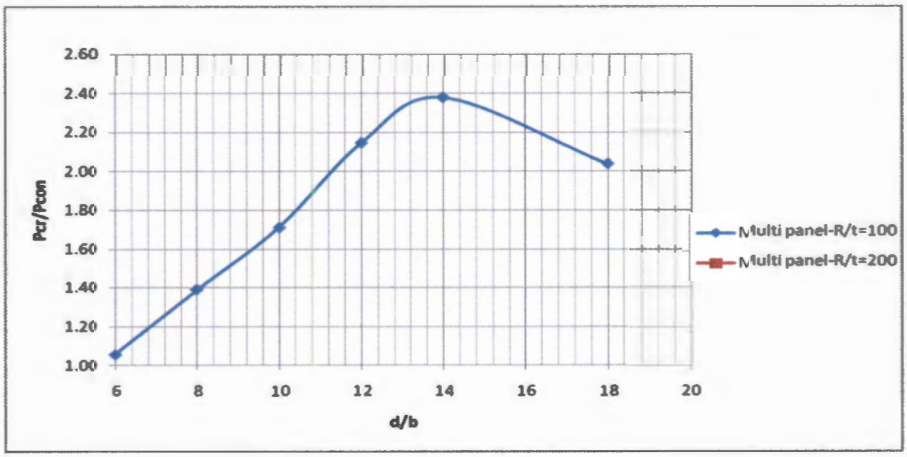

Fig. 6. 24 Axial compression: normalized elastic buckling strength vs stringer slenderness (d/b)

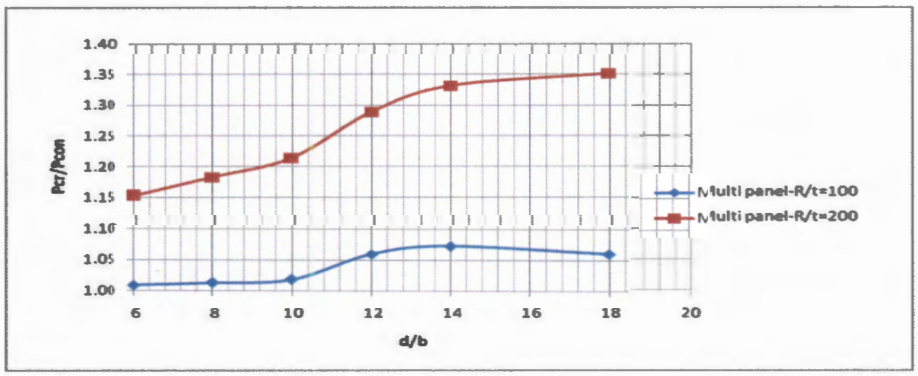

Fig. 6. 25 External pressure: normalized elastic buckling strength vs stringer slenderness (d/b)

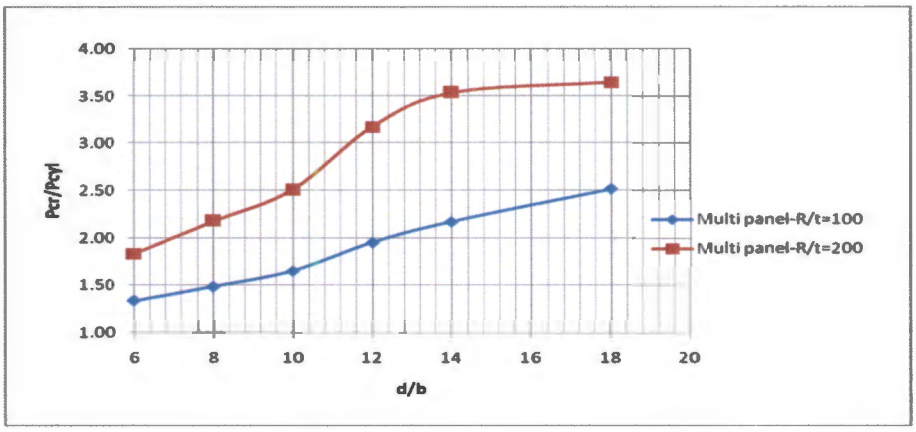

Fig. 6. 26 Shear: normalized elastic buckling strength vs stringer slenderness (d/b)

6.4.4.4 Effect of varying stringer slenderness (d/t) on elastic buckling loads of conical frustum.

Fig. 6.27 to 6.29 shows results of the effects of ratio of shell thickness to stiffener depth on the buckling load of conical shells subjected to different load configurations.

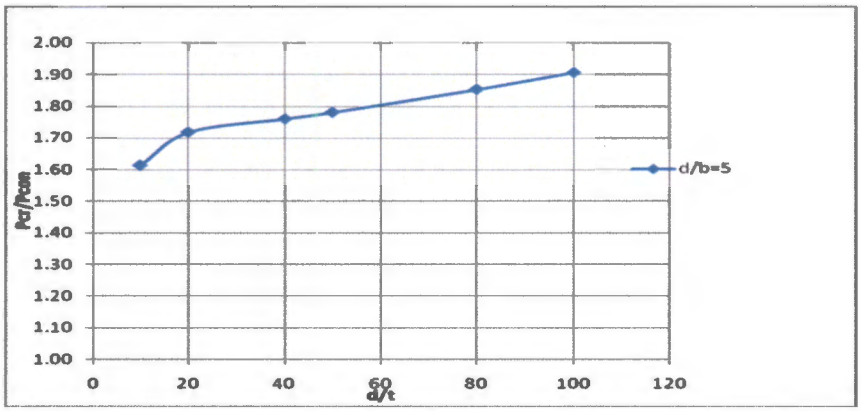

Fig. 6. 27 Axial compression: normalized elastic buckling strength vs stringer slenderness (d/t)

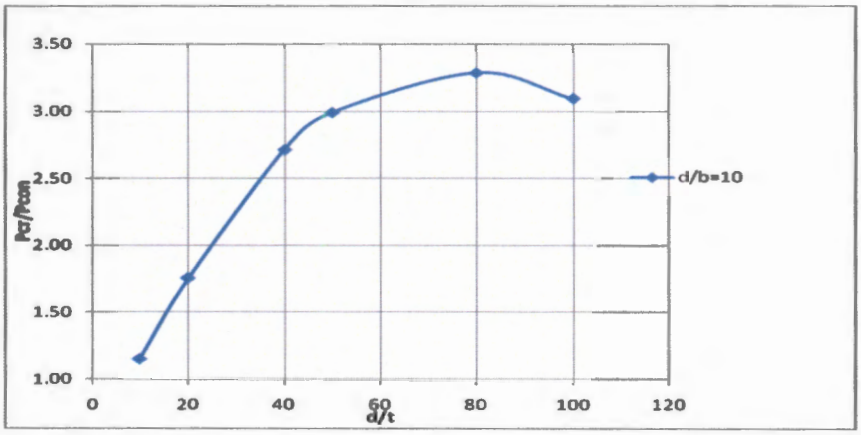

Fig. 6. 28 External pressure: normalized elastic buckling strength vs stringer slenderness (d/t)

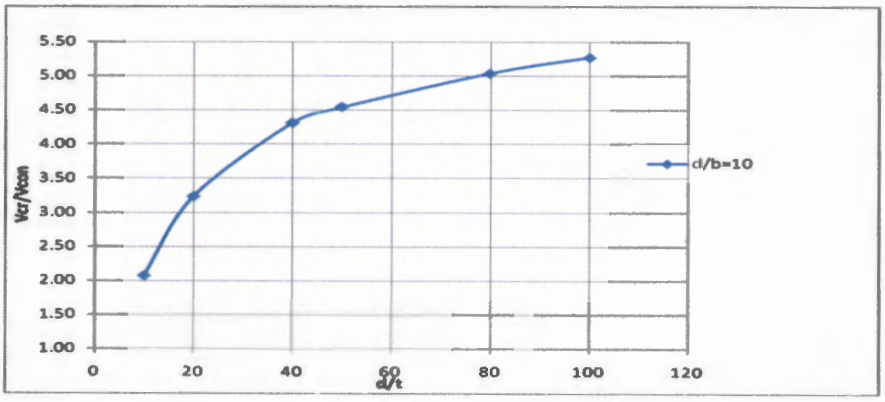

Fig. 6. 29 Shear: normalized elastic buckling strength vs stringer slenderness (d/t)

6.4.5 Circumferentially stiffened conical shell frustum

6.4.5.1 Deformed shapes of elastic buckled conical shell frustum subjected to various load cases

Different deformed shapes of buckled ring stiffened conical shells subjected to different load cases are shown in Fig.6.30(a-c).

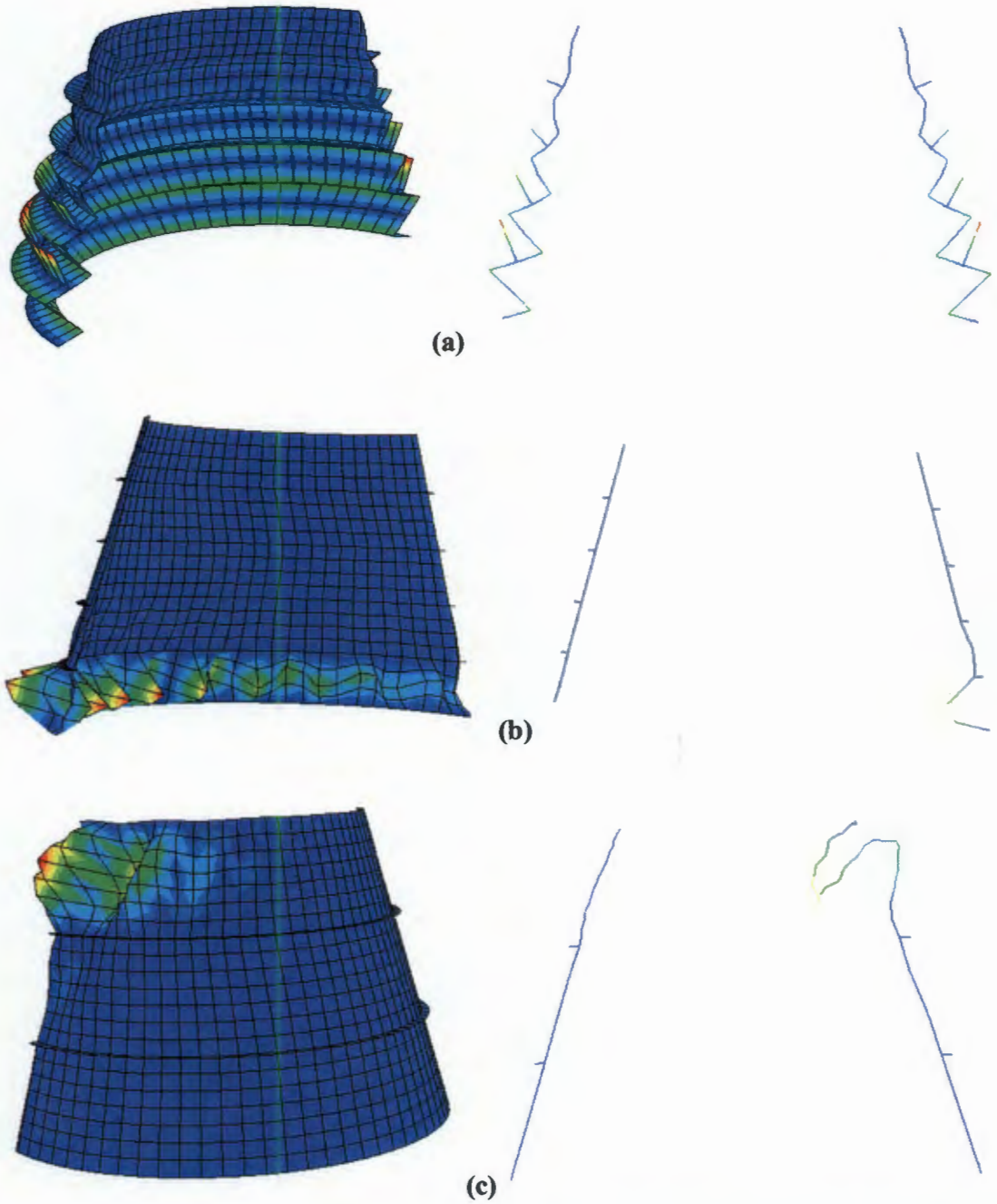

Fig. 6. 30 Deformed shapes of elastic buckled cylinders subjected to (a) axial compression (b) external pressure (c) shear load

6.4.5.2 Variation of elastic buckling load for conical frustum of varying R/t and number of stiffeners (N).

For different panel lengths, elastic buckling load was investigated for conical shells with different R/t ratios. Results are presented for these conical shells for different load configurations in Fig.6.31 to 6.33.

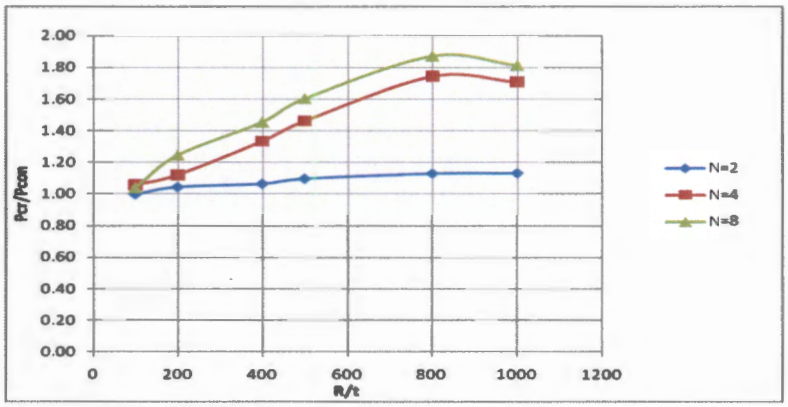

Fig. 6. 31 Axial compression: normalized elastic buckling strength vs R/t

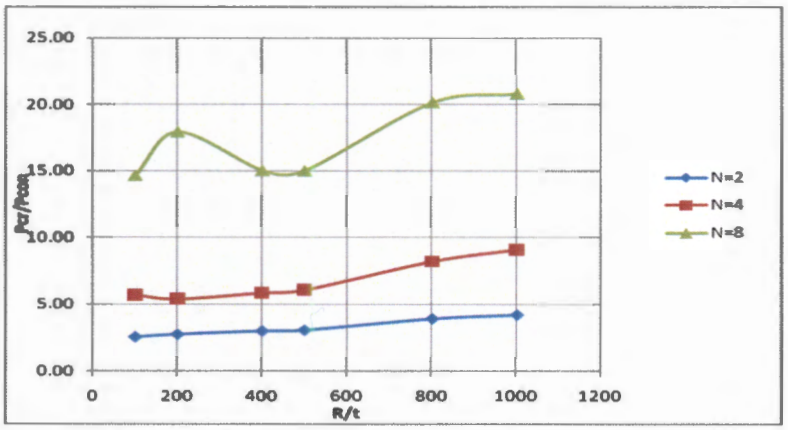

Fig. 6. 32 External pressure: normalized elastic buckling strength vs R/t

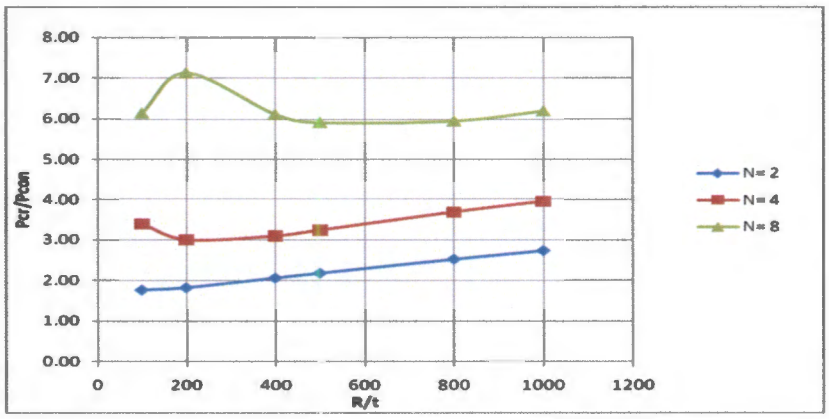

Fig. 6. 33 Shear: normalized elastic buckling strength vs R/t

6.4.5.3 Effect of varying ring stiffener slenderness (d/b) on elastic buckling loads on conical frustum of varying R/t.

Fig.6.34 to 6.36 shows the effect of varying ring stiffener slenderness on elastic buckling load, for different load cases.

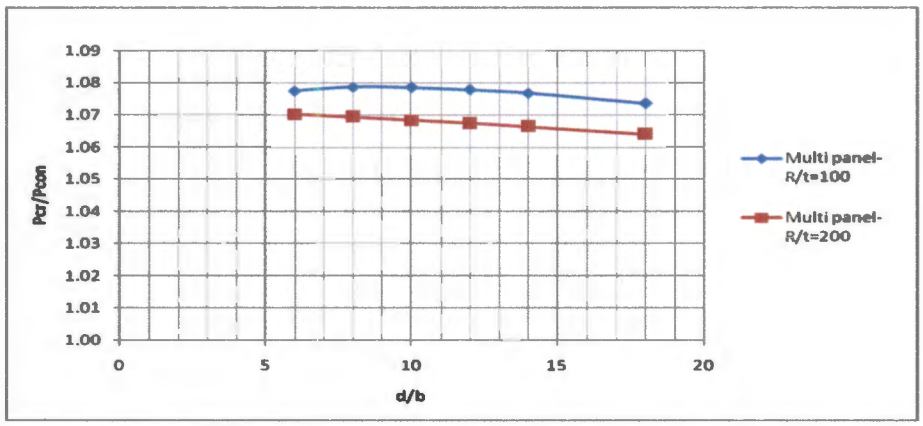

Fig. 6. 34 Axial compression: normalized elastic buckling strength vs stiffener slenderness (d/b)

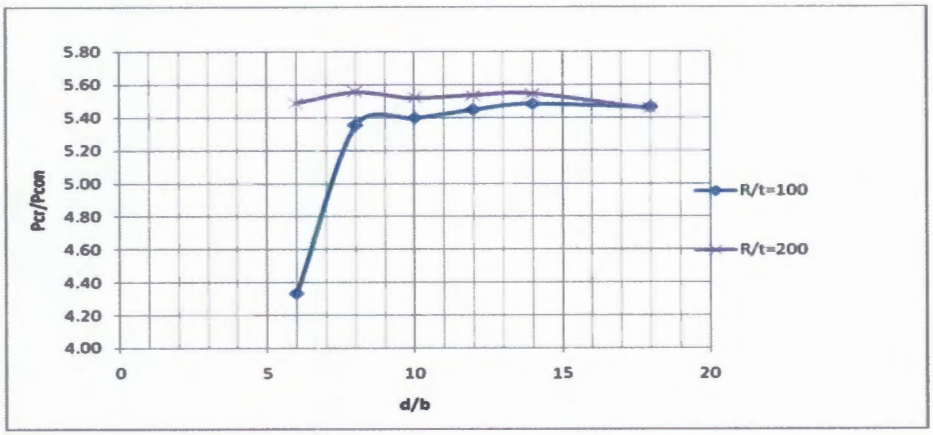

Fig. 6. 35 External pressure: normalized elastic buckling strength vs stiffener slenderness (d/b)

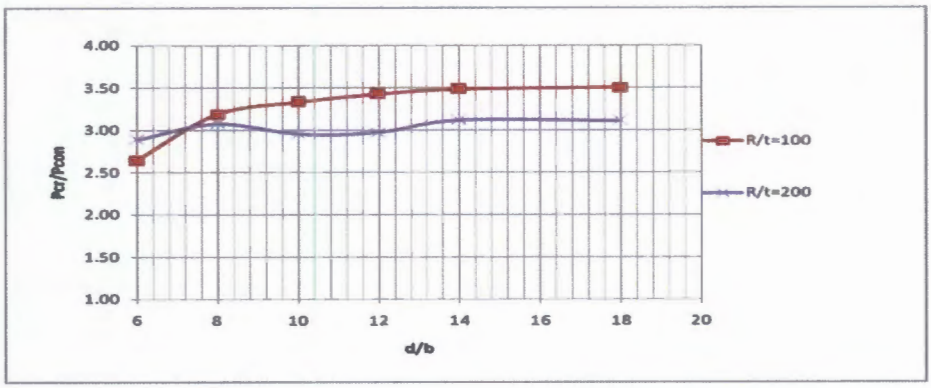

Fig. 6. 36 Shear: normalized elastic buckling strength vs stiffener slenderness (d/b)

6.4.5.4 Effect of varying ring stiffener slenderness (d/t) on elastic buckling loads of conical frustum.

The effect of varying stringer slenderness (d/t) on elastic buckling loads of conical frustum under different load cases is shown in graphs in Fig.6.37 to 6.39.

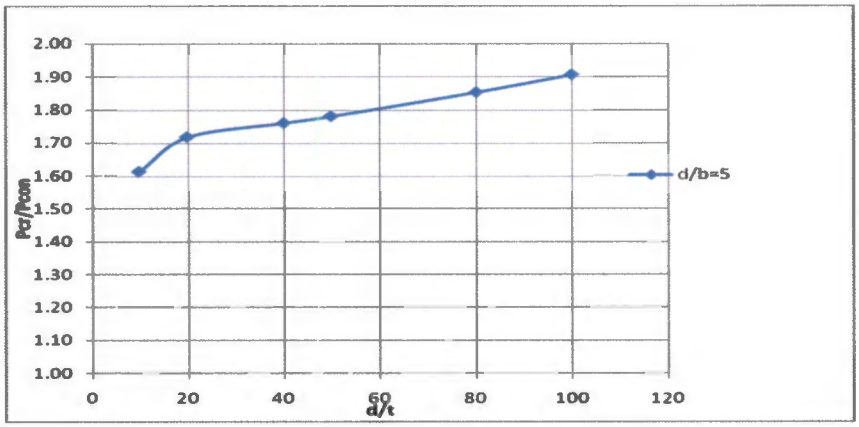

Fig. 6. 37 Axial compression: normalized elastic buckling strength vs stiffener slenderness (d/t)

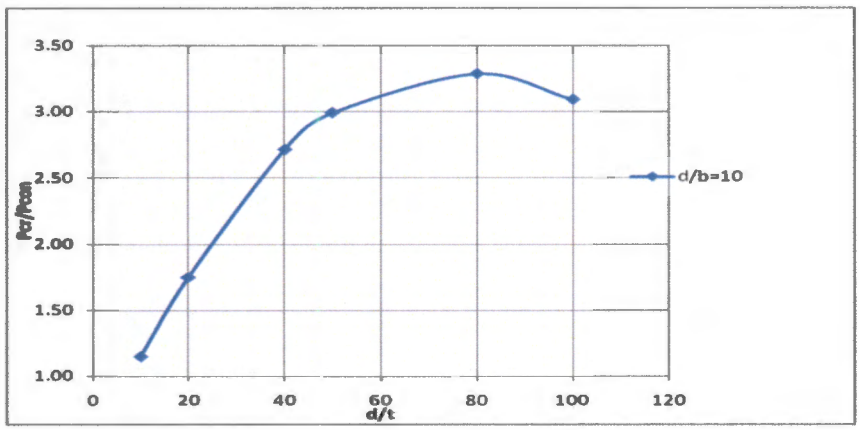

Fig. 6. 38 External pressure: normalized elastic buckling strength vs stiffener slenderness (d/t)

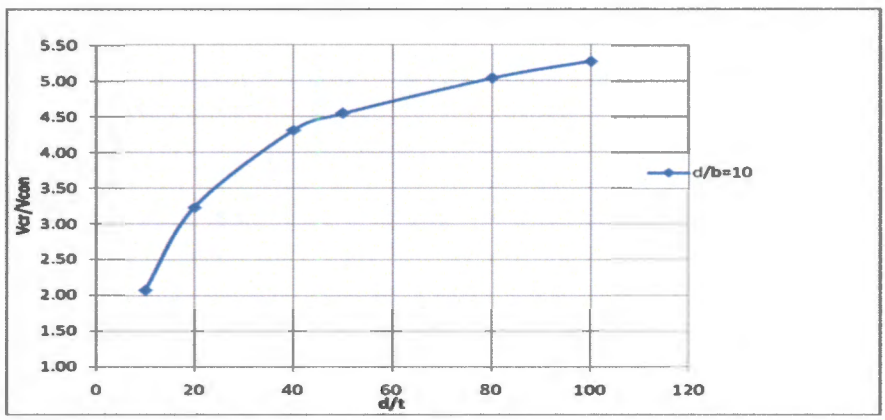

Fig. 6. 39 Shear: normalized elastic buckling strength vs stiffener slenderness (d/t)

6.5 Effect of varying key parameters of stiffened cylindrical shells on buckling modes

6.5.1 Introduction

Elastic buckling loads, normalized with respect to the classical buckling load for un-stiffened cylinders (P_{cyl}) for different buckling modes are presented against different parameters for cylindrical and conical shells.

6.5.2 Stringer stiffened cylindrical shells under axial compression

Results from an investigation of the dominance of certain buckling modes as parameters of axially compressed stringer stiffened cylindrical shells varies, are presented from sections 6.5.2.1 to 6.5.2.4.

6.5.2.1 Buckling mode shape for stiffened cylinders subjected to axial compression

A typical buckling mode shape is shown in Fig. 6.40 for a stringer stiffened cylinder subjected to axial compression.

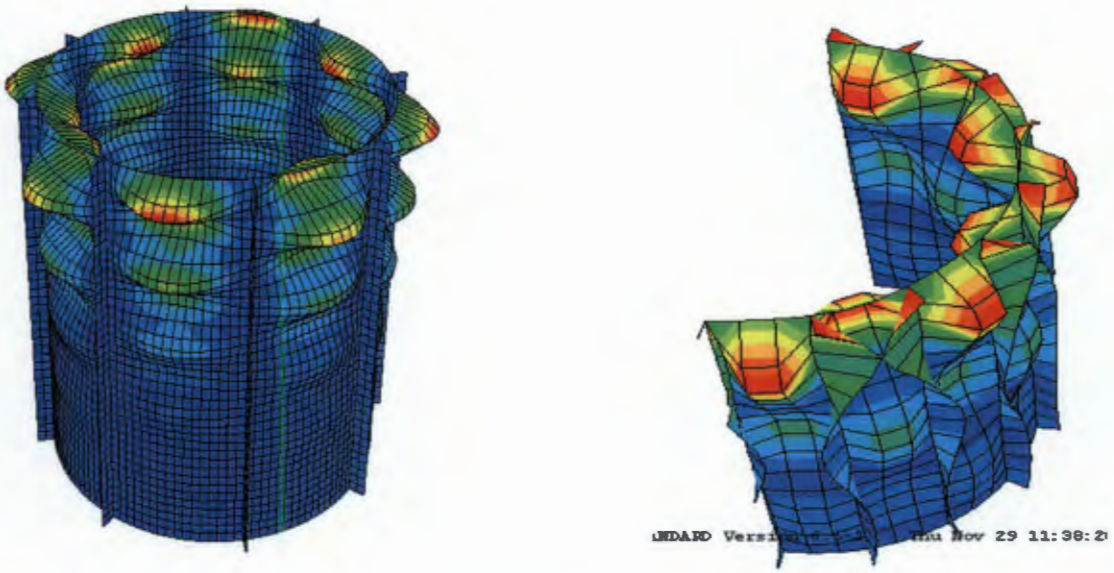

Fig. 6. 40 Deformed shape of stiffened cylinders subjected to axial compression

6.5.2.2 Stringer and local shell modes

Results of an investigation of stringer and local shell modes are presented in Fig. 6.41.

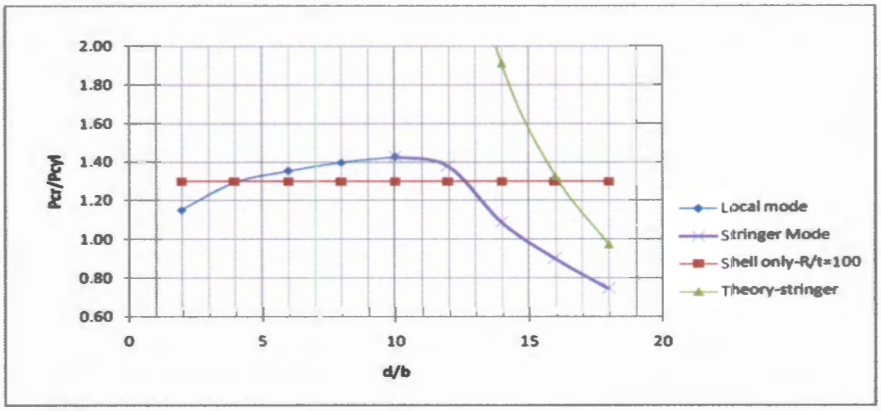

Fig. 6. 41 Axial compression: Normalised Buckling load vs d/b

6.5.2.3 Local shell and global modes

The influence of number of stiffeners (N) on the dominant mode is illustrated in Fig. 6. 42 ,where the results for a stringer stiffened cylinder under axial compression are presented.

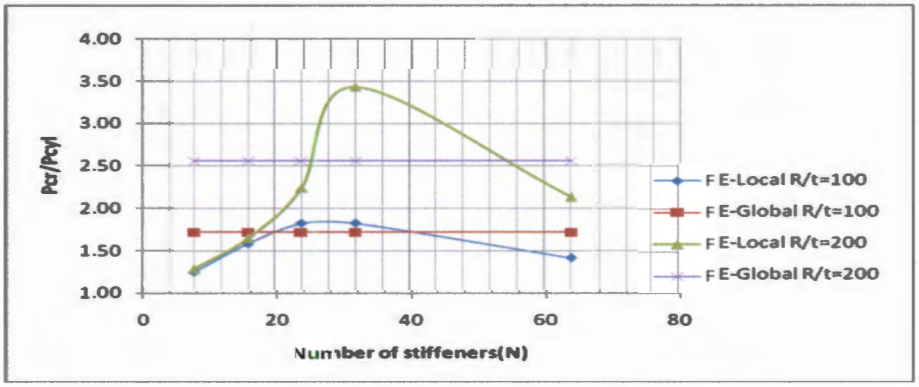

Fig. 6. 42 Axial compression: Normalised Buckling load vs N

6.5.2.4 Effect of varying stringers slenderness (d/t) on elastic buckling loads cylinders of varying number of stiffeners (N)

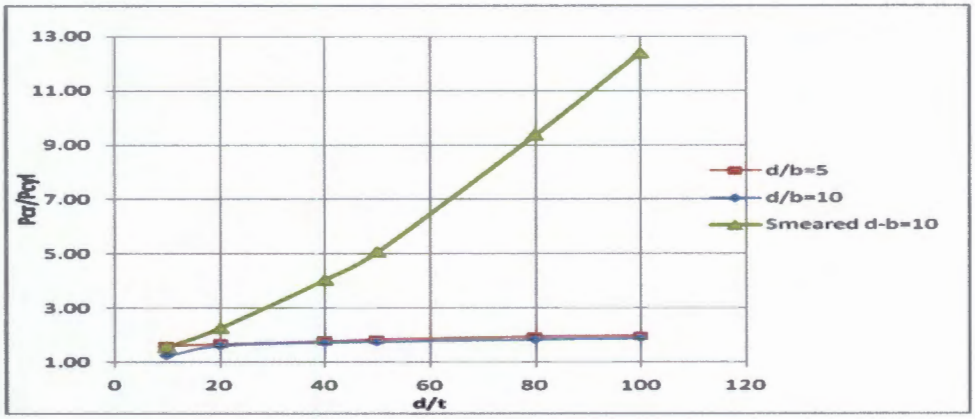

Fig. 6. 43 Axial compression: Normalised Buckling load vs d/t

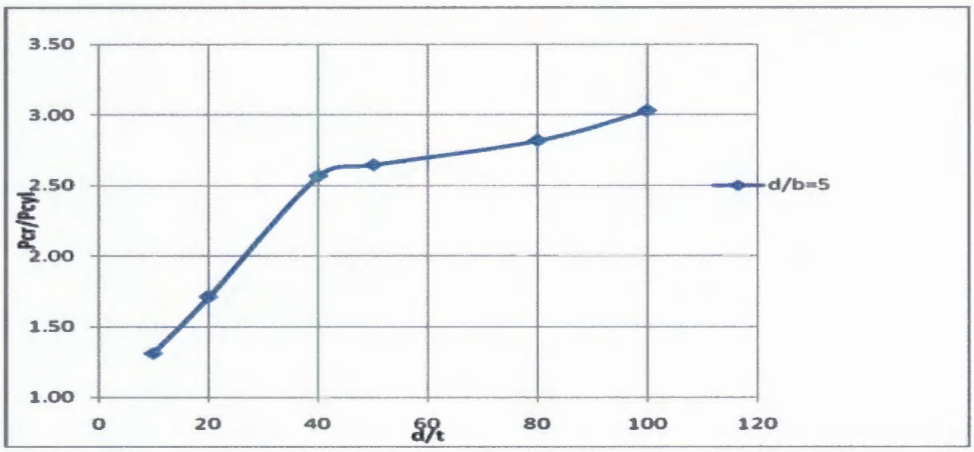

Fig. 6. 44 External pressure: Normalised Buckling load vs d/t

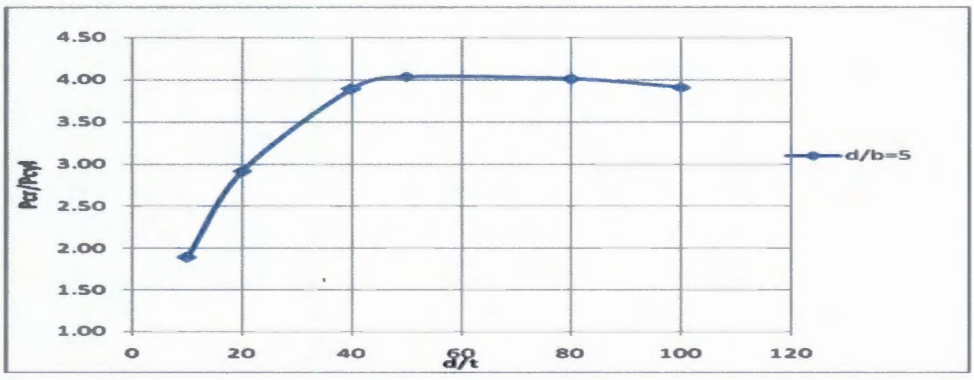

Fig. 6. 45 Shear: Normalised Buckling load vs d/t

6.5.3 Stringer stiffened cylindrical shells under uniform external pressure

Results from an investigation of the buckling behavior of meridionally stiffened cylinders loaded with a uniform external pressure are presented from section 6.5.3.1 to 6.5.3.3.

6.5.3.1 Deformed shapes of different buckling modes for stiffened cylinders subjected to various load cases

A typical buckling mode of a stringer stiffened cylindrical shell under uniform external pressure is shown in Fig. 6. 46.

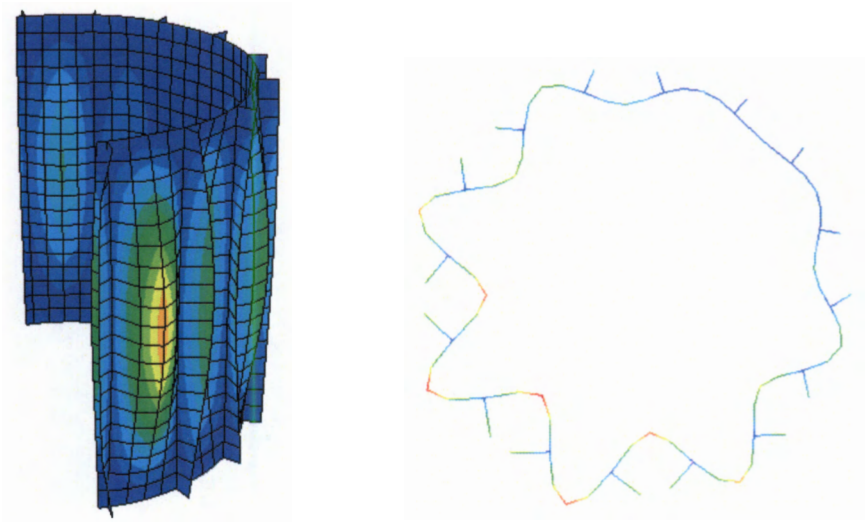

Fig. 6. 46 Deformed shape of stiffened cylinders subjected to axial compression

6.5.3.2 Panel and local shell modes

Buckling behavior of meridionally stiffened cylindrical shells as slenderness of the stiffener varies is investigated and the results are shown in Fig. 6. 47.

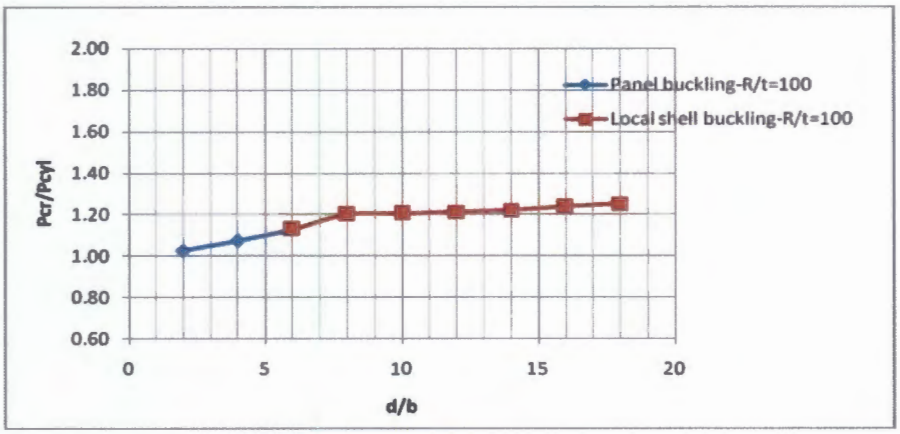

Fig. 6. 47 External pressure: Normalised Buckling load vs d/b

6.5.3.3 Global and local shell modes

Changeover of buckling modes of stringer stiffened cylinders is captured by varying the number of stiffeners, thus panel width and the results are presented in Fig. 6. 48.

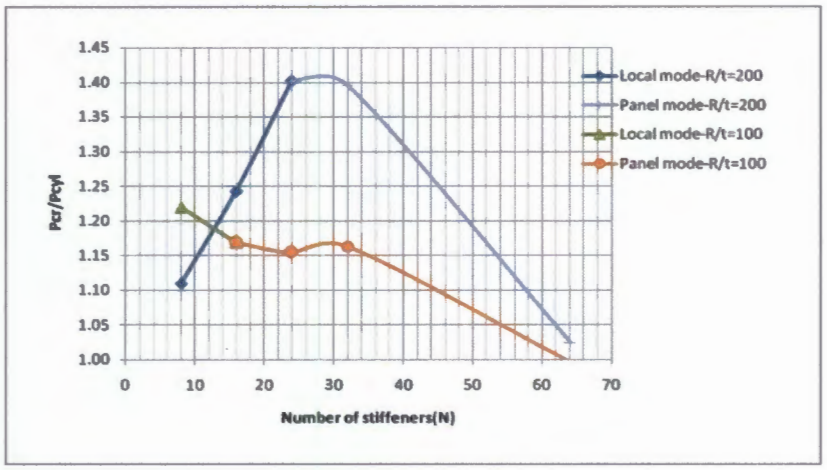

Fig. 6. 48 External pressure: Normalised Buckling load vs N

6.5.4 Stringer stiffened cylindrical shells under shell edge shear load

Results from an investigation of buckling modes of stringer stiffened cylindrical shells under a shell edge shear load are presented from section 6.5.4.1 to 6.5.4.3.

6.5.4.1 Deformed shapes of different buckling modes for stiffened cylinders subjected to shear load

A common buckling mode shape of stringer stiffened cylinders subjected to shell edge shear load is shown in Fig. 6. 49.

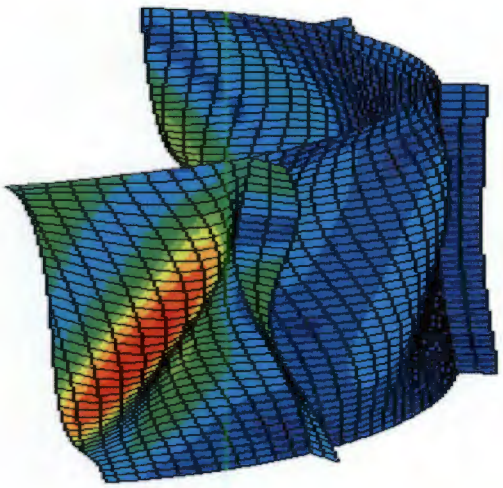

Fig. 6. 49 Deformed shape of stringer stiffened cylinders subjected to shell edge shear load

6.5.4.2 Stringer and local shell modes

Slenderness ratio of stringer of cylindrical shells is varied to note how the buckling mode changes under shell edge shear load. The results are shown in Fig. 6. 50.

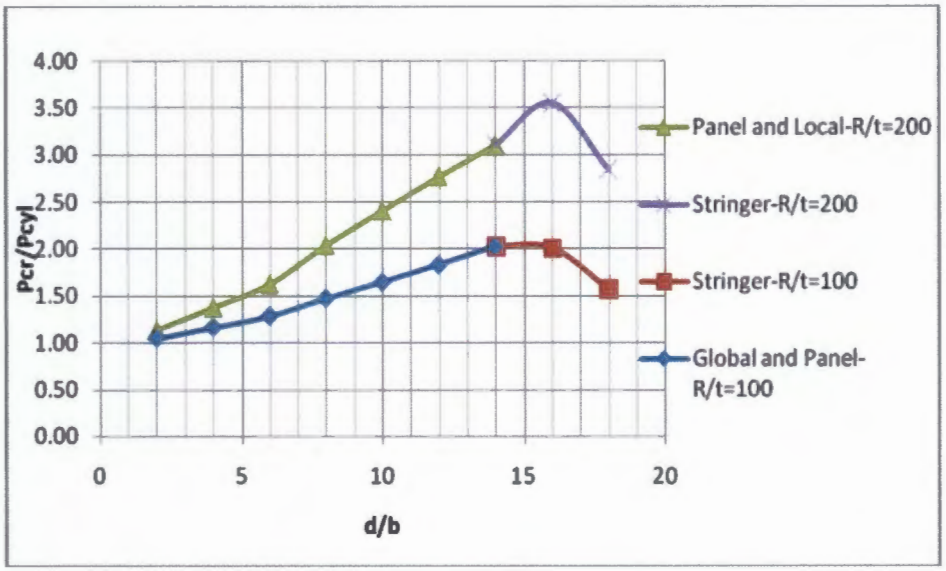

Fig. 6. 50 Shear: Normalised Buckling load vs d/b

6.5.4.3 Global and local shell modes

Panel width is varied by varying the number of stiffeners on the cylindrical shell subjected to shear load to investigate how this affects the shell buckling mode shapes. The results are presented in Fig. 6. 51.

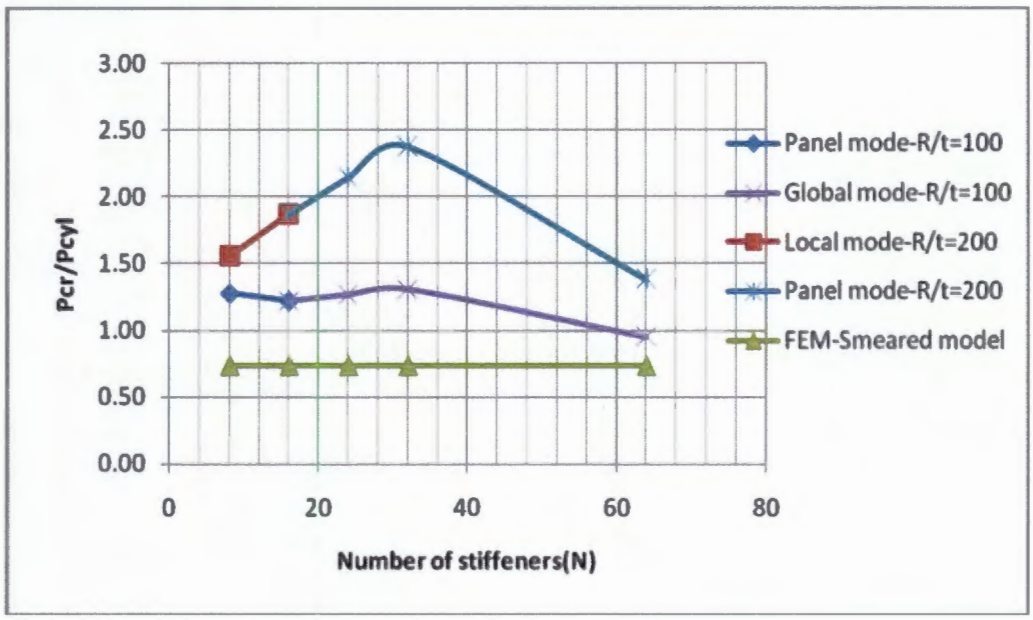

Fig. 6. 51 Shear: Normalised Buckling load vs N

6.5.5 Ring stiffened cylindrical shells under axial compression

Results from an investigation of influence of different parameters on buckling behavior of ring stiffened cylindrical shell under axial compression are presented from section 6.5.5.1 to 6.5.5.3.

6.5.5.1 Deformed shapes of different buckling modes for stiffened cylinders subjected to various load cases

A buckling mode shape peculiar to circumferentially stiffened shells under axial compression is shown in Fig. 6. 52.

Fig. 6. 52 Deformed shape of ring stiffened cylinders subjected to axial compression

6.5.5.2 Stringer and local shell modes

Results in Fig. 6. 53 show the variation of buckling modes as ring slenderness varies for cylinders under axial compression.

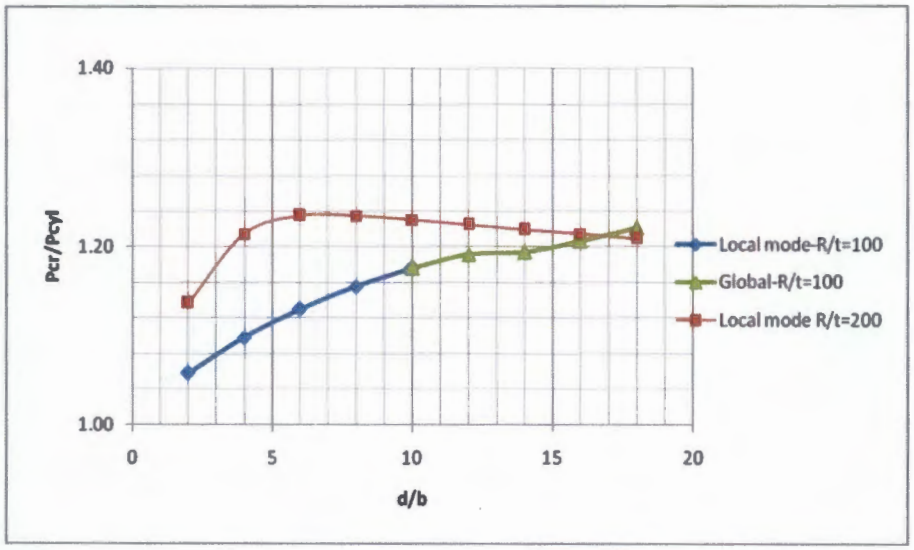

Fig. 6. 53 Axial compression: normalized elastic buckling strength vs stringer slenderness (d/b)

6.5.5.3 Global and local shell modes

Fig. 6. 54 show the influence of number of stiffeners (N) buckling mode on the buckling behavior of ring stiffened cylindrical shells.

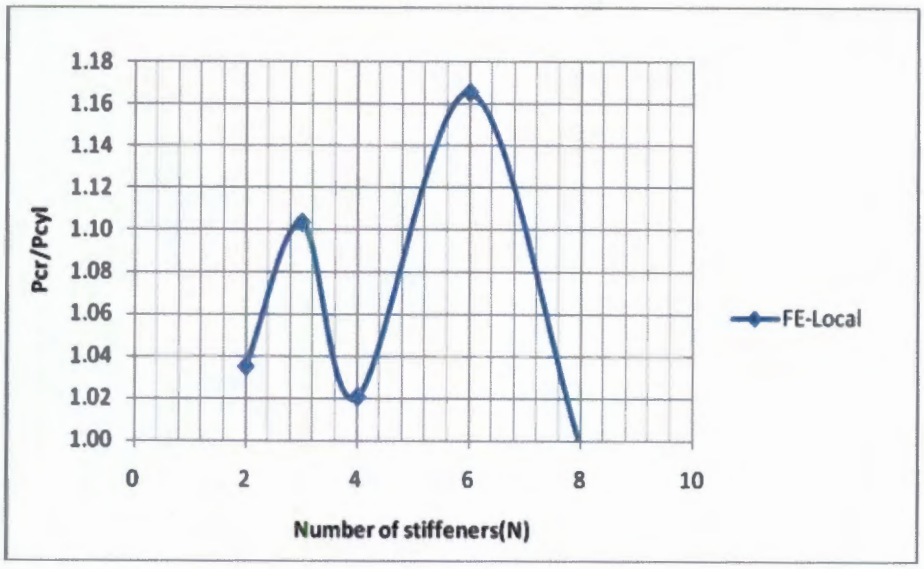

Fig. 6. 54 Axial compression: normalized elastic buckling strength vs number of stiffeners (N)

6.5.6 Ring stiffened cylindrical shells under external pressure

6.5.6.1 Deformed shapes of different buckling modes of ring stiffened cylinders subjected to uniform external load.

Various buckling mode shapes of ring stiffened cylinders subjected to external pressure are shown if Fig. 6. 55.

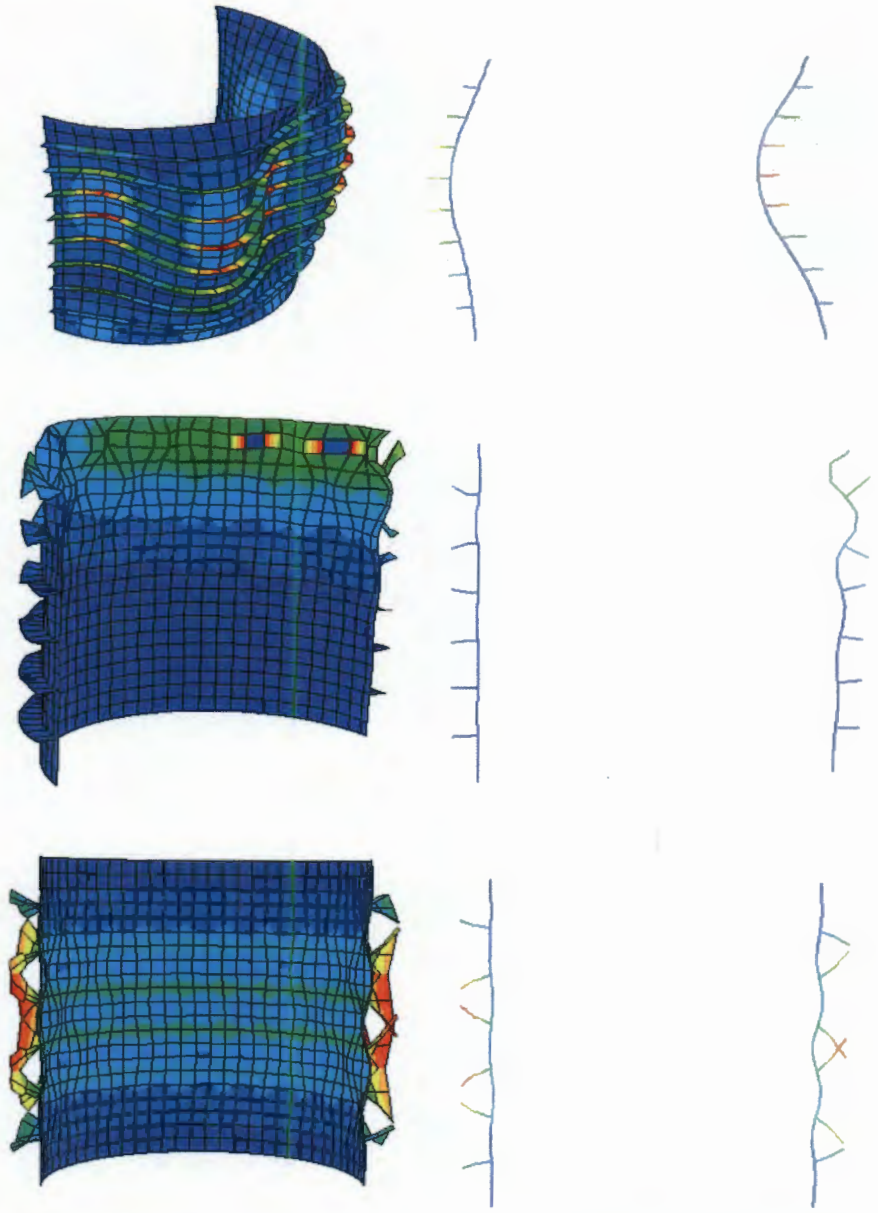

Fig. 6. 55 Deformed shape of stringer stiffened cylinders subjected to external pressure

6.5.6.2 Panel and local shell modes

The change over from panel to local shell buckling mode is captured by varying the d/b ratio of the ring stiffener and results are shown in Fig. 6. 56.

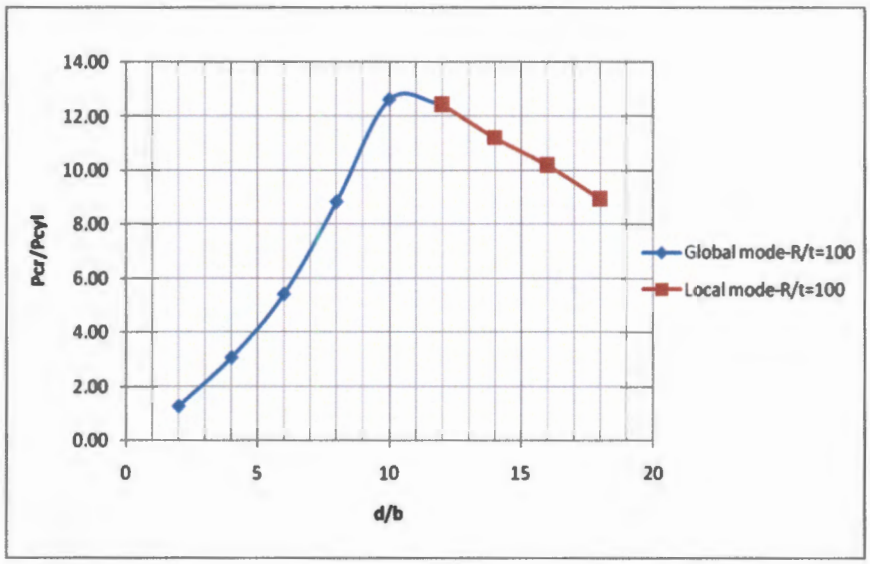

Fig. 6. 56 External pressure: normalized elastic buckling strength vs stringer slenderness (d/b)

6.5.6.3 Global and local shell modes

In Fig. 6. 57, the change between local shell and global mode is shown for ring stiffened cylinders by varying number of stiffeners.

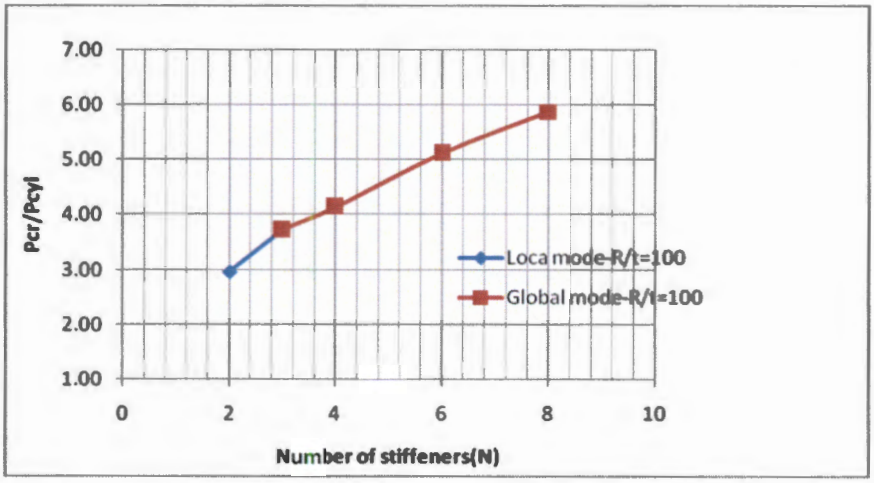

Fig. 6. 57 External pressure: normalized elastic buckling strength vs number of stiffeners (N)

6.5.7 Ring stiffened cylindrical shells under shear load

6.5.7.1 Deformed shapes of different buckling modes for stiffened cylinders subjected to various load cases

Different deformed shapes of ring stiffened cylinders subjected to shell edge shear are shown in Fig. 6. 58.

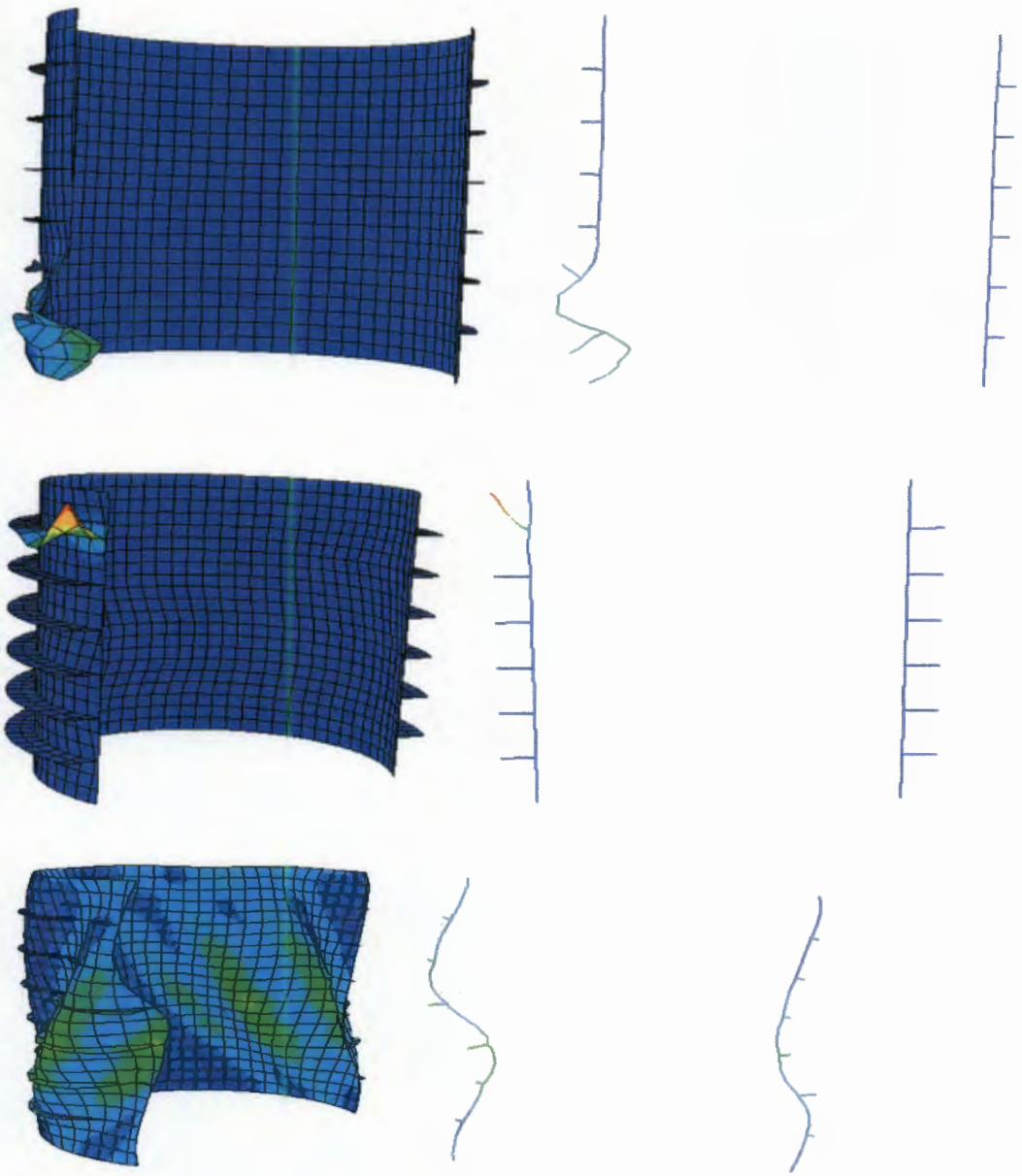

Fig. 6. 58 Deformed shape of ring stiffened cylinders subjected to shell edge shear

6.5.7.2 Stringer and local shell modes

Prevalence of different buckling modes as stiffener slenderness varies is depicted in Fig. 6. 59.

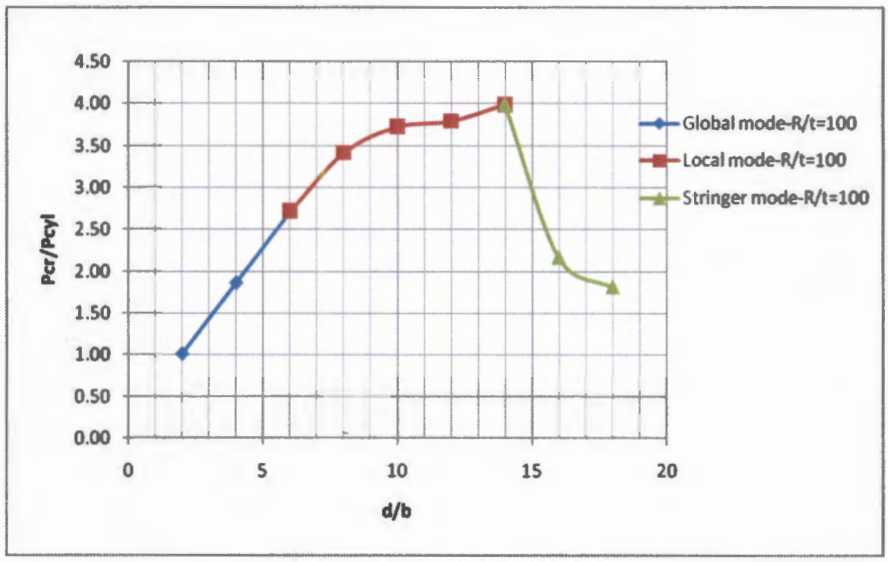

Fig. 6. 59 Shear: normalized elastic buckling strength vs stiffener slenderness (d/b)

6.5.7.3 Global and local shell modes

Fig. 6. 60 shows the buckling behavior of ring stiffened cylindrical shells under shear load as the number of stiffeners vary on the shell.

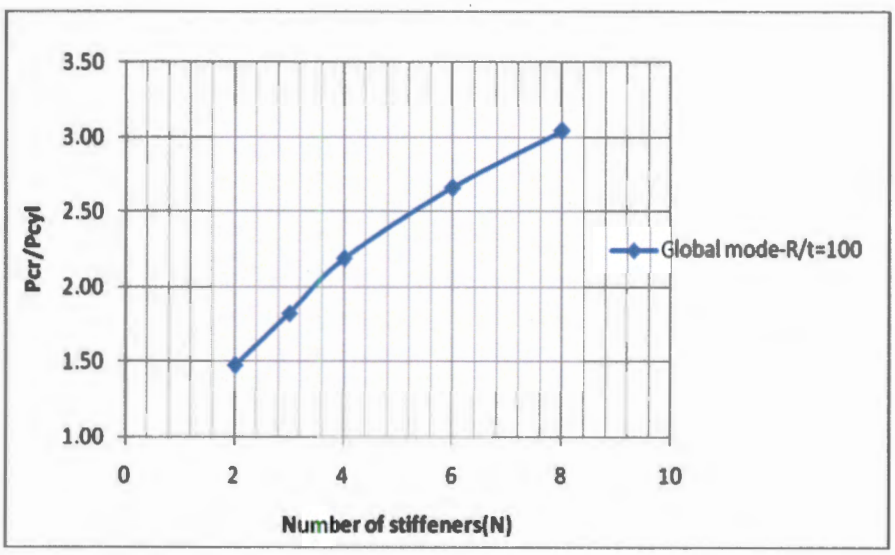

Fig. 6. 60 Shear: normalized elastic buckling strength vs number of stiffeners (N)

6.6 Effect of varying key parameters of stiffened conical shell frustum on buckling modes

6.6.1 Introduction

Results of the effect of varying key parameters of stiffened conical shell frustum, on buckling modes are presented.

6.6.2 Stringer stiffened conical shell frustum under axial compression

Results of the investigation of stringer stiffened conical shell frustum under axial compression as certain key parameters change are presented from section 6.6.2.1 to 6.6.2.3.

6.6.2.1 Deformed shapes of different buckling modes for stiffened cylinders subjected to axial compression.

Different typical mode shapes of stringer stiffened conical shells under axial load are shown in Fig. 6. 61.

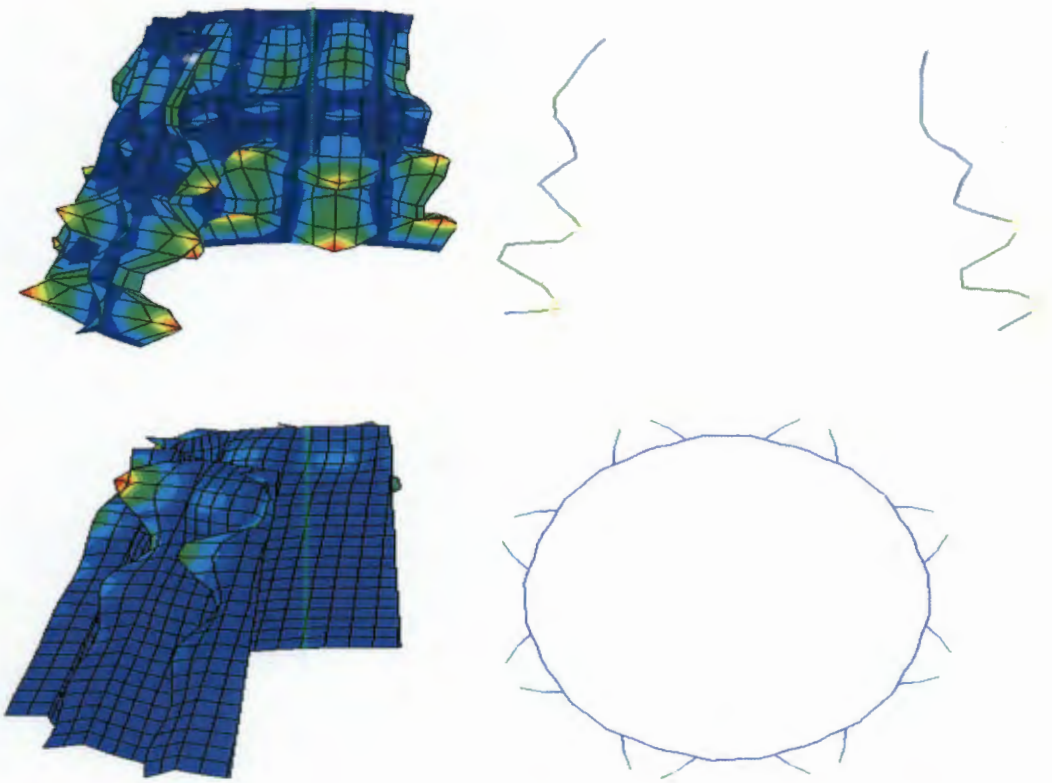

Fig. 6. 61 Deformed shape of stringer stiffened conical shell frustum subjected to axial compression

6.6.2.2 Stringer and local shell modes

Results of an investigation of stringer and local shell modes are presented in Fig. 6. 62.

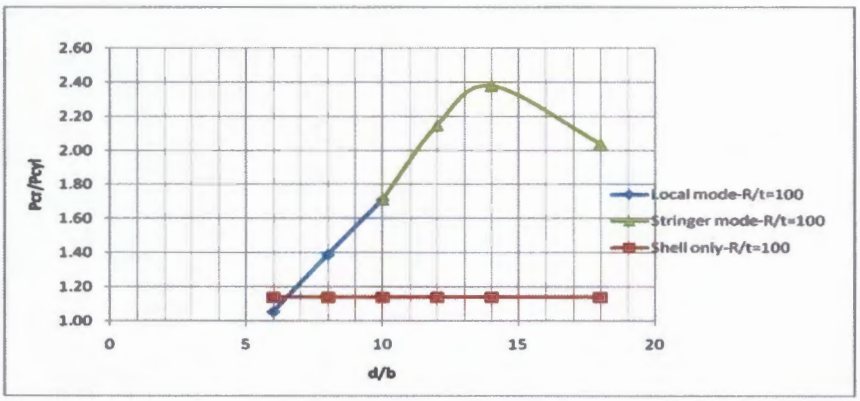

Fig. 6. 62 Axial compression: normalized elastic buckling strength vs stringer slenderness (d/b)

6.6.2.3 Global and local shell modes

The influence of number of stiffeners (N) on the dominant mode is illustrated in Fig. 6. 63, where the results for a stringer stiffened conical frustum under axial compression are presented. Also two extreme cases (N=8 and N=32) were considered for the investigation of tapering angle of the cone in Fig. 6.64.

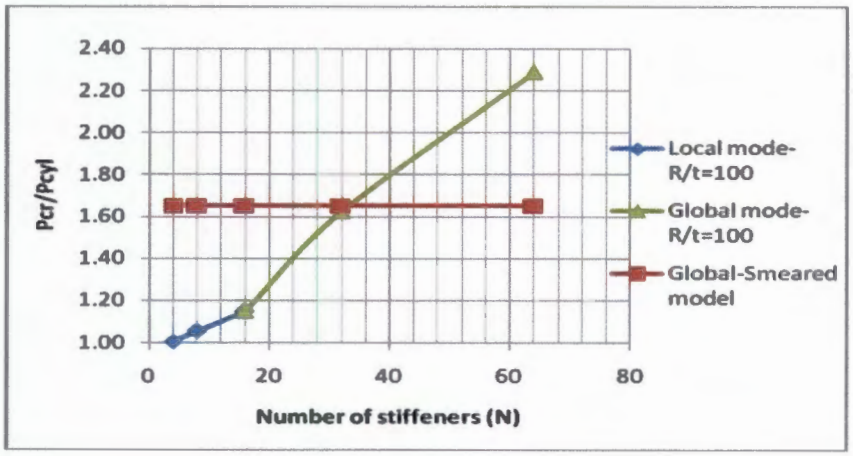

Fig. 6. 63 Axial compression: normalized elastic buckling strength vs number of stiffeners (N)

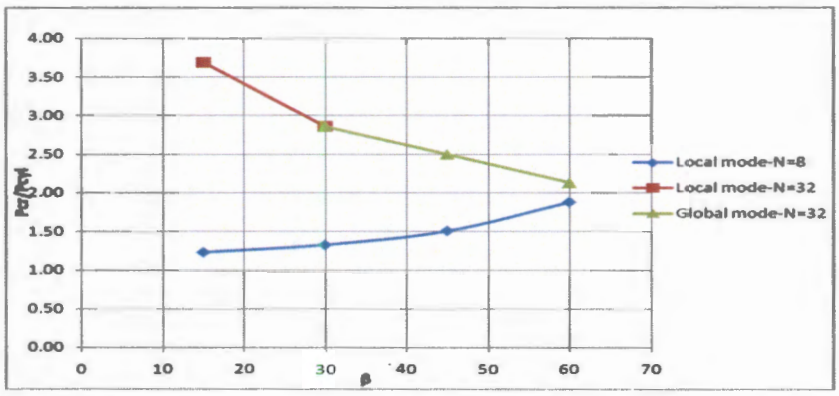

Fig. 6. 64 Axial compression: normalized elastic buckling strength vs tapering angle

6.6.3 Stringer stiffened conical shell frustum under external pressure

In this section, results of prevalence of different buckling modes on a stringer stiffened conical shells under external pressure are presented from section 6.6.3.1 to 6.6.3.3.

6.6.3.1 Deformed shapes of different buckling modes for stiffened conical frustum subjected to uniform external pressure.

A typical buckling mode shape is shown in Fig. 6. 65 for a stringer stiffened conical frustum subjected to axial compression.

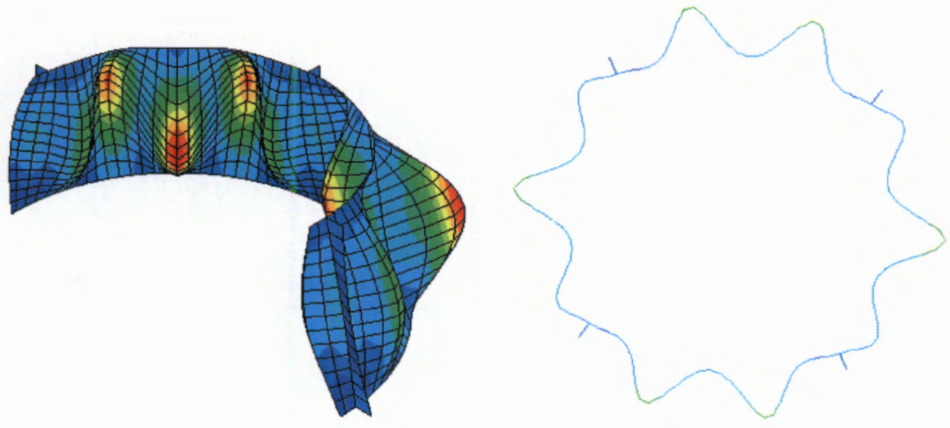

Fig. 6. 65 Deformed shape of stringer stiffened conical shell frustum subjected to external pressure

6.6.3.2 Stringer and local shell modes

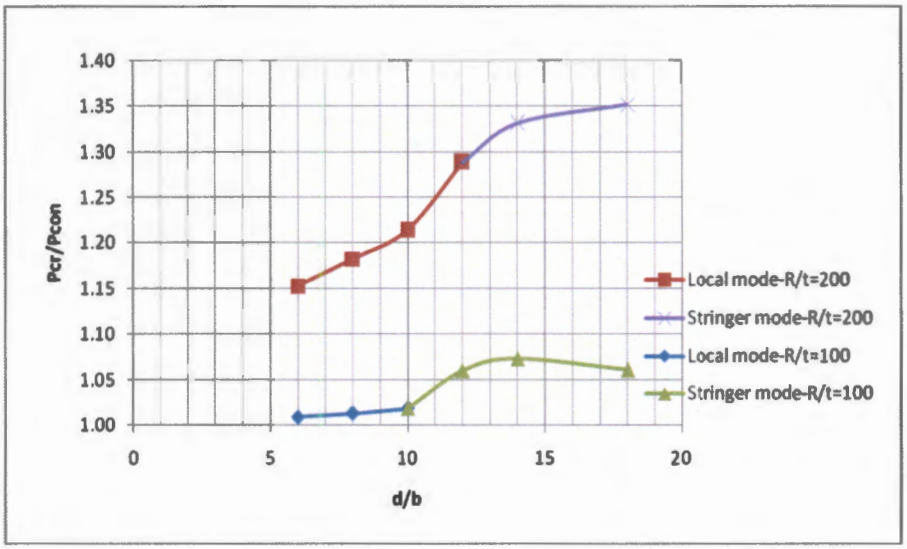

Fig. 6. 66 External pressure: normalized elastic buckling strength vs stringer slenderness (d/b)

6.6.3.3 Global and local shell modes

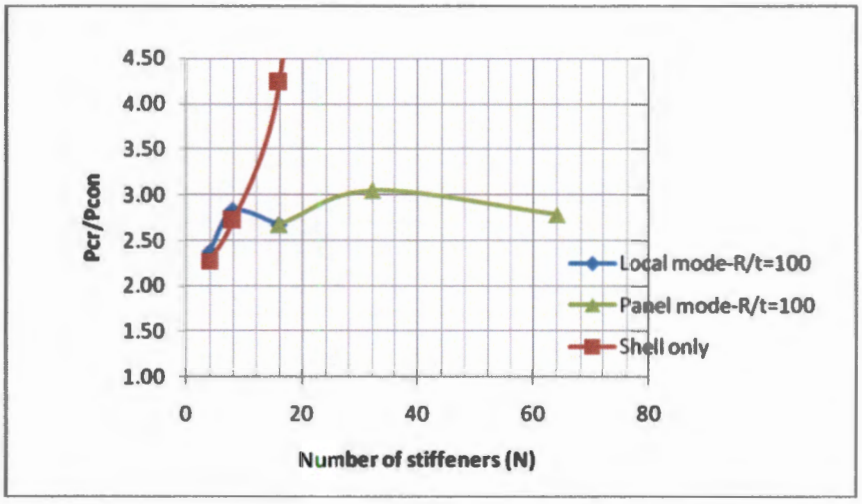

Fig. 6. 67 External pressure: normalized elastic buckling strength vs number of stiffeners (N)

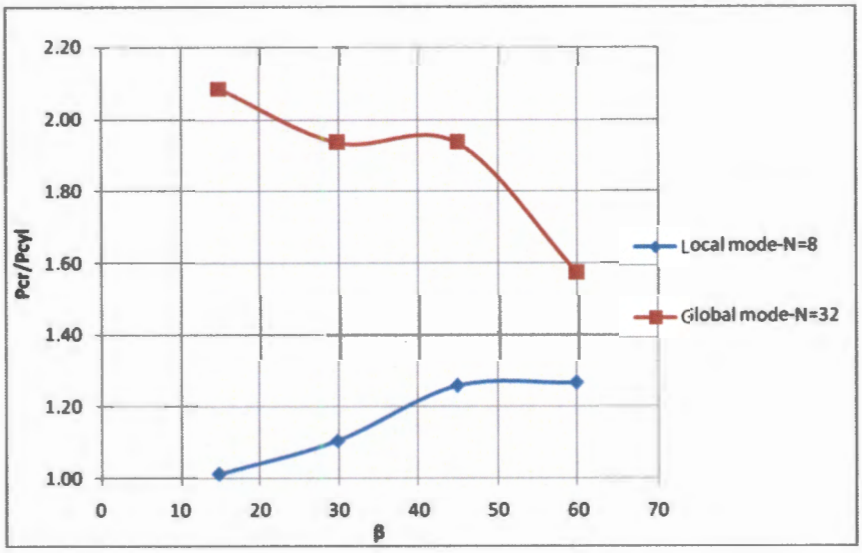

Fig. 6. 68 External pressure: normalized elastic buckling strength vs tapering angle

6.6.4 Stringer stiffened conical shell frustum under shell edge shear

6.6.4.1 Deformed shapes of different buckling modes for stiffened cylinders subjected to various load cases

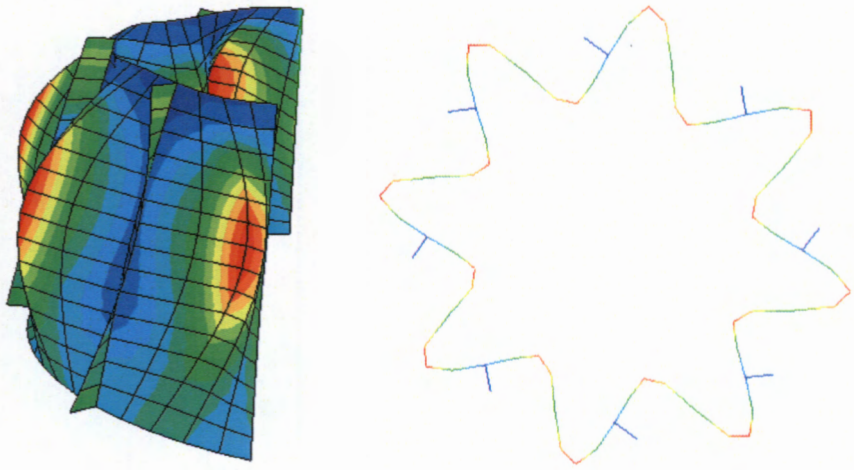

Fig. 6. 69 Deformed shape of stringer stiffened conical shell frustum subjected to shear load

6.6.4.2 Stringer and local shell modes

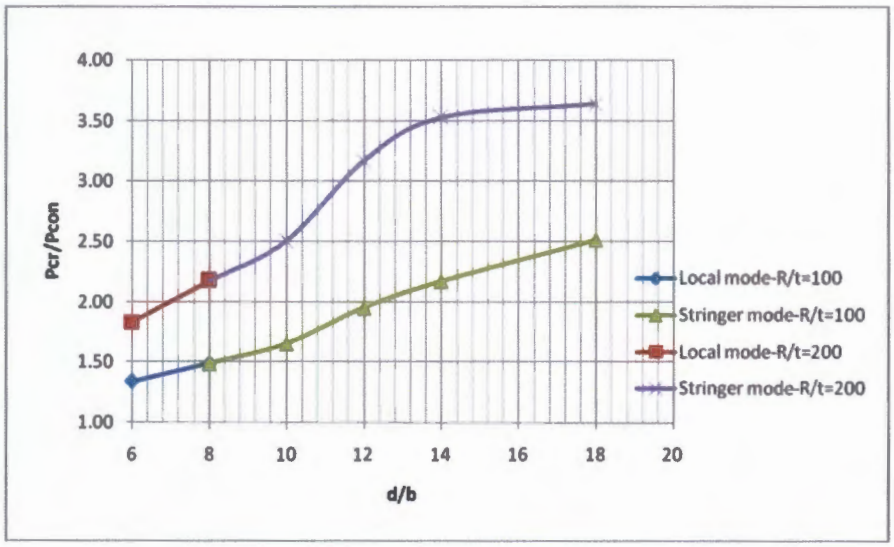

Fig. 6. 70 Shear: normalized elastic buckling strength vs stringer slenderness (d/b)

6.6.4.3 Global and local shell modes

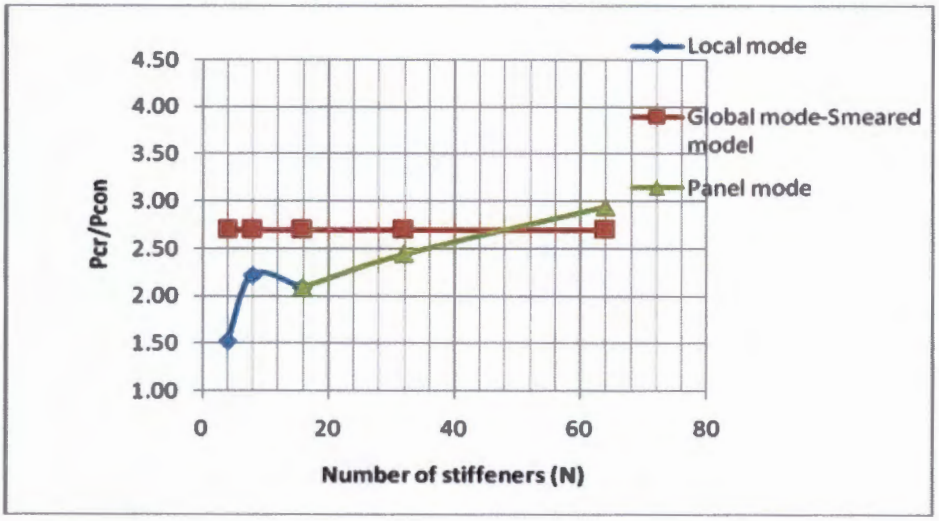

Fig. 6. 71 Shear: normalized elastic buckling strength vs number of stiffeners (N)

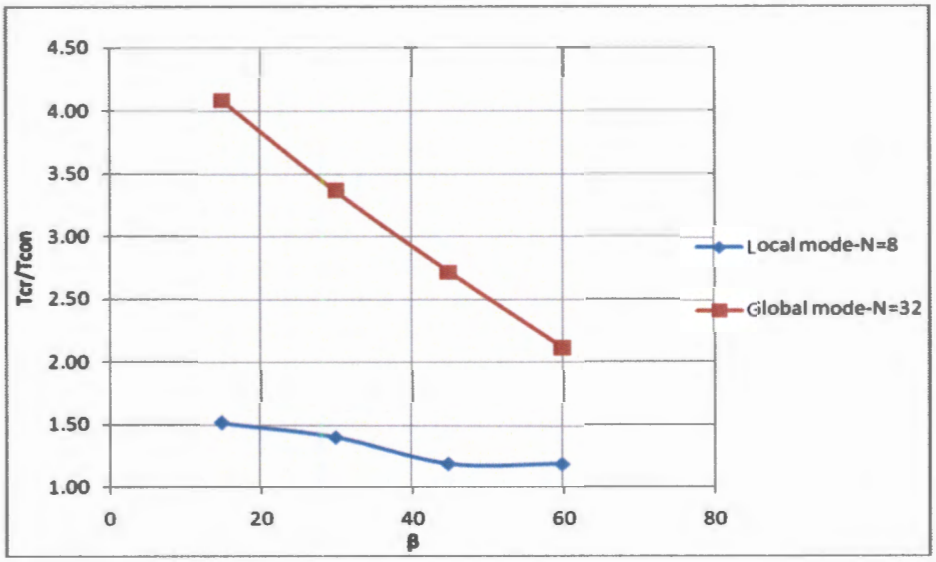

Fig. 6. 72 Shear: normalized elastic buckling strength vs tapering angle

6.6.5 Ring stiffened conical shell frustum under axial compression

6.6.5.1 Deformed shapes of different buckling modes for stiffened cylinders subjected to various load cases

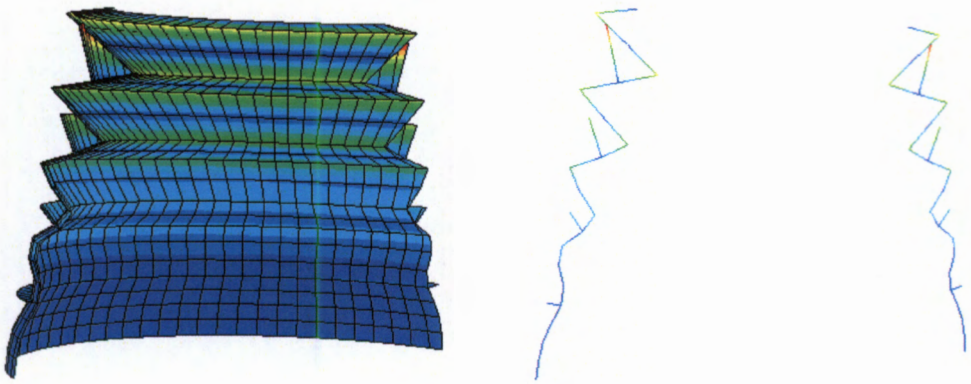

Fig. 6. 73 Deformed shape of ring stiffened conical shell frustum subjected to axial compression

6.6.5.2 Stringer and local shell modes

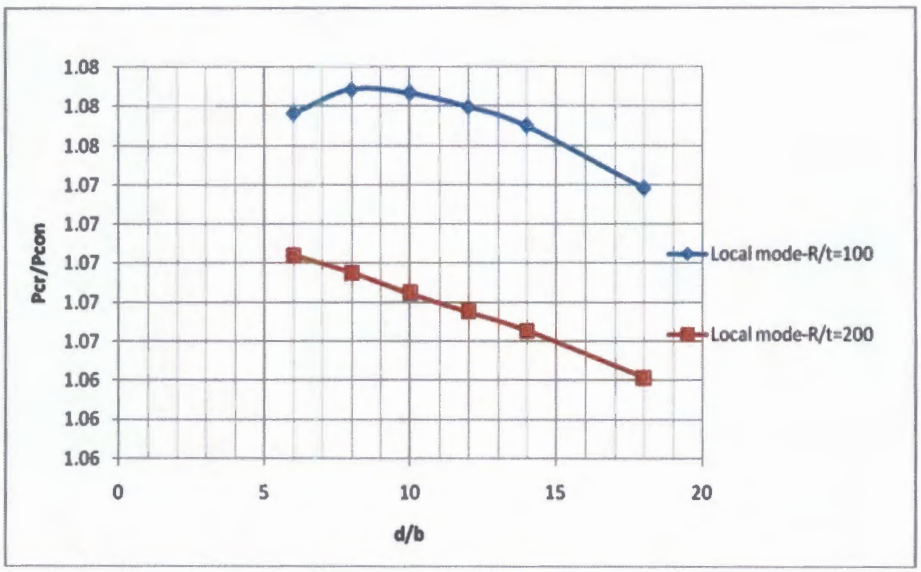

Fig. 6. 74 Axial compression: normalized elastic buckling strength vs stiffener slenderness (d/b)

6.6.5.3 Global and local shell modes

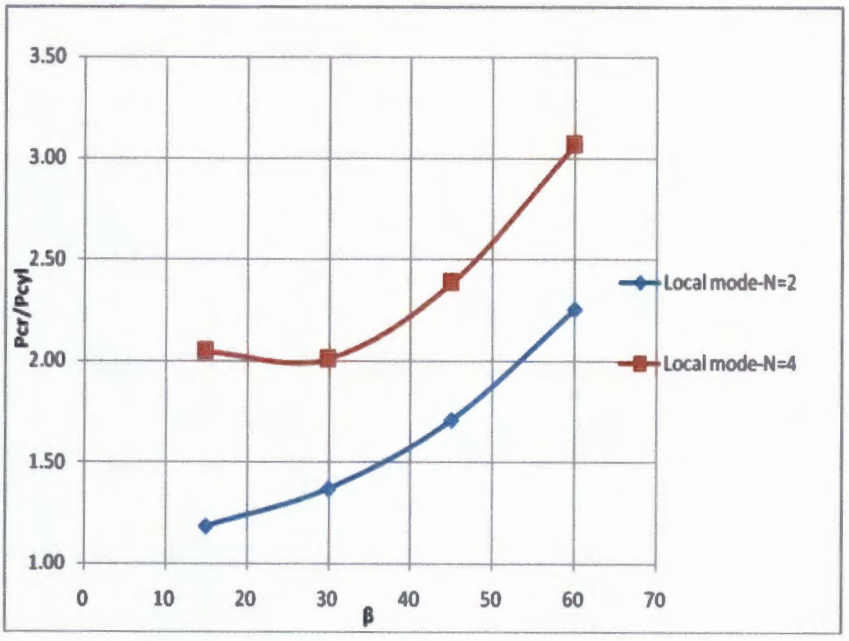

Fig. 6. 75 Axial compression: normalized elastic buckling strength vs tapering angle

6.6.6 Ring stiffened conical shell frustum under external pressure

6.6.6.1 Deformed shapes of different buckling modes for stiffened cylinders subjected to various load cases

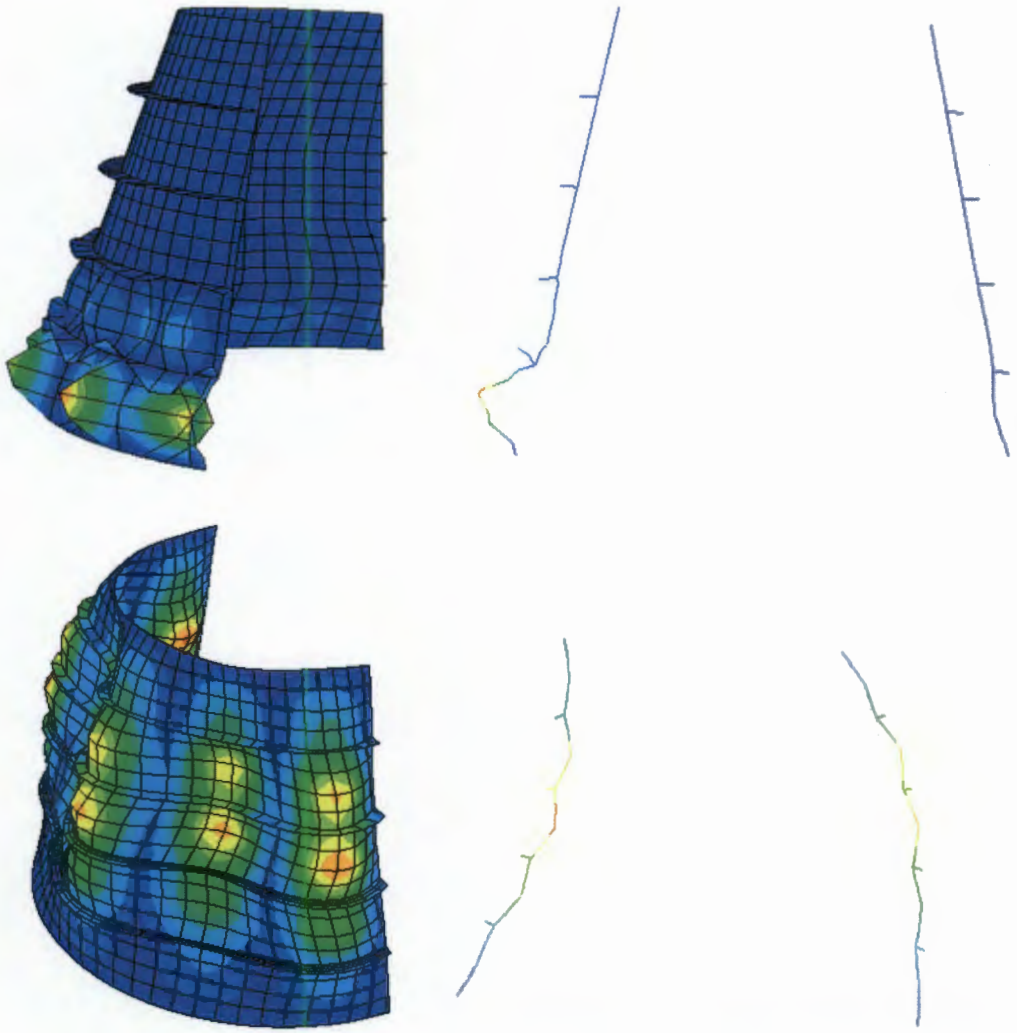

Fig. 6. 76 Deformed shape of ring stiffened conical shell frustum subjected to external pressure

6.6.6.2 Ring stiffener and local shell modes

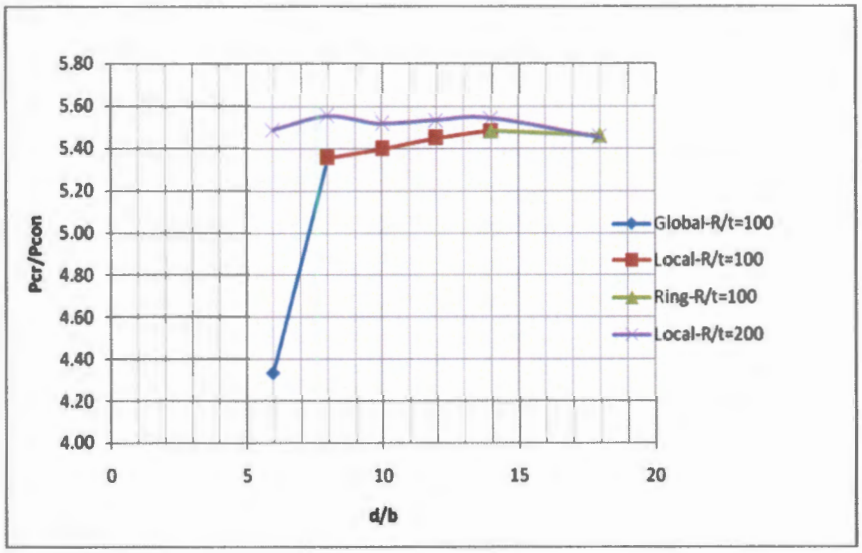

Fig. 6. 77 External pressure: normalized elastic buckling strength vs stiffener slenderness (d/b)

6.6.6.3 Global and local shell modes

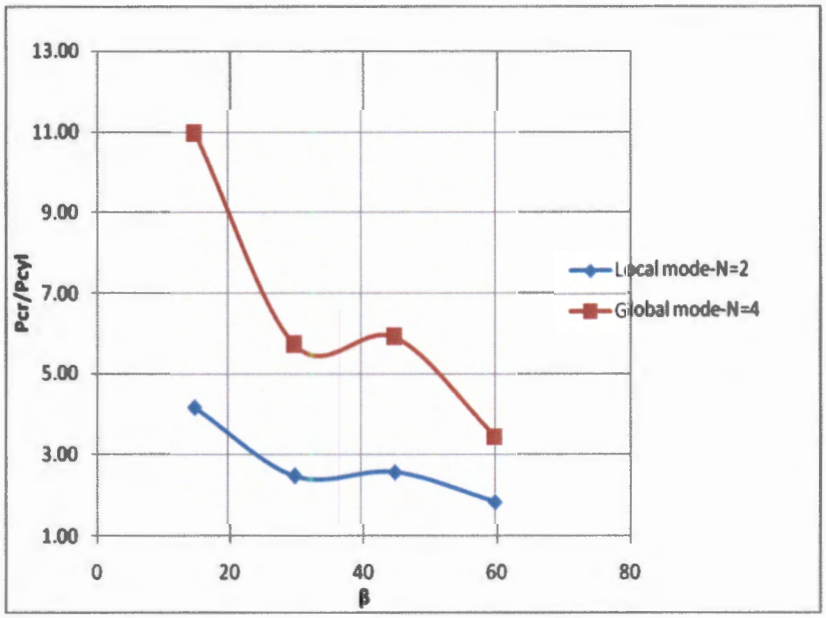

Fig. 6. 78 External pressure: normalized elastic buckling strength vs tapering angle

6.6.7 Ring stiffened conical shell frustum under shell edge shear

6.6.7.1 Deformed shapes of different buckling modes for stiffened cylinders subjected to various load cases

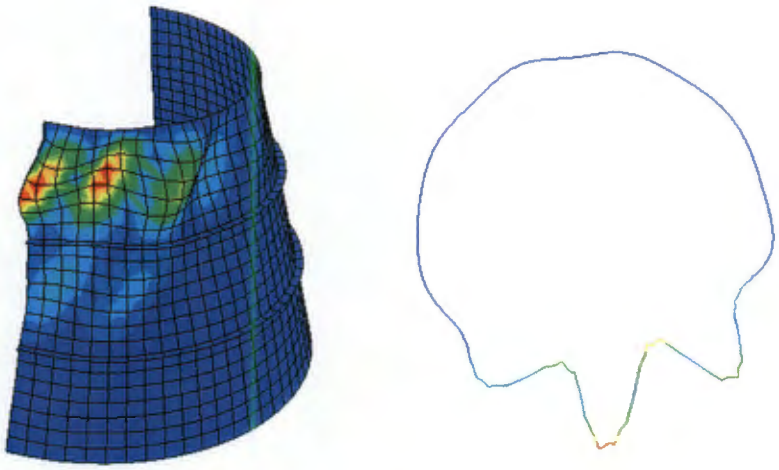

Fig. 6. 79 Deformed shape of ring stiffened conical shell frustum subjected to shear load

6.6.7.2 Panel and local shell modes

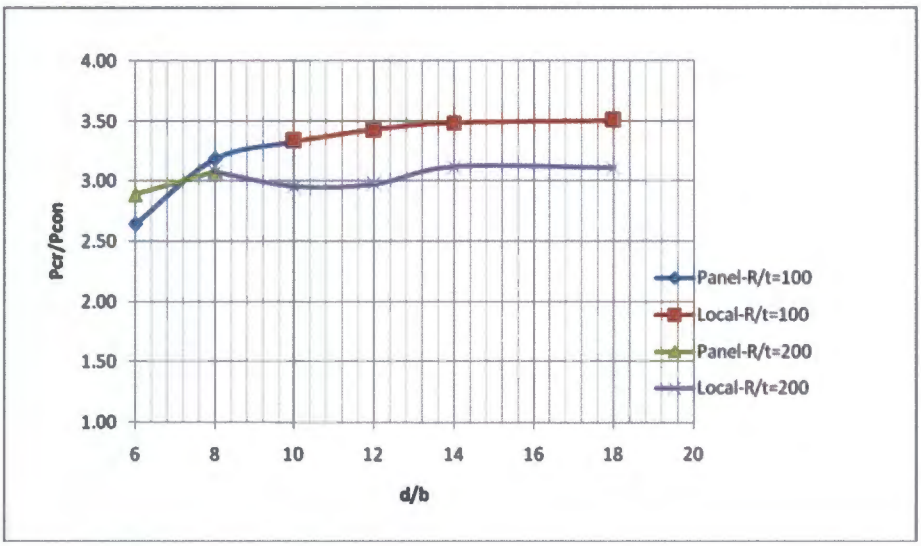

Fig. 6. 80 Shear: normalized elastic buckling strength vs stiffener slenderness (d/b)

6.6.7.3 Global and local shell modes

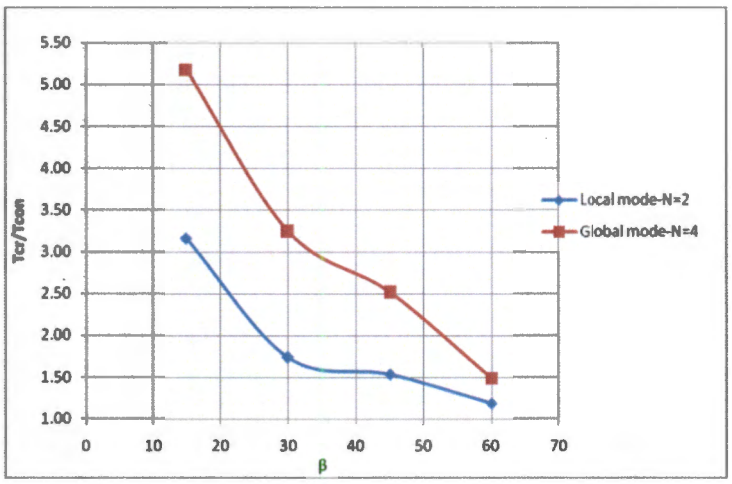

Fig. 6. 81 Shear: normalized elastic buckling strength vs tapering angle

Chapter 7

Discussion of Results

7.1 Introduction

A discussion of experimental results and finite element parametric studies which were presented in Chapter 5 and Chapter 6 respectively are presented in this chapter. Elastic stability analyses of stiffened shells have been undertaken to study the effect of various parameters on buckling capacity and buckling modes of cylindrical and conical steel shell structures subjected to different loadings.

The role of stiffeners is proved to be vital in the design of steel containment structures. Optimal stiffener design involves the determination of the best location and orientation of stiffeners (Luo et al, 1998). In recent works, it was shown that the optimum geometric properties of the stiffeners correspond to the shape when the buckling shape of a shell changes from the local mode to the overall mode (Alinia, 2004). This criterion specifies that the critical buckling load in local and global modes should be equal, thus maintaining equal safety reserves against either mode of failure (Spagnoli, 2000).

In this chapter, the discussion of results starts with a mesh convergence study and validation of finite element models against analytical results, previous research results and experimental results. The results are discussed in three sections. Firstly, the effect of stiffeners on load carrying capacity is discussed. Secondly, a discussion of the results on the effect of stiffeners on buckling modes is presented. Finally, the effect of type or geometry of stiffeners is discussed.

7.2 Mesh convergence study

By varying the number of longitudinal stiffeners thus the panel width, different combinations of axial and circumferential elements were tested and results presented in Table 6.1 of chapter 6. The number of circumferential elements was determined on the basis of panel angular width (2π/N).

The meshes chosen are shown in Table 7.1 and have an accuracy which is within 1.5% of the critical load relative to the most refined mesh.

	Mesh	
Number of meridional stiffeners (N)	Axial	Circumference
4	28	32
8	14	16
16	14	8
32	14	4

Table 7. 1 Convergence study for single panel model

7.3 Finite element model validation with analytical results and previous researchers' results

Major studies of stiffened shells have been conducted by various authors including Spagnoli (Spagnoli and Chryssanthopoulos, 1999),Chryssanthopoulos and Koiter. Henceforth, finite element results presented by Spagnoli are also used herein to validate the current finite element work.

Finite element results from single panel model were validated by referring to the limiting case of cylindrical panels. Koiter and Timoshenko's theoretical critical buckling stress for cylindrical panels is calculated as a function of the total curvature parameter (η) of the panel using equation 2.52 in chapter 2. These classical buckling equations will be complemented by Baker's equations presented in the literature review (Baker, Kovalevsky and Rish, 1972). Also finite element results obtained by Spagnoli on analytical studies will be presented for comparison (Spagnoli and Chryssanthopoulos, 1999).

Comparison of theory with FE predictions related to single panel and shell only model is performed by varying N for R/t=100. For simplicity, we adopt the same boundary conditions along the shell stringer junction as those adopted in formulation of classical solutions and those assumed by Koiter in his derivations. The results are presented by plotting normalized buckling strength against total curvature in the Fig. 6.1.

Fig. 6.1 shows all the curves following a similar trend of dropping sharply in the range $\eta<1$, then the curve becomes almost constant.

However, significant decrease of up to 74% in finite element results of single panel model when compared with shell only finite element model requires an explanation. Spagnoli attributed the difference to the more detailed idealization of the actual assembly in the single panel finite element model in comparison to that assumed in theory. In a different research, Spagnoli and Chryssanthopoulos argued that the lower results for very narrow panels ($\eta < 0.4$) obtained by the single panel model compared to those of the shell only model indicate a modal interaction between stringer and panel buckling which can only be picked up by the former FE model.

In conclusion it is believed that, in general, the ABAQUS program is capable of predicting the elastic buckling strength of perfect structures accurately.

7.4 Discussion of experimental results

Discussion of experimental results and validation of FEM results using those experimental results is presented in the following sections.

7.4.1 Description of failure mechanism

Description of failure mechanisms of different experimental specimen are presented in Table 7. 2 and Table 7. 3.

Stiffening option	Model	N	Description of failure mechanism
Un-stiffened	**CYL01**	-	Axisymmetric bulge at the top
Stringer	**CYL03**	8	Stringer failure before the skin failed
	CYL05	20	Mechanism was initially in the form of an axisymmetric bulge but later developed to stringer failure mode
Ring	**CYL07**	8	Nearly axisymmetric ring in the outer bay close to end supports
	CYL09	20	Axisymmetric bulge at the top

Table 7. 2 Failure mechanisms of cylindrical shells

Stiffening option	Model	N	Description of failure mechanism
Un-stiffened	**CON01**	-	Axisymmetric bulge at the top and inward bulge at the bottom
Stringer	**CON03**	8	Local folding of stringers before the skin failed
	CON05	20	Mechanism was initially in the form of an axisymmetric bulge but later developed to stringer failure mode
Ring	**CON07**	8	Nearly axisymmetric ring in the outer bay close to end supports
	CON09	20	Axisymmetric bulge at the top

Table 7. 3 Failure mechanisms of conical frustum shells

There seem to be consistence in results for stringer stiffened shells as load capacity is noted to increase with increase in number of stiffeners. However, in contrast, there is no logical consistence for the results obtained for ring stiffened shells.

7.4.2 Finite element model validation with experimental results

Although literature acknowledges discrepancies between the theoretical and experimental results to be as high as 70%, in this study discrepancies in the order of 94% were obtained as shown in

Table 7. **4**.

It is evident that the main reason for discrepancies between the experimental, finite element and theoretical values of loads of overall buckling and failure modes is initial imperfections and residual stresses from welding. The linear buckling analysis performed in finite element analysis which does not include these non-linearities.

Chen et al. categories imperfections from fabricated shells into three divisions: out of straightness, variation of radii and out of roundness. The variation in radii along the meridian is primarily caused by the shrinkage of the circumferential girth weld (Chen et al, 1996). Deformation of the stiffener wall out of plane initiated by local undulation of the shell causes a reduction in the shell rigidity both to tension-compression and bending. These imperfections are

the combined consequences of ovalization and fabrication procedures (rolling, seam welding, and welding of stiffeners) (Chen et al., 1996). This is the main reason for the significant difference between experimental and the estimated critical loads and buckling modes (Krasovsky and Kostyrko, 2007). These types of imperfections are essentially functions of the radius and position along the length of shell (Chen et al., 1996).

Residual stresses resulting from welding of stiffeners to the shell and along the seam line were shown experimentally by Chen et al to be significant in the longitudinal direction (Chen et al., 1996).

Estimation of carrying capacity for such shells is only possible when all the mentioned effects are taken into account, especially the ones that have a clear expressed non-linear nature (Krasovsky and Kostyrko, 2007). Therefore finite element model should be built with residual stresses and measured imperfections.

Model	N	Pcr[kN]	σcr[Mpa]	FEM, σcr[Mpa]	Discrepancy of Experimental from FEM [%]
CYL01	0	288	286.48	2031	85.9
CYL03	8	305	269.12	2430	88.9
CYL05	20	358	270.13	3705	92.7
CYL07	8	260	258.63	4119	93.7
CYL09	20	300	298.42	5127	94.2
CON01	0	200	206	654	68.5
CON03	8	225	253	707	64.2
CON05	20	260	290	1350	78.5
CON07	8	190	195	670	70.8
CON09	20	165	169	680	75.1

Table 7. 4 A comparison of FEM results with results from experimental tests on stiffened cylindrical and conical shells

Results of research effort by Walker et al.(1981) at the University College, on stiffened steel cylindrical shells are shown in Table 7.5. Interestingly, a strong correlation exists between these results and the results found in this current study.

Model	R/t	d/b	N	σcr[Mpa]
UC1	200	8	20	324
UC2	200	8	40	320
UC3	200	16	20	322
UC4	200	16	30	320
UC5	200	16	40	338
UC6	280	8	40	311
UC7	280	16	40	311
UC8	360	16	20	309
UC9	360	16	40	340

Table 7. 5 Results of experimental tests conducted at University College, London (Walker et al., 1981)

7.5 Load carrying capacity

7.5.1 Introduction

The purpose of this part of the study is to examine the advantage of stiffening cylindrical and conical frustum shells over their un-stiffened counterparts. First, the effect of number of stiffeners is discussed to reveal the optimum number of stiffeners; then, the optimum stiffener size for different shell geometry and load cases is discussed. Also elastic buckling loads for stiffened shells that have the same volume of steel (iso-weight) as un-stiffened shells is assessed. Furthermore, a comparison between the option of stiffening in the meridional direction and stiffening in the circumferential direction will be conducted.

It is also important to note that constant reference will be made in all sections that follow to figures in Chapter 6 (Results of FEM studies).

7.5.2 Meridionally stiffened cylindrical and conical frustum shells

In order to assess the variation of load carrying capacity as different parameters of stringer stiffened shells varies, normalized buckling strength is evaluated. Normalized buckling strength is the ratio of elastic buckling load of stiffened cylinders over classical buckling load of cylinders. A value of normalized strength more than 1 means that introduction of stiffeners

increase the buckling load. Meanwhile, if normalized strength less than 1 means that stiffeners are not advantageous for that configuration.

7.5.2.1 Variation of elastic buckling load for cylinders of varying R/t and number of stringers (N)

Elastic critical loads for different N values are depicted against different R/t ratios in Fig. 6.3 for axially compressed cylindrical shells stiffened in the meridional direction. Generally the elastic buckling load of stiffened cylinders increases due to the introduction of stiffeners. This is indicated by the normalized buckling strength in Fig. 6.3 for all different curves (N=8, 16 and 32) which is greater than 1. The curves remain almost constant with insignificant increase in normalized buckling load as R/t increases. This also reflects a strong agreement with the theoretical formulations. Expectedly, this same trend is observed for the same load configuration but with stiffened conical frustum in Fig. 6.21. However absolute value of critical buckling load used to plot the curves, shows that R/t is a function of critical buckling load. Increase in buckling load is generally attributed to the increase in both extensional and bending stiffness of the shell due to introduction of meridional stiffeners for both cylindrical and conical shells. Again it can be observed in Fig.6.3 and 6.21 that buckling load increases an N increases. This is because the stiffeners reduce the load carried by the shell panel by as both beam and column actions.

Again a similar trend is observed for cylindrical shells under uniform external load in Fig. 6.4 and shell edge shear in Fig. 6.5. However increase in buckling load due to introduction of stiffeners for the load case of uniform external pressure is because the stiffeners assist the shell panel to carry stresses by bending action developed by the stiffener. On the other hand stiffened shells under shear resist applied load by developing torsion in the stiffeners. Also the same observation is made in Fig. 6.22 and 6.23 for stiffened conical shells while the explanation given for cylindrical shells applies in this case as well.

In the same graphs Fig. 6.3 to Fig. 6.5, it can also be noted that the percentage of increase of strength across cylinder of varying R/t with the same number of stiffeners seem to be constant with exceptions of two cases of N=32 for both uniform external pressure and shear load.

7.5.2.2 Effect of varying number of stringers (N) on elastic buckling loads for iso-weight cylinders

The effect of varying total curvature (η) on elastic buckling strength of stiffened cylindrical shells loaded axially with a compressive load is presented in Fig. 6.6. As the numbers of stiffeners were varied, different panel widths were considered. As panels becomes narrower (η decreases) that is in the range η<1, the two curves (R/t=100 and R/t=500) rises rapidly. However, for η>1 (panels become wider), the curve becomes almost horizontal and increase in curvature seem to bring no significant increase in elastic buckling load.

This behavior is similar to that noted in studies by Spagnoli and Chryssanthopoulus. The buckling strength starts to increase after a particular value of curvature (η) is reached. For the stiffened conical shell, it is noted that η parameter defines a limit below which the buckling strength starts increasing from that of un-stiffened cone. This value depends on R/t. This behavior is also similar to that studied by theoretically Kioter for the case of cylindrical panels (Koiter, 1956).

7.5.2.3 Effect of varying stringers slenderness (d/b) on elastic buckling loads cylinders of varying R/t

Results for stringer stiffened cylindrical shells loaded with axial compression in Fig. 6.7 shows that as slenderness ratio (d/b) increases, the buckling load increases in the range d/b=2 to 10, then starts to decrease for d/b>10. Variation of load carrying capacity with d/b ratio for stringer stiffened conical shells under axial compressive load is depicted in Fig. 6.24. In the range d/b=6 to 14 the curve rises gently indicating an increase in buckling strength as d/b increases in this range. This increases reaches a pick value at d/b=14 and as d/b increases from this point (d/b>14) the curve drops at a rate equal to that it was rising with. Generally, the trends in the initial range of all the graphs (Fig. 6.7 and 6.24) indicate clearly that the larger the d/b ratio, the higher the load carrying capacity. This can be attributed to a general increase in extensional stiffness of the stiffened shell. Moreover, for the case of a shell under axial compression, there is also a change in flexural rigidity of the shell as d/b varies. Since the parameter b is kept constant, by increasing the d/b ratio, the moment inertia about the strong axis increases. Bending is primarily in meridional direction hence the meridional stiffeners are increasing the stiffness of shell in the meridional direction. Consequently the bending resistance of the stiffeners would increase. However, for the case of a shell under axial compression, load carrying capacity continues to

increase up to a point when buckling begin to be controlled by stiffener slenderness and the load carrying capacity begins to decrease as slenderness increases.

Similar trends are observed in Fig. 6.8 for stiffened cylinders loaded with uniform external pressure and that for stiffened conical frustum under the same loading configuration (Fig.6.25). On this graph, the buckling load initially increases almost gently up to a peak value at d/b=10 for cylindrical shells and d/b=14 for conical shells as d/b increases but for d/b>10 the rate of increase decreases to the extent that the graph is almost constant. Since stiffeners carry load by beam action, this change in load carrying capacity is primarily due to a change in flexural rigidity of the shell as d/b varies.

		Optimum d/b	
	Load case	R/t=100	R/t=200
Stiffened cylinders	Axial compression	10	-
	External pressure	18	-
	Shear	16	15
Stiffened conical frustum	Axial compression	14	-
	External pressure	14	18
	Shear	18	18

Table 7. 6 Optimum stringer slenderness ratio for cylindrical and conical frustum (N=16)

However, in Fig. 6.9 the graph for shell edge shear shows a similar trend to the one for cylindrical shells under axial compression but the load carrying capacity peak value is at d/b>15. The graph for conical shells under shell edge shear (Fig. 6.26) rises gently up to a peak buckling load at d/b=14. Both curves for the load case of uniform external pressure rise at a gentle rate. The d/b values at which load carrying capacity is at its peak are shown in Table 7. 6. This

increase in elastic load capacity is attributed to the fact that shells under shell edge shear which resist its load by torsional resistance of the stiffener shell combination. Again the drop in load carrying capacity after reaching a certain slenderness ratio can be attributed to failure of stiffeners before the shell buckles. Increasing torsional stiffness of stringers is an efficient means of increasing the buckling load. However, if the torsional stiffness becomes too large, the effective stiffness of the stringers may be much less than the nominal value, due to local deformations of the shell wall.

The d/b values at which load carrying capacity is at its peak are shown in Table 7. 6.

7.5.2.4 Effect of varying stringers slenderness (d/t) on elastic buckling loads cylinders of varying number of stiffeners (N)

The curves in Fig. 6.10 for axially compressed cylindrical shell rise almost at the same rate as d/t increases. The curve for d/b=5 shows a greater increase in buckling load than that of d/b=10. No peak values of buckling load were noted except for points when the rate of increase decreases. Results for the case of uniform external load is shown Fig. 6.11, with the curve rising sharply in the initial stages and the rate of increase decreases in the range d/t>40. Fig. 6.12 depicts results for shear loading and the graph rises steeply in the range d/t=10 to 40. In the range d/t>40 the curve is almost constant. Points were picked when the increase in elastic buckling load declines and are shown in Table 7. 7.

Fig. 6.27 shows the curve of axially compressed stiffened conical shell which reflects that load carrying capacity increases as d/t increases. For the same model under uniform external load the graph rises steeply as d/t increases as shown in Fig. 6.28. Similarly for the load case of shell edge shear load the load carrying capacity rises initially at a steep gradient but becomes less steep for d/t>40. Points were picked when the increase in elastic buckling load declines and are shown in Table 7. 7.

It can be concluded that increase in buckling load is result of increase in shell thickness. Since R and d were held constant, the load carrying capacity varies because t is varying and is a function of buckling load as shown in Equations 2.9, 2.12 and 2.13. However, the graph for uniform external pressure is almost uniform for d/t>40 which shows less sensitivity of larger values of d/t ratio to change in buckling load as shell thickness increases.

		Optimum d/t
Stiffened cylinders	Axial compression	80
	External pressure	40
	Shear	50
Stiffened conical frustum	Axial compression	20
	External pressure	80
	Shear	50

Table 7. 7 Optimum d/t ratio for stiffened cylindrical and conical frustum (N=16)

7.5.3 Circumferentially stiffened cylindrical and conical frustum shells

7.5.3.1 Variation of elastic buckling load for cylinders of varying R/t and number of ring stiffeners (N).

An increase in buckling capacity is noted as both R/t and number of ring stiffeners (N) increases for all load cases. However the percentage of increase differed for different load cases. The graph for axially loaded cylindrical shells, Fig. 6.14, shows that the rate of increase of load carrying capacity is less for N=2 and N=3. However, the rate picks up for N=4 and N=6 and very steep for N=8. Buckling strength increase ranged between 3% and 40% for axially compressed cylindrical shells depending on the R/t ratio.

This variation is because, an axially compressed un-stiffened shell buckles into a defined number of meridional waves and this number is a function of R/t. the number of half waves of shell buckles is calculated using equation 2.10 in section 2.4.2 of Chapter 2 which gives the wave

length of a buckle. As a result, significant increase in strength is realized when the position of the ring stiffener coincides with the peak of the meridional wave buckle.

A greater increase in strength is noted for shells under uniform external pressure than when it is axially compressed. Fig. 6.15, the graph for stiffened cylinders under uniform external loading shows gentle and almost uniform gradient curves shows for N=2, 3 and 4. This reflects that there is less increase in buckling load these cases as R/t ratio increases. However different trends are noted on the same graph for N=6 and 8, where the curves fluctuates as R/t changes. Ring stiffeners increase the stiffness of the structure transverse direction hence ring stiffened shells are more efficient increasing load carrying capacity of shells resisting external pressure. R/t ratio is a function buckling shear stress hence its variation influences the magnitude of buckling strength.

The graph for the case of shell edge shear, Fig. 6.16 exhibit similar trends to that of uniform external pressure in Fig. 6.15 as both R/t and N varies. The curves for N=2, 3 and 4 are almost of uniform gradient, but for N=6 and 8 the curves are initially inconsistent but as R/t increases the load carrying capacity rises sharply. The ring stiffeners resist applied shear load by developing torsional restoring forces besides increased rigidity.

The variation of load carrying capacity with R/t ratio for ring stiffened conical shells is depicted in Fig. 6.31 for the load case of axial compression. The three different curves for N=2, 4 and 8 shows that load carrying capacity increases as R/t increases.

Fig. 6.32 depicts the variation of load carrying capacity of conical shells under uniform external pressure which is also similar to the case of shell edge shear in Fig. 6.33. In both graphs the increase in elastic buckling load with increase in R/t is small but significant.

7.5.3.2 Effect of varying ring stiffener slenderness (d/b) on elastic buckling loads stiffened cylindrical shells

The curve for axially compressed ring stiffened cylindrical shell in Fig. 6.17 shows that the buckling load increases as d/b increases in the range d/b=2 to 6. For d/b>6 the load starts to decrease and the gradient of the curve becomes gentle. However for cylindrical shells under uniform external pressure, the curve in Fig. 6.18 rises steeply as d/b increases in the range d/b=2 to 10. After a peak load carrying capacity is reached at d/b =10, the curves drops as d/b increases

which indicates a decrease in buckling load for d/b>10. The results for stiffened cylindrical shells under shell edge shear load shows a trend similar to both the case of cylindrical shells under axial compression and external pressure. However the increase in buckling load is in a range broader that of the former cases. The curve rises as d/b increases in the range d/b=2 to14. A sudden drop in buckling load occurs after a peak value of buckling load is reached at d/b=14. Optimum ring stiffener slenderness ratios for circumferentially stiffened cylinders are shown in Table 7. 8.

		Optimum d/b	
	Load case	R/t=100	R/t=200
Stiffened cylinders	Axial compression	-	6
	External pressure	11	-
	Shear	14	-

Table 7. 8 Optimum ring stiffener slenderness ratio for circumferentially stiffened cylinders

The effect of ring slenderness on stiffened conical shells under axial compression is depicted in Fig. 6.34. The curves for both R/t=100 and 200 are almost constant with slight decrease in load carrying capacity as d/b increases. This reflects that d/b ratio does not play a major role in the elastic buckling load of ring stiffened conical shells under axial compression. This trend is noted in Fig. 6.36 for the case of conical shells under shell edge shear load.

In Fig. 6.35 the results for conical shells under uniform external load is shows that there is no consistence between the curve for R/t=100 and 200. The curve for R/t=100 shows a remarkable increase in load carrying capacity as d/b increases.

In all cases, the increase in elastic buckling load as d/b increases is primarily due to an increase in extensional stiffness of the shell. Ring stiffeners increase stiffness of the shell in the circumferential directions.

The optimum number of stiffeners was chosen to model ring stiffener slenderness problem. Table 7. 8 shows optimum slenderness ratio for cylinders under different load configurations. The optimum slenderness ratio for ring stiffened cylinder under axial compression is lower than that of stringer stiffened cylinders under the same load.

7.6 Effect of varying key parameters of stiffened cylindrical and conical frustum shells on buckling modes

7.6.1 Introduction

Dominance of stringer, local shell or global shell buckling modes depends on the stiffening arrangement and geometry of shell and stiffeners. Change over between these modes is captured as certain key design parameters vary. Elastic buckling loads, normalized with respect to the classical buckling load of their un-stiffened counterpart (P_{cyl} or P_{con}) for different buckling modes are presented against different parameters for cylindrical and conical shells.

7.6.2 Meridionally stiffened shells

A study of prevalence of stringer or local shell mode as the stringer slenderness (d/b) varies is presented. Also an analysis of results of change over between local shells and global buckling mode as number of stiffener varies is presented. The results for the shell only model are in agreement with the theoretical predictions for a cylindrical panel. This is because the model presents the same boundary conditions along the shell-stringer junction as those assumed by theory for instance Koiter (Spagnoli, 2001).

7.6.2.1 Stringer, local and panel shell modes

The region in which either shell or stringer mode prevails was evaluated by treating shell and stringer as isolated components. Stringer mode was captured using a single panel model and theoretical prediction for buckling stress of a stringer (flat plate). Both multi panel and shell only models are used to predict local shell mode.

A clear change over is shown in Fig. 6.41 for a cylinder under axial compression. The curve shows that local buckling mode is dominant in the initial stages (d/b=2 to 10) while buckling load is also rising gradually. The curve starts to decrease rapidly when a certain slenderness ratio

(d/b=10) is reached and at this point again the stringer buckling mode becomes dominant as d/b ratio increases. Results for conical shells under axial compression on Fig.6.62 shows trend which is similar to that of their cylindrical counterpart. This graph shows a curve which rises gradually and in that process the buckling mode which was initially of a local mode changes to a stringer mode for d/b>10. The curve drops down from a peak buckling mode at d/b=14. From results of both stiffened cylindrical and conical shells a general conclusion can be drawn that the critical load of a stringer is a function of its slenderness. This implies that moving from a low to high d/b values implies moving from shell buckling to stringer buckling mode. When the slenderness ratio d/b increases beyond a certain limiting value the critical load starts to decreases in general agreement with theoretical results. From this particular value of d/b the buckling load on the stringer is less than that of the stiffener hence it buckles before the shell panel and stringer buckling dominates in this range of d/b.

Fig. 6.47, the graph of a cylinder under external pressure, shows the curve rising gently and at d/b=8 the rate of increase drops that the curve is almost flat. Contrary to the axial compressed cylinder curve, the change over from panel to local shell buckling mode is not marked by a peak buckling load but the load continues to increase after the changeover. Fig. 6.66 shows the behavior of conical shells under uniform external pressure. The curve rises initially at a gentle rate but the rate of increase picks up after d/b=10. The mode of buckling changes from local to stringer at d/b, which is the point at which the rate of load increase increases. There is an increase in load as d/b increases because the stringer is acting as a beam in flexure to carry load. Panel buckling is prevalent in the lower values of because the flexural rigidity of the stringer is less than that of higher d/b hence the beam offers less resistance and moves out of plane together with shell panel. The failure mode changes to local shell buckling because the stringer flexural rigidity increase as d/b increases.

The buckling behavior of cylinders under shear is shown in Fig. 6.50. The graph shows a curve which rises steeply as the shell buckles panel/local and simultaneously drops and changes over to buckle in the stringer mode at d/b=15. The buckling behavior of conical shell under shell edge shear load is depicted in Fig. 6.70. The curve rises at a uniform rate and the buckling mode changes from local mode to stringer mode at d/b=8. A similar trend is shown for the case of R/t=200 but the load carrying capacity is higher than that of case of R/t=100. These trends are

explained by the fact that, stringers in this case are resisting load by developing torsion. Stringers offer a greater torsional rigidity for lower values of d/b hence panel buckling is inevitable. Torsional buckling of stiffener might occur before the shell buckles locally if they are relatively slender.

Load case	Optimum d/b	
	Cylindrical	Conical frustum
Axial compression	11	14
External pressure	6	14
Shear	16	8

Table 7. 9 Change over between panel buckling, local shell and stringer modes for different load cases

In summary the change over between local and stringer as a result of varying stringer slenderness are presented in Table 7. 9. The clustering of Eigen modes is evidence of mode interaction between local and stringer modes of failure. According to the European code of Construction steel recommendations (ECCS, 1988), the slenderness ratio at which the mode changes from local to stringer is 10. The results optimum d/b ratio obtained are in the range of the one adopted in normal design practice. These ratios can be adopted as limits for sizing stiffeners in order to preclude local buckling of stiffeners.

7.6.2.2 Local shell, panel and global modes

The conventional criterion of optimization is that critical buckling loads in local and global modes should be equal, thus maintaining equal safety reserves against either mode of failure (Spagnoli, 2000). The change over between local shell and global mode is shown for both cylinders and cone by varying the number of stringers.

In Fig.6.42, the behavior of axially compressed cylindrical shells is shown. From the two curves from different models, the curve for local buckling is lower than that of global mode which shows that the local buckling mode is dominant initially and at N=20 there is a mode change

over to global buckling since the curve for global mode is lower than that of local mode. But an unexpected change of mode occurs again at N=40 as the mode changes back to become local mode. The graph for the case of R/t=200 follows exactly the same trend as the one for R/t=100. Fig. 6.63 shows results of two models of axially compressed conical frustum. The first curve analyses global buckling of a smeared model and shows a constant graph since the buckling load is normalized. The second curve of multi panel model shows the buckling load increasing gently as number of stiffeners increases. As the number of stiffeners increases, the buckling mode changes from local buckling mode to global mode at N=36. This point coincide which the point at which the two graphs crosses each other. A conclusion can be drawn that stiffened shells with wider panels fail by local buckling while that with narrower panels fail globally. This is due to the fact that local critical load increases as panel becomes narrower (as N increases).

The buckling behavior of cylindrical shells under uniform external pressure is depicted in Fig. 6.48. Two buckling modes are noted on this graph. Local buckling mode is dominant in the initial stages and changes to panel buckling at N=24. The buckling behavior of stiffened conical shells under uniform external pressure load is depicted in Fig. 6.67. Although the curve does not reflect a defined trend (buckling load fluctuates as N increases), it shows that local buckling mode is dominant in the initial stages (N=4 to 16) but for N>16 the panel buckling mode of failure becomes more pronounced. Again as with axially compressed shells, local critical load increases as panel becomes narrower hence panel buckling is more prevalent as N increases.

Fig. 6.51 shows the graph of a cylinder under shell edge shear load. The curve is almost constant in the initial stages with local mode dominating and it changes to panel buckling mode at N=16. The load carrying capacity generally decreases when in panel buckling mode range. A trend similar to the one shown in the investigation of axially compressed cones in Fig. 6.63 is reflected in Fig. 6.71, results of buckling behavior of conical shells under shell edge shear. Again the first curve of a smeared model shows a buckling load being constant as N increases. However the curve for the multi panel model shows that local buckling mode is prevalent in the range of N=2 to 16 and for N>16, panel buckling mode becomes the dominant mode of failure. It is evident from results that local shell mode governs for wide panels. Global mode is associated with closely spaced stiffeners. This is mainly due to the fact that local critical load increases as the

panel becomes narrower. The multi panel model shows good agreement with respect to the dominant buckling mode identified by identified by orthotropic models (Spagnoli, 2001).

In Table 7. 10, the number of stiffeners (N) at which the change over from local shell to global mode occurs, is shown for different load cases for stiffened cylindrical and conical shells.

Load case	Optimum number of stiffeners (N)		
	Cylindrical		Conical frustum
	R/t=100	R/t=200	R/t=100
Axial compression	28	32	34
External pressure	24	30	32
Shear	28	30	44

Table 7. 10 Change over between local shell, panel buckling and global modes for different load cases

The following discussion pertains to the influence of tapering angle of stiffened conical frustum on two extreme cases, one with wide panels and the other with narrow panels.

The influence of tapering angle of stiffened conical shells under axial compression is depicted in Fig. 6.64. Results shows that the curve for wide panels (N=8) increases gradually as tapering angle increases while the mode of failure remains as local mode. Contrary to the curve for narrow panels (N=32), the curve shows that buckling load decreases gradually as tapering angle increases. Also the mode of failure changes from local to global mode of failure at $\alpha=30^{o}$. This is analogous to the case of N variation.

A trend similar to that of stiffened conical under axial loading is noted for the case of stiffened shells under uniform external pressure. The curve for N=8 (wide panels) rises gradually as tapering angle but the shell fails by local buckling mode throughout this range. Again on the contrary, the curve for N=32 (narrow panels) drops gradually as tapering angle increases. However the buckling mode remains predominantly global.

The buckling behavior of stiffened conical shells under shear edge shear is depicted in Fig. 6.72. Both curves (N=8 and N=32), unlike the two previous load cases, drops gradually as tapering angle increases. However, besides the buckling mode for narrow panels is global while that of wide panels (N=8) is local.

With exception of axially compressed conical frustum, no clear trend was found in the buckling mode with respect to the tapering angle of the cone (α). For conical frustum, in the case of narrow panels having an intermediate number of stiffeners (N=32), changeover between local and global modes may be induced by varying α (Spagnoli, 2001). The mode changeover from local to global mode was observed between $\alpha=30^0$ and $\alpha=40^0$.

7.6.3 Circumferentially stiffened shells

A study of prevalence of stringer or local shell mode as the ring stiffener slenderness (d/b) varies is presented. Also an analysis of results of change over between local shells and global buckling mode as number of stiffener varies is presented.

7.6.3.1 Stiffener buckling and local shell modes

The behavior of ring stiffened cylinders under axial compression is depicted in Fig. 6.53. The curve for R/t=100 rises gently with local buckling mode being the predominant failure mode for d/b<10. Afterwards the buckling mode changes over to become of global nature. However the curve for R/t=200 rises sharply from d/b=2 to d/b=6. For d/b>6 the graph drops at a gentle rate. Strange enough, there is no mode changeover which was noted for this case of R/t=200. The buckling behavior of axially compressed ring stiffened conical shells is depicted in Fig. 6.74. Both curves for the case of R/t=100 and 200 shows that the cone buckles by local buckling mode in the whole range of d/b. Ring stiffeners increases extensional stiffness of shell, hence as d/b increases for both cylindrical and conical shells the buckling load increases. Local buckling was observed for shells having relatively heavy frames. The sheet will buckle between stiffeners and the ring stiffener remains circular in cross section.

Fig. 6.56 shows the behavior of cylindrical shells under external load. An initial rapid increase in buckling load as d/b increases is noted by the steep curve but the graph drops gently at d/b=10. From d/b=2 to d/b=10, panel buckling mode prevails and the failure mode changes to local mode

for d/b>10. Fig. 6.77 shows the behavior of conical shells under uniform external pressure. The curve for R/t=100 shows that the cone fails by local buckling mode in the range d/b=6 to 14 and by global buckling mode for d/b>14. For R/t=200 the cone buckles by local buckling mode in the full range of d/b. panel buckling dominates lower range of d/b ratio because the flexural rigidity is lower hence the ring stiffener buckles with the sheet at the critical load.

Fig. 6.59 depicts the behavior of ring stiffened cylindrical shells under shell edge shear load. Three different buckling modes are noted on the graph. The buckling mode is initially global in the d/b=2 to 6 range then change to local in the range d/b=6 to 14. Finally the curve drops and also the failure mode becomes stringer in nature. Results of behavior of ring stiffened conical shells under shell edge shear are shown in Fig. 6.80. The curve of R/t=100 shows that for the range of d/b=6 to10 panel buckling mode dominates and for d/b>10 for the failure mode is local buckling. This trend is similar to that noted for R/t=200 with panel buckling in the range d/b=6 to 8 and local buckling in the range d/b>8. Prevalence of local failure mode in the lower range of d/b is because the ring stiffener resist applied shear load by developing in plane stresses which are compressive in nature. This makes the behavior of stiffeners similar to that of a strut, hence as slenderness of the stiffener increases (d/b) the load carrying capacity decreases and stringer buckling dominates.

Load case	**Optimum d/b**
	Cylindrical
Axial compression	10
External pressure	11
Shear	14

Table 7. 11 Change over between stiffener and local shell modes for different load cases

7.6.3.2 Global and local shell modes

Fig. 6.54 shows the curve for an axially compressed cylinder as number of stiffeners varies. The curve shows that the buckling load fluctuates as number of stiffeners changes, with load peaking at certain values of N. However the buckling mode remained local throughout the range of N values. Results show that stiffeners have got more effectiveness when N coincides with the number of buckle waves.

The behavior of ring stiffened cylinders under uniform external pressure is shown in Fig. 6.57. For the range of N=2 to 3, the mode of failure is local buckling but the mode changes to global mode for the range of N>3.

No mode change over is noted for cylindrical shells under shell edge shear in Fig.6.60. There is an increase in buckling mode as N increases while global buckling mode dominates the whole range of N.

Load case	Number of stiffeners (N) at mode changeover point
	Cylindrical
	R/t=100
Axial compression	6
External pressure	8
Shear	8

Table 7. 12 Change over between local shell and global modes for different load cases

For ring stiffened conical shells under axial compression, Fig. 6.75 shows that for N=2 and 4 there is no mode change over as tapering angle varies. For the both curves the cone buckles by local buckling mode.

The behavior of ring stiffened conical shells under uniform external pressure is depicted in Fig. 6.78. The curve for N=2 shows the cone buckles by local buckling mode and that there no mode

Chapter 8

Conclusions and recommendations

8.1 Introduction

This thesis has presented a finite element based parametric investigation of stiffened cylindrical and truncated conical steel containment shell structures. Emphasis was placed on their buckling modes under different load configurations (axial compression, external pressure and shell edge shear). New and unexpected findings that have emerged from the numerical study discussion in Chapter 7 are summarized below.

8.2 Validity of FEM to model elastic buckling of stiffened shells

From the results and discussion of validation of FE models in Chapter 7, it can be concluded that the ABAQUS program is capable of predicting the elastic buckling strength of perfect structures accurately. Local buckling of stiffened shells can be effectively investigated using the shell only model. Both shell panel and overall buckling can be investigated using multi panel model. This was well authenticated by the experimental results and previous studies by different independent researchers. However more accurate results can be obtained if proper and practical boundary conditions are integrated into the FE models. Most importantly there is need to include imperfections and residual stresses into the model to obtain more accurate results.

8.3 Elastic load carrying capacity

By stiffening steel cylindrical and a truncated conical shell, its critical buckling stress increases. The amount of increase depends on the different geometric parameters of a shell and its stiffeners such as aspect ratio and number of stiffeners.

Following the discussion in section 7.5.2.1, a conclusion can be drawn that for different R/t ratios increase in elastic buckling load relative to their corresponding un-stiffened counterparts is almost the same for a particular number of stiffeners. To clarify with an example, percentage load increase between un-stiffened shell (R/t =100) and stiffened shell (N=8, R/t=100) is the same as for un-stiffened shell (R/t =500) and stiffened shell (N=8, R/t=500). In view of this, to a designer it can be concluded that R/t does not affect the choice of number of stiffeners (N).

change over as tapering angle varies. This trend is noted again for N=4 but it fails by global buckling mode.

A trend similar to that noted for the case of conical shells under external load is observed in the case of conical shells under shell edge shear load in Fig. 6.81. The curve of N=2 reflects that there is no mode change over as tapering angle varies and the shell buckles by local buckling mode. Also the case of N=4 displays the same behavior but fails by global buckling.

For circumferentially stiffened shells, the change over point does not coincide with the maximum normalized strength as expected. The load capacity, in all cases continued to increase after the mode changeover. They seem to be distinct trend on the optimum number of stiffeners as the graphs indicate a fluctuating load carrying capacity as number of stiffeners changes. This can be explained by the fact that, when the shell buckles, it buckles into a unique number of stiffeners. If the ring stiffener is located to coincide with the peak buckling wave, a significant load increase is expected. On the hand if the ring stiffener is located at the neutral point of the buckling sine wave, no load increase is expected.

A comparison of the critical buckling loads of un-stiffened with those of stiffened shells having the same volume of steel in section 7.5.2.2 undoubtedly leads to a conclusion that stiffening option offers major enhancement of buckling capacity than merely increasing the thickness of the shell. The ratio of increase varied between 1.2 and 3.7.Subsequently, stiffening option is more economic than the option of increasing the thickness of the shell, if the labor cost of welding does not offset the cost.

A conclusion was draw from section 7.5.2.3 that by raising the aspect ratio of stiffeners, the critical buckling load increases up to a certain point beyond which the critical load decreases. Load carrying capacity of both cylindrical and conical shells can be increased by increasing the shell wall bending stiffness, if the load on the shell causes bending and buckling considerations are included. The stiffness of the shell wall can be increased by attaching meridional and circumferential stiffeners to a shell. In addition, if the bending is primarily in the meridional direction, the stiffeners added in the meridional direction would be made much larger than the circumferential stiffeners.

From section 7.5.3 on circumferentially stiffened shells, it is noted that optimum increase in load carrying capacity is obtained when the stiffeners are located at points along the meridian where the crests of buckling waves are likely to occur. Consequently, for structural optimization a design engineer should take this into account and locate ring stiffeners at points of expected crests along the shell wall.

Strangely enough, results of variation of tapering angle of conical frustum seem to lead to two separate conclusions that buckling load increases as tapering load increases for wide panels. Conversely, buckling load decreases as tapering angle of cone increases for the case of narrow panels. Most importantly this conclusion suggest use of an elastic buckling equation for stiffened conical shells which takes curvature into account so that these distinctions can be capture accurately. Alternatively, one can adopt different sets of equations for different ranges of total curvature which is a function of number of stiffeners (N).

8.4 Failure mode shapes

Changeover between buckling modes in stiffened shells may be obtained by varying aspect ratio of stiffener and its shell and number of stiffeners. In particular, changeover from local to overall

mode corresponds to the optimum value of the stiffener rigidity (flexural or torsional) hence the critical stress is at its highest possible value. This changeover point varies with the load configuration and form of shell structure. In comparison with the design standard set by the European Convention for Construction steelwork (ECCS), the ECCS guide line seem to be more conservative and safe to use.

Also following the discussion in section 7.6.2 and 7.6.3, a conclusion can be drawn that for both stiffened cylindrical and conical frustum shells, local buckling mode is more dominant on wide panels while the most inevitable failure mode for narrow panels is global buckling.

Oddly enough the discussion on buckling modes as tapering angle varies seem to lead to a conclusion that it does not influence the buckling mode of a conical shell with R/t=100. However further investigation is needed for shells of different R/t ratios in order to make a more sound conclusion.

8.5 Recommendations

- In practice pre-buckling rotations exist hence linear buckling analysis (LBA) yield overestimated buckling loads which are un-conservative. Since LBA is not sufficient to predict the stability of the structure, a good prediction of the buckling load can be made by properly combining LBA with geometrically nonlinear pre-buckling analysis. This methodology is computationally cheaper and efficient than nonlinear analysis and more reliable than LBA (Bagchi and Paramasvam, 1996).

- Since imperfection and residual stresses strongly influence the buckling of shells, an investigation which incorporates these parameters will yield results which are more practical for development of design tables and charts.

- For further study, a continuation into the post buckling range of the stiffened shells will yield a deeper and more comprehensive understanding of the buckling behavior of stiffened shells.

References

1. ABAQUS , "Theory ans user's manual; version 5.6" Hibbit, Karsson and Soren Inc, Providence (1995).
2. Bagchi A., Paramasivam V., "Stability analysis of axisymmetric thin shells" Journal of engineering mechanics, March (1996).
3. Baker E.H., Kovalevsky L., Rish F.L. "Structural Analysis of Shells" McGraw Hill (1972).
4. Berry P. A., Rotter J. M., Bridge R. Q., "Compression tests on cylinders with circumferential weld depression" J. Engineering Mechanics ASCE (April 2000)
5. Brush D.O., Almroth B.O., "Buckling of bars, plates and shells" Mc Graw Hill (1975).
6. Chajes A., "Principles of structural stability theory" Prentice Hall (1974)
7. Chapelle D., Bathe K.J.,"The Finite element analysis of shells-fundamentals", Springer (2003).
8. Chen Q., Elwi A.E., "Finite element analysis of longitudinally stiffened cylinders in bending" J. Engineering Mechanics ASCE (November 1996)
9. El Damatty A.A, El Attar M., Korol R.M. "Inelastic stability of conical tanks" Thin walled structures 31 (1998).
10. El Damatty A.A, Marroquin E.G, El Attar M. "Behaviour of stiffened liquid-filled conical tanks" Thin walled structures 39 (2001).
11. Esslinger M., Geier B., "Post buckling behaviour of structures: CISM courses and lectures No. 236" Springer-Verlag (1975).
12. European Convention for Construction steelwork (ECCS), "Buckling of steel shells European recommendations", ECCS TWG 8.4 (1988).
13. European Convention for Construction steelwork (ECCS), "EC3 Part 1.6 Eurocode 3: Design of steel structures. Part 1.6: Strength and stability of shell structures". prEN 1993-1-6. Brussels: CEN, (2004).

14. European Convention for Constructional Steel Work, Buckling of Steel Shells, 4th ed. Brussels,1988; 56.

15. Flugge W., "Stresses in shells", Second edition. Springer-Verlag (1973)

16. Green D.R., Nelson H.M., "Compression tests on large scale stringer stiffened tubes" Buckling of shells in offshore structures, Granada (1981).

17. Koiter, W. T. ''The effect of axisymmetric imperfections on the Buckling of cylindrical shells under axial compression.'' *Proc., Koninklijke Nederlandse Akademie van Wetenschappen*, Series B, Vol. 66(5), North-Holland, Amsterdam, 265–279 (1963).

18. Krasovsky V.L., Kostyrko V.V., "Experimental studying of buckling of stringer cylindrical shells under axial compression" Thin walled structures (2007).

19. Libai A., Simmonds J.G., "The non-linear theory of elastic shells" 2nd Edition, Cambridge University Press (1998).

20. Logan D.L., "A first course in the Finite element method" Third edition. Thomson learning (2002).

21. Pircher M., Bridge R.Q. "Buckling of Thin Walled Silos and Tanks under axial load-some new aspects" J. Structural engineering .ASCE (October 2001).

22. Proceeding of a state-of-the-art colloquium, Universitat Stuttgart, Germany, Buckling of shells. Berlin: Springer Verlag KG, (1982).

23. Rotter J.M., "Shell structures: the new European standard and current research needs", Thin walled structures (1998).

24. Spagnoli A. "Different buckling modes in axially stiffened conical shells" Engineering structures 23 (2001).

25. Spagnoli A., Chryssanthopoulos M.K. , "Buckling design of stringer stiffened conical shells in compression" Journal for Structural Engineering ,January (1999).

26. Spagnoli A., Chryssanthopoulus M.K, "Elastic buckling and post buckling behaviour of widely stiffened conical shells under axial compression" Engineering structures (1999).

27. Sridharan S., Zeggane M., "Stiffened plate and cylindrical shells under interactive buckling" Finite element in analysis and design, 38(2001).

28. Sturm RG. "University of Illinois Bulletin No. 329, EE5". Urbana (IL): University of Illinois, 1941.

29. Timoshenko S. "Theory of Elastic stability" McGraw Hill (1936).

30. Ugural A.C. , "Stresses in plates and shell" McGraw Hill (1981).

31. Vandepitte D, Rathe J, Verhegghe B, Paridaens R, Verschaeve C. "Experimental investigation of hydrostatically loaded conical shells and practical evaluation of buckling loads". In: Ramm E, editor.

32. Walker A.C, Andronicou A.,Shridhan S., "Experimental investigation of the buckling of stiffened shells using small scale models" Buckling of shells in offshore structures, Granada (1981).

33. Winterstetter T.A., Schmidt H. "Stability of circular cylindrical steel shells under combined loading" Thin walled structures 40 (2002).

34. Zingoni A. "Shell structures in civil and mechanical engineering".London: Thomas Telford (1997).

Appendix A-FEM Results

UNSTIFFENED CYLINDRICAL SHELLS BUCKLING

AXIAL COMPRESSION

E= 2.00E+11 Pa
μ= 0.3
L= 1 m

$$\sigma_{cr} = \frac{E}{\sqrt{3\left(1-\mu^2\right)}}\left(\frac{t}{R}\right)$$

THEORETICAL

R	t [m]	R/t	σcyl[Mpa]	Pcyl[kN]
1	0.01	100	1210	76026.54
1	0.005	200	605	19006.64
1	0.0025	400	302.5	4751.66
1	0.002	500	242	3041.06
1	0.00125	800	151.25	1187.91
1	0.001	1000	121	760.27

FEM-ABAQUS

R/t	λ	Pcr[kN]	σcr[Mpa]	Pcr/Pcyl
100	12187	76573.18	1218.7	1.01
200	3135.5	19700.93	627.1	1.04
400	777.35	4884.234	310.94	1.03
500	489.35	3074.677	244.675	1.01
800	203.53	1278.817	162.824	1.08
1000	123.84	778.1097	123.84	1.02

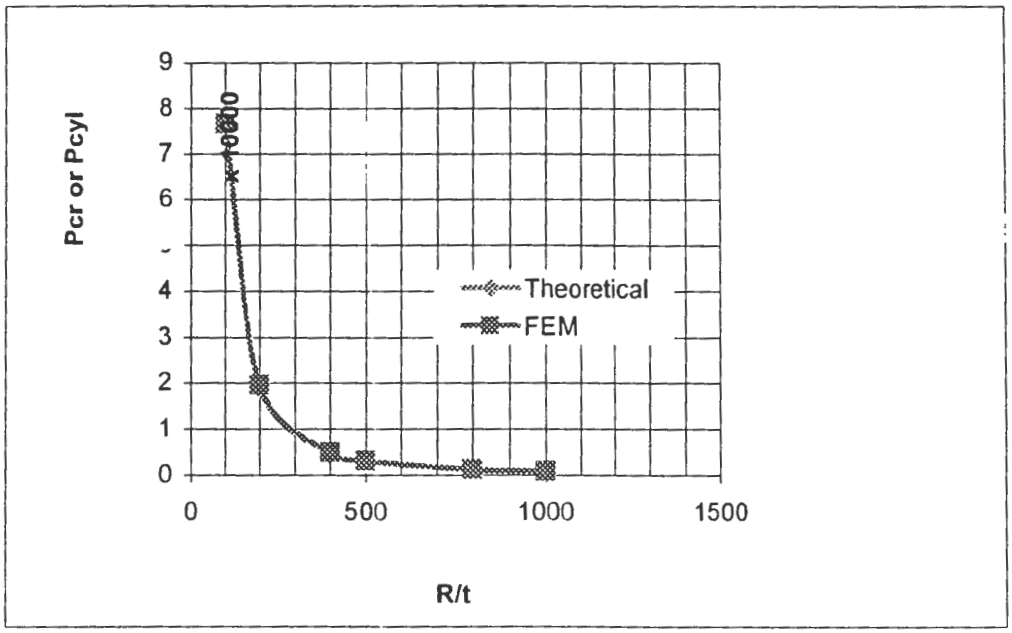

1 **Normalised Buckling load vs R/t for cylinders with varying number of stringer stiffeners**

R= 1 d/b= 5 d= 0.1 b= 0.02

R/t	100	200	400	500	800	1000
t [m]	0.01	0.005	0.0025	0.002	0.0013	0.0010

	N= 8				N= 16				N= 32			
R/t	λ	Pcr[kN]	σcr[Mpa]	Pcr/Pcyl	λ	Pcr[kN]	σcr[Mpa]	Pcr/Pcyl	λ	Pcr[kN]	σcr[Mpa]	Pcr/Pcyl
100	12971	91876	1165.468	1.20	15574	122772.7	1294.636	1.60	25882	245443.8	1935.191	3.21
200	3357	23778.25	501.482	1.21	4164.3	32827.95	517.661	1.67	6254.8	59315.43	621.651	3.01
400	891.05	6311.47	199.050	1.29	1099.9	8670.716	181.746	1.78	1491	14139.43	177.390	2.89
500	584.89	4142.9	145.027	1.35	715.79	5642.705	126.614	1.84	914.74	8674.649	113.296	2.82
800	261.19	1850.057	77.558	1.45	316.48	2494.87	62.600	1.95	376.68	3572.126	49.714	2.79
1000	160.44	1136.426	50.999	1.46	194.96	1536.906	40.146	1.98	238.67	2263.352	32.203	2.91

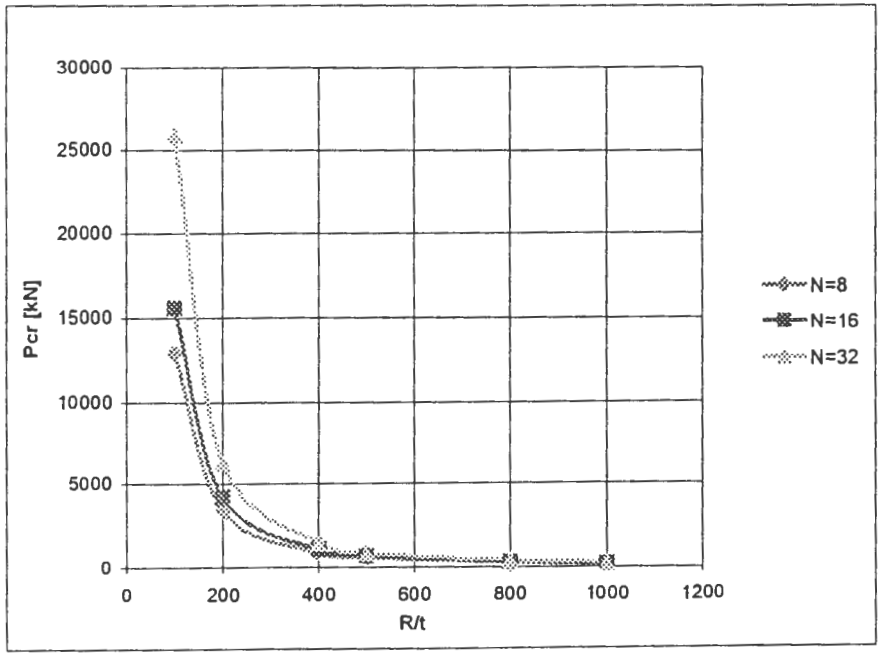

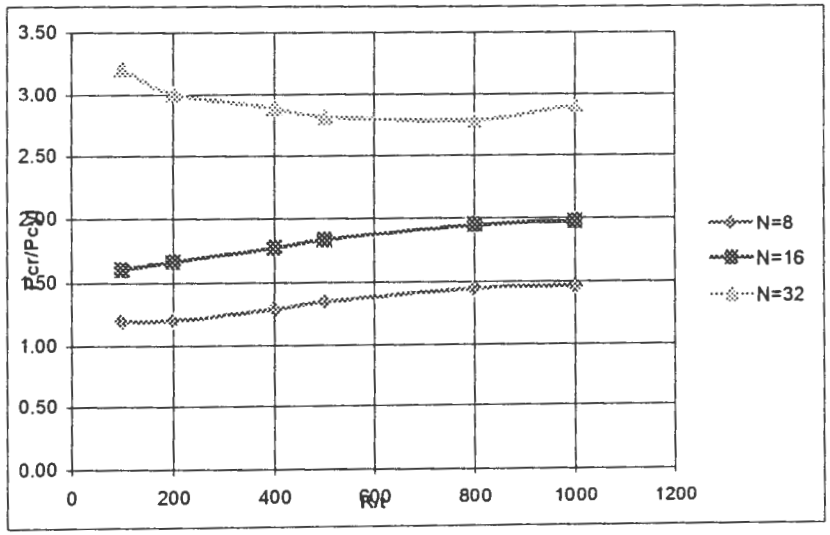

3 **Normalised Buckling load vs d/b of stringer stiffeners**

R/t= 100 d/t= 2
R= 1 N= 16 s= 0.393

Local			R/t= 100			t= 0.01
d/b	d [m]	b [m]	λ	Pcr[kN]	σcr[Mpa]	Pcr/Pcyl
2	0.02	0.0100	13290	87756.3327	1329	1.15
4	0.04	0.0100	14260	98724.6225	1426	1.30
6	0.06	0.0100	14234	103099.5	1423.4	1.36
8	0.08	0.0100	14084	106519.902	1408.4	1.40
10	0.10	0.0100	13788	108693.359	1378.8	1.43
12	0.12	0.0100	12777	104812.099	1277.7	1.38

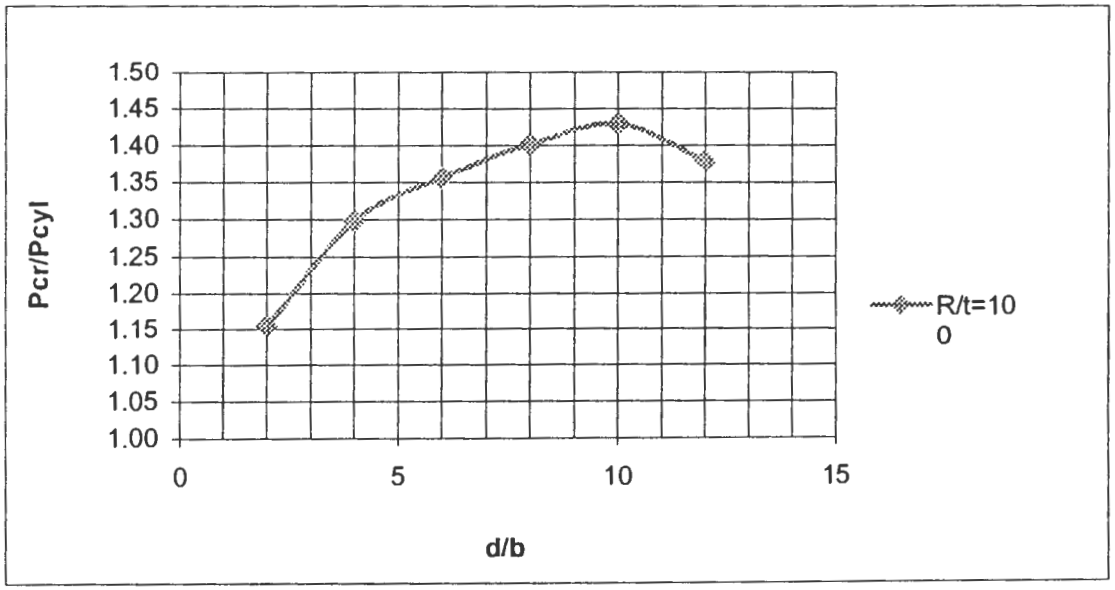

Local and Global Modes-Normalised Buckling load vs Number of stringer stiffeners

R= 1 ζ= 0.3

Note: Mode- Buckling mode Glo- Global buckling mode λ- eigenvalue
Loc- Local buckling mode Str- Stringer buckling mode

Local and Global					FE-Multi panel R/t=100 t= 0.01					FE-Multi panel R/t=200 t= 0.005				
N	s[m]	d/b	d[m]	b[m]	λ	Pcr[kN]	σcr[Mpa]	Pcr/Pcyl	Mode	λ	Pcr[kN]	σcr[Mpa]	Pcr/Pcyl	Mode
8	0.79	4.24	0.1	0.0236	13486	95523.8	1520.309	1.26	Loc	3457.9	24492.946	779.6347	1.29	Loc
16	0.39	2.12	0.05	0.0236	17032	120640.8	1920.058	1.59	Loc	4425.2	31344.512	997.7268	1.65	Loc
24	0.26	3.18	0.05	0.0157	18608	139247.1	2216 187	1.83	Glo	5691.8	42592.794	1355.771	2.24	Loc
32	0.20	4.24	0.05	0.0118	17639	139051.5	2213.073	1.83	Glo	8285.2	65313.767	2079.002	3.44	Glo
64	0.10	2.12	0.025	0.0118	13707	108054.8	1719.746	1.42	Glo	5137.7	40501.441	1289.201	2.13	Glo

Global					FEM-Smeared model				FEM-Smeared model			
R/t	s[m]	d[m]	b[m]	ts[m]	λ	Pcr[kN]	σcr[Mpa]	Pcr/Pcyl	λ	Pcr[kN]	σcr[Mpa]	Pcr/Pcyl
8	0.79	0.1	0.0236	0.013	20834	130903.9	2083.4	1.72	7757.3	48740.6	775.73	2.56
16	0.39	0.05	0.0236	0.013	20835	130910.2	2083.5	1.72	7758.3	48746.8	775.83	2.56
24	0.26	0.05	0.0157	0.013	20836	130916.4	2083.6	1.72	7759.3	48753.1	775.93	2.57
32	0.20	0.05	0.0118	0.013	20837	130922.7	2083.7	1.72	7760.3	48759.4	776.03	2.57
64	0.10	0.025	0.0118	0.013	20838	130929.0	2083.8	1.72	7761.3	48765.7	776.13	2.57

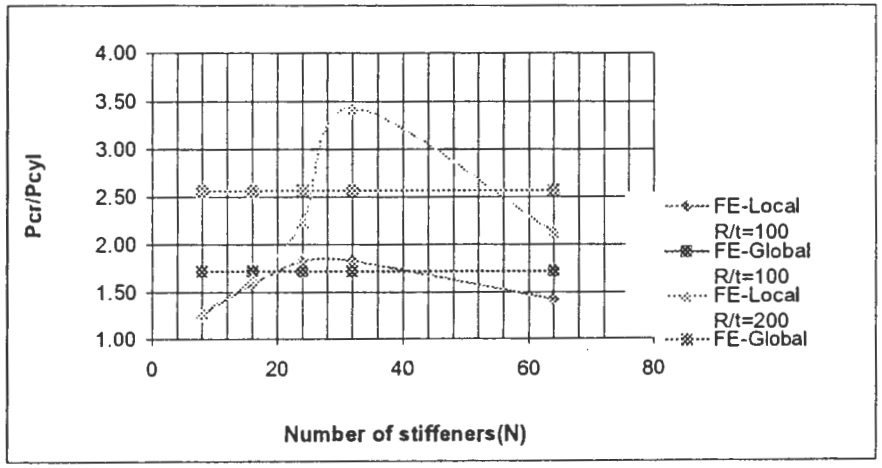

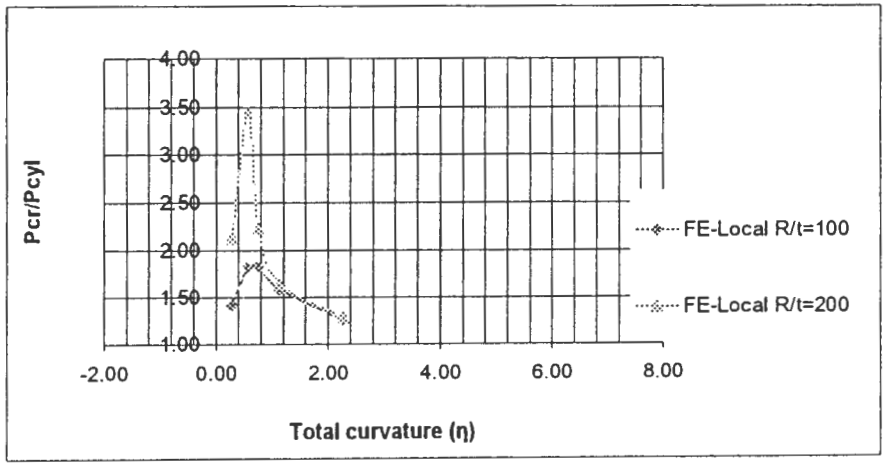

3 Local and Stringer Modes-Normalised Buckling load vs d/b of stringer stiffeners

R/t= 100 d/t= 2 E= 2.00E+11
R= 1 N= 16 s= 0.393 KST= 1.28

Local				Multi panel-R/t=100 t= 0.01					Shell only- t= 0.01					Theory-Stringers		
d/b	d [m]	b [m]	ts	λ	Pcr[kN]	σcr[Mpa]	Pcr/Pcyl	Buckling Mode	λ	Pcr[kN]	σcr[Mpa]	Pcr/Pcyl	Mode	σcr[Mpa]	Pcr[kN]	Pcr/Pcyl
2	0.02	0.0100	0.0105	13290	87756.33	1396.7	1.15	Loc	15740	98897.337	1574.0	1.30	Loc	57843.835	11568.77	47.80
4	0.04	0.0100	0.0110	14260	98724.62	1571.3	1.30	Loc	15740	98897.337	1574.0	1.30	Loc	14460.959	5784.384	11.95
6	0.06	0.0100	0.0115	14234	103099.5	1640.9	1.36	Loc	15740	98897.337	1574.0	1.30	Loc	6427.0928	3856.256	5.31
8	0.08	0.0100	0 0120	14084	106519.9	1695.3	1.40	Loc	15740	98897.337	1574.0	1.30	Loc	3615.2397	2892.192	2.99
10	0.10	0.0100	0.0125	13788	108693.4	1729.9	1.43	Loc	15740	98897.337	1574.0	1.30	Loc	2313.7534	2313.753	1.91
12	0.12	0.0100	0.0131	12777	104812.1	1668.1	1.38	Str	15740	98897.337	1574.0	1.30	Loc	1606.7732	1928.128	1.33
14	0.14	0.0100	0.0136	9717.5	82824.05	1318.2	1.09	Str	15740	98897.337	1574.0	1.30	Loc	1180.4864	1652.681	0.98
16	0.16	0.0100	0.0141	7740.7	68452.44	1089.5	0.90	Str	15740	98897.337	1574.0	1.30	Loc	903.80993	1446.096	0.75
18	0.18	0.0100	0.0146	6191.4	56732.95	902.9	0.75	Str	15740	98897.337	1574.0	1.30	Loc	714.12142	1285.419	0.59

Note: Mode- Buckling mode
λ- eigenvalue

Glo- Global buckling mode
Str- Stringer buckling mode
Loc- Local buckling mode

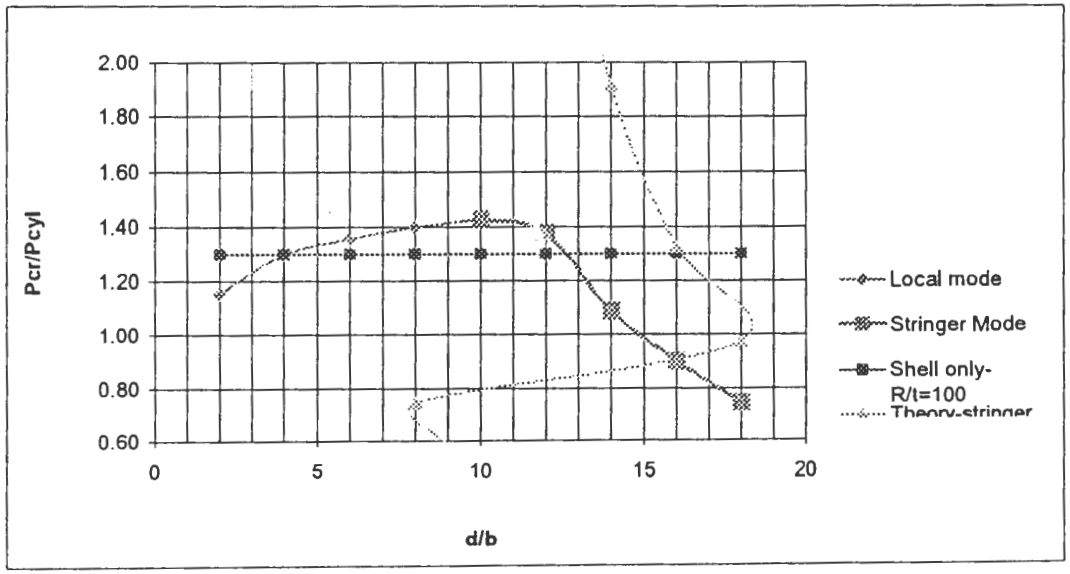

6 Local and Global Modes-Normalised Buckling load vs d/t of stringer stiffeners

R/t= 100 t= 0.01 d/b= 10.0 b= 0.01
R= 1 N= 16 s= 0.393

Local				FE-Multi Panel					FE-Smeared			
d/t	d [m]	t [m]	t_s	λ	Pcr[kN]	σcr[Mpa]	Pcr/Pcyl	Buckling Mode	λ	Pcr[kN]	σcr[Mpa]	Pcr/Pcyl
10	0.10	0.0100	0.0125	12064	95102.75	1206.4	1.25	Glo	18956	119104.1	1510.862	1.57
20	0.10	0.0050	0.0075	3891	30673.47	433.0463	1.61	Loc	6851.3	43047.99	907.8803	2.26
40	0.10	0.0025	0.0050	1044	8230.045	123.1456	1.73	Loc	3059.5	19223.41	606.2643	4.05
50	0.10	0.0020	0.0045	680.67	5365.848	81.2615	1.76	Loc	2458.3	15445.95	540.7041	5.08
80	0.10	0.0013	0.0038	278.86	2198.305	33.90779	1.85	Loc	1770.3	11123.12	466.3005	9.36
100	0.10	0.0010	0.0035	184.25	1452.477	22.54284	1.91	Loc	1497.8	9410.955	422.3344	12.38

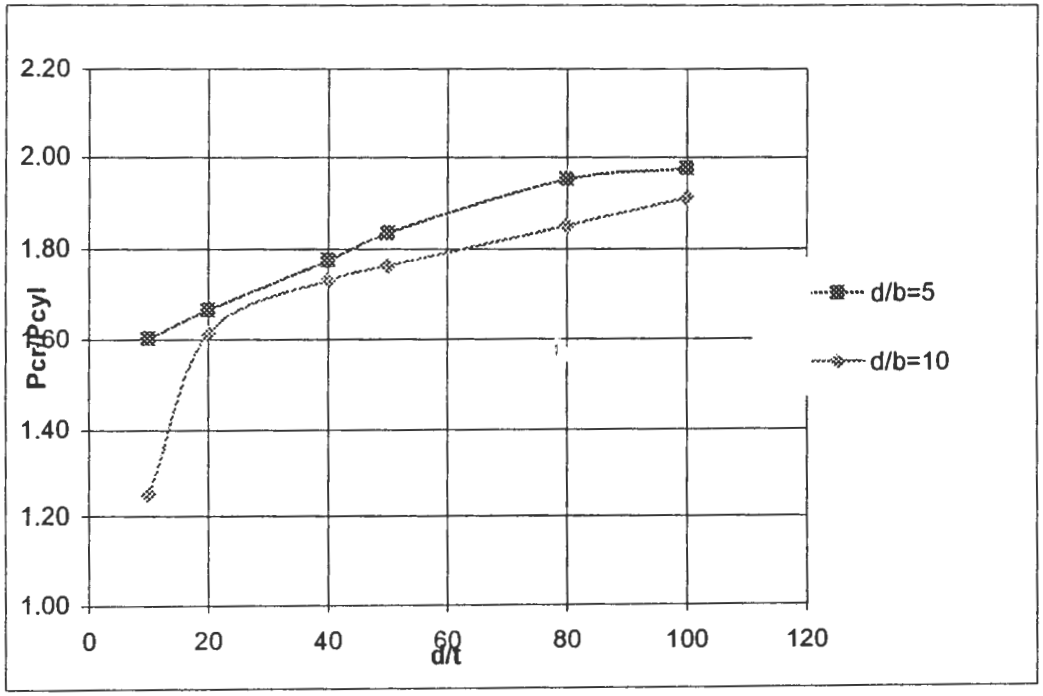

Local and Global Modes-Normalised Buckling load vs Number of ring stiffeners

R/t= 100 ζ= 0.3 H= 2 m
R= 1 t= 0.01 As= 0.005

Local					FEM-Multi Panel				FEM-Single Panel			
N	s[m]	d/b	d [m]	b [m]	λ	Pcr[kN]	σcr[Mpa]	Pcr/Pcyl	λ	Pcr[kN]	σcr[Mpa]	Pcr/Pcyl
2	0.67	1.00	0.05	0.0500	12525	78696.9	1252.5	1.04	13313	83648.05	1331.3	1.10
3	0.50	1.50	0.05	0.0333	13353	83899.37	1335.3	1.10	14562	91495.74	1456.2	1.20
4	0.40	2.00	0.05	0.0250	12351	77603.62	1235.1	1.02	18163	114121.5	1816.3	1.50
6	0.29	3.00	0.05	0.0167	14104	88618.05	1410.4	1.17	23019	144632.6	2301.9	1.90
8	0.22	4.00	0.05	0.0125	12069	75831.76	1206.9	1.00	27688	173968.8	2768.8	2.29

Global					FEM-Smeared model			
N	s [m]	d [m]	b [m]	ts	λ	Pcr[kN]	σcr[Mpa]	Pcr/Pcyl
2	0.67	0.05	0.0500	0.01375	23066	144928	2306.6	1.91

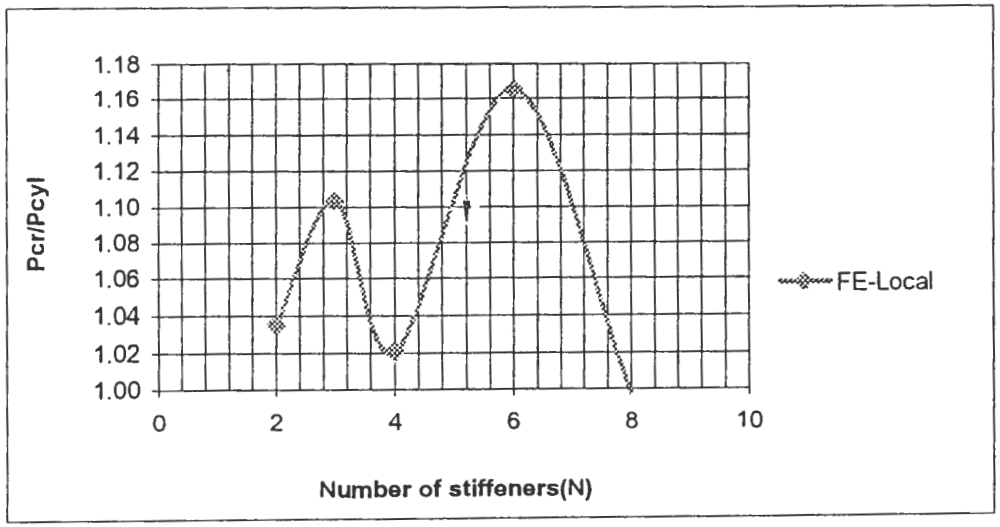

3 Local and Stringer Modes-Normalised Buckling load vs d/b of ring stiffeners

R/t= 100 E= 2.00E+11
R= 1 N= 6 s= 0.286 m Kst= 1.28

Local			Multi panel-R/t=100 t= 0.01					Multi panel-R/t=200 t= 0.005				
d/b	d [m]	b [m]	λ	Pcr[kN]	σcr[Mpa]	Pcr/Pcyl	uckling Mod	λ	Pcr[kN]	σcr[Mpa]	Pcr/Pcyl	Mode
2	0.02	0.0100	12811	80493.89	1281.1	1.06	Loc	3440	21614.16	344.0	1.14	Loc
4	0.04	0.0100	13294	83528.67	1329.4	1.10	Loc	3673.5	23081.28	367 4	1.21	Loc
6	0.06	0.0100	13679	85947.69	1367.9	1.13	Loc	3735.9	23473.35	373.6	1.24	Loc
8	0.08	0.0100	13987	87882.91	1398.7	1.16	Loc	3734.7	23465.81	373.5	1.23	Loc
10	0.10	0.0100	14237	89453.71	1423.7	1.18	Loc	3721	23379.73	372.1	1.23	Loc
12	0.12	0.0100	14421	90609.82	1442.1	1.19	Glo	3705.6	23282.97	370.6	1.22	Loc
14	0.14	0.0100	14460	90854.86	1446.0	1.20	Glo	3689.1	23179.3	368.9	1.22	Loc
16	0.16	0.0100	14605	91765.92	1460.5	1.21	Glo	3674	23084.42	367.4	1.21	Loc
18	0.18	0.0100	14786	92903.18	1478.6	1.22	Glo	3658.4	22986.41	365.8	1.21	Loc

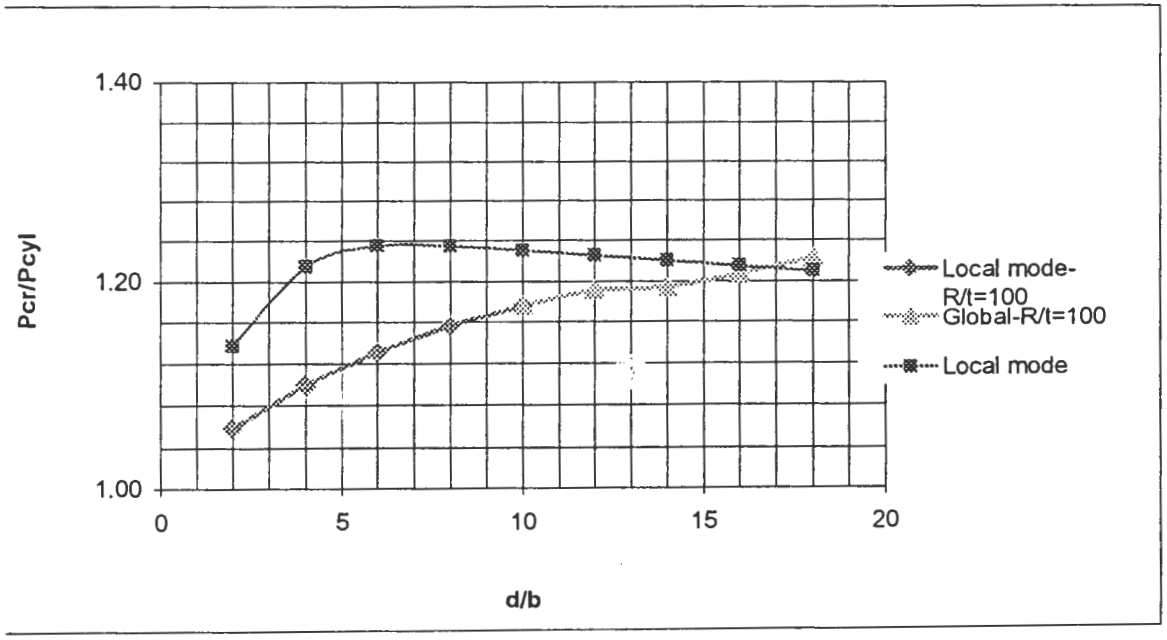

Note: Mode- Buckling mode
λ- eigenvalue
Glo- Global buckling mode
Str- Stringer buckling mode
Loc- Local buckling mode

5 Local and Global Modes-Normalised Buckling load vs d/t of ring stiffeners

R/t= 100 t= 0.01 b= 0.01

R= 1 N= 6 s= 1.047

Local				FE-Multi Panel			d/b= 1		d/b= 10				
d/t	d [m]	t [m]	ts	λ	Pcr[kN]	σcr[Mpa]	Pcr/Pcyl	Mode	λ	Pcr[kN]	σcr[Mpa]	Pcr/Pcyl	Mode
10	0.10	0.0100	0.0125	15421	96893	1229.11	1.27	Glo	14237	89453.71	1134.741	1.18	Loc
20	0.10	0.0050	0.0075	4190	26326.55	371.6767	1.39	Loc	3721	23379.73	493.0776	1.23	Loc
40	0.10	0.0025	0.0050	1315.4	8264.902	123.6671	1.74	Loc	782.27	4915.147	155.013	1.03	Loc
50	0.10	0.0020	0.0045	900.64	5658.888	85.69937	1.86	Loc	526.26	3306.589	115.7511	1.09	Loc
80	0.10	0.0013	0.0038	380.87	2393.077	36.91205	2.01	Loc	265.7	1669.442	69.9859	1.41	Loc
100	0.10	0.0010	0.0035	237.53	1492.445	23.16316	1.96	Loc	199.61	1254.187	56.28399	1.65	Loc

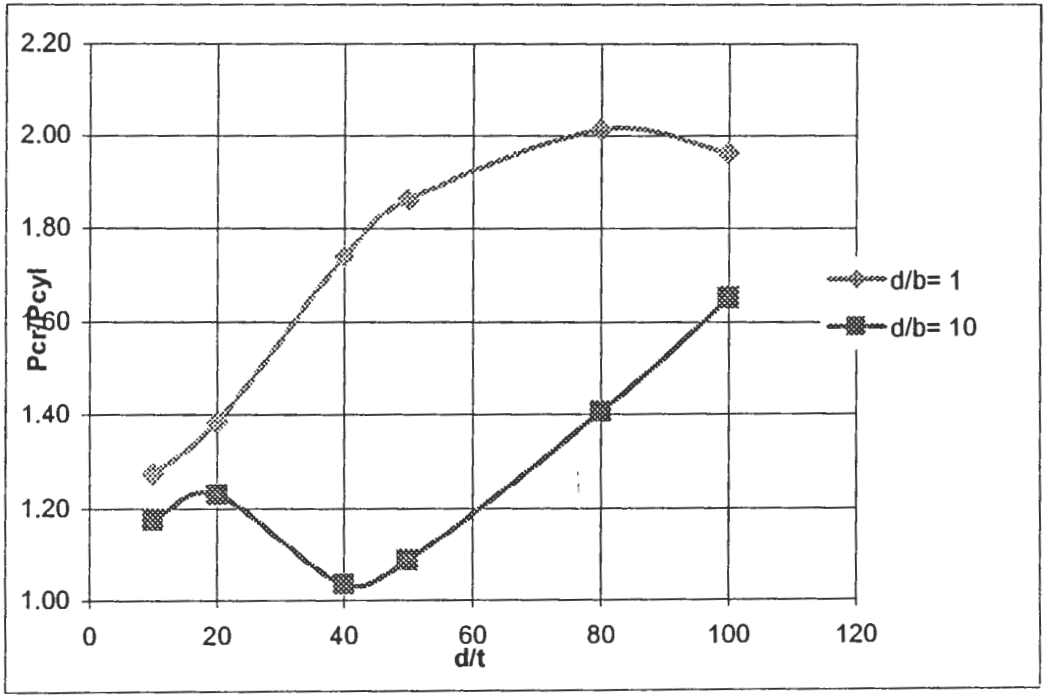

Note: Mode- Buckling mode
λ- eigenvalue
Glo- Global buckling mode
Str- Stringer buckling mode
Loc- Local buckling mode

UNSTIFFENED CYLINDRICAL SHELLS BUCKLING

EXTERNAL PRESSURE

E= 2.00E+11 Pa

μ= 0.3

L= 1 m

Z= 476.97 → Kp = 22.713229

$$\sigma_{cr} = K_P \frac{\pi^2 E}{12\,(1-\mu^2)}\left(\frac{t}{L}\right)^2$$

R	t [m]	R/t	σcyl[Mpa]	pcr[kN/m2]	Z	Kp
1	0.01	100	135.57	1355.70	95.39392	7.5
1	0.005	200	58.747	293.74	190.7878	13
1	0.0025	400	19.20575	48.01	381.5757	17
1	0.002	500	13.37624	26.75	476.9696	18.5
1	0.00125	800	7.343375	9.18	763.1514	26
1	0.001	1000	5.4228	5.42	953.9392	30

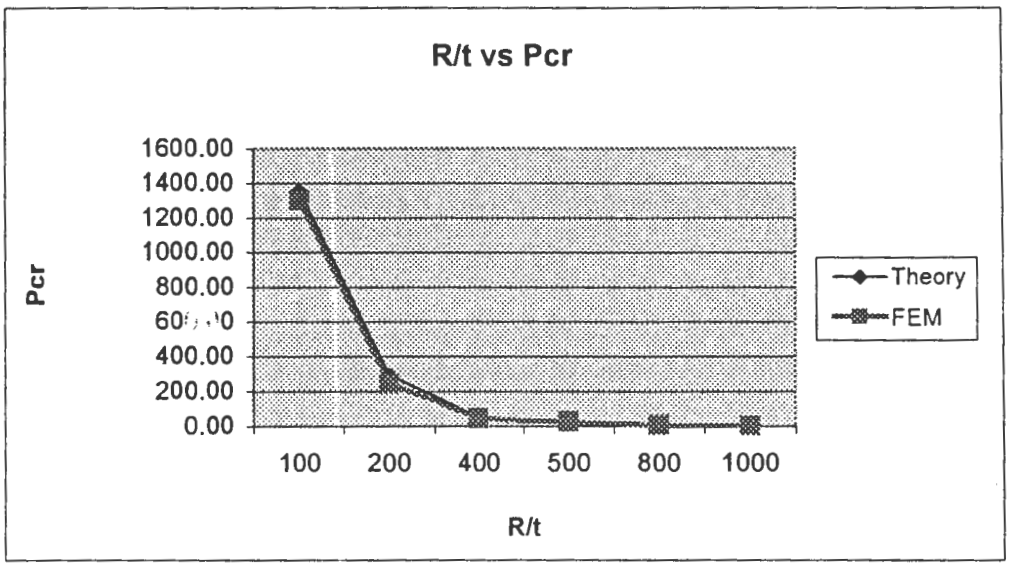

1 **Normalised Buckling load vs R/t for cylinders with varying number of stringer stiffeners**

R= 1 d/b= 5 d= 0.1 b= 0.02

R/t	100	200		400	500	800	1000
t [m]	0.01	0.005		0.0025	0.002	0.00125	0.001

	N=8				N=16				N=32			
R/t	λ	pcr[kN/m2]	σcr[Mpa]	Pcr/Pcyl	λ	Pcr[kN]	σcr[Mpa]	Pcr/Pcyl	λ	Pcr[kN]	σcr[Mpa]	Pcr/Pcyl
100	1593.1	1593.1	159.31	1.22	1708	1708	2.091479477	1.31	3184.5	3184.5	4.180727	2.45
200	302.98	302.98	60.596	1.24	416.76	416.76	0.51869021	1.71	1255.1	1255.1	2.148683	5.16
400	64.394	64.394	25.7576	1.43	115.58	115.58	0.165465952	2.57	329	329	0.845394	7.31
500	39	39	19.5	1.47	70.298	70.298	0.103239268	2.65	200.22	200.22	0.530015	7.54
800	13.721	13.721	10.9768	1.57	24.619	24.619	0.038684986	2.82	57.912	57.912	0.163277	6.63
1000	7.3566	7.3566	7.3566	1.42	15.67	15.67	0.022306099	3.03	30.454	30.454	0.09234	5.89

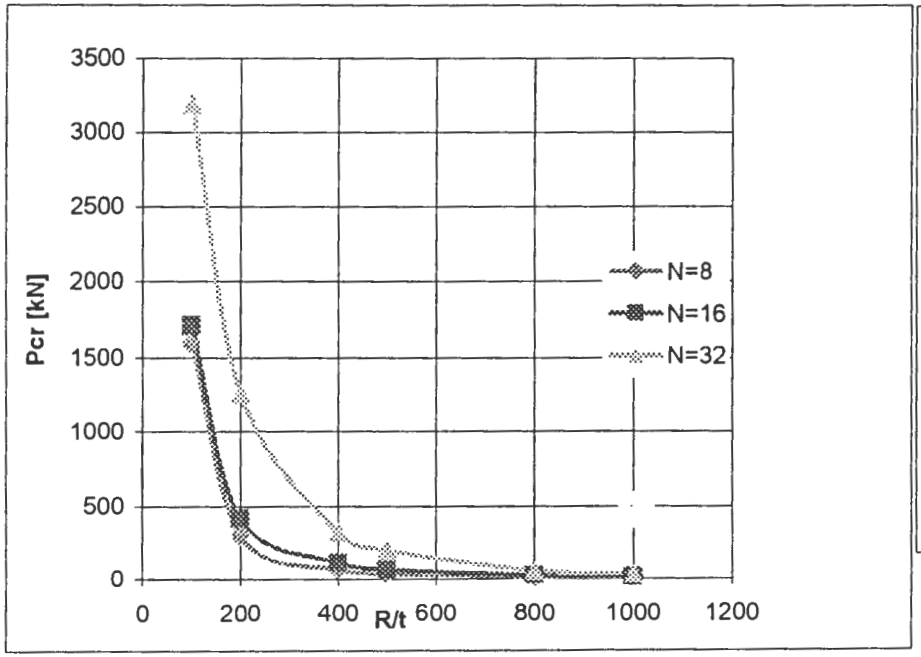

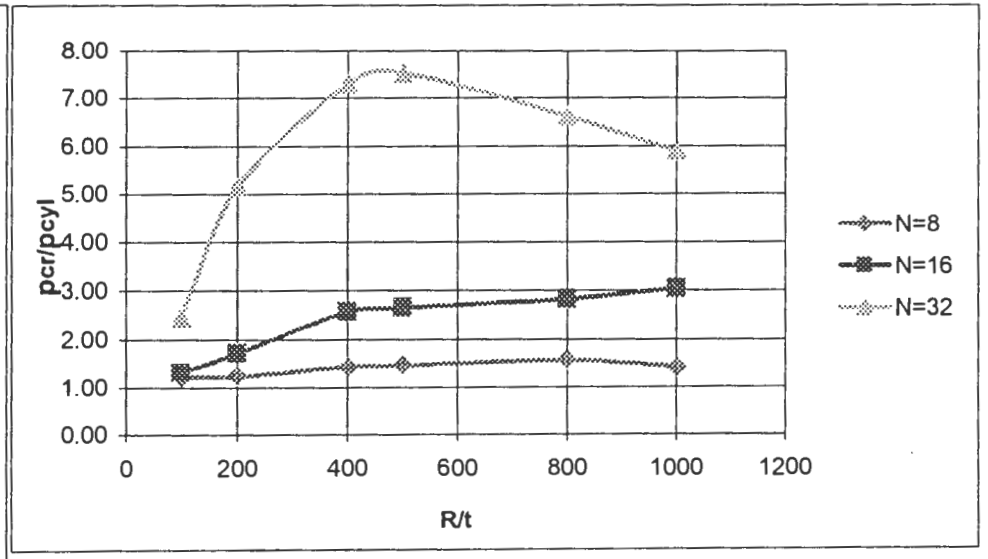

1 **Normalised Buckling load vs R/t for cylinders with varying number of stringer stiffeners**

R= 1 d/b= 5 d= 0.1 b= 0.02

R/t	100	200		400	500	800	1000
t [m]	0.01	0.005		0.0025	0.002	0.00125	0.001

	N= 2				N= 3				N= 4				N= 6				N= 8			
R/t	λ	pcr[kN/m2]	σcr[Mpa]	Pcr/Pcyl	λ	Pcr[kN]	σcr[Mpa]	Pcr/Pcyl	λ	Pcr[kN]	σcr[Mpa]	Pcr/Pcyl	λ	Pcr[kN]	σcr[Mpa]	Pcr/Pcyl	λ	Pcr[kN]	σcr[Mpa]	Pcr/Pcyl
100	4025.3	4025.3	402.53	3.09	5642.7	5642.7	564.27	4.34	7068.2	7068.2	706.82	5.43	11492	11492	1149.2	8.83	15086	15086	1508.6	11.60
200	729.94	729.94	145.988	3.00	1068.8	1068.8	213.76	4.39	1495.5	1495.5	299.1	6.14	3015.4	3015.4	603.08	12.39	9322.8	9322.8	1864.56	38.30
400	140.84	140.84	56.336	3.13	210.11	210.11	84.044	4.67	284.67	284.67	113.868	6.33	525.28	525.28	210.112	11.68	1401.2	1401.2	560.48	31.15
500	84.494	84.494	42.247	3.18	127.18	127.18	63.59	4.79	172.23	172.23	86.115	6.49	314.68	314.68	157.34	11.85	799.78	799.78	399.89	30.12
800	31.856	31.856	25.4848	3.65	48.884	48.884	39.1072	5.60	67.268	67.268	53.8144	7.70	123.22	123.22	98.576	14.11	309.47	309.47	247.576	35.44
1000	17.66	17.66	17.66	3.42	27.507	27.507	27.507	5.32	38.528	38.528	38.528	7.46	71.309	71.309	71.309	13.80	184.63	184.63	184.63	35.73

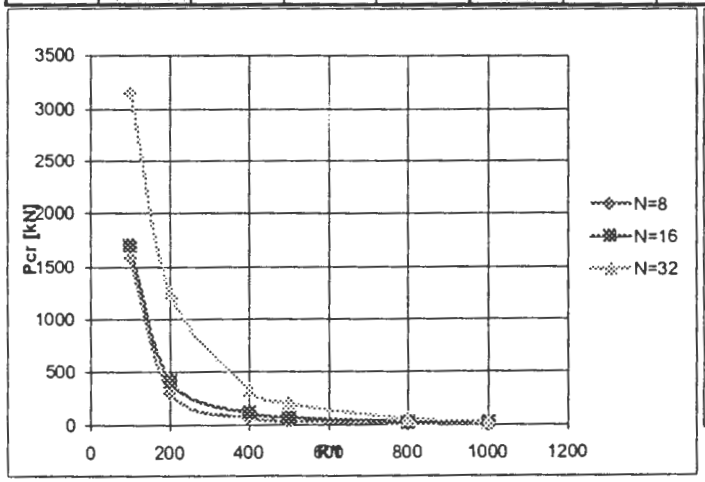

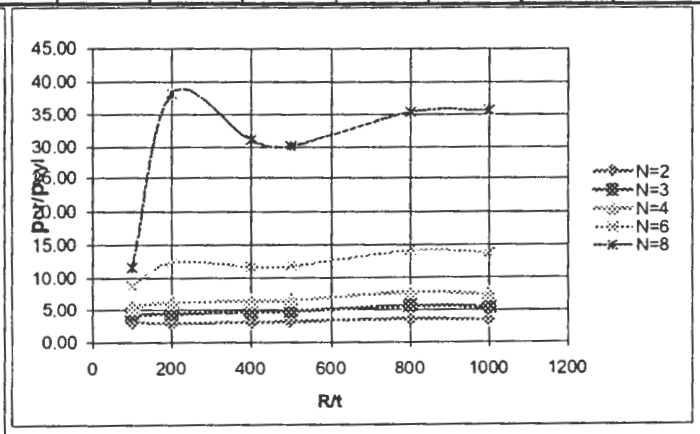

Local and Global Modes-Normalised Buckling load vs Number of stringer stiffeners

R= 1 ζ= 0.3

Local and Global					FE-Multi panel R/t=10(t= 0.01					FE-Multi panel R/t=20(t= 0.005				
N	s[m]	d/b	d[m]	b[m]	λ	Pcr[kN/m2]	σcr[Mpa]	Pcr/Pcyl	Mode	λ	Pcr[kN/m2]	σcr[Mpa]	Pcr/Pcyl	Mode
8	0.79	4.24	0.1	0.0236	1653.5	1653.5	26.3	1.22	Loc	326	326	10.4	1.11	Loc
16	0.39	2.12	0.05	0.0236	1584.5	1584.5	25.2	1.17	Loc	365.21	365.21	11.6	1.24	Loc
24	0.26	3.18	0.05	0.0157	1565.1	1565.1	24.9	1.15	P	411.97	411.97	13.1	1.40	P
32	0.20	4.24	0.05	0.0118	1576.5	1576.5	25.1	1.16	P	410	410	13.1	1.40	P
64	0.10	2.12	0.025	0.0118	1351.2	1351.2	21.5	1.00	P	300.92	300.92	9.6	1.02	P

Global					FEM-Smeared model				FEM-Smeared model			
R/t	s[m]	d[m]	b[m]	ts[m]	λ	Pcr[kN/m2]	σcr[Mpa]	Pcr/Pcyl	λ	Pcr[kN/m2]	σcr[Mpa]	Pcr/Pcyl
8	0.79	0.1	0.1	0.0236	2310.7	2310.7	15.6	1.70	699.26	699.3	4.7	2.38
16	0.39	0.05	0.05	0.0236	2310.7	2310.7	15.6	1.70	699.26	699.3	4.7	2.38
24	0.26	0.05	0.05	0.0157	2310.7	2310.7	23.4	1.70	699.26	699.3	7.1	2.38
32	0.20	0.05	0.05	0.0118	2310.7	2310.7	31.2	1.70	699.26	699.3	9.4	2.38
64	0.10	0.025	0.025	0.0118	2310.7	2310.7	31.2	1.70	699.26	699.3	9.4	2.38

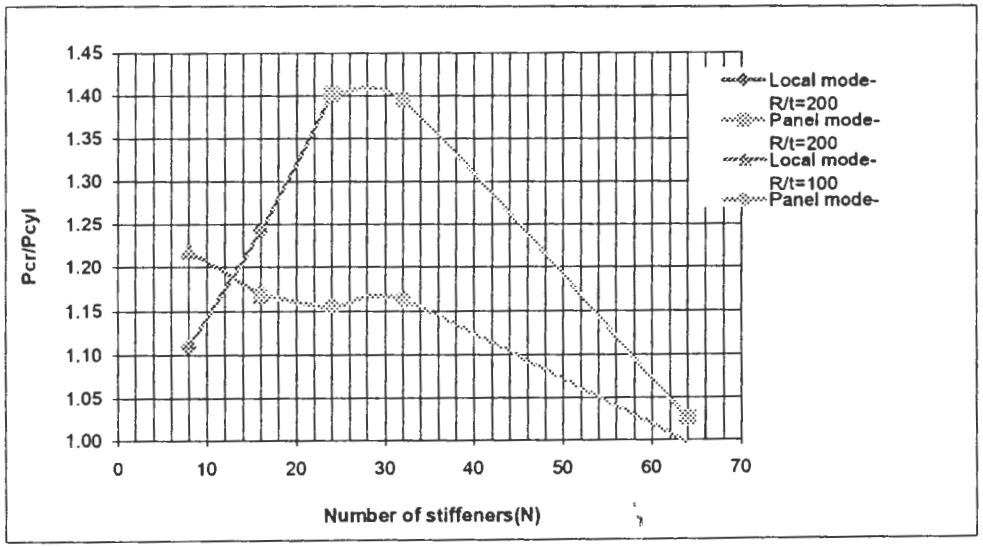

6 Local and Global Modes-Normalised Buckling load vs d/t of stringer stiffeners

R/t= 100 t= 0.01 d/b= 5.0 b= 0.01
R= 1 N= 16 s= 0.393

Local				FE-Multi Panel					FE-Smeared			
d/t	d [m]	t [m]	ts	λ	Pcr[kN]	σcr[Mpa]	Pcr/Pcyl	uckling Mod	λ	Pcr[kN]	σcr[Mpa]	Pcr/Pcyl
10	0.10	0.0100	0.0125	1708	1708	21.67	1.31	Glo	18956	18956	240.46	13.98
20	0.10	0.0050	0.0075	416.76	416.76	5.88	1.71	Loc	6851.3	6851.3	144.49	23.32
40	0.10	0.0025	0.0050	115.58	115.58	1.73	2.57	Loc	3059.5	3059.5	96.49	63.72
50	0.10	0.0020	0.0045	70.298	70.298	1.06	2.65	Loc	2458.3	2458.3	86.06	91.89
80	0.10	0.0013	0.0038	24.619	24.619	0.38	2.82	Loc	1770.3	1770.3	74.21	192.86
100	0.10	0.0010	0.0035	15.67	15.67	0.24	3.03	Loc	1497.8	1497.8	67.22	276.20

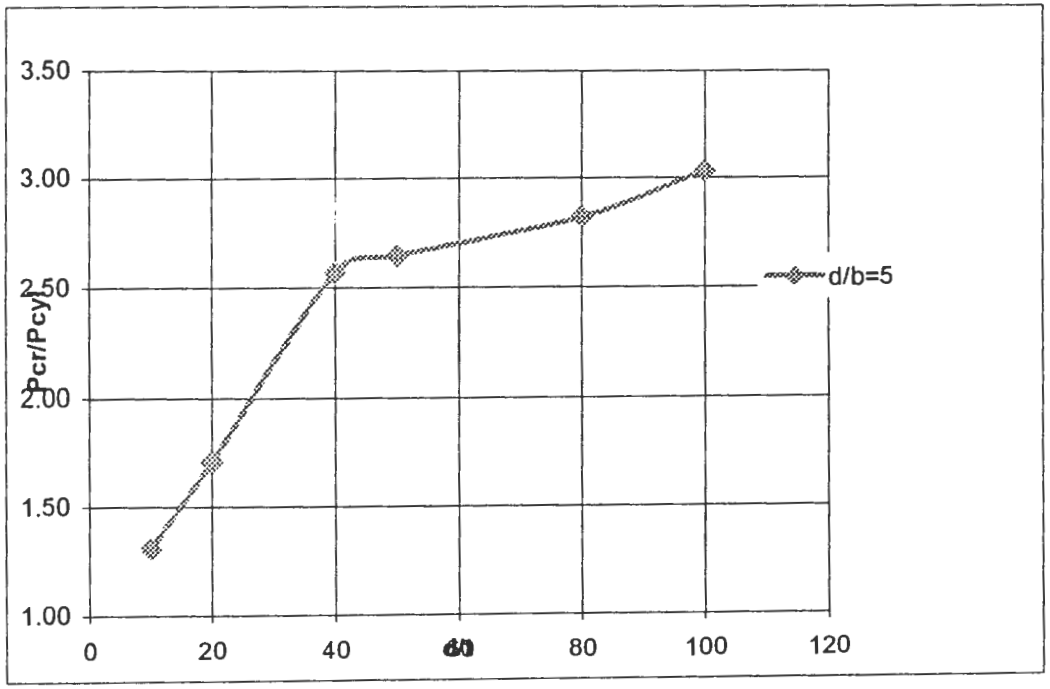

Local and Global Modes-Normalised Buckling load vs Number of ring stiffeners

R/t= 100 ζ= 0.3 H= 2 m
R= 1 t= 0.01 As= 0.005

Local					FEM-Multi Panel				
N	Str	d/b	d [m]	b [m]	λ	Pcr[kN]	σcr[Mpa]	Pcr/Pcyl	Mode
2	0.67	1.00	0.05	0.0500	4025.3	4025.3	64.06	2.97	Loc
3	0.50	1.50	0.05	0.0333	5053.1	5053.1	80.42	3.73	Glo
4	0.40	2.00	0.05	0.0250	5620.2	5620.2	89.45	4.15	Glo
6	0.29	3.00	0.05	0.0167	6944.7	6944.7	110.53	5.12	Glo
8	0.22	4.00	0.05	0.0125	7975.4	7975.4	126.93	5.88	Glo

Global					FEM-Smeared model			
N	s	d [m]	b [m]	t_s	λ	Pcr[kN]	σcr[Mpa]	Pcr/Pcyl
2	0.67	0.05	0.0500	0.01375	23066	23066	266.9868	17.01

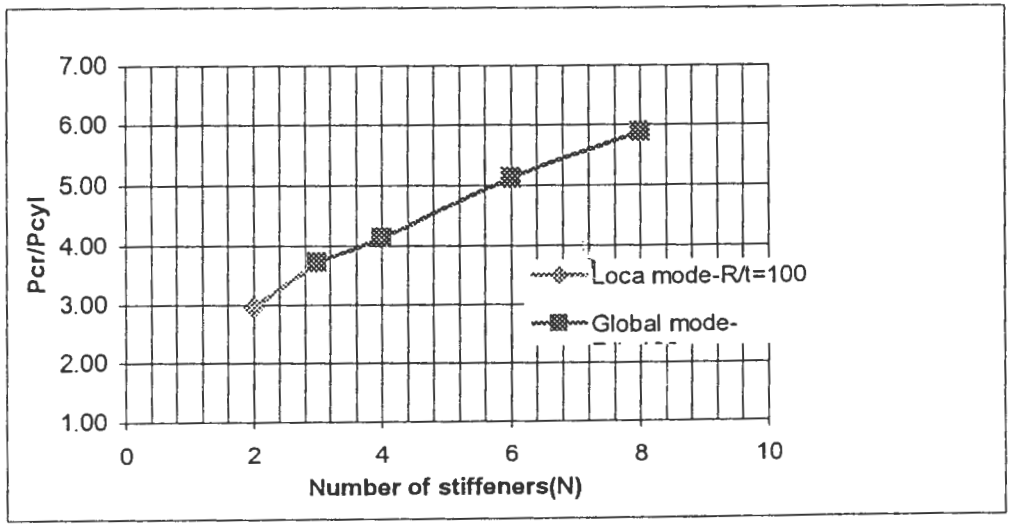

3 Local and Stringer Modes-Normalised Buckling load vs d/b of ring stiffeners

R/t= 100 s= 0.286 m
R= 1 N= 6

Local			Multi panel-R/t=100			t= 0.01	
d/b	d [m]	b [m]	λ	Pcr[kN]	σcr[Mpa]	Pcr/Pcyl	Mode
2	0.02	0.0100	1741.6	1741.6	27.7	1.28	Glo
4	0.04	0.0100	4185.8	4185.8	66.6	3.09	Glo
6	0.06	0.0100	7361.5	7361.5	117.2	5.43	Glo
8	0.08	0.0100	12003	12003	191.0	8.85	Glo
10	0.10	0.0100	17123	17123	272.5	12.63	Glo
12	0.12	0.0100	16909	16909	269.1	12.47	Glo
14	0.14	0.0100	15235	15235	242.5	11.24	Loc
16	0.16	0.0100	13854	13854	220.5	10.22	Loc
18	0.18	0.0100	12166	12166	193.6	8.97	Loc

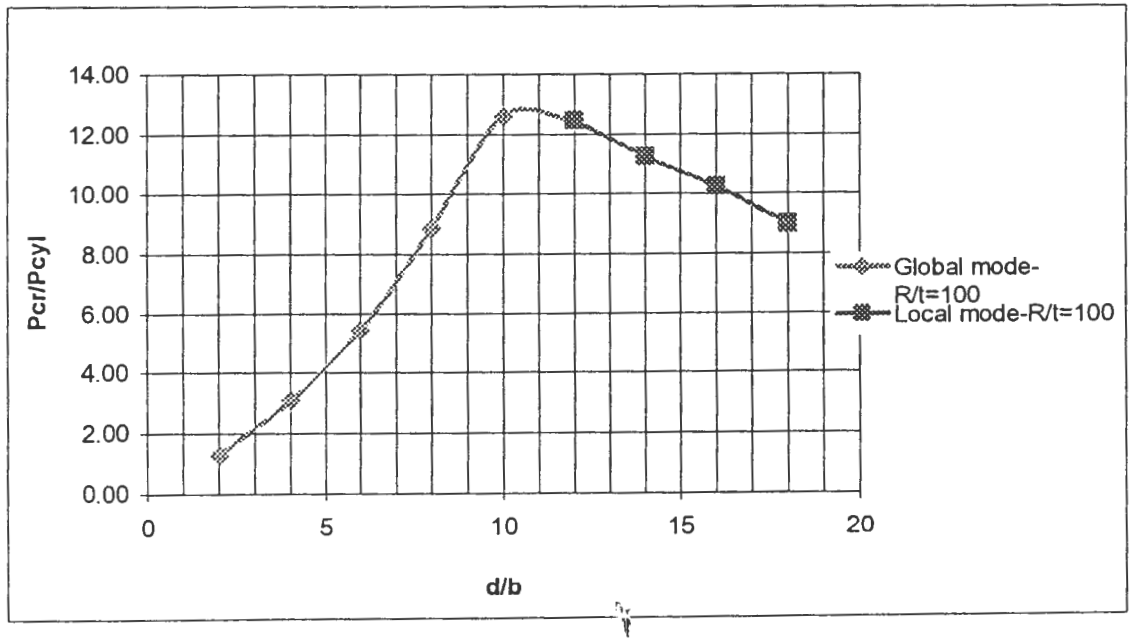

1 Normalised Buckling load vs R/t for cylinders with varying number of stringer stiffeners

R= 1 d/b= 5 d= 0.1 b= 0.02

R/t	100	200	400	500	800	1000
t [m]	0.01	0.005	0.0025	0.002	0.00125	0.001

	N=8				N=16				N=32			
R/t	λ	Tcr[kN/m]	Tcr[Mpa]	Tcr/Tcyl	λ	Tcr[kN/m]	Tcr[Mpa]	Tcr/Tcyl	λ	Tcr[kN/m]	Tcr[Mpa]	Tcr/Tcyl
100	5267.9	5267.9	526.79	1.23	8106.3	8106.3	810.63	1.90	17182	17182	1718.2	4.02
200	1510	1510	302	1.52	2891.8	2891.8	578.36	2.91	9421	9421	1884.2	9.49
400	341.51	341.51	136.604	1.42	937.86	937.86	375.144	3.89	5503	5503	2201.2	22.84
500	206.39	206.39	103.195	1.34	621.77	621.77	310.885	4.04	4444	4444	2222	28.86
800	73.7	73.7	58.96	1.21	244.92	244.92	195.936	4.01	2851.2	2851.2	2280.96	46.71
1000	46.417	46.417	46.417	1.17	155.17	155.17	155.17	3.91	2100	2100	2100	52.93

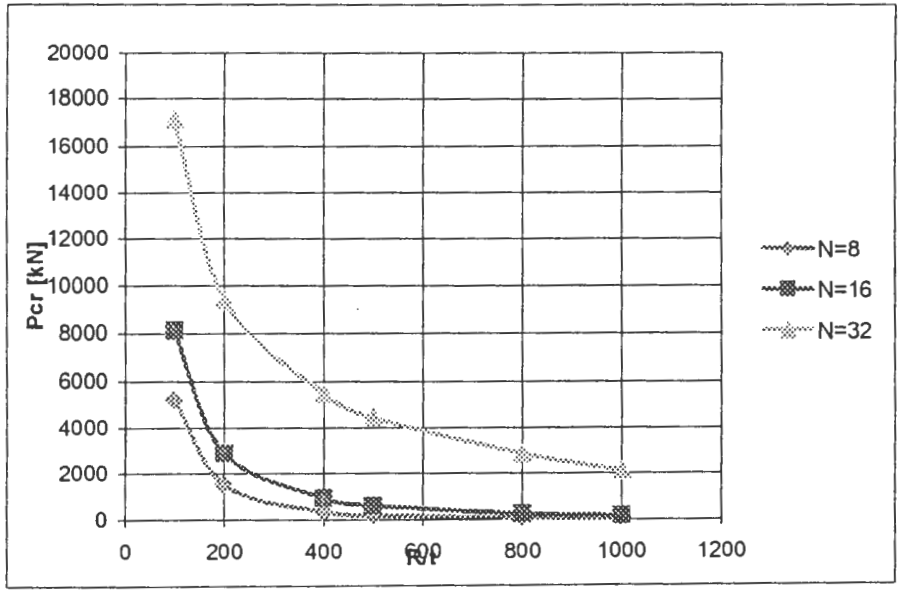

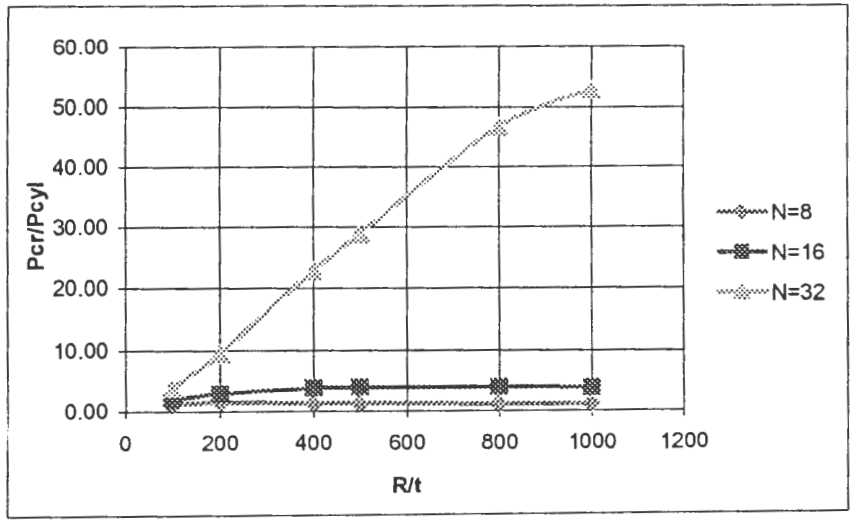

1 Normalised Buckling load vs R/t for cylinders with varying number of ring stiffeners

R= 1 d/b= 1 d= 0.05 b= 0.05

R/t	100	200	400	500	800	1000
t [m]	0.01	0.005	0.0025	0.002	0.00125	0.001

	N= 2				N= 3				N= 4				N= 6				N= 8			
R/t	λ	Tcr[kN/m]	Tcr[Mpa]	Tcr/Tcyl	λ	Tcr[kN/m]	Tcr[Mpa]	Tcr/Tcyl	λ	Tcr[kN/m]	Tcr[Mpa]	Tcr/Tcyl	λ	Tcr[kN/m]	Tcr[Mpa]	Tcr/Tcyl	λ	Tcr[kN/m]	Tcr[Mpa]	Tcr/Tcyl
100	6962	6962	696.2	1.63	8934	8934	893.4	2.09	11518	11518	1151.8	2.70	17422	17422	1742.2	4.08	23586	23586	2358.6	5.52
200	1684.2	1684.2	336.84	1.70	2206.3	2206.3	441.26	2.22	2794.4	2794.4	558.88	2.81	4797	4797	959.4	4.83	5033.7	5033.7	1006.74	5.07
400	423.1	423.1	169.24	1.76	573.24	573.24	229.296	2.38	702.39	702.39	280.956	2.92	1198.2	1198.2	479.28	4.97	1353.4	1353.4	541.36	5.62
500	276.15	276.15	138.075	1.79	381	381	190.5	2.47	470	470	235	3.05	765.65	765.65	382.825	4.97	954.44	954.44	477.22	6.20
800	123.9	123.9	99.12	2.03	176.54	176.54	141.232	2.89	228.97	228.97	183.176	3.75	359	359	287.2	5.88	518.87	518.87	415.096	8.50
1000	76.69	76.69	76.69	1.93	110.74	110.74	110.74	2.79	150.59	150.59	150.59	3.80	238.48	238.48	238.48	6.01	363.79	363.79	363.79	9.17

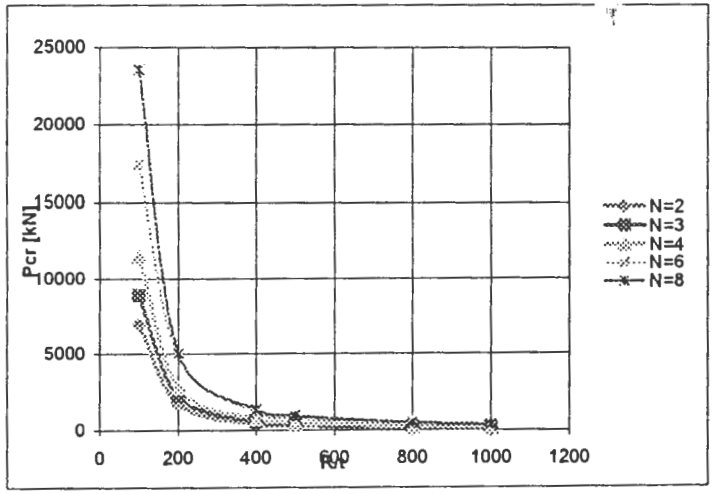

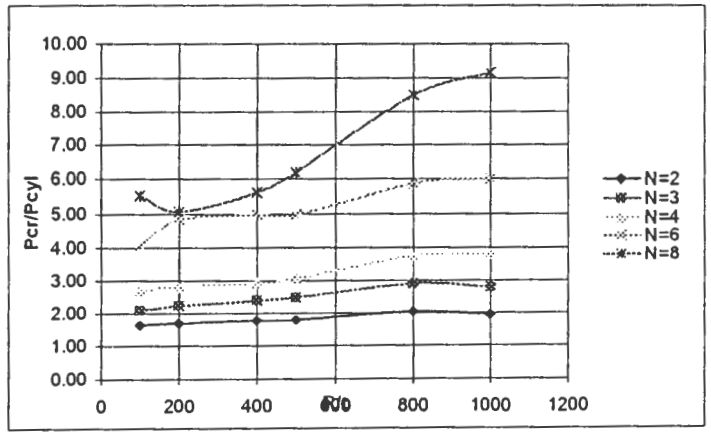

Local and Global Modes-Normalised Buckling load vs Number of stringer stiffeners

R= 1 ζ= 0.3

Local and Global					FE-Multi panel R/t=10 t= 0.01					FE-Multi panel R/t=20 t= 0.005				
N	s[m]	d/b	d[m]	b[m]	λ	Tcr[kN/m]	Tcr[Mpa]	Tcr/Tcyl	Mode	λ	Tcr[kN/m]	Tcr[Mpa]	Tcr/Tcyl	Mode
8	0.79	4.24	0.1	0.0236	6023.5	6023.5	602.35	1.28	P	1541.7	1541.7	308.34	1.56	Loc
16	0.39	2.12	0.05	0.0236	5759.9	5759.9	575.99	1.22	P	1850.7	1850.7	370.14	1.87	P
24	0.26	3.18	0.05	0.0157	5979	5979.0	597.9	1.27	Glo	2125.1	2125.1	425.02	2.15	P
32	0.20	4.24	0.05	0.0118	6166.2	6166.2	616.62	1.31	Glo	2356	2356	471.2	2.38	P
64	0.10	2.12	0.025	0.0118	4491.4	4491.4	449.14	0.95	Glo	1371	1371	274.2	1.39	P

Global					FEM-Smeared model			
R/t	s[m]	d[m]	b[m]	ts[m]	λ	Tcr[kN/m]	Tcr[Mpa]	Tcr/Tcyl
8	0.79	0.1	0.1	0.0236	3461.7	3461.7	23.3829	0.74
16	0.39	0.05	0.05	0.0236	3461.7	3461.7	23.3829	0.74
24	0.26	0.05	0.05	0.0157	3461.7	3461.7	35.07435	0.74
32	0.20	0.05	0.05	0.0118	3461.7	3461.7	46.76581	0.74
64	0.10	0.025	0.025	0.0118	3461.7	3461.7	46.76581	0.74

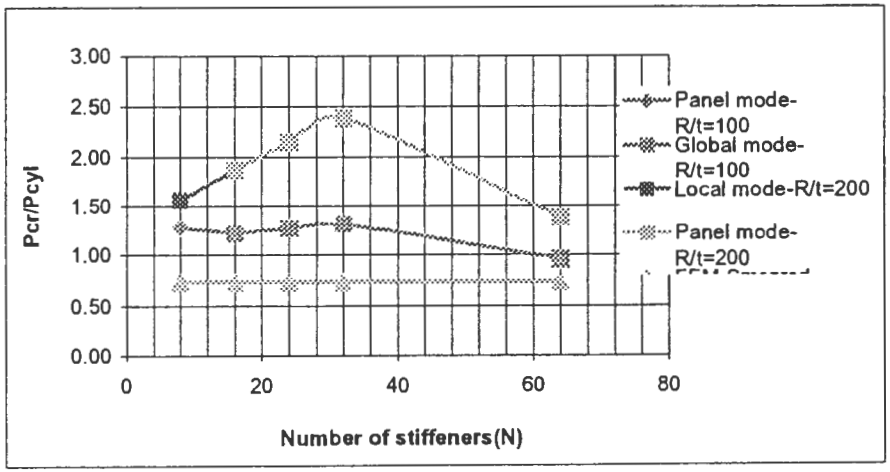

3 Local and Global Modes-Normalised Buckling load vs d/b of stringer stiffeners

R/t= 100 E= 2.00E+11
R= 1 N= 16 s= 0.393 Kst= 1.28

Local				FE-R/t=100				t= 0.01	FE-R/t=200				t= 0.005
d/b	d [m]	b [m]	ts	λ	Tcr[kN/m]	Tcr[Mpa]	Tcr/Tcyl	Mode	λ	Tcr[kN/m]	Tcr[Mpa]	Tcr/Tcyl	Mode
2	0.02	0.0100	0.0105	3972.2	3972.2	397.2	1.05	Glo	950.48	950.48	190.096	1.14	Glo
4	0.04	0.0100	0.0110	4410	4410	441.0	1.17	Glo	1151.5	1151.5	230.3	1.38	P
6	0.06	0.0100	0.0115	4865.2	4865.2	486.5	1.29	Glo	1360.8	1360.8	272.16	1.63	P
8	0.08	0.0100	0.0120	5583.1	5583.1	558.3	1.48	P	1706.9	1706.9	341.38	2.05	P
10	0.10	0.0100	0.0125	6239.3	6239.3	623.9	1.65	P	2014.9	2014.9	402.98	2.41	Loc
12	0.12	0.0100	0.0131	6941.5	6941.5	694.2	1.83	P	2316.1	2316.1	463.22	2.78	Loc
14	0.14	0.0100	0.0136	7687.5	7687.5	768.8	2.03	P	2596.3	2596.3	519.26	3.11	Loc
16	0.16	0.0100	0.0141	75..6	7599.6	760.0	2.01	Str	2968.5	2968.5	593.7	3.56	Str
18	0.18	0.0100	0.0146	5925.5	5925.5	592.6	1.57	Str	2379.2	2379.2	475.84	2.85	Str

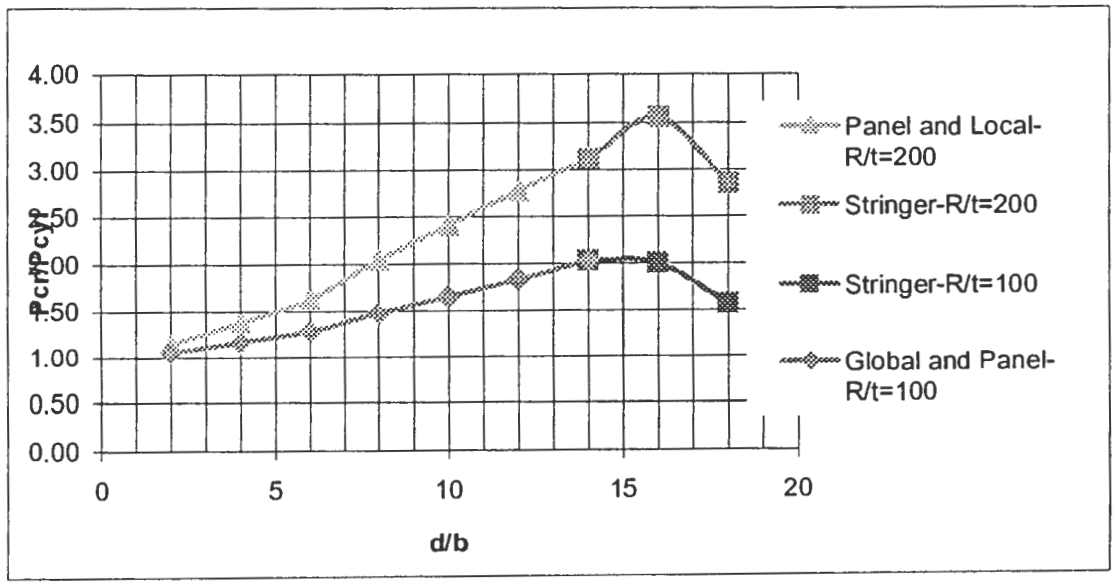

5 Local and Global Modes-Normalised Buckling load vs d/t of stringer stiffeners

R/t= 100 t= 0.01 d/b= 5.0
R= 1 N= 16 s= 0.393
b= 0.01

Local			FE-Multi Panel				
d/t	d [m]	t [m]	λ	Pcr[kN]	σcr[Mpa]	Pcr/Pcyl	Mode
10	0.10	0.0100	8106.3	8106.3	102.83	1.90	Glo
20	0.10	0.0050	2891.8	2891.8	40.83	2.91	Loc
40	0.10	0.0025	937.86	937.86	14.03	3.89	Loc
50	0.10	0.0020	621.77	621.77	9.42	4.04	Loc
80	0.10	0.0013	244.92	244.92	3.78	4.01	Loc
100	0.10	0.0010	155.17	155.17	2.41	3.91	Loc

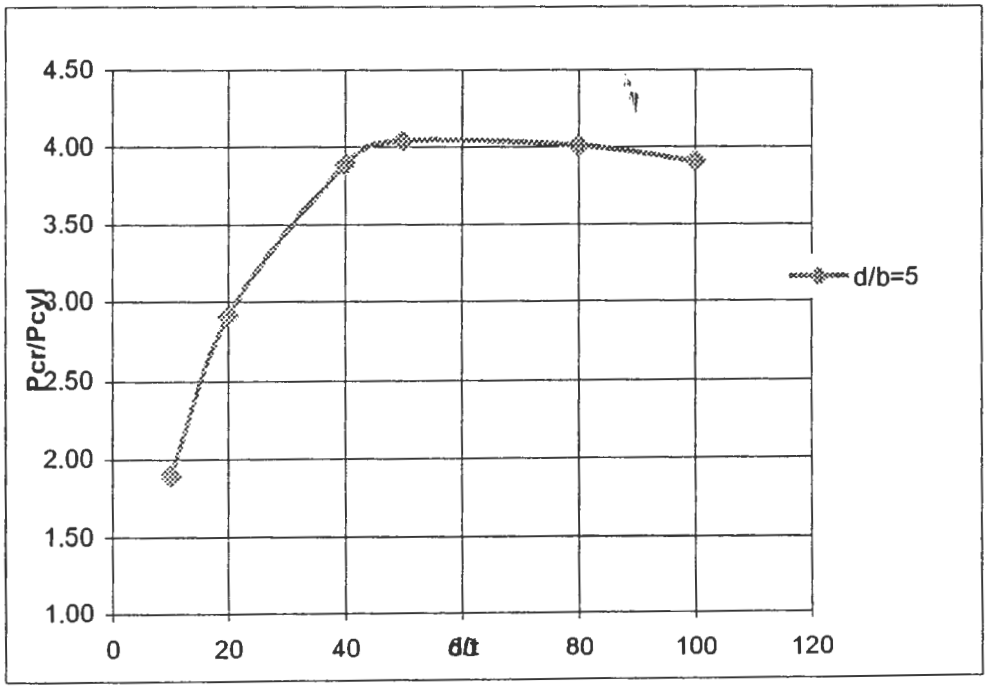

Local and Global Modes-Normalised Buckling load vs Number of ring stiffeners

R= 1 ζ= 0.3
L= 2 As= 0.005

Local					FEM-Multi Panel			t=	0.01
N	Str	d/b	d [m]	b [m]	λ	Pcr[kN]	σcr[Mpa]	Pcr/Pcyl	Mode
2	0.67	1.00	0.05	0.0500	6962.8	6962.8	110.82	1.48	Glo
3	0.50	1.50	0.05	0.0333	8592.8	8592.8	136.76	1.83	Glo
4	0.40	2.00	0.05	0.0250	10316	10316	164.18	2.19	Glo
6	0.29	3.00	0.05	0.0167	12537	12537	199.53	2.67	Glo
8	0.22	4.00	0.05	0.0125	14327	14327	228.02	3.05	Glo

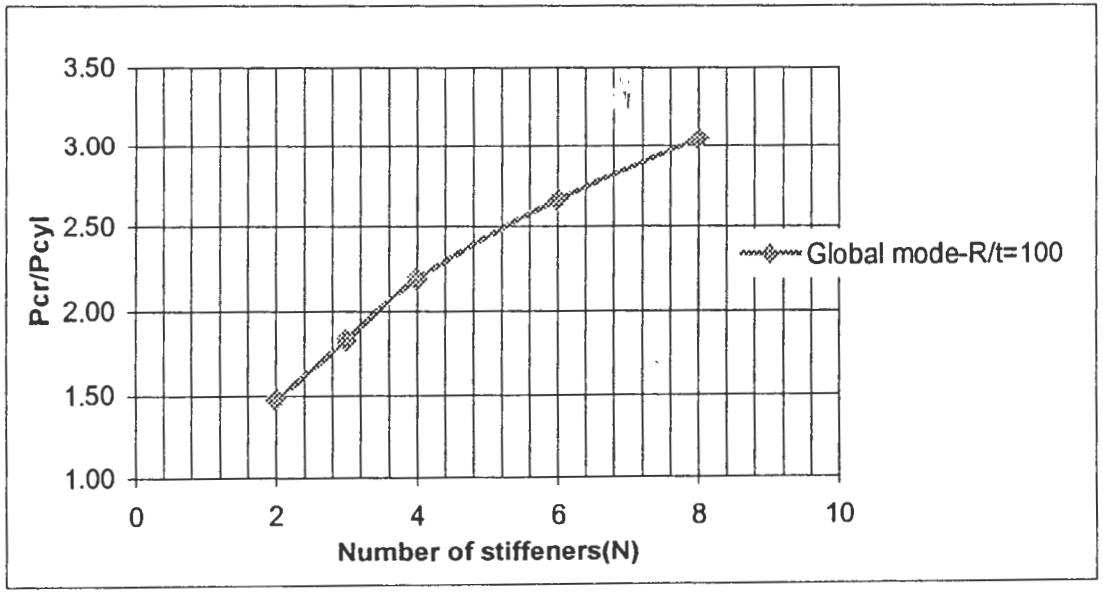

3 Local and Stringer Modes-Normalised Buckling load vs d/b of ring stiffeners

R/t= 100 s= 0.286 m
R= 1 N= 6

Local			Multi panel-R/t=100			t= 0.01	
d/b	d [m]	b [m]	λ	Pcr[kN]	σcr[Mpa]	Pcr/Pcyl	Mode
2	0.02	0.0100	4840	4840	77.0	1.03	Glo
4	0.04	0.0100	8831.7	8831.7	140.6	1.88	Glo
6	0.06	0.0100	12801	12801	203.7	2.72	Glo
8	0.08	0.0100	16055	16055	255.5	3.41	Loc
10	0.10	0.0100	17519	17519	278.8	3.72	Loc
12	0.12	0.0100	17831	17831	283.8	3.79	Loc
14	0.14	0.0100	18764	18764	298.6	3.99	Loc
16	0.16	0.0100	10235	10235	162.9	2.18	Str
18	0.18	0.0100	8578.7	8578.7	136.5	1.82	Str

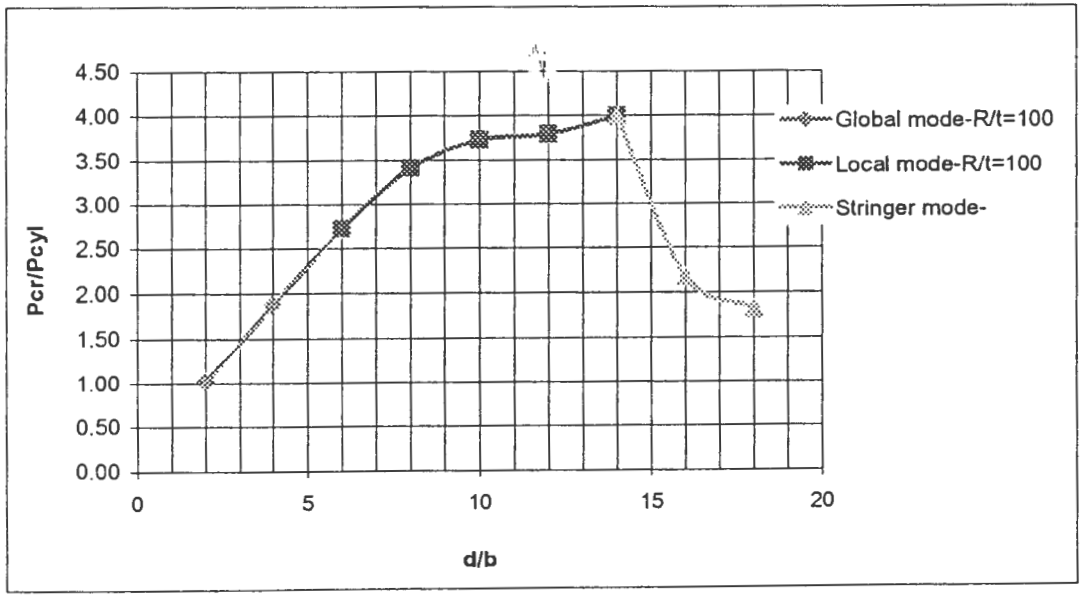

3 Normalised Buckling load vs d/b stringer stiffeners

R/t= 100
R= 1 N= 16

				Multi panel-R/t=100				t= 0.01
d/b	d [m]	b [m]	ts	λ	Pcr[kN]	σcr[Mpa]	Pcr/Pcyl	Mode
6	0.06	0.0100	0.0060	12485	74910	1234.286988	1.06	Loc
8	0.08	0.0100	0.0080	12323	98584	1624.36188	1.39	Loc
10	0.10	0.0100	0.0100	12145	121450	2001.123411	1.71	Loc
12	0.12	0.0100	0.0120	12690	152280	2509.107229	2.15	Str
14	0.14	0.0100	0.0140	12058	168812	2781.503871	2.38	Str
18	0.18	0.0100	0.0180	8032.9	144592.2	2382.43587	2.04	Str

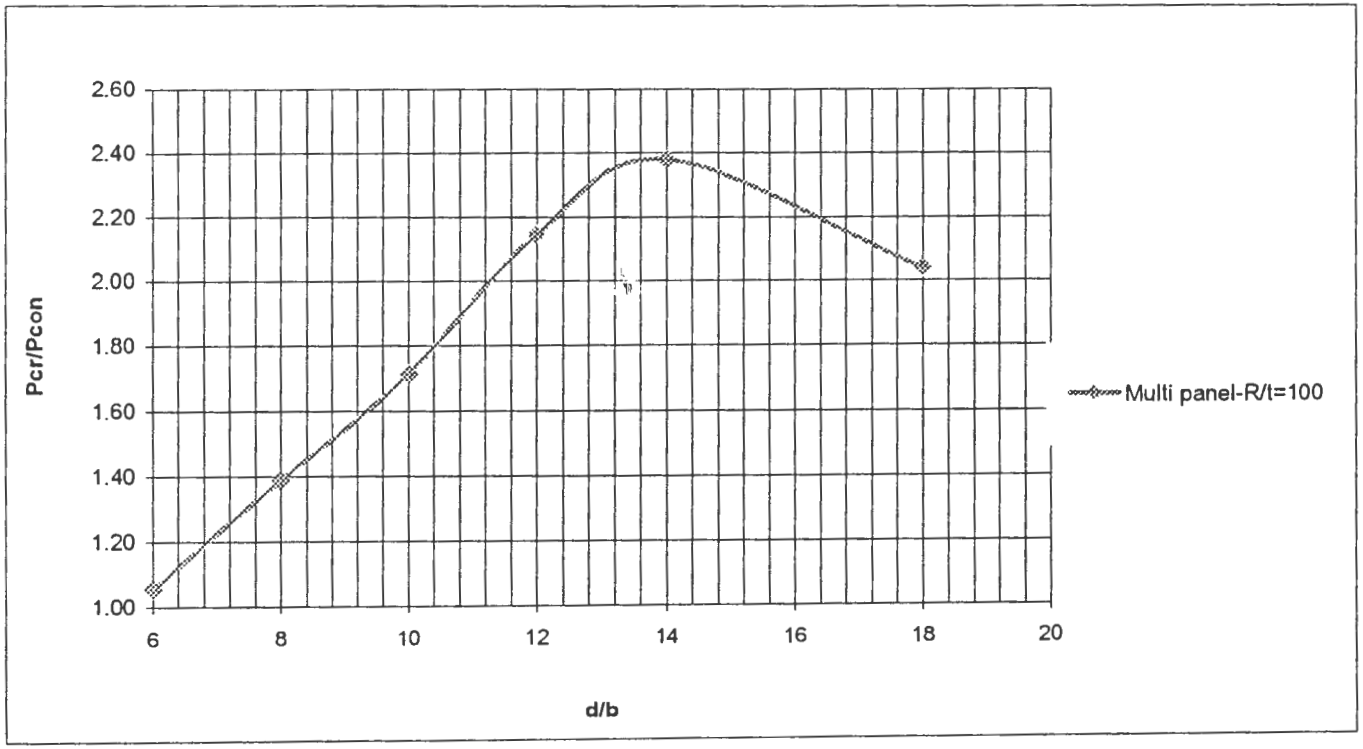

1 **Normalised Buckling load vs R/t for cones with varying number of ring stiffeners**

R= 1 d/b= 1 d= 0.05 b= 0.05

α= 15 □ = 0.262 rad

R/t	100	200	400	500	800	1000
t [mm]	0.01	0.005	0.0025	0.002	0.00125	0.001

	N= 2				N= 4				N= 8			
R/t	λ	Pcr[kN]	σcr[Mpa]	Pcr/Pcyl	λ	Pcr[kN]	σcr[Mpa]	Pcr/Pcyl	λ	Pcr[kN]	σcr[Mpa]	Pcr/Pcyl
100	12090	70875.10665	1167.804	1.00	12783	74937.6748	1234.743	1.06	12566	73665.5575	1213.782	1.04
200	3162.5	18539.4975	610.948	1.05	3388.1	19862.03051	654.531	1.12	3770	22100.83971	728.308	1.25
400	806.6	4728.524485	311.646	1.07	1009.1	5915.638554	389.886	1.33	1101	6454.383162	425.394	1.46
500	531.87	3117.977086	256.873	1.10	707.4	4146.985149	341.648	1.46	776.44	4551.717768	374.992	1.60
800	214.07	1254.940784	165.421	1.13	329.66	1932.563082	254.742	1.74	354.33	2077.185818	273.805	1.87
1000	137.29	804.8340275	132.612	1.13	206.52	1210.680482	199.48	1.71	219.56	1287.124766	212.08	1.81

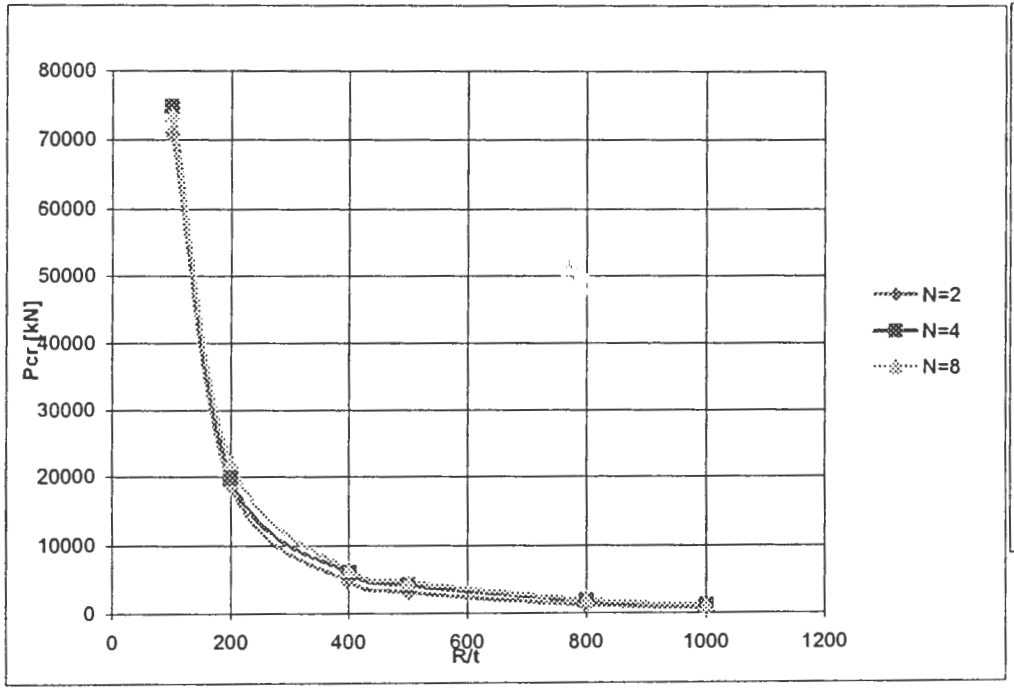

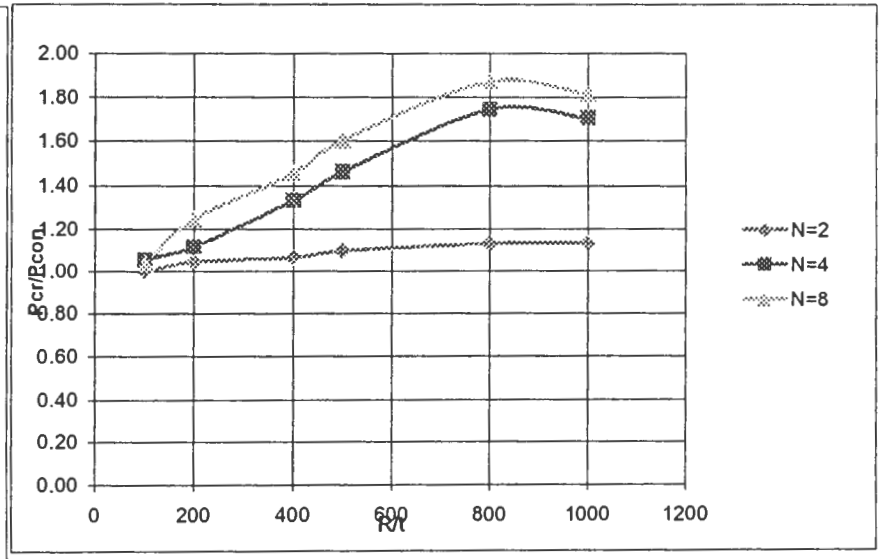

2 Local and Global Modes-Normalised Buckling load vs β

R/t= 100 d= 0.1

R1= 1 d/b= 5 Pcyl= 76055.10 kN

t= 0.01

				N= 8					N= 32				
α	R□	β[rad.]	Pcon	λ	Pcr[kN]	σcr[Mpa]	Pcr/Pcon	Mode	λ	Pcr[kN]	σcr[Mpa]	Pcr/Pcon	Mode
15	1.54	0.262	70960.37	12358	87534	1442.292	1.23	Loc	27612	261849.7	4314.48	3 69	Loc
30	2.15	0.524	57041.33	10698	75775.92	1392.582	1.33	Loc	17181	162930.6	2994.278	2.86	Loc
45	3.00	0.785	38027.55	8095.9	57344.76	1290.711	1.51	Loc	10019	95012.03	2138.522	2.50	Glo
60	4.46	1.047	19013.78	5047	35748.84	1137.921	1.88	Loc	4276.9	40558.64	1291.021	2.13	Loc

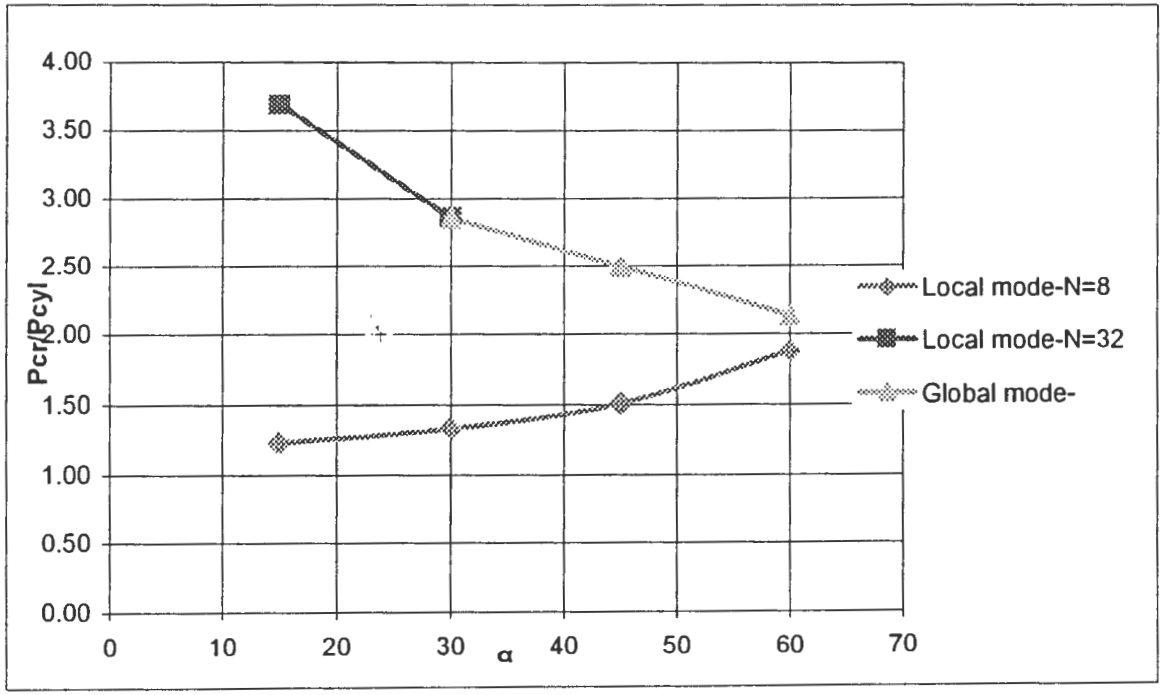

2 Local and Global Modes-Normalised Buckling load vs β

R/t= 100 d= 0.1

R1= 1 d/b= 10 Pcyl= 76055.10 kN

t= 0.01

				N= 2					N= 4				
α	RL	β[rad.]	Pcon	λ	Pcr[kN]	σcr[Mpa]	Pcr/Pcon	Mode	λ	Pcr[kN]	σcr[Mpa]	Pcr/Pcon	Mode
15	1.54	0.262	70960.37	11879	84141.16	1386.388	1.19	Loc	15305	145140.2	2391.464	2.05	Loc
30	2.15	0.524	57041.33	11040	78198.37	1437.101	1.37	Loc	12081	114566.4	2105.458	2.01	Loc
45	3.00	0.785	38027.55	9175.4	64991.06	1462.813	1.71	Loc	9553	90592.87	2039.056	2.38	Loc
60	4.46	1.047	19013.78	6052.7	42872.4	1364.671	2.25	Loc	6147	58293.14	1855.528	3.07	Loc

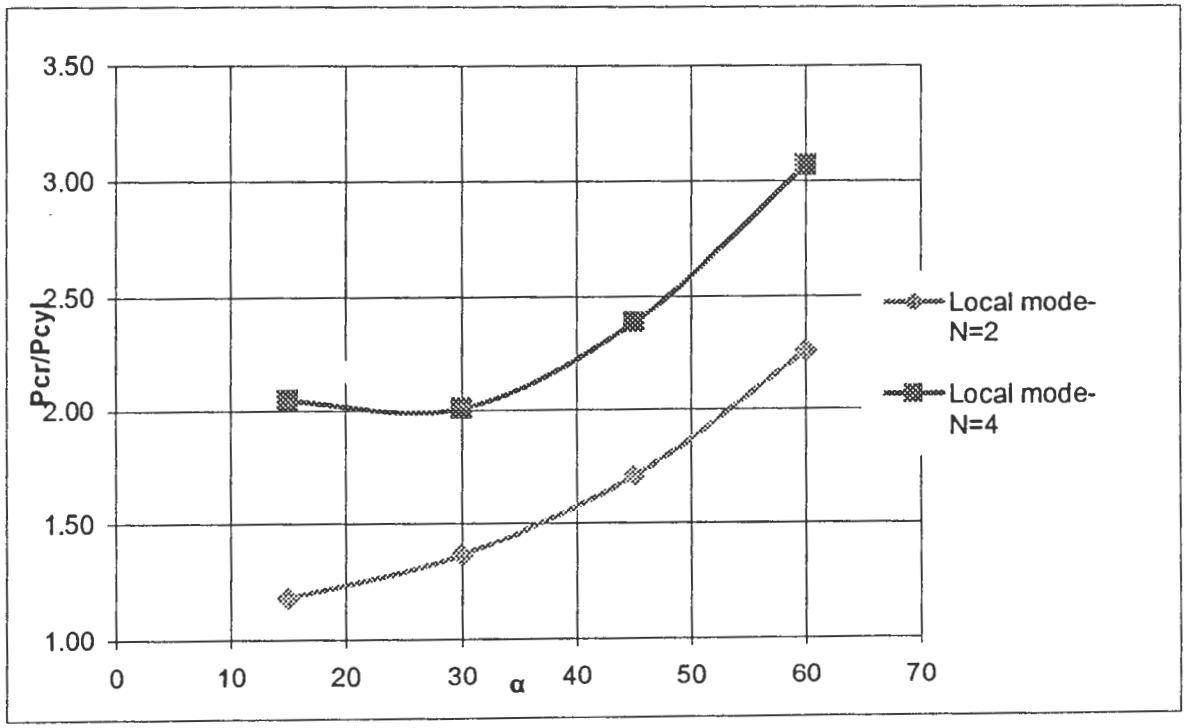

3 Local and Stringer Modes-Normalised Buckling load vs d/b of ring stiffeners

R/t= 100
R= 1 N= 4 s= 0.400 m

Local			Multi panel-R/t=100			t= 0.01		Multi panel-R/t=200			t= 0.005	
d/b	d [m]	b [m]	λ	Pcr[kN]	σcr[Mpa]	Pcr/Pcyl	uckling Moc	λ	Pcr[kN]	σcr[Mpa]	Pcr/Pcyl	Mode
6	0.06	0.0100	12166	76441.23	1259.517	1.08	Loc	3021.1	18982.13	625.5346	1.07	Loc
8	0.08	0.0100	12180	76529.2	1260.966	1.08	Loc	3018.6	18966.42	625.0169	1.07	Loc
10	0.10	0.0100	12178	76516.63	1260.759	1.08	Loc	3015.6	18947.57	624.3958	1.07	Loc
12	0.12	0.0100	12170	76466.37	1259.931	1.08	Loc	3012.9	18930.61	623.8367	1.07	Loc
14	0.14	0.0100	12159	76397.25	1258.792	1.08	Loc	3010.2	18913.64	623.2777	1.07	Loc
18	0.18	0.0100	12123	76171.06	1255.065	1.07	Loc	3003.4	18870.92	621.8697	1.06	Loc

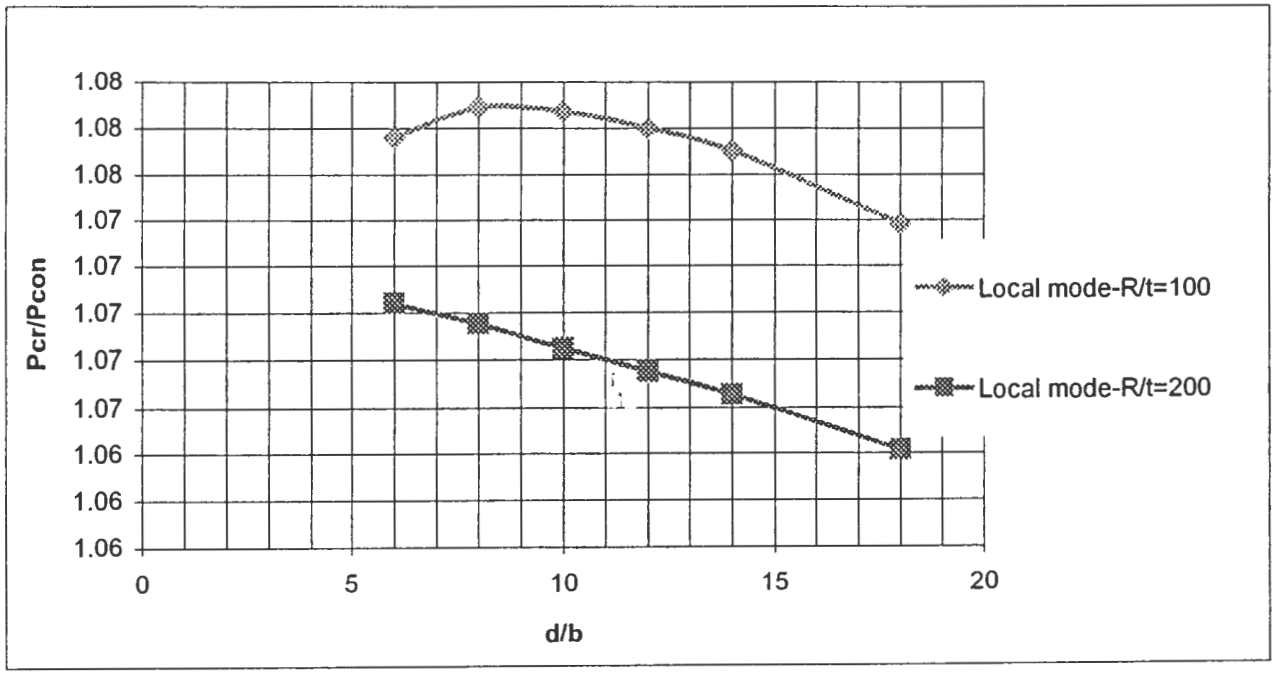

UNSTIFFENED CONICAL SHELLS BUCKLING

AXIAL COMPRESSION

$$\sigma_{cr} = \frac{E}{\sqrt{3\left(1-\mu^2\right)}}\left(\frac{t}{R}\right) COS\,\alpha$$

E= 2.00E+11 Pa
μ= 0.3
Le= 2 m
α= 15 □ = 0.262 rad L= 2.071 m
R1= 1 R2= 1.536 m Re= 1.313 m

R	t [m]	R/t	σCON[Mpa]	PCON[kN]	Z	Kp
1	0.01	100	143.01	899.36	312	28
1	0.005	200	51.07	160.60	623	40
1	0.0025	400	19.15	30.11	1246	60
1	0.002	500	14.30	17.99	1558	70
1	0.00125	800	6.38	5.02	2492	80
1	0.001	1000	4.60	2.89	3116	90

ABAQUS-Unstiffened

R/t	λ	Pcr[kN]	σcr[Mpa]	Pcr/PCON
100	849.83	849.83	135.12968	0.94
200	152.52	152.52	48.50377	0.95
400	28	28	17.808885	0.93
500	16.286	16.286	12.948013	0.91
800	5.2192	5.2192	6.6391523	1.04
1000	3.0251	3.0251	4.810148	1.05

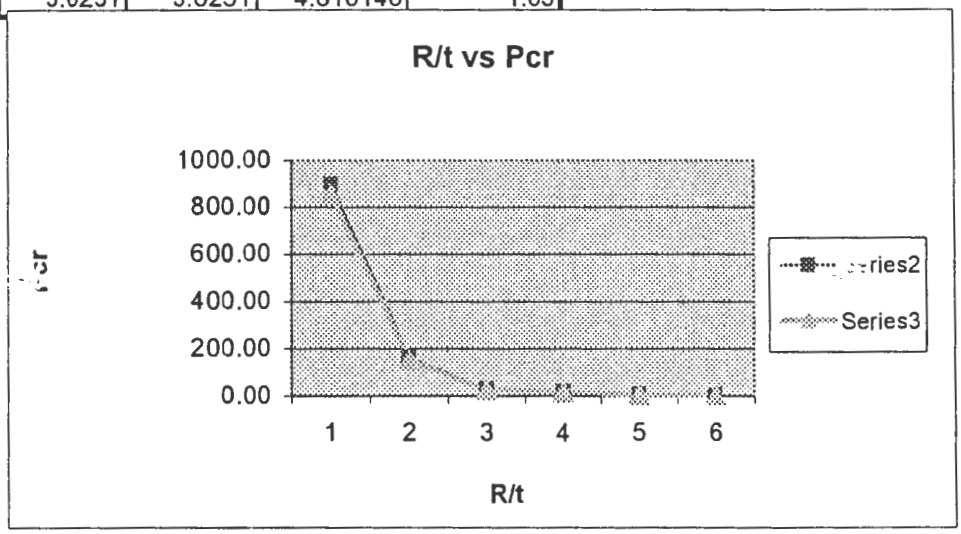

1 **Normalised Buckling load vs R/t for cones with varying number of stringer stiffeners**

R= 1 d/b= 5 d= 0.1 b= 0.02

α= 15 □ = 0.262 rad

R/t	100	200	400	500	800	1000
t [mm]	0.01	0.005	0.0025	0.002	0.00125	0.001

	N= 8				N= 16				N= 32			
R/t	λ	Pcr[kN]	σcr[Mpa]	Pcr/Pcyl	λ	Pcr[kN]	σcr[Mpa]	Pcr/Pcyl	λ	Pcr[kN]	σcr[Mpa]	Pcr/Pcyl
100	912.32	912.32	145.07	1.01	978.69	978.69	155.62	1.09	1876.3	1876.3	298.35	2.09
200	205	205	65.19	1.28	267.59	267.59	85.10	1.67	613.61	613.61	195.14	3.82
400	44.127	44.127	28.07	1.47	75.976	75.976	48.32	2.52	199.59	199.59	126.95	6.63
500	24.677	24.677	19.62	1.37	48.706	48.706	38.72	2.71	127.17	127.17	101.11	7.07
800	7.2665	7.2665	9.24	1.45	17.151	17.151	21.82	3.42	39.706	39.706	50.51	7.91
1000	4.177	4.177	6.64	1.44	9.3555	9.3555	14.88	3.24	21.819	21.819	34.69	7.55

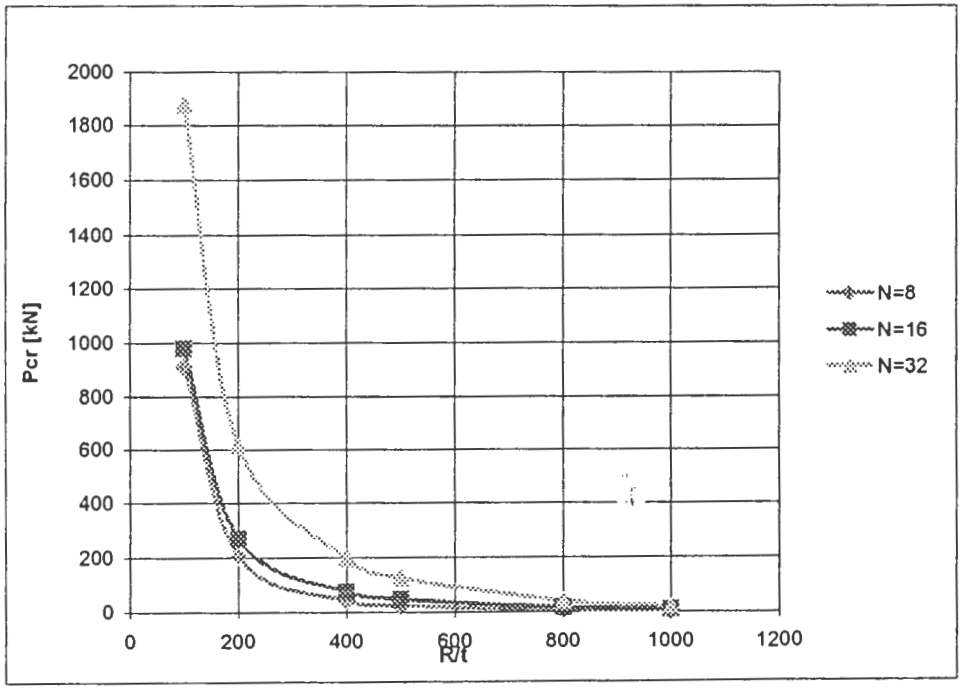

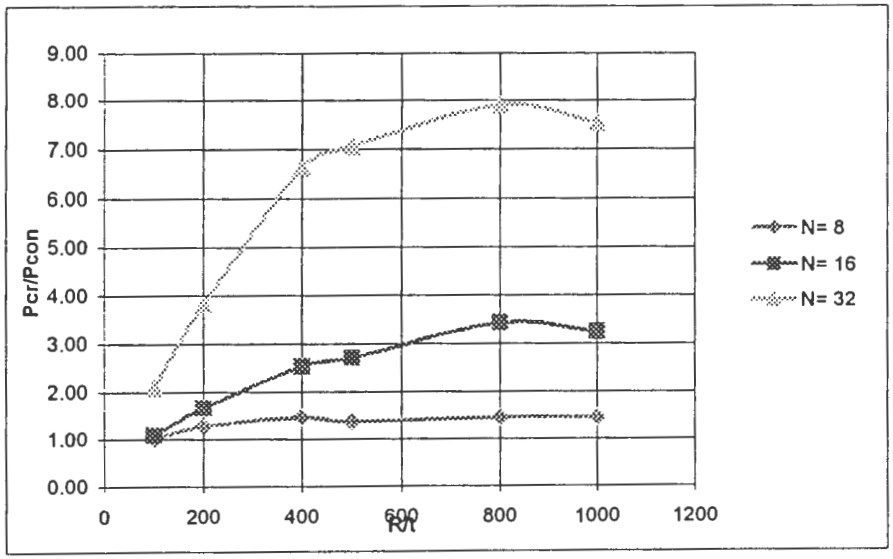

3 Normalised Buckling load vs d/b stringer stiffeners

R/t= 100 E= 2.00E+11 Pa
R= 1 N= 16 s= 0.393

			Multi panel-R/t=100				t= 0.01	Multi panel-R/t=200				t= 0.005
d/b	d [m]	b [m]	λ	pcr[kN]	σcr[Mpa]	pcr/pcon	Mode	λ	pcr[kN]	σcr[Mpa]	pcr/pcon	Mode
6	0.06	0.0100	857.74	857.74	136.3874373	1.01	Loc	175.83	175.83	27.95836	1.15	Loc
8	0.08	0.0100	861.14	861.14	136.9280642	1.01	Loc	180.38	180.38	28.68185	1.18	Loc
10	0.10	0.0100	865.83	865.83	137.6738112	1.02	Loc	185.18	185.18	29.44508	1.21	Loc
12	0.12	0.0100	900.85	900.85	143.2422679	1.06	Str	196.57	196.57	31.25618	1.29	Loc
14	0.14	0.0100	912.06	912.06	145.0247465	1.07	Str	203.1	203.1	32.2945	1.33	Str
18	0.18	0.0100	901.72	901.72	143.3806048	1.06	Str	206.18	206.18	32.78425	1.35	Str

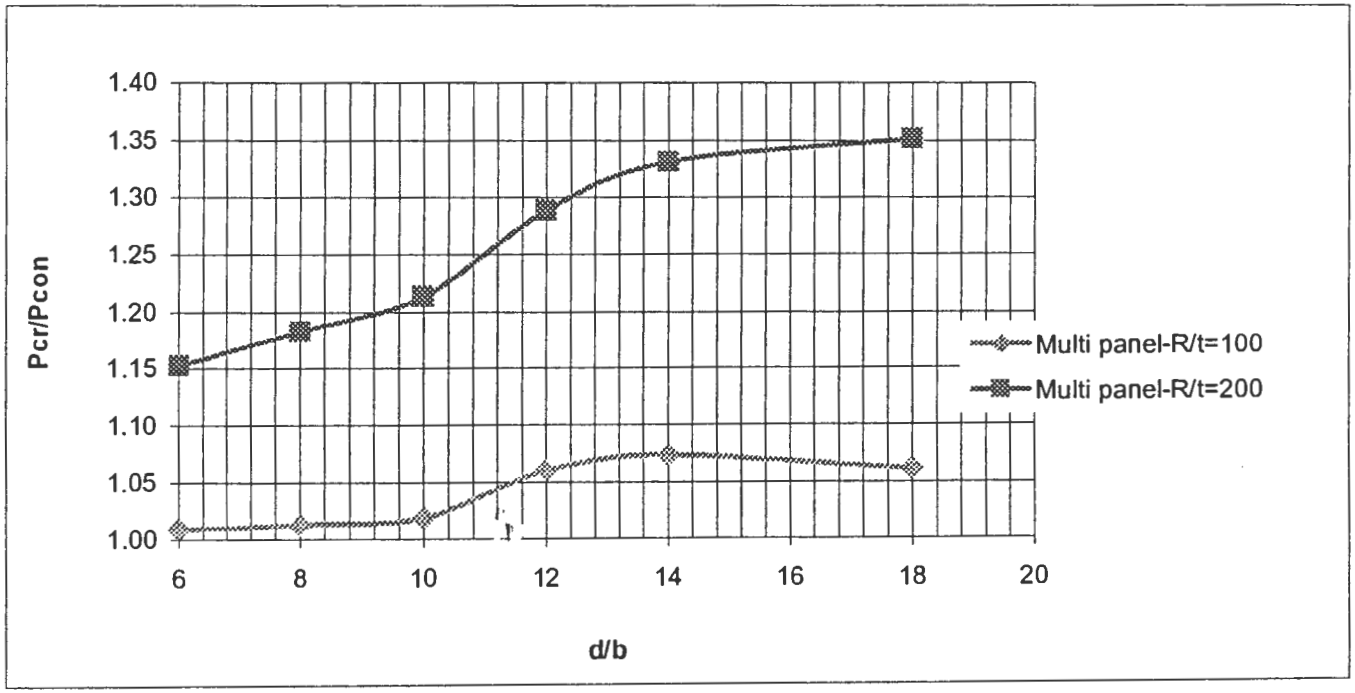

4 **Normalised Buckling load vs d/t of stringer stiffeners**

t= 0.01 d/b= 5 d= 0.1

R= 1 N= 16 s= 0.393 b= 0.02

			d/b=10			
d/t	d [m]	t [m]	λ	pcr[kN]	σcr[Mpa]	Pcr/Pcyl
10	0.10	0.0100	978.69	978.69	155.619443	1.15
20	0.10	0.0050	267.59	267.59	42.54892432	1.75
40	0.10	0.0025	75.976	75.976	12.08078431	2.71
50	0.10	0.0020	48.706	48.706	7.744638843	2.99
80	0.10	0.0013	17.151	17.151	2.727144516	3.29
100	0.10	0.0010	9.3555	9.3555	1.487598421	3.09

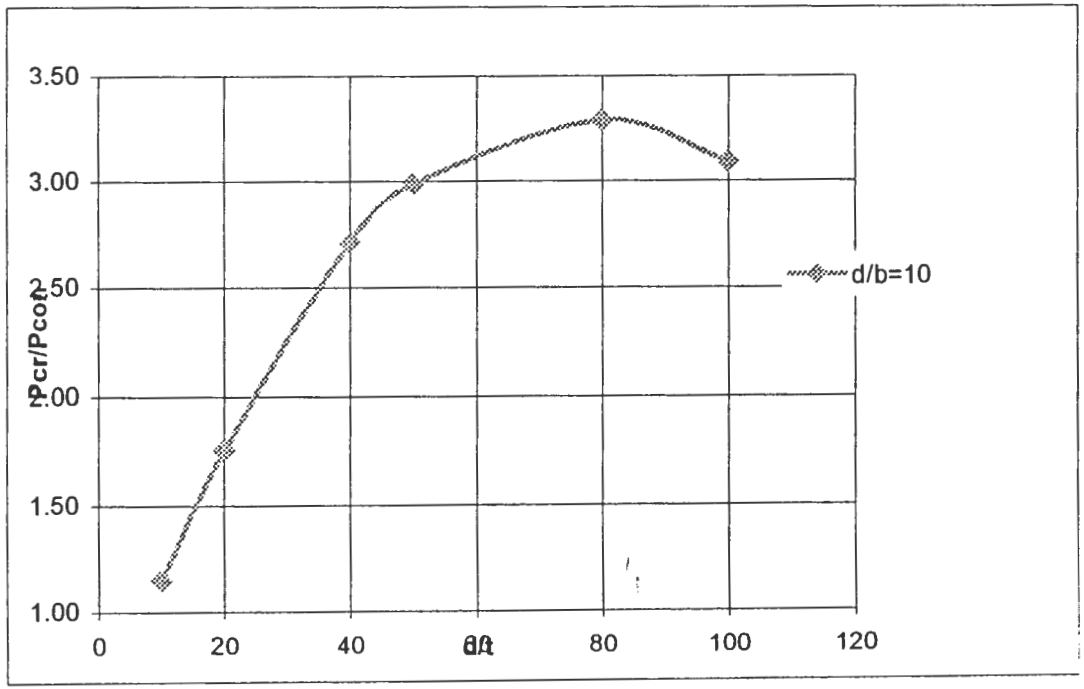

1 Normalised Buckling load vs R/t for cones with varying number of ring stiffeners

R= 1 d/b= 1 d= 0.05 b= 0.05

α= 15 □ = 0.262 rad

R/t	100	200	400	500	800	1000
t [mm]	0.01	0.005	0.0025	0.002	0.00125	0.001

	N= 2				N= 4				N= 8			
R/t	λ	Pcr[kN]	σcr[Mpa]	Pcr/Pcyl	λ	Pcr[kN]	σcr[Mpa	Pcr/Pcy	λ	Pcr[kN]	σcr[Mpa]	Pcr/Pcyl
100	2306.1	2306.1	366.688	2.56	5110	5110	812.530	5.68	13198	13198	2098.586	14.67
200	442.62	442.62	140.760	2.76	862.82	862.82	274.390	5.37	2884.9	2884.9	917.444	17.96
400	90.486	90.486	57.552	3.00	175.87	175.87	111.859	5.84	453.25	453.25	288.281	15.05
500	55.099	55.099	43.806	3.06	108.89	108.89	86.572	6.05	270.15	270.15	214.780	15.02
800	19.678	19.678	25.032	3.92	41.097	41.097	52.278	8.19	101.23	101.23	128.771	20.17
1000	12.155	12.155	19.327	4.20	26.266	26.266	41.77	9.09	60.234	60.234	95.777	20.84

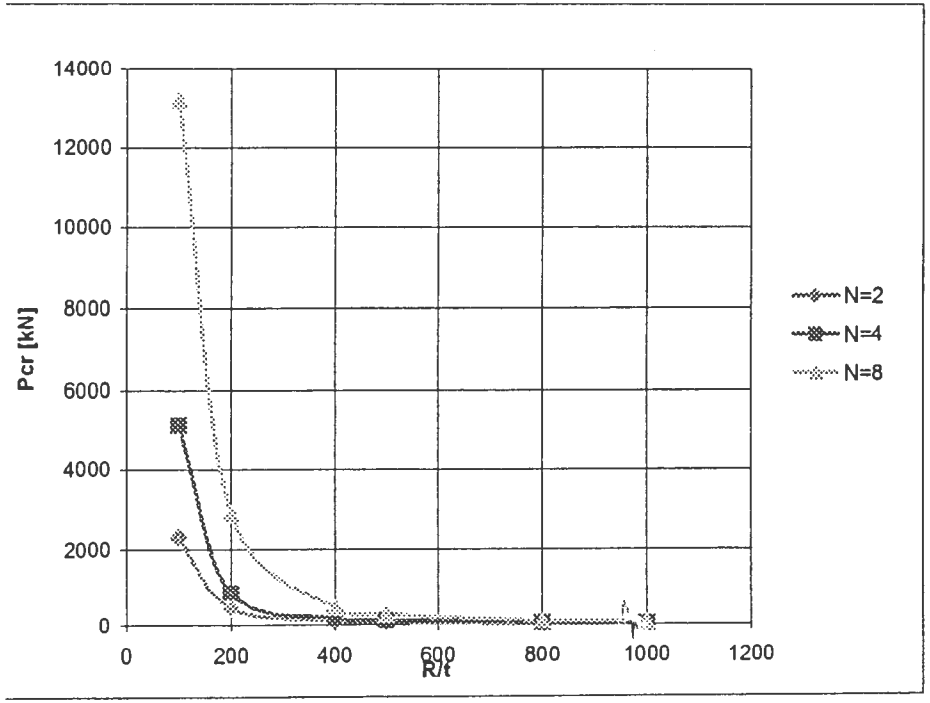

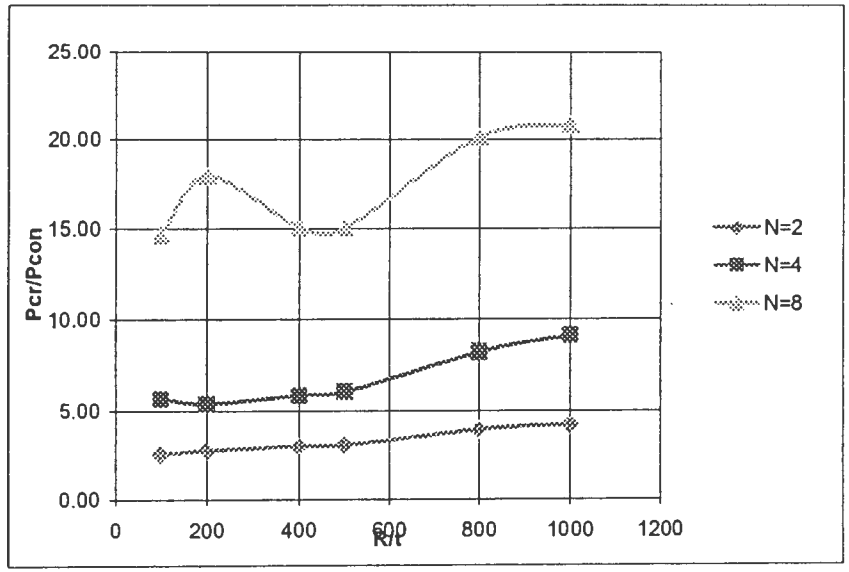

Local and Global Modes-Normalised Buckling load vs Number of stringer stiffeners

R/t= 100 ζ= 0.3
R= 1 t= 0.01

Local

N	Str	d/b	d [m]	b [m]	λ	Pcr[kN]	σcr[Mpa]	Pcr/Pcyl	Mode
4	1.57	2.12	0.1	0.0471	2141.9	2141.9	340.579	2.38	Loc
8	0.79	4.24	0.1	0.0236	2543.3	2543.3	404.4048	2.83	Loc
16	0.39	2.12	0.05	0.0236	2403.3	2403.3	382.1437	2.67	Loc
32	0.20	1.06	0.025	0.0236	2738.9	2738.9	435.5067	3.05	P
64	0.10	0.13	0.00625	0.0471	2505.2	2505.2	398.3466	2.79	P
Smeared					3843.4	3843.4	611.131	4.27	

Shell

N	Str	d [m]	b [m]	ts	λ	Pcr[kN]	σcr[Mpa]	Pcr/Pcyl
4	1.57	0.1	0.0471	0.013	2042	2042	324.6941	2.27
8	0.79	0.1	0.0236	0.013	2443.3	2443.3	388.504	2.72
16	0.39	0.05	0.0236	0.013	3810.1	3810.1	605.836	4.24
32	0.20	0.05	0.0118	0.013	12991	12991	2065.672	14.44
64	0.10	0.025	0.0118	0.013	88671	88671	14099.39	98.59

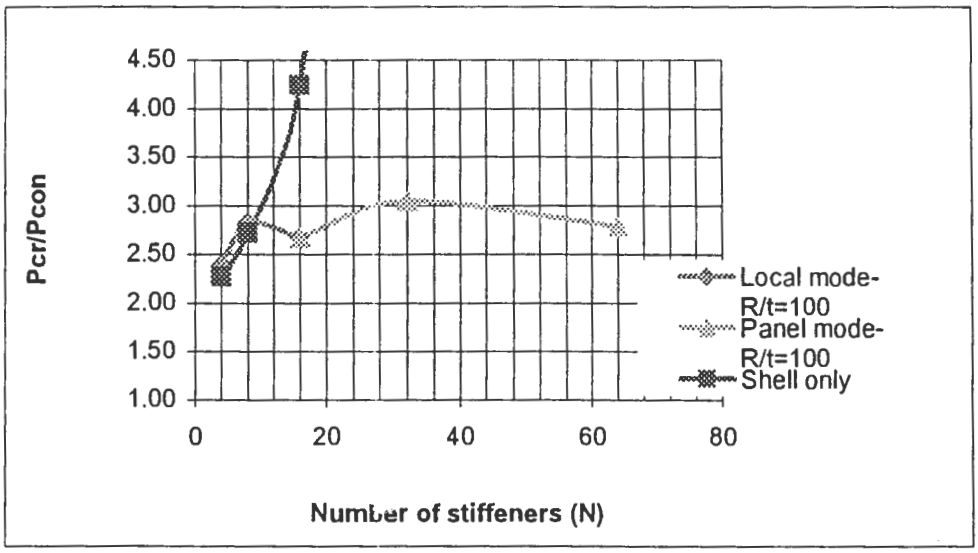

2 Local and Global Modes-Normalised Buckling load vs β

R/t= 100 d= 0.1

R1= 1 d/b= 5 Pcyl= 76055.10 kN

t= 0.01 H= 2

							N= 8					N= 32				
α	R□[m]	β[rad.]	Re[m]	L[m]	Kp	Pcon	λ	pcr[kN]	σcr[Mpa]	pcr/pcon	Mode	λ	pcr[kN]	σcr[Mpa]	pcr/pcon	Mode
15	1.54	0.262	1.31	2.07	28	899.36	912.32	912.32	123.9828	1.01	Loc	1876.3	1876.3	254.9861	2.09	Glo
30	2.15	0.524	1.82	2.31	26	483.82	535.64	535.64	112.6523	1.11	Loc	936.41	936.41	196.9395	1.94	Glo
45	3.00	0.785	2.83	2.83	24	191.73	241.69	241.69	96.676	1.26	Loc	371.09	371.09	148.436	1.94	Glo
60	4.46	1.047	5.46	4.00	22	45.49	57.72	57.72	63.07759	1.27	Loc	71.512	71.512	78.14977	1.57	Glo

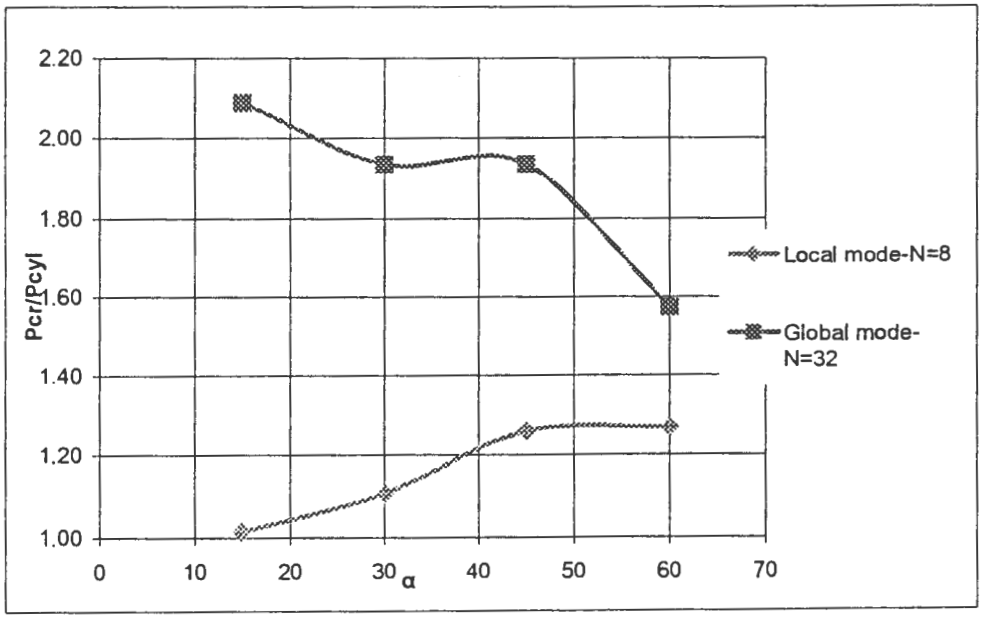

Local and Stringer Modes-Normalised Buckling load vs d/b of stringer stiffeners

R/t= 100 E= 2.00E+11 Pa
R= 1 N= 16 s= 0.393

			Multi panel-R/t=100				t= 0.01	Multi panel-R/t=200				t= 0.005
d/b	d [m]	b [m]	λ	pcr[kN]	σcr[Mpa]	pcr/pcon	Mode	λ	pcr[kN]	σcr[Mpa]	pcr/pcon	Mode
6	0.06	0.0100	857.74	857.74	136.3874	1.01	Loc	175.83	175.83	27.95836	1.15	Loc
8	0.08	0.0100	861.14	861.14	136.9281	1 01	Loc	180.38	180.38	28.68185	1.18	Loc
10	0.10	0.0100	865.83	865.83	137.6738	1.02	Loc	185.18	185.18	29.44508	1.21	Loc
12	0.12	0.0100	900.85	900.85	143.2423	1.06	Str	196.57	196.57	31.25618	1.29	Loc
14	0.14	0.0100	912.06	912.06	145.0247	1.07	Str	203.1	203.1	32.2945	1.33	Str
18	0.18	0.0100	901.72	901.72	143.3806	1.06	Str	206.18	206.18	32.78425	1.35	Str

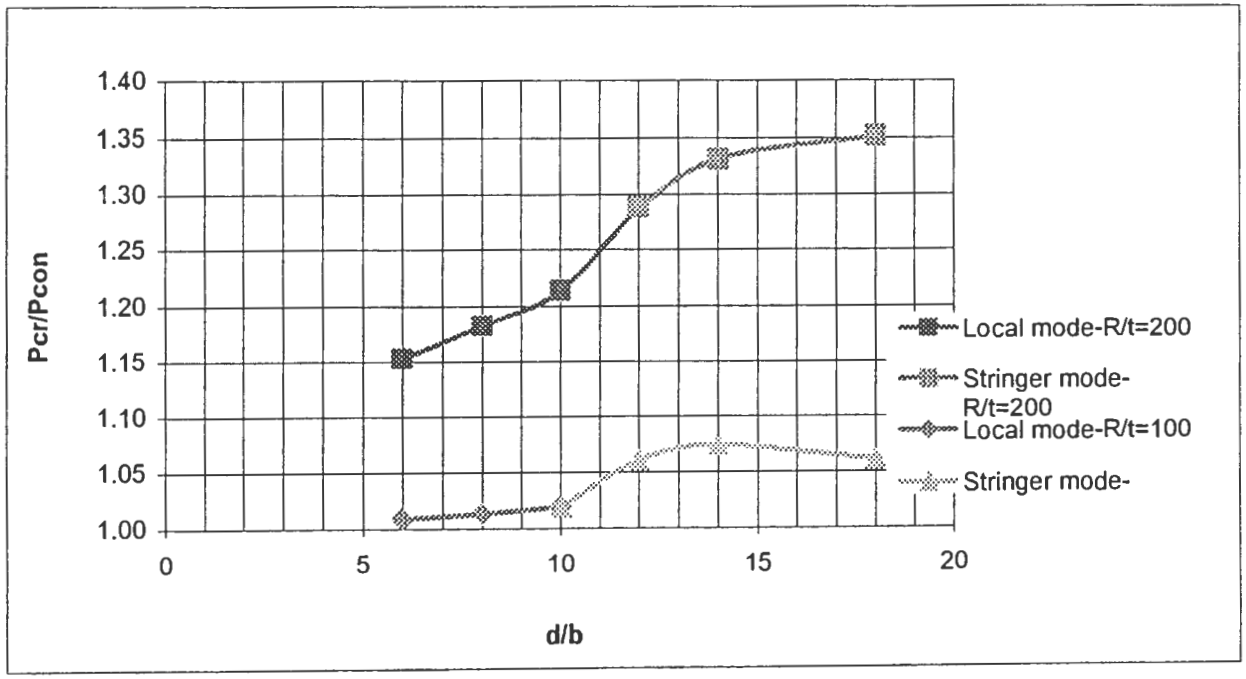

2 Local and Global Modes-Normalised Buckling load vs β

R/t= 100 d= 0.1

R1= 1 d/b= 10 Pcyl= 76055.10 kN

t= 0.01 H= 2

							N= 2					N= 4				
α	R□[m]	β[rad.]	Re[m]	L[m]	Kp	Pcon	λ	Pcr[kN]	σcr[Mpa]	Pcr/Pcon	Mode	λ	Pcr[kN]	σcr[Mpa]	Pcr/Pcon	Mode
15	1.54	0.262	1.31	2.07	28	899.36	3750	3750	509.6189	4.17	Loc	9858.2	9858.2	1339.713	10.96	Glo
30	2.15	0.524	1.82	2.31	26	483.82	1204.5	1204.5	253.3225	2.49	Loc	2769.4	2769.4	582.4418	5.72	Glo
45	3.00	0.785	2.83	2.83	24	191.73	496.65	496.65	198.66	2.59	Loc	1133.3	1133.3	453.32	5.91	Glo
60	4.46	1.047	5.46	4.00	22	45.49	84.31	84.31	92.13568	1.85	Loc	157.34	157.34	171.9443	3.46	Glo

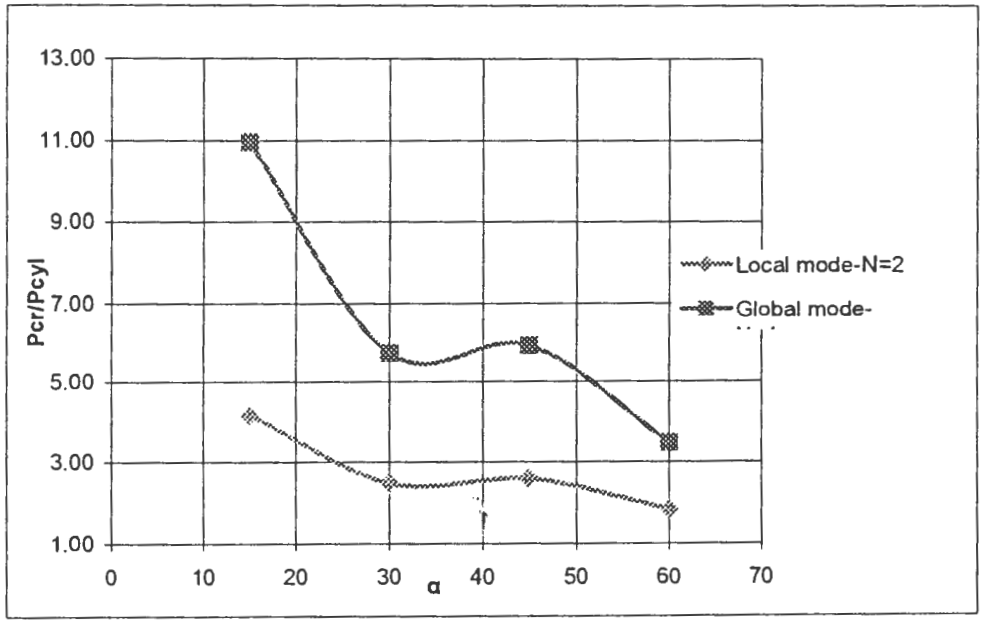

3 Local and Stiffener buckling Modes-Normalised Buckling load vs d/b of ring stiffeners

R/t= 100
R= 1 N= 4 s= 0.400 m

Local			Multi panel-R/t=100 t= 0.01					Multi panel-R/t=200 t= 0.005				
d/b	d [m]	b [m]	λ	pcr[kN]	σcr[Mpa]	pcr/pcyl	Mode	λ	pcr[kN]	σcr[Mpa]	pcr/pcon	Mode
6	0.06	0.0100	3685.7	3685.7	586.0554	4.34	P	837.11	837.11	133.1071	5.49	Loc
8	0.08	0.0100	4551.2	4551.2	723.6768	5.36	Loc	847.27	847.27	134.7226	5.56	Loc
10	0.10	0.0100	4587.1	4587.1	729.3851	5.40	Loc	841.68	841.68	133.8338	5.52	Loc
12	0.12	0.0100	4629.4	4629.4	736.1112	5.45	Loc	844.24	844.24	134.2408	5.54	Loc
14	0.14	0.0100	4659.9	4659.9	740.9609	5.48	Loc	845.68	845.68	134.4698	5.54	Loc
18	0.18	0.0100	4642.4	4642.4	738.1783	5.46	Str	831.59	831.59	132.2294	5.45	Loc

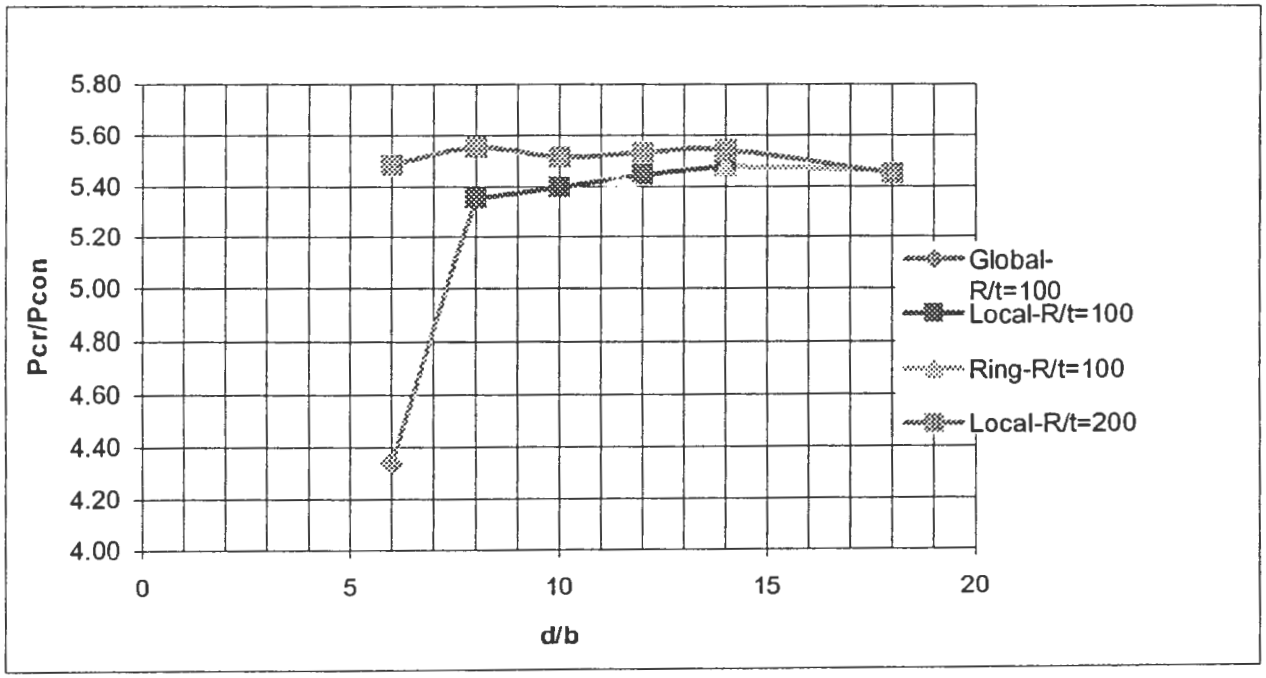

UNSTIFFENED CONICAL SHELLS BUCKLING

SHEAR

E= 2.00E+11 Pa
μ= 0.3
H= 2 m

L= 2.071 m
Re= 1.196 m
R1= 1
R2= 1.536 m

α= 15 □ = 0.262 rad

R	t [m]	R/t	TCON[Mpa]	TCON[kN]	Z	Re/t
1	0.01	100	419.1	13165.28	319.1029101	119.6
1	0.005	200	180.4	2834.16	660.7192839	239.2
1	0.0025	400	75.8	595.37	1321.438568	478.3
1	0.002	500	57.3	360.32	1651.79821	597.9
1	0.00125	800	31.9	125.13	2642.877135	956.6
1	0.001	1000	24.1	75.73	3303.596419	1195.8

ABAQUS-Unstiffened

R/t	λ	Tcr[kN]	TCON[Mpa]	Pcr/PCON
100	4530.4	14232.67136	453.04	1.08
200	988,57	3105.68425	197.714	1.10
400	222.2	698.0618876	88.88	1.17
500	138.32	434.5450958	69.16	1.21
800	51.488	161.7543225	41.1904	1.29
1000	32.373	101.702779	32.373	1.34

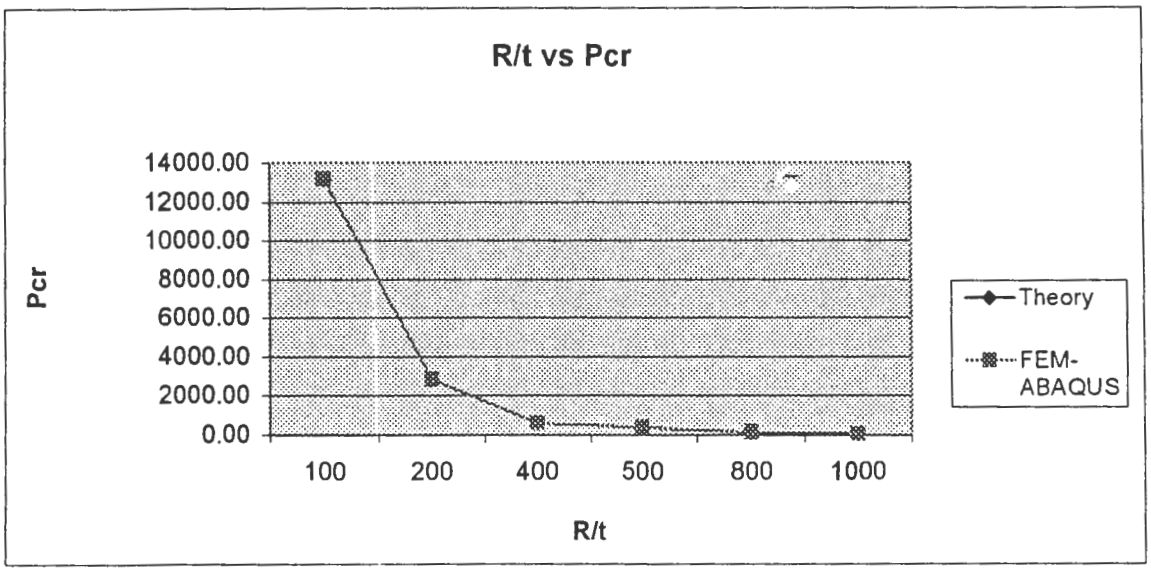

1 **Normalised Buckling load vs R/t for cones with varying number of stringer stiffeners**

R= 1 d/b= 5 d= 0.1 b= 0.02

α= 15 = 0.262 rad

R/t	100	200	400	500	800	1000
t [mm]	0.01	0.005	0.0025	0.002	0.00125	0.001

	N= 8				N= 16				N= 32			
R/t	λ	Tcr[kN]	Tcr[Mpa]	Tcr/Tcyl	λ	Tcr[kN]	Tcr[Mpa]	Tcr/Tcyl	λ	Tcr[kN]	Tcr[Mpa]	Tcr/Tcyl
100	6359.5	19979.0	636.0	1.52	8687.5	27292.6	868.8	2.07	17137	53837.5	1713.7	4.09
200	1559.6	4899.6	311.9	1.73	2915.9	9160.6	583.2	3.23	7217.2	22673.5	1443.4	8.00
400	331.93	1042.8	132.8	1.75	817.59	2568.5	327.0	4.31	1901	5972.2	760.4	10.03
500	204.64	642.9	102.3	1.78	521.54	1638.5	260.8	4.55	1270	3989.8	635.0	11.07
800	73.455	230.8	58.8	1.84	200.8	630.8	160.6	5.04	649.37	2040.1	519.5	16.30
1000	44.658	140.3	44.7	1.85	127.12	399.4	127.1	5.27	503.16	1580.7	503.2	20.87

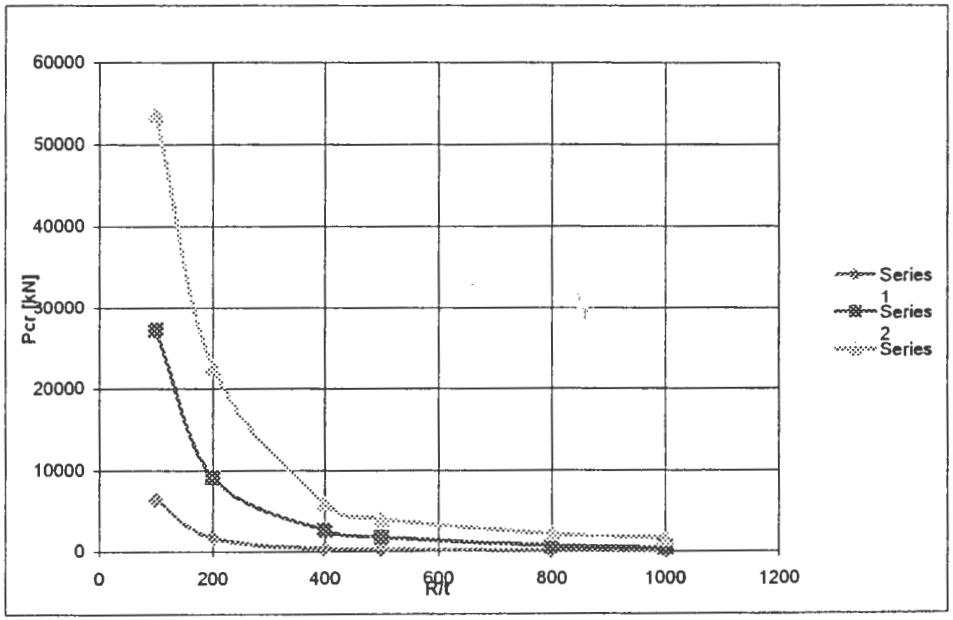

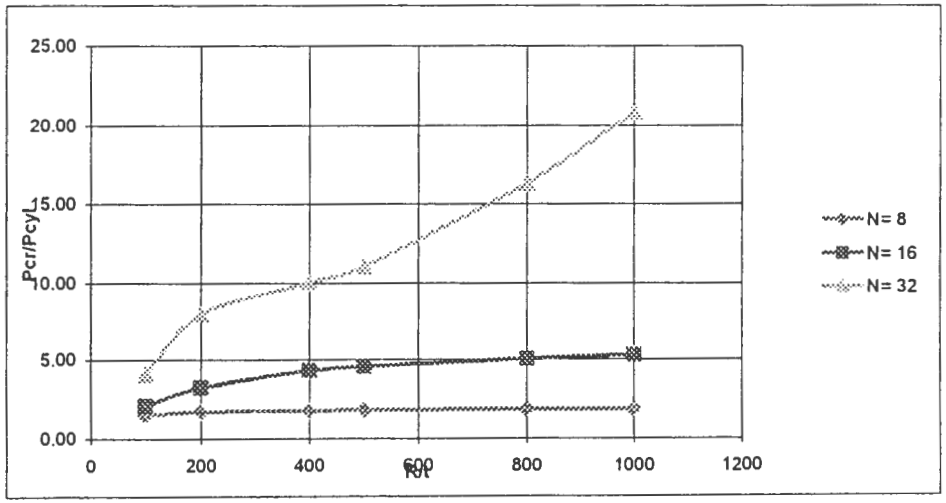

4 **Normalised Buckling load vs d/t of stringer stiffeners**

t= 0.01 d/b= 5 d= 0.1

R= 1 N= 16 s= 0.393 b= 0.02

			d/b=10			
d/t	d [m]	t [m]	λ	Vcr[kN]	Tcr[Mpa]	Vcr/Vcon
10	0.10	0.0100	8687.5	27292.5862	868.8	2.07
20	0.10	0.0050	2915.9	9160.57002	583.2	3.23
40	0.10	0.0025	817.59	2568.53474	327.0	4.31
50	0.10	0.0020	521.54	1638.46623	260.8	4.55
80	0.10	0.0013	200.8	630.831805	160.6	5.04
100	0.10	0.0010	127.12	399.359258	127.1	5.27

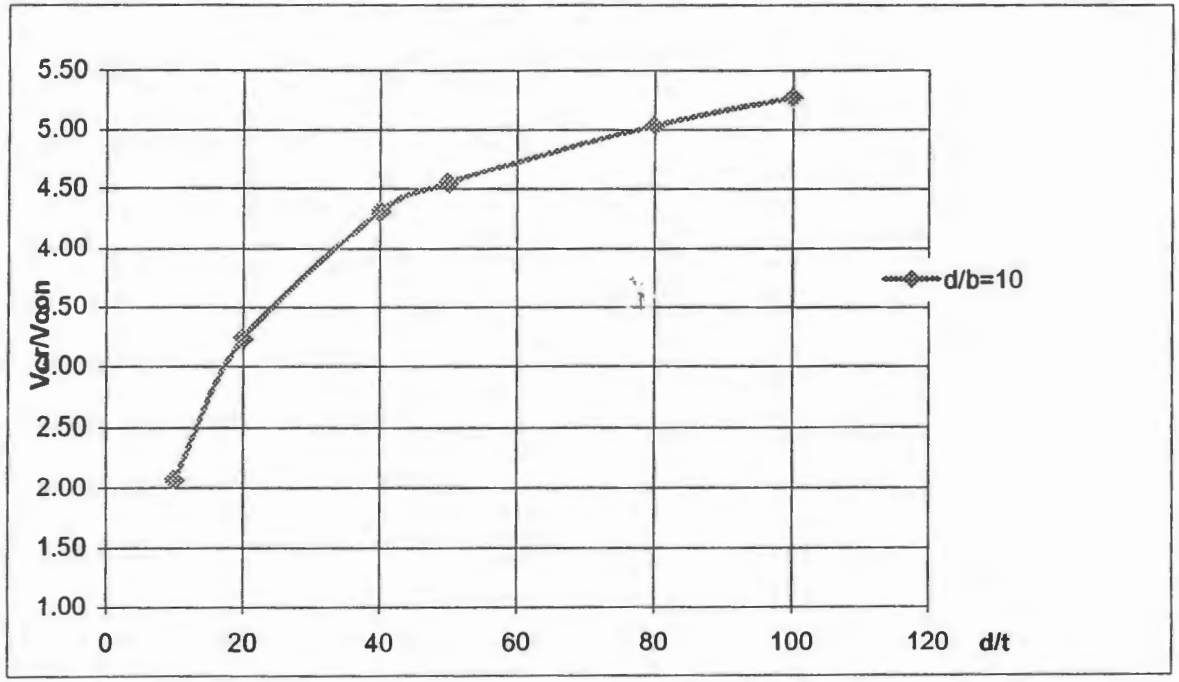

Local and Global Modes-Normalised Buckling load vs β

R/t= 100 d= 0.1
R1= 1 d/b= 5 Pcyl= 76055.10 kN
t= 0.01 H= 2

							N= 2					N= 4				
α	R□[m]	β[rad.]	Re[m]	L[m]	Z	Tcon	λ	Vcr[kN]	Tcr[Mpa]	Vcr/Vcon	Mode	λ	Vcr[kN]	Tcr[Mpa]	Vcr/Vcon	Mode
15	1.54	0.262	1.20	0.00	319.0	13167.0	13276	41707.8	1327.6	3.17	Loc	21717	68226.0	2171.7	5.18	Glo
30	1.15	0.524	1.26	0.00	301.8	14607.4	8112.6	25486.5	811.3	1.74	Loc	15085	47390.9	1508.5	3.24	Glo
45	2.00	0.785	1.21	0.00	316.1	15058.0	7387	23206.9	738.7	1.54	Loc	12064	37900.2	1206.4	2.52	Glo
60	3.46	1.047	1.02	0.00	372.7	10838.1	4115	12927.7	411.5	1.19	Loc	5148.9	16175.7	514.9	1.49	Glo

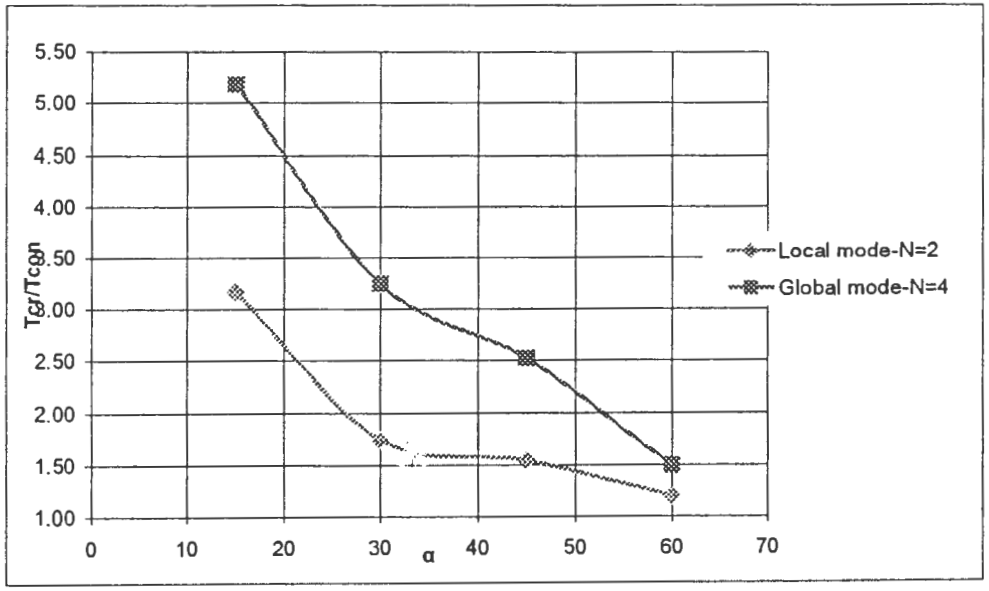

```
*Heading
** Job name: N8 Model name: Axial N=8
*Preprint, echo=NO, model=NO, history=NO, contact=NO
**
** PARTS
**
*Part, name=N8
*Node
      1,           1., -0.555000007,           0.
      2,           0., -0.555000007,   1.04999995
      3,           0., -0.555000007,           1.
      4,           0.,  -0.77700001,           1.
      5,           1.,  -0.77700001,           0.
   1701,  0.994617581,  0.888499975, -0.103614062
*Element, type=S4R
 1,    1, 134, 135,  41
 2,   41, 135, 136,  40
 3,   40, 136, 137,  39
 4,   39, 137, 138,  38
 5,   38, 138, 139,  37

*Nset, nset=_PickedSet3, internal
    1,    3,    4,    5,    6,    8,   10,   11,   13,   14,   16,   17,   18,
19,   21,   22
   23,   26,   27,   28,   29,   30,   31,   32,   33,   34,   35,   36,   37,
38,   39,   40
   41,   42,   43,   44,   45,   46,   47,   48,   49,   50,   51,   52,   53,
54,   55,   56
   57,   58,   59,   60,   61,   62,   63,   64,   65,   66,   67,   68,   69,
70,   71,   72
*Elset, elset=_PickedSet4, internal
    1,    2,    3,    4,    5,    6,    7,    8,    9,   10,   11,   12,   13,
14,   15,   16
   17,   18,   19,   20,   21,   22,   23,   24,   25,   26,   27,   28,   29,
30,   31,   32
   33,   34,   35,   36,   37,   38,   39,   40,   41,   42,   43,   44,   45,
46,   47,   48
   49,   50,   51,   52,   53,   54,   55,   56,   57,   58,   59,   60,   61,
62,   63,  190
  191,  192,  193,  194,  195,  196,  197,  198,  199,  200,  201,  202,  203,
204,  205,  206
  207,  208,  209,  210,  211,  212,  213,  214,  215,  216,  217,  218,  219,
220,  221,  222
  223,  224,  225,  226,  227,  228,  229,  230,  231,  232,  233,  234,  235,
236,  237,  238
  239,  240,  241,  242,  243,  244,  245,  246,  247,  248,  249,  250,  251,
252,  379,  380
  381,  382,  383,  384,  385,  386,  387,  388,  389,  390,  391,  392,  393,
394,  395,  396
  397,  398,  399,  400,  401,  402,  403,  404,  405,  406,  407,  408,  409,
410,  411,  412
  413,  414,  415,  416,  417,  418,  419,  420,  421,  422,  423,  424,  425,
426,  427,  428
  429,  430,  431,  432,  433,  434,  435,  436,  437,  438,  439,  440,  441,
568,  569,  570
  571,  572,  573,  574,  575,  576,  577,  578,  579,  580,  581,  582,  583,
584,  585,  586
  587,  588,  589,  590,  591,  592,  593,  594,  595,  596,  597,  598,  599,
600,  601,  602
  603,  604,  605,  606,  607,  608,  609,  610,  611,  612,  613,  614,  615,
** Section: Shell t=10mm
```

```
*Shell Section, elset=_PickedSet3, material=steel
0.01, 5
*End Part
**
**
** ASSEMBLY
**
*Assembly, name=Assembly
**
*Instance, name=N8-1, part=N8
*End Instance
**
*Nset, nset=_PickedSet38, internal, instance=N8-1
  10, 399, 400, 401, 402, 403, 404, 405, 406, 407, 408, 409, 410, 411, 412, 413
 414, 415, 416, 417, 418, 419, 420, 421, 422, 423, 424, 425, 426, 427, 428, 429
 430, 431, 432, 433, 434, 435, 436, 437, 438, 439, 440, 441, 442, 443, 444, 445
 446, 447, 448, 449, 450, 451, 452, 453, 454, 455, 456, 457, 458, 459, 460
*Elset, elset=_PickedSet38, internal, instance=N8-1
 442, 444, 446, 448, 450, 452, 454, 456, 458, 460, 462, 464, 466, 468, 470, 472
 474, 476, 478, 480, 482, 484, 486, 488, 490, 492, 494, 496, 498, 500, 502, 504
 506, 508, 510, 512, 514, 517, 519, 521, 523, 525, 527, 529, 531, 533, 535, 537
 539, 541, 543, 545, 547, 549, 551, 553, 555, 557, 559, 561, 563, 565, 567
*Nset, nset=_PickedSet39, internal, instance=N8-1
   26, 1082, 1083, 1084, 1085, 1086, 1087, 1088, 1089, 1090, 1091, 1092, 1093,
1094, 1095, 1096
 1097, 1098, 1099, 1100, 1101, 1102, 1103, 1104, 1105, 1106, 1107, 1108, 1109,
1110, 1111, 1112
 1113, 1114, 1115, 1116, 1117, 1118, 1119, 1120, 1121, 1122, 1123, 1124, 1125,
1126, 1127, 1128
 1129, 1130, 1131, 1132, 1133, 1134, 1135, 1136, 1137, 1138, 1139, 1140, 1141,
1142, 1143
*Elset, elset=_PickedSet39, internal, instance=N8-1
 1514, 1516, 1518, 1520, 1522, 1524, 1526, 1528, 1530, 1532, 1534, 1536, 1538,
1540, 1542, 1544
 1546, 1548, 1550, 1552, 1554, 1556, 1558, 1560, 1562, 1564, 1566, 1568, 1570,
1572, 1574, 1576
 1578, 1580, 1582, 1584, 1586, 1587, 1589, 1591, 1593, 1595, 1597, 1599, 1601,
1603, 1605, 1607
 1609, 1611, 1613, 1615, 1617, 1619, 1621, 1623, 1625, 1627, 1629, 1631, 1633,
1635, 1637
*Elset, elset=__PickedSurf37_E2, internal, instance=N8-1, generate
 1514,  1586,     2
*Elset, elset=__PickedSurf37_E4, internal, instance=N8-1, generate
 1587,  1637,     2
*Surface, type=ELEMENT, name=_PickedSurf37, internal
__PickedSurf37_E2, E2
__PickedSurf37_E4, E4
*End Assembly
**
** MATERIALS
**
*Material, name=steel
*Elastic
 2e+11, 0.3
** ----------------------------------------------------------------
**
** STEP: Step-1
**
*Step, name=Step-1, perturbation
*Buckle, eigensolver=lanczos
3, , ,
```

```
**
** BOUNDARY CONDITIONS
**
** Name: BC-1 Type: Symmetry/Antisymmetry/Encastre
*Boundary, op=NEW, load case=1
_PickedSet38, PINNED
*Boundary, op=NEW, load case=2
_PickedSet38, PINNED
** Name: BC-2 Type: Displacement/Rotation
*Boundary, op=NEW, load case=1
_PickedSet39, 1, 1
*Boundary, op=NEW, load case=2
_PickedSet39, 1, 1
**
** LOADS
**
** Name: Axial1000N   Type: Shell edge load
*Dsload
_PickedSurf37, EDSHR, 1000.
**
** OUTPUT REQUESTS
**
*Restart, write, frequency=0
**
** FIELD OUTPUT: F-Output-1
**
*Output, field
*Node Output
U,
*Element Output, directions=YES
S,
*End Step
```

Appendix B-Experimental Results

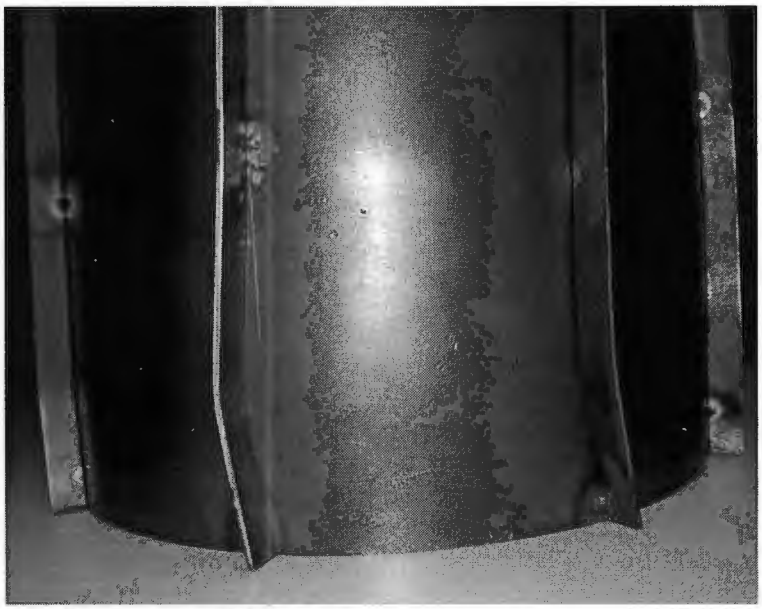

Fig. B1 Stringer failure

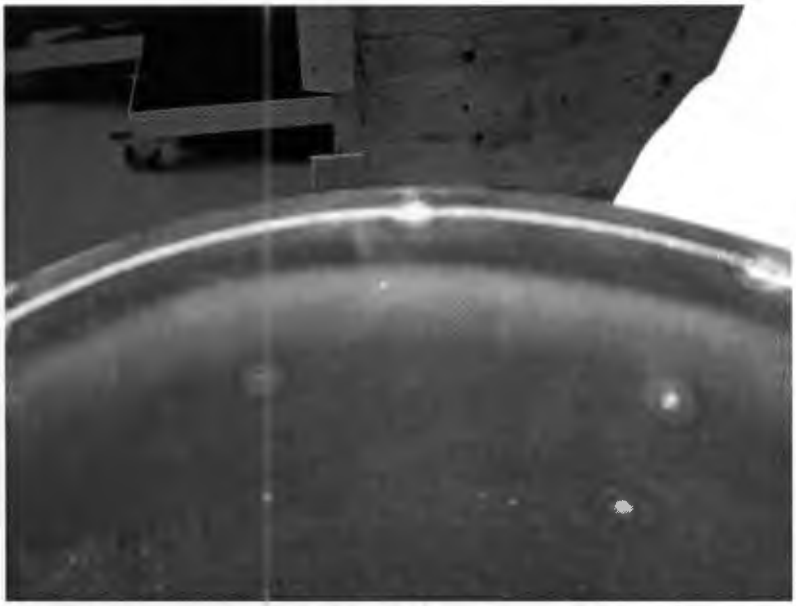

Fig. B2 Axisymmetric bulge at the top support

Fig. B3 Shell buckling between ring stiffeners

Test No. CYL01

	LOAD [kN]	Dial gauge reading [mm]	Deflection [mm]
	0	13.86	0
	10	13.76	0.1
	20	13.67	0.19
	30	13.61	0.25
	40	13.54	0.32
	50	13.49	0.37
	60	13.45	0.41
	70	13.41	0.45
	80	13.38	0.48
	90	13.34	0.52
	100	13.31	0.55
	110	13.27	0.59
	120	13.24	0.62
	130	13.21	0.65
	140	13.18	0.68
	150	13.16	0.7
	160	13.14	0.72
	170	13.11	0.75
	180	13.09	0.77
	190	13.07	0.79
	200	13.04	0.82
	210	13.01	0.85
	220	12.98	0.88
	230	12.94	0.92
	240	12.89	0.97
	250	12.86	1
	260	12.81	1.05
	270	12.76	1.1
	288	12.67	1.19

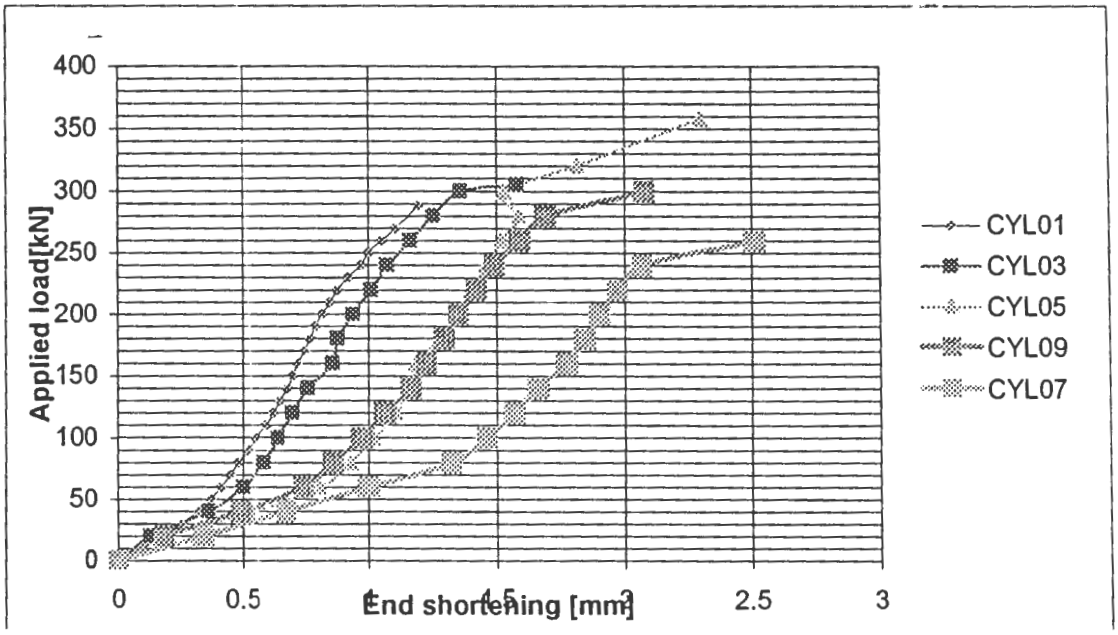

Test No. CYL03

	LOAD [kN]	Dial gauge reading [mm]	Deflection [mm]
	0	11.36	0
	20	11.23	0.13
	40	11	0.36
	60	10.86	0.5
	80	10.78	0.58
	100	10.72	0.64
	120	10.66	0.7
	140	10.6	0.76
	160	10.5	0.86
	180	10.48	0.88
	200	10.42	0.94
	220	10.35	1.01
	240	10.29	1.07
	260	10.2	1.16
	280	10.11	1.25
	300	10	1.36
	305	9.78	1.58

Test No. CYL05

	LOAD [kN]	l gauge reading [r	Deflection [mm]
	0	11.31	0
	20	11.12	0.19
	40	10.77	0.54
	60	10.5	0.81
	80	10.38	0.93
	100	10.29	1.02
	120	10.21	1.1
	140	10.15	1.16
	160	10.13	1.18
	180	10.03	1.28
	200	9.97	1.34
	220	9.91	1.4
	240	9.85	1.46
	260	9.79	1.52
	280	9.72	1.59
	300	9.78	1.53
	320	9.5	1.81
	358	9.01	2.3

Test No. CYL07

	LOAD [kN]	Dial gauge reading [mm]	Deflection [mm]
	0	13.7	0
	20	13.36	0.34
	40	13.03	0.67
	60	12.7	1
	80	12.38	1.32
	100	12.24	1.46
	120	12.13	1.57
	140	12.04	1.66
	160	11.93	1.77
	180	11.86	1.84
	200	11.8	1.9
	220	11.73	1.97
	240	11.63	2.07
	260	11.19	2.51

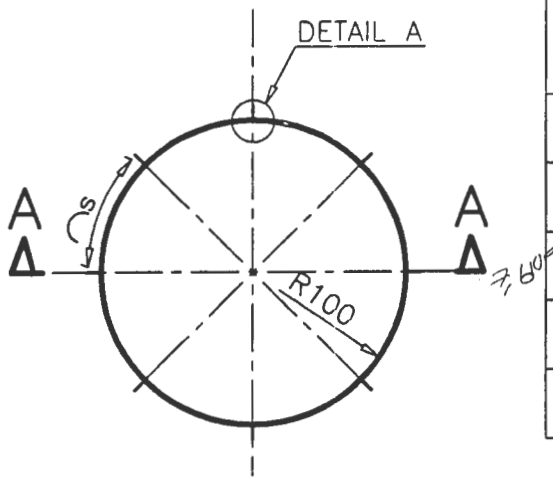

PLAN VIEW
SCALE 1:5

Model reference	STIFFENER DIMENSIONS			No. of Stiffeners
	b	d	s	
CYL01	No stiffeners			0
CYL03	1.6	10	157	8
CYL05	1.6	10	63	20

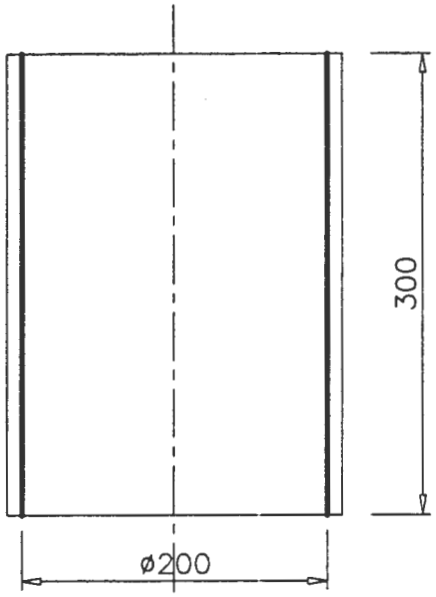

SECTION A–A
SCALE 1:5

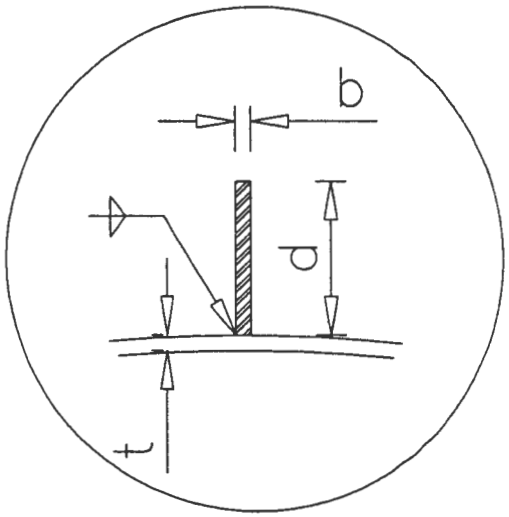

DETAIL A
NTS

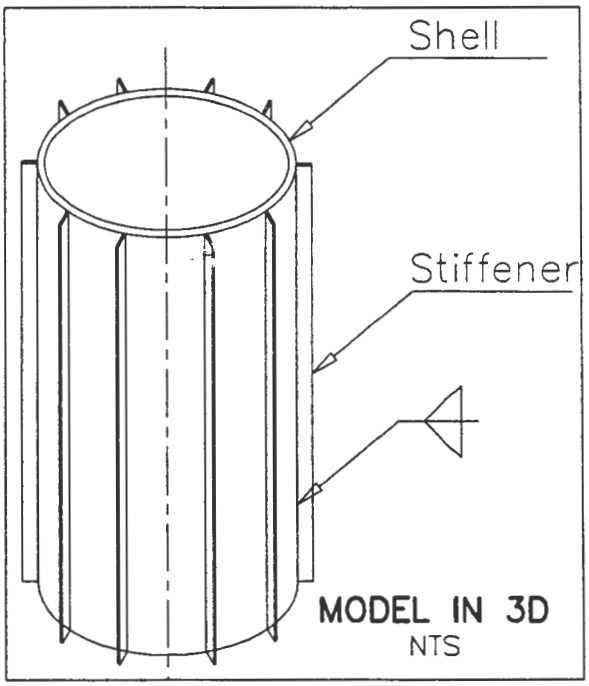

MODEL IN 3D
NTS

NOTES

- All dimensions are in mm
- Material–Use grade 350MPa steel for all parts
- Longitudinal stiffeners to be spot welded to the out side of cylinder or cone surface
- Each model has Stiffener dimensions(b and d) and different stiffener spacing(s) as shown in table above

UNIVERSITY OF CAPE TOWN DEPT. OF CIVIL ENG. STRUCTURAL ENG. RESEARCH GROUP	TITLE	LONGITUDINALLY STIFFENED CYLINDRICAL SHELLS				
	DRWN BY	RUGARE	SCALE	AS SHOWN	PAGE	1 of 4

Model reference	STIFFENER DIMENSIONS			No. of Stiffeners
	b	d	s	
CYL07	1.6	10	38	8
CYL09	1.6	10	15	20

6591,8

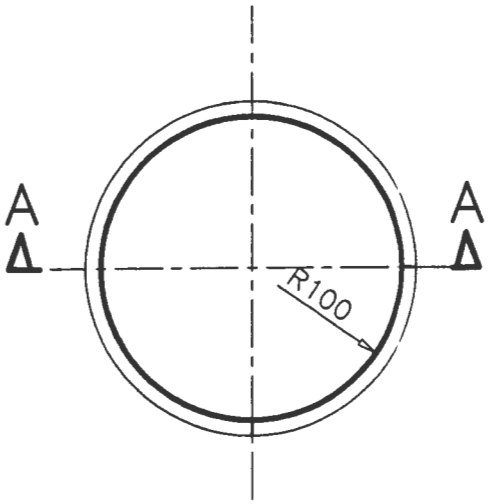

PLAN VIEW
SCALE 1:5

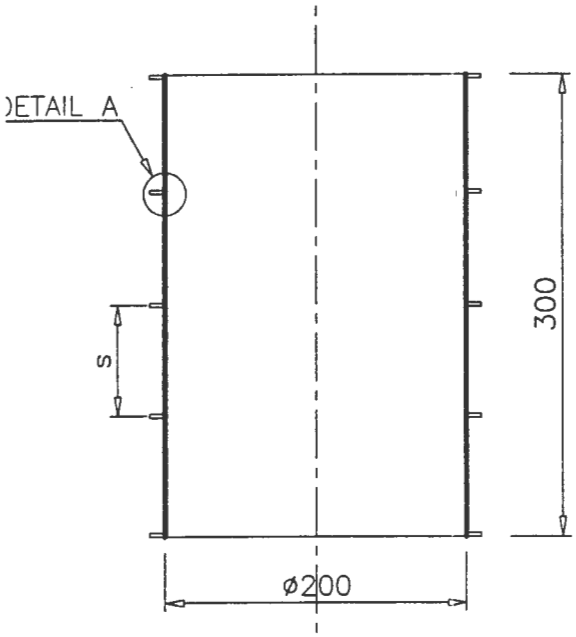

SECTION A–A
SCALE 1:5

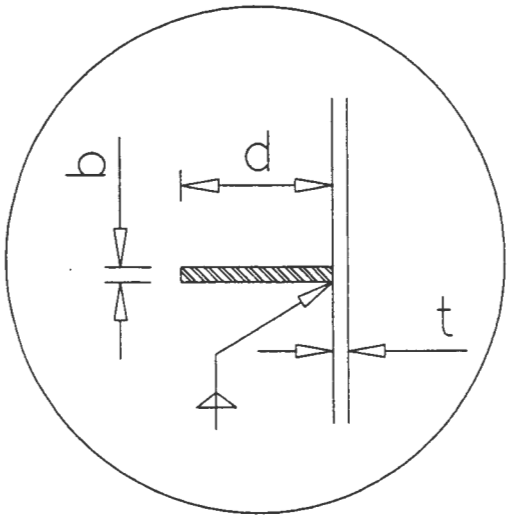

DETAIL A
NTS

NOTES

- All dimensions are in mm
- Material–Use grade 350MPa steel for all parts
- Longitudinal stiffeners to be spot welded to the out side of cylinder or cone surface
- Each model has Stiffener dimensions(b and d) and different stiffener spacing(s) as shown in table above

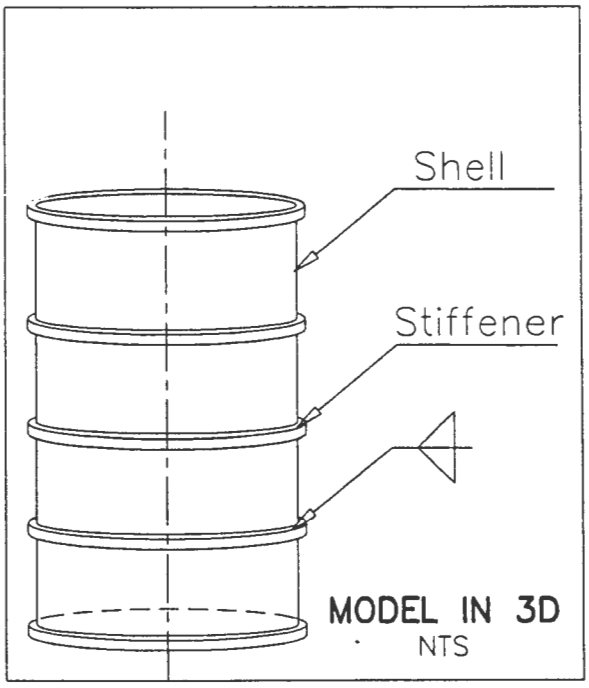

MODEL IN 3D
NTS

UNIVERSITY OF CAPE TOWN DEPT. OF CIVIL ENG. STRUCTURAL ENG. RESEARCH GROUP	TITLE	RING STIFFENED CYLINDRICAL SHELLS				
	DRWN BY	RUGARE	SCALE	AS SHOWN	PAGE	2 of 4

Model reference	STIFFENER DIMENSIONS			No. of Stiffeners
	b	d	s	
CON01	No stiffeners			0
CON03	1.6	10	79	8
CON05	1.6	10	31	20

3045,5

3419,1

6283,0

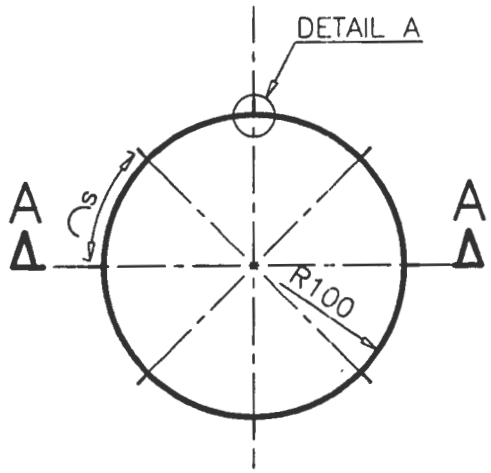

PLAN VIEW
SCALE 1:5

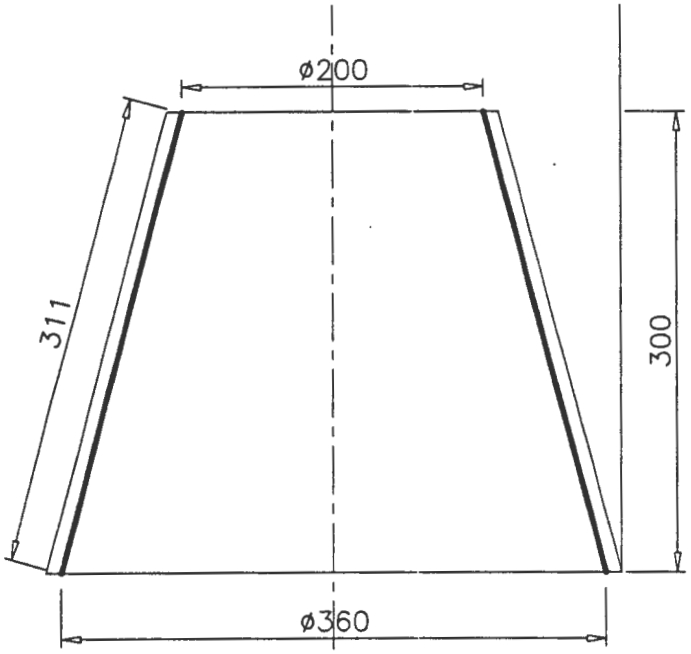

SECTION A–A
SCALE 1:5

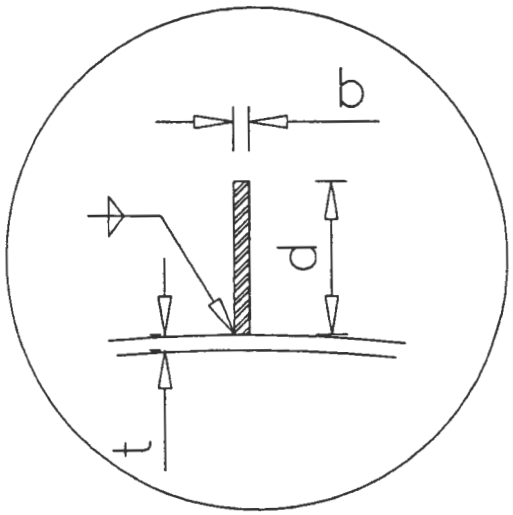

DETAIL A
NTS

NOTES

- All dimensions are in mm
- Material–Use grade 350MPa steel for all parts
- Longitudinal stiffeners to be spot welded to the out side of cylinder or cone surface
- Each model has Stiffener dimensions(b and d) and different stiffener spacing(s) as shown in table above

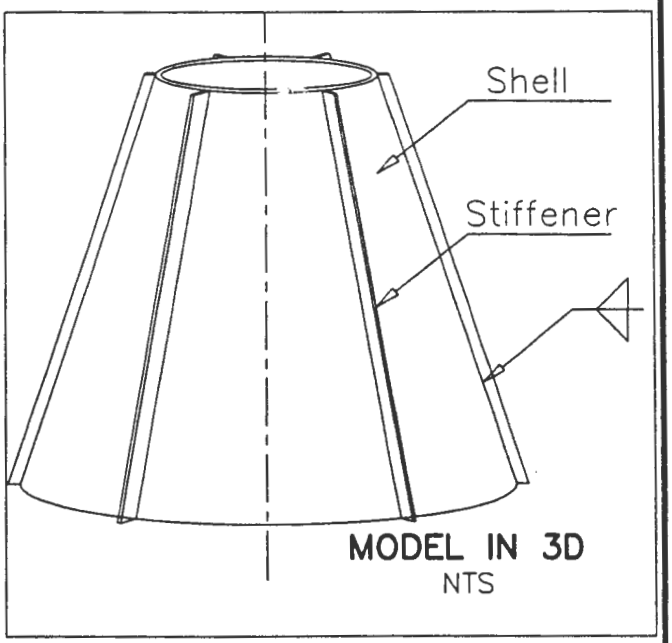

MODEL IN 3D
NTS

UNIVERSITY OF CAPE TOWN DEPT. OF CIVIL ENG. STRUCTURAL ENG. RESEARCH GROUP	TITLE	LONGITUDINALLY STIFFENED CONICAL SHELLS				
	DRWN BY	RUGARE	SCALE	AS SHOWN	PAGE	3 of 4

Model reference	STIFFENER DIMENSIONS			No. of Stiffeners
	b	d	s	
CON07	1.6	10	39	8
CON09	1.6	10	16	20

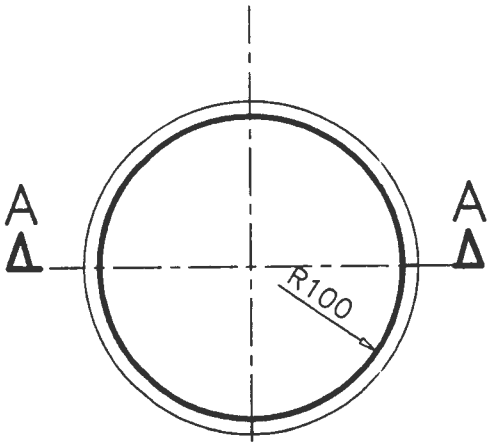

PLAN VIEW
SCALE 1:5

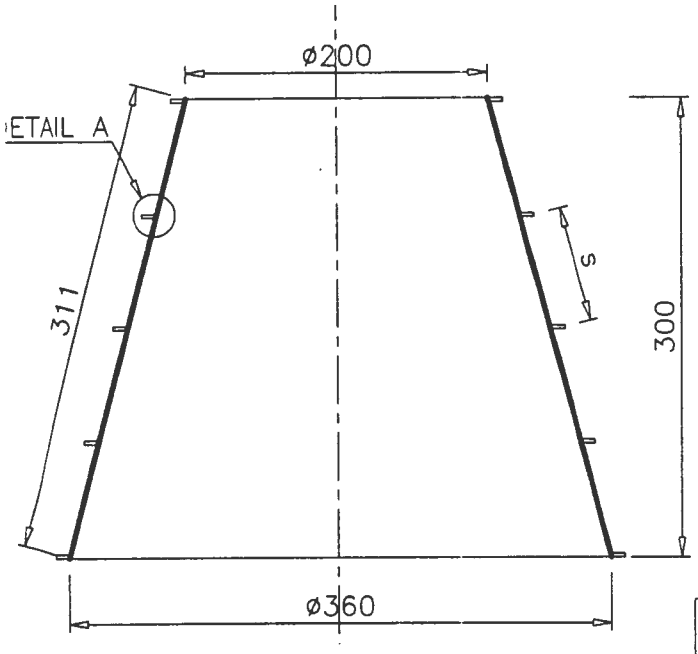

SECTION A–A
SCALE 1:5

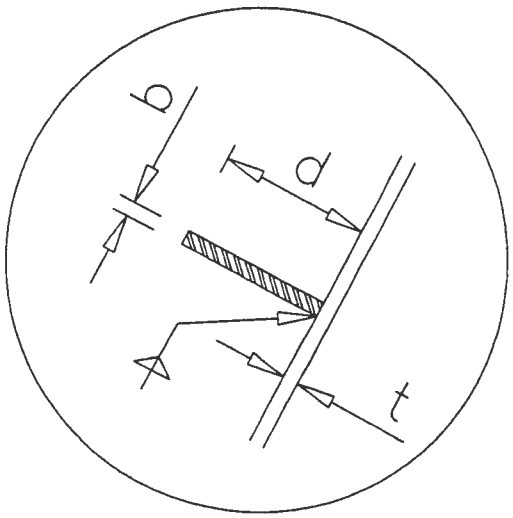

DETAIL A
NTS

NOTES

- All dimensions are in mm
- Material–Use grade 350MPa steel for all parts
- Longitudinal stiffeners to be spot welded to the out side of cylinder or cone surface
- Each model has Stiffener dimensions(b and d) and different stiffener spacing(s) as shown in table above

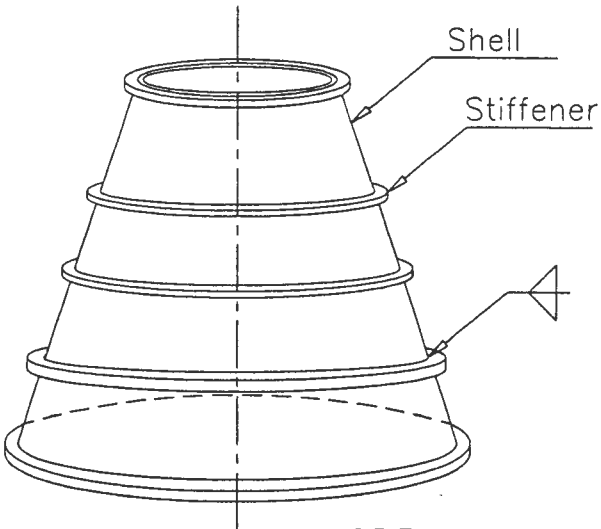

MODEL IN 3D
NTS

UNIVERSITY OF CAPE TOWN DEPT. OF CIVIL ENG. STRUCTURAL ENG. RESEARCH GROUP	TITLE	RING STIFFENED CONICAL SHELLS				
	DRWN BY	RUGARE	SCALE	AS SHOWN	PAGE	4 of 4

Parameter table:

Customer	:	Load cell	:
Tester	:	Extensometer (path)	:
Test standard	:	Specimen grips	:
Material	:	Machine data	: Control SN: 94851 Crosshead SN: 94851 Force SN: 94834 200 kN
Specimen ID	:		

Results:

Nr	Rp 0.2 N/mm²	Rm N/mm²	ε Break %
1	330.77	393.11	27.38
2	335.45	389.71	35.16
3	371.12	395.47	26.25
4	368.00	389.39	32.22
5	397.88	402.99	37.17

Series graph:

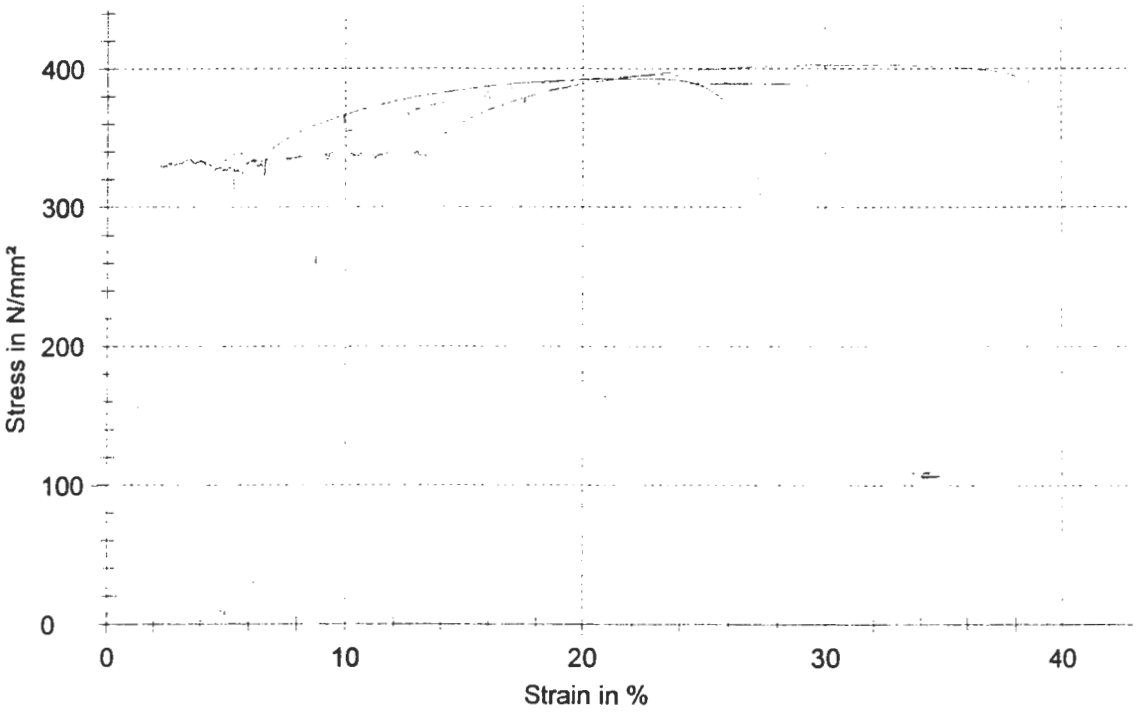

Statistics:

Series n = 5	Rp 0.2 N/mm²	Rm N/mm²	ε Break %
x̄	360.64	394.13	31.64
s	27.74	5.55	4.76
v	7.69	1.41	15.03

Appendix C-Buckling coefficient graphs

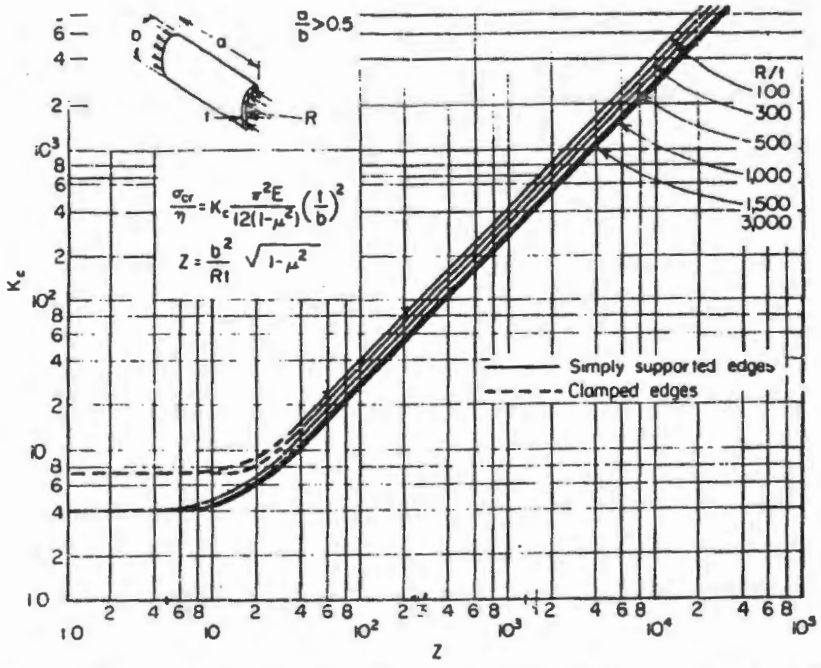

figure 10-1 *Buckling-stress coefficient K_c for unpressurized curved panels subjected to axial compression.*

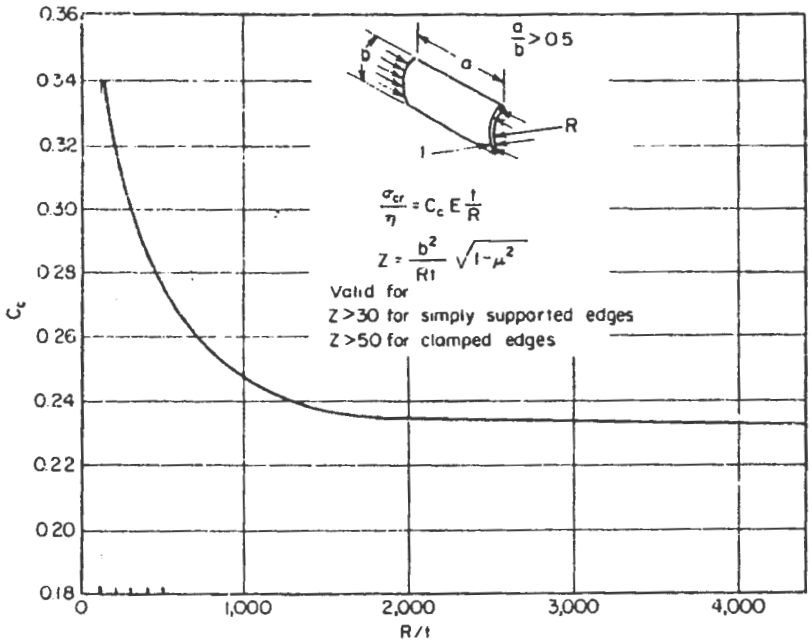

figure 10-2 *Buckling-stress coefficient C_c for unpressurized curved panels subjected to axial compression.*

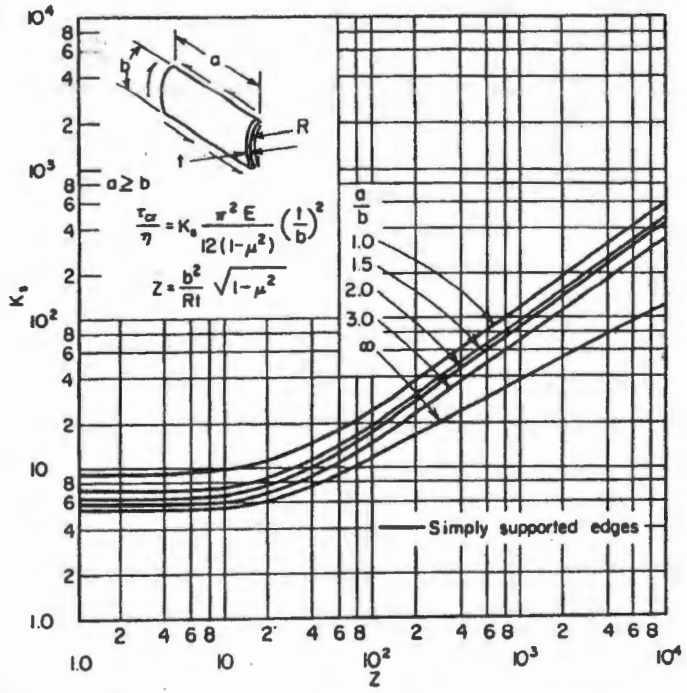

figure 10-5 *Buckling-stress coefficient K_s for unpressurized curved panels subjected to shear.*

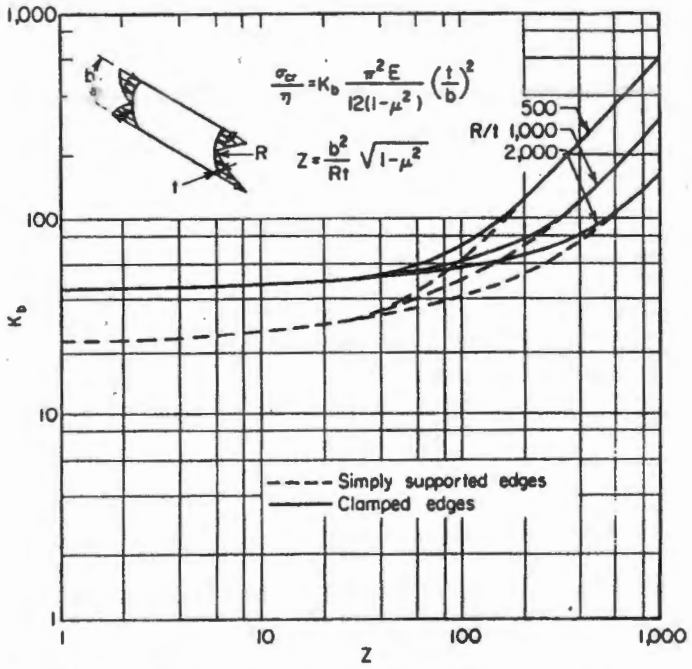

figure 10-7 *Critical buckling-stress coefficients for long, curved panels subjected to bending.*